# Geology of the Navajo Gap area between the Ladron Mountains and Mesa Sarca, Socorro County, New Mexico: A Structural Analysis

by

Charles M. Hammond

Submitted in Partial Fulfillment
of the Requirements for the Degree of
Master of Science in Geology

New Mexico Institute of Mining and Technology,

Socorro, New Mexico

August, 1987

# ABSTRACT

Navajo Gap is the topographic low area between Mesa Sarca and the Ladron Mountains. Mesa Sarca is the southeastern edge of Colorado Plateau and the Ladron Mountains are an uplift within the Rio Grande rift at the southern end of Albuquerque basin. The Navajo Gap area lies along the border fault of Monte Largo embayment, the southwestern region of Albuquerque basin. Strata in the area include: Proterozoic granite and metavolcanics; Mississippian, Pennsylvanian, and Permian limestones, sandstones and shales; a small outcrop of Cretaceous conglomerate; late Oligocene-early Miocene mafic dikes; and Pleistocene- Pliocene gravels and travertine. Detailed mapping reveals three styles of structural deformation: compressional, strike-slip, and tensional.

Three episodes of Phanerozoic structural deformation are recognized in the Navajo Gap area. The earliest episode includes late Paleozoic folding. The nature of late Paleozoic deformation, and the location of the structural zone are indeterminate.

The second episode of deformation was presumably Laramide. Early Laramide deformation was compressional and late Laramide deformation was strike-slip. Prominent early Laramide structures consist of a near vertical, north- to north-northwest-trending, down-to-west fault at the location of the Ladron fault, and a northwest-trending and northeast-dipping reverse fault at the location of the Saiz fault. Fold belts developed within the foot walls paralleling these faults. Other structures include minor reverse faults, minor thrust faults (both within the fold belts), north-northeast- to northeast-trending left-shears, and east-trending right-shears. Early Laramide structures were primary to an approximately N60 ° E-trending maximum principle horizontal stress.

Folds, reverse faults, and thrust faults continued to develop during late Laramide, but north-trending left-slip faults and shears, and north-northeast-

trending right-slip faults and shears became the dominant style of deformation. Strike-slip faulting, especially right-slip, was the most common. These structures were most likely secondary to an approximately N21 ° E-trending maximum principle horizontal stress.

The early Laramide tectonic setting for the Navajo Gap area is interpreted to have been on the west side of the northern Sierra uplift of Eocene age, or an uplift between the Sierra and Lucero uplifts. During late Laramide, this tectonic setting is interpreted to have become a zone of strike-slip within a right-wrench zone.

The third episode of deformation was possibly a three-stage event, including early rift (late Oliogocene-early Miocene), middle rift (?), and late rift (Pleistocene-Pliocene) extension. Early rift extension was evident by the emplacement of north- to north-northeast-trending mafic dikes. Middle rift extension reactivated a Laramide reverse fault forming the north-west-trending and northeast-dipping tensional Saiz fault zone. The early Laramide uplift collapsed into the southwestern Albuquerque basin during this tension.

Late rift tensional stuctures include north-trending, high-angle normal faults. These structures include the Ladron and Mesa Sarca faults, and other less prominent faults that parallel Mesa Sarca fault. The Saiz fault zone, Mesa Sarca fault, and the Ladron fault are interpreted to reflect control by preexisting structures. The Navajo Gap area tilted approximately seven degrees westward during late rift tensional faulting. Navajo Gap was the site of a paleovalley that drained to the northeast into the Albuquerque basin during late Tertiary.

# TABLE OF CONTENTS

# LIST OF FIGURES

# LIST OF PLATES

# INTRODUCTION

## Field Area Setting

The Navajo Gap study area is approximately 4 km (2.5 mi) wide and 12 km (7.5 mi) long. It stretches north-northwestward from the northwest slope of Ladron Mountains, elevation approximately 7900 ft, to the high point of Mesa Sarca, elevation 6965 ft. Navajo Gap is located at the intersections of Riley, Ladron Peak, and Mesa Sarca 7 1/2 minute quadrangles, about 56 km (35 mi) northwest of Socorro, and 32 km (20 mi) west of Bernardo, in central-north Socorro County, New Mexico. The location is shown in Figure 1 and its relationships to surrounding physiographic features and access routes are shown in Figure 2.

Navajo Gap, elevation approximately 5700 ft, is the topographic low between Mesa Sarca and Ladron Mountains. The Navajo Gap area crosses between the southeastern margin of Colorado Plateau and the Sierra Ladron massif, a horst block within the Rio Grande rift.

From north to south, the Navajo Gap area is comprised of: (1) the southeastern side of a faulted and dissected mesa of gently west-dipping Pennsylvanian strata (Mesa Sarca); (2) a faulted and gently folded east-facing cuesta (northwest extension of Ladron Mountains, here informally named Saiz Ridge after Saiz Ranch on which it lies) and adjacent low hills of folded, faulted, and gently west-dipping Pennsylvanian and Permian strata; and (3) ridges and canyons of Proterozic granitic and metamorphic rocks (northwest side of Ladron Mountains). Most bedrock consists of upper Paleozoic strata; a lesser amount is of Proterozoic and Tertiary rocks.

The area is bounded to the northeast by a major rift (extensional) fault and Monte Largo Embayment, a southwestern prong of the Albuquerque basin. To the southwest, pediment gravels cover the Paleozoic strata and

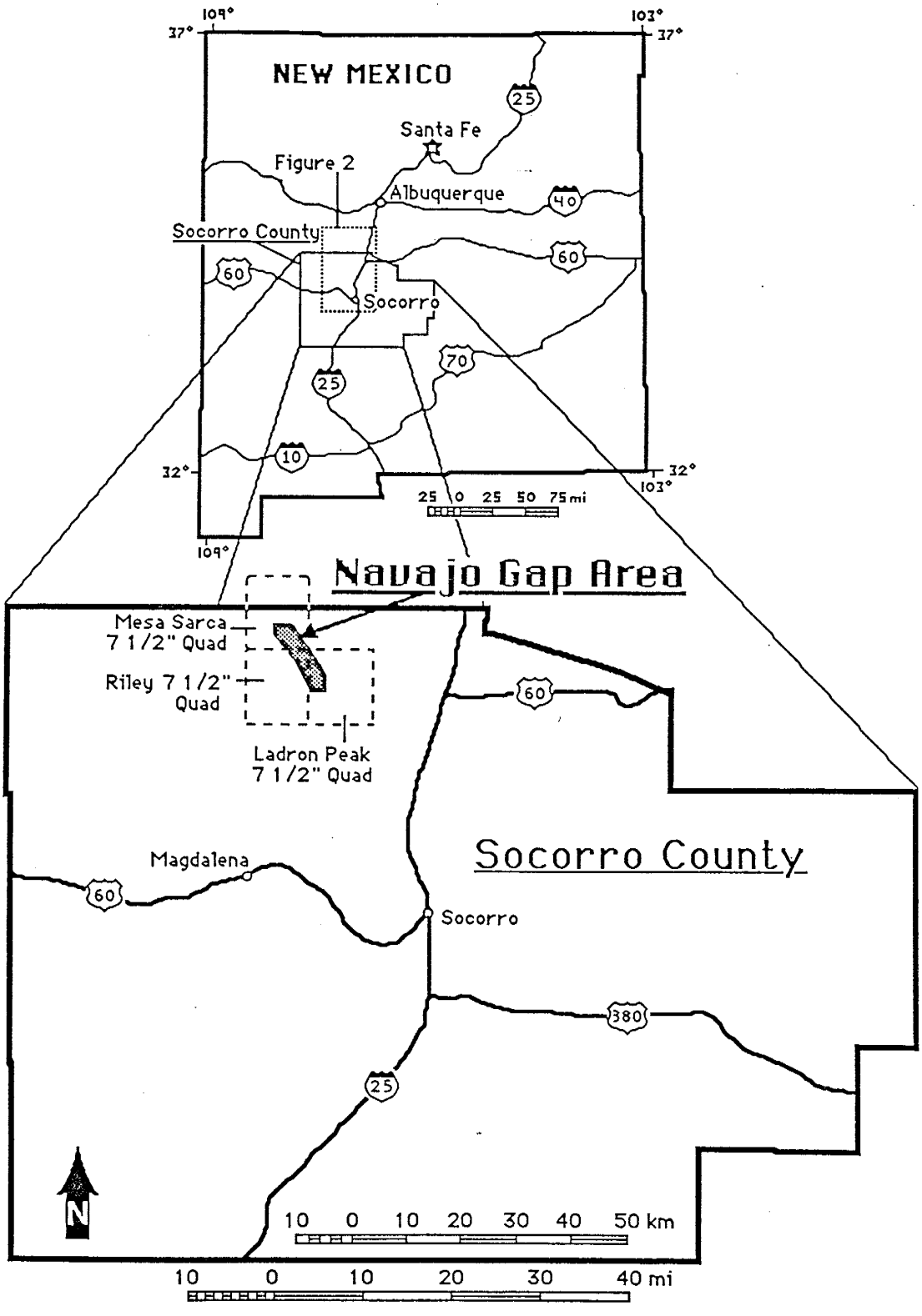


Figure 1. Location of Navajo Gap field study area within Mesa Sarca, Riley, and Ladron Peak 7 1/2' quadrangles.

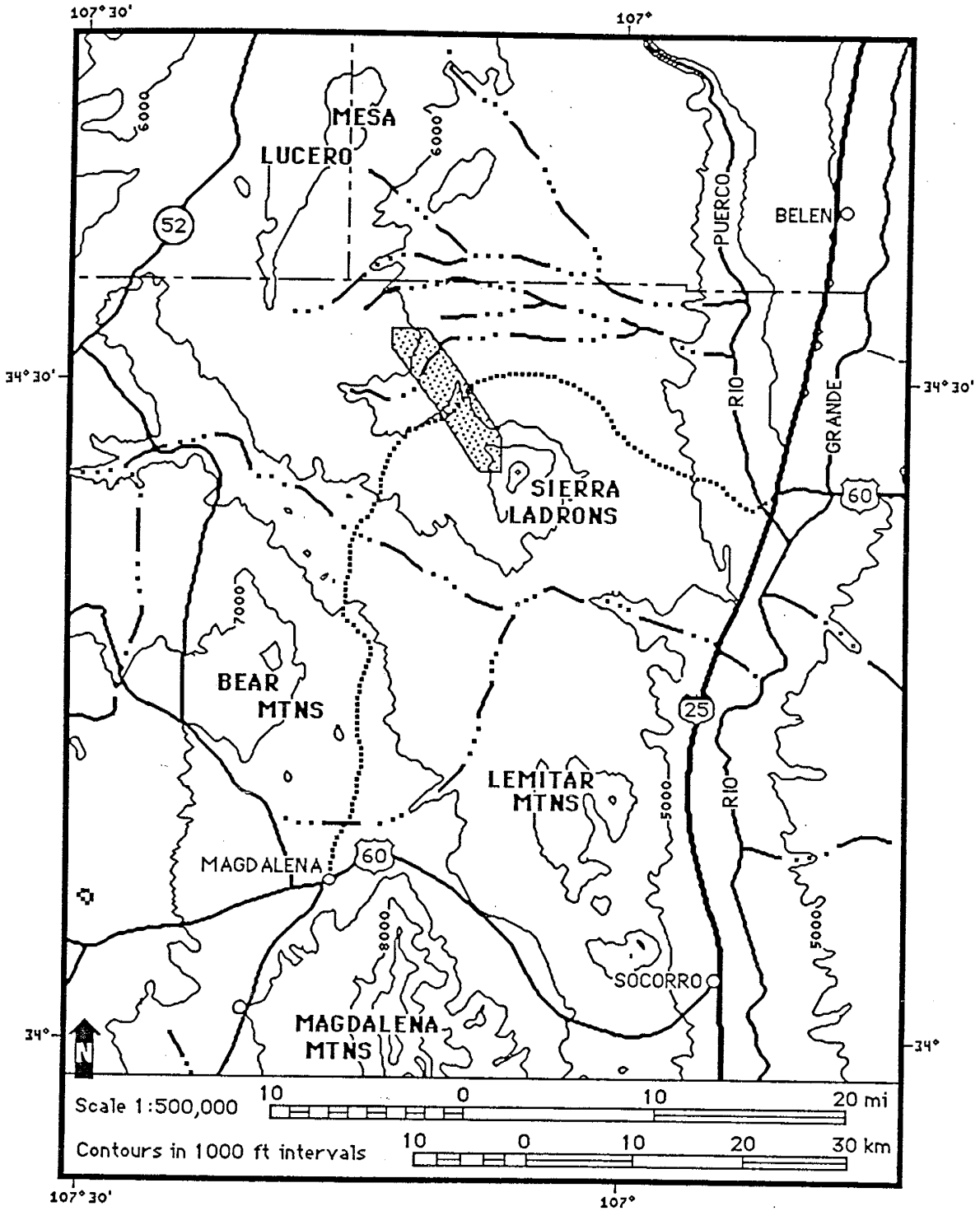


Figure 2. Location of Navajo Gap area (stippled) and surrounding topographic features. Access to Navajo Gap on gravel road (dashed ·····) from intersection of (25) and (60), or from Magdalena. See Figure 1 for location of this map.

upper Santa Fe Group deposits of Cenozoic age.

## Objectives

The primary objectives of this study were to: (1) map the geology of Navajo Gap; (2) detail Pennsylvanian stratigraphy using Thompson's (1942) nomenclature, modified by Rejas (1965); (3) determine the nature of the Comanche (Saiz) fault zone and the Ladron fault; (4) determine the style of extensional faulting in the area; (5) determine if Laramide strike-slip faulting occurred in the area; (6) formulate ideas toward understanding the structural control of Monte Largo embayment; and (7) delineate any structural or stratigraphic features that can aid in interpreting the nature of the west margin of the Albuquerque basin as shown on the COCORP Socorro line 1A seismic-reflection profile.

## Methods of Investigation

I mapped the geology at a scale of 1:12,000 on a base made from parts of Riley, Ladron Peak, and Mesa Sarca preliminary topographic quadrangles of the U.S.G.S. 7 1/2 minute series. Color aerial photographs of the BLM LCS project, 8/26/75, at a scale of approximately 1:36,000, aided in mapping. Mapping began in early summer, 1985, and was completed in late summer 1986.

Field work emphasized analysis of structural style and kinematic indicators. These indicators are: (a) extension veins, (b) shear veins, (c) internal fibrous vein minerals, (d) slickensides, (e) fault-breccia fabric, (f) fault-fold spatial relationship, and (g) offset stratigraphy. Detailed stratigraphic sections were measured prior to mapping. Locations of these sections are included with the stratigraphic descriptions in Appendices B through F. I

revised these sections many times throughout the course of mapping. Classifications of limestone, sandstone, grain size, sorting, roundness, bed thickness, and bed internal structure are listed in Appendix A.

Extension veins, faults, and striations were plotted on equal-area stereographic nets. Thirteen thin sections were prepared from samples of veins collected in the study area. Internal fibrous vein minerals were analyzed to determine incremental and finite strain. Structural analyses revealed stress fields related to tectonic activity in the area. Schematic maps were drawn to aid in determining the style of structural deformation.

## Previous Work

Oil and Gas Investigation map number 47, at a scale of 1:62,500, includes the Navajo Gap area (Kelley and Wood,1946). Kelley and Wood mapped the major structures but did not record many minor faults. Folds were located, but mapping at such a small scale did not allow their true nature to be shown. They also measured and described stratigraphic sections of Paleozoic strata. The geologic map of Albuquerque basin, at a scale of 1:190,000 (Kelley,1977), also includes Navajo Gap. Duschatko (1953) described structures in the Gray Mesa area (Navajo Gap area) from reconnaissance field work.

Siemers (1978) measured and described a generalized stratigraphic section of the Paleozoic strata. But, only the Sandia Formation and lower limestone member of the Madera Limestone were studied in the Navajo Gap area. Chamberlin and others (1982) produced an excellent overview of the Ladron Mountains and its surrounding area. Thompson (1942), Read and Wood (1947), Kottlowski (1960, 1963), Armstrong and others (1979), and Bachman (1975) discussed this area in regional studies of the Paleozoic system. Parts of the Navajo Gap area are mentioned briefly by Armstrong (1958), Black (1964)

and Condie (1976).

Two useful nomenclatures have evolved for Pennsylvanian strata in central New Mexico; Myers (1973) and Thompson (1942) modified (Rejas, 1965). The use of either would depend on author's discretion and scale of study. In this study, the desire for precise structural control and the large scale of field mapping (1:12,000) warranted the more detailed Thompson (1942) modified (Rejas, 1965) nomenclature. For field studies at a smaller scale, this nomenclature may be too detailed and impractical. In this case I would recommend Myers (1973) nomenclature.

Acknowledgments

Special thanks to my thesis advisor, Dr. Charles E. Chapin, for suggesting the area of study, his constructive advice and criticism, and for patience while I learned and struggled to finish. New Mexico Bureau of Mines and Mineral Resources supplied aerial photographs, base maps, drafting supplies, and thin section materials.

Dr. David B. Johnson served on my committee and gave substantial constructive criticism. Dr. Clay T. Smith served on my committee and gave constructive advice. Eddy Saiz allowed access to his ranch land and showed me "unknown" back roads. John F. Callender gave me many ideas during a structural analysis class, spring semester 1986. Dr. Paul E. Hammond assisted through his geoscience writing skills.

Insight was gained from discussions with S.M. Cather, Pascal Cabezas, Karen Brown, and R. P. Lozinsky. Charles Ferguson assisted with his mastery at drafting. Bill Macintosh provided me with a lower hemisphere equal-area computer plotting program and assisted in the collection of most of the vein samples with the New Mexico Bureau of Mine's paleomagnetics-drill.

Cara N. Francke pushed me through hard times and assisted through her technical-editor skills. Many other peers unknowingly assisted in many ways with their own ideas and techniques of study.

Final portions of this research were supported in part by a Richard A. Matuszeski Graduate Research Fund Grant-in-Aid received from the Graduate Student Association of New Mexico Institute of Mining and Technology, Socorro, New Mexico. Lastly, I would like to thank my parents, Dr. Paul E. Hammond and Jean M. Hammond, for their continuous moral and financial support. Without them this would not have been possible.

## PROTEROZOIC ROCKS

Proterozoic rocks are well exposed in the Ladron Mountains. A small exposure also crops out at the foot of Mesa Sarca (Plate 1). Proterozoic rocks consist of a granitoid, related to the Capriote Granite in the Ladron Mountains (Condie, 1976), and a metavolcanic sequence. Aplite and diabase dikes intrude the metavolcanic sequence; only aplite intrudes the granite. Field relations indicate that the granite is younger than the metavolcanics. Mapped in the Ladron Mountains (Black, 1964; Condie, 1976), metasedimentary rocks and the Ladron pluton granite do not crop out in the study area.

The metavolcanic sequence consists of foliated siliceous rocks with minor black and green amphibolite in thin layers. Condie (1976) stated that "the metavolcanic sequence is composed chiefly of pink to purple siliceous volcanic rocks", of which 75 percent was originally ash-flow tuffs. "The remainder is composed of siliceous air-fall tuffs and lava flows, and perhaps 5 percent of basalt flows" (Condie, 1976).

The Capriote Granite, more recently labeled a granitoid (Chamberlin and others, 1982), is medium- to coarse-grained and has a reddish-brownish-orange color. Most of the granitoid is non-foliated, but small areas of foliated granitic gneiss crop out along the Ladron fault (SE/4, section 25, T3N, R3W) and at the foot of Mesa Sarca (western SE/4, section 32, T4N, R3W) (Plate 1). The outcrop of granitic gneiss at the foot of Mesa Sarca has not been previously recorded. Along the Ladron fault, Precambrian rocks are in contact with lower Pennsylvanian strata.

Similar packages of granitic rocks in association with felsic metavolcanic (and metasedimentary) rocks crop out south of the Ladron Mountains in the Magdalena, Lemitar, and Chupadera Mountains, and to the east in the Manzano and Los Pinos Mountains. In the Manzano Mountains, Bowring and Condie

(Bowring and others, 1983) obtained U-Pb zircon ages of 1,650-1,680 m.y. from the metavolcanic rocks. To the south, Bowring and others (1983) have dated the accumulation of volcanics and intrusion of granites at 1,650±10 m.y. using the U-Pb zircon method. No reliable ages have been obtained from these rocks in the Ladron Mountains (J.M. Robertson, personal communication, 1986). Thus, from a regional correlation the granitoid and associated felsic metavolcanics at the south end of Navajo Gap have an age of about 1,650 m.y. (J.M. Robertson, personal communication 1986).

# PALEOZOIC ROCKS

## General Features

Paleozoic strata cropping out in the Navajo Gap area include limestones, sandstones, and shales of the Mississippian, Pennsylvanian, and Permian periods. Mississippian strata consist of the Caloso Formation. Pennsylvanian strata consist of, from bottom to top, the Sandia, Elephant Butte, Whiskey Canyon, Garcia, Bartolo, Amado, Coane, Adobe, Council Spring, Burrego, Story, Del Cuerto, and Moya Formations (Fig. 3). Permian strata consist of, from bottom to top, the Bursum, Abo, and Yeso Formations.

Complete sections are measurable from the base of the Sandia Formation upwards to the top of the Bursum Formation. Incomplete sections include the Caloso, Abo, and Yeso Formations. An angular unconformity is recognized between Mississippian and Pennsylvanian strata. Total thickness of these strata are about 945 m (3,100 ft). Mississippian strata are 4.5 m (14.8 ft) thick. Pennsylvanian strata are about 574 m (1,883 ft) thick. Permian strata are about 367 m (1,204 ft) thick.

Due to gently dipping strata, several Pennsylvanian formations were unmappable on the steep east faces of Mesa Sarca and Saiz Ridge. The lower eight Pennsylvanian formations were mapped as the Armendaris, Socorro, and Veredas Groups (Fig. 3 and Plate 1).

## Mississippian Strata

Caloso Formation. The oldest Paleozoic strata in the Navajo Gap area are part of the Caloso Formation of Osagean age (Armstrong, 1958). While studying these strata in the southern Ladron Mountains, Armstrong (1958) noted

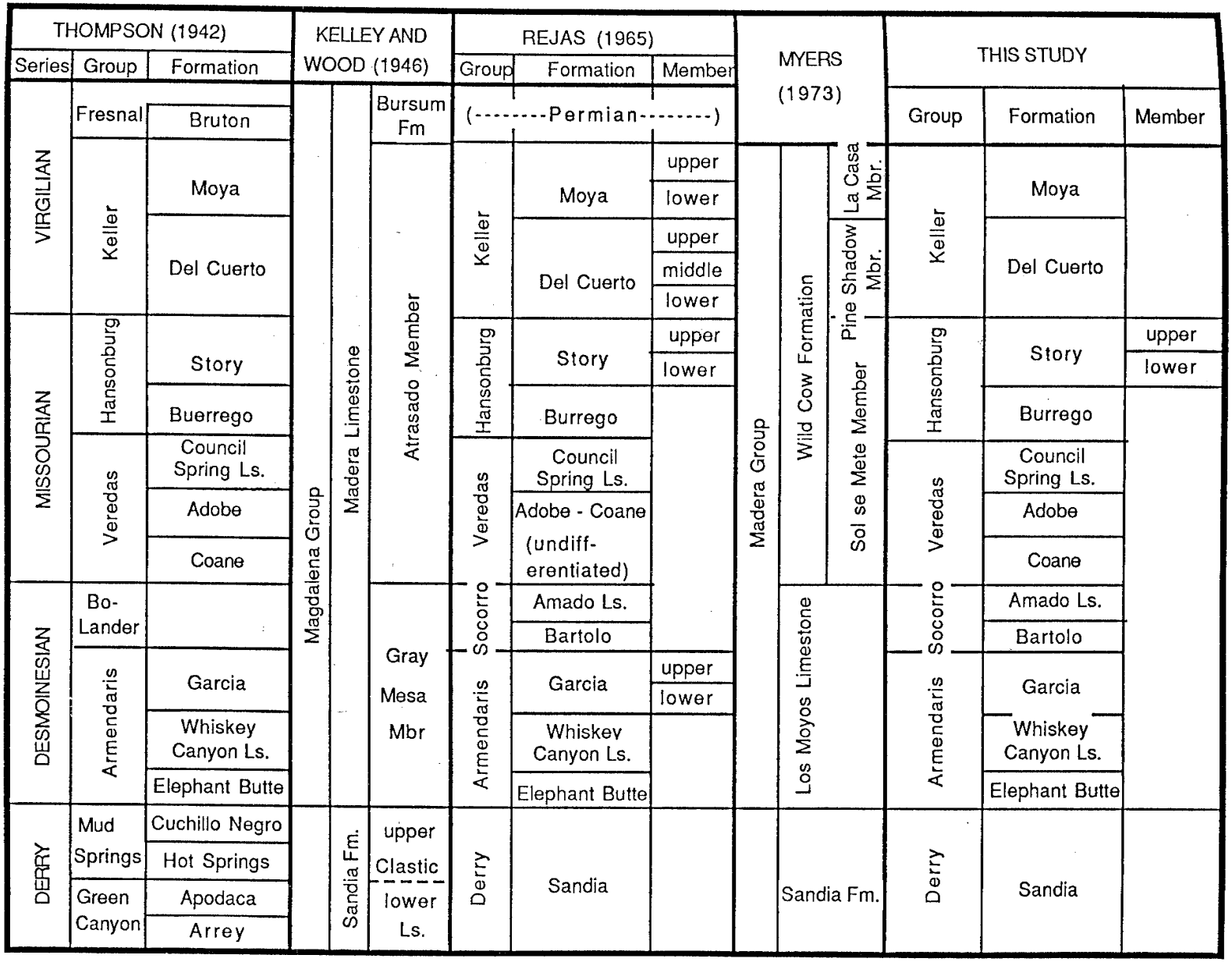


Figure 3. Nomenclature for Pennsylvanian stratigraphic units.

an erosional outlier of what he regards as Caloso Formation in the northern Ladron Mountains. I mapped this outlier (Plate 1) but field relations indicate that what Armstrong (1958) described as the basal Caloso Formation, "a pure white quartzitic conglomerate", is actually the basal bed of the overlying Pennsylvanian Sandia Formation (discussed below). Below this quartizitic conglomerate is an angular unconformity separating Mississippian strata from Pennsylvanian strata. The Caloso Formation lies nonconformably upon Proterozoic granitoid.

The Mississippian strata are 4.5 m (14.8 ft) thick. They consist of a basal brownish-white quartzose sandstone and a brown and gray carbonate mudstone. The sandstone is thick-bedded, medium-grained, and shows small-scale, low-angle, wedge- and trough-shaped cross-beds. Overlying this sandstone is a medium-bedded, arenaceous carbonate mudstone. This limestone contains $<5\%$ coarse-grained sand, and a few crinoid columnals and small brachiopods.

Besides the location of the measured section, Mississippian strata crop out in a small area at the east base of Mesa Sarca (Plate 1). They overlie Precambrian granitic gneiss and underlie basal Pennsylvanian sandstones and consist of thin- to medium-bedded, arenaceous and cherty carbonate mudstone. The basal 0.8 m (2.6 ft) of this unit is altered and contains lenses of coarse-grained quartz, feldspars, and small pebbles of quartz and sandstone. The upper 3.7 m (12.1 ft) has a sandy base and contains chert nodules.

## Pennsylvanian Strata

Introduction. Studies of Pennsylvanian strata in central New Mexico have lithologically divided it using either a broad generalized nomenclature or a detailed nomenclature. Broad generalized studies have divided Pennsylvanian strata lithologically into three units; (1) a basal clastic unit, the Sandia

Formation; (2) a middle limestone unit; and (3) an upper arkosic limestone unit. Kelley and Wood (1946) and Siemers (1978) used this style of nomenclature in their studies of the Navajo Gap area (Fig. 3). Myers (1973) produced a slightly more detailed stratigraphy of Pennsylvanian strata using a broad generalized approach (Fig. 3) east of Navajo Gap in the Manzano Mountains.

Thompson (1942) divided the Pennsylvanian strata lithologically using a very detailed approach into Derry (Atokan), Des Moines, Missouri, and Virgil Series with eight groups containing 16 formations and members (Fig. 3). Thompson's (1942) work was in the Mud Springs Mountains, Sierra County, and Oscura Mountains, Socorro County, New Mexico. Rejas (1965) modified Thompson's Pennsylvanian nomenclature in his field study of the Cerros de Amado area, Socorro County, New Mexico. Maulsby (1981) and Bauch (1982) used this nomenclature in their studies of the Rancho de Lopez area and Lomas de las Cañas quadrangle, respectively, both in Socorro County, New Mexico.

Thompson's (1942) Pennsylvanian modified (Rejas, 1965) nomenclature can be applied to the Navajo Gap area. In the study area, lithologies of each formation are recognizable across the entire area even though some units or beds change dramatically in thickness and lithology over distances of less than one to several kilometers. However, an important consideration is that the lithologic formation boundaries in the Navajo Gap area are probably not coeval with those of Thompson's (1942). This is due to the distance from Thompson's type sections and lateral variation in Pennsylvanian facies.

In central New Mexico, some Pennsylvanian lithologic formations are correlatable between the Navajo Gap area and Manzano Mountains (see Myers, 1973), Lomas de las Cañas quadrangle (see Bauch, 1982), Cerros de Amado area (see Rejas, 1965), and Mud Springs and Oscura Mountains (see Thompson, 1942). The most readily recognizable units are: (a) the Sandia Formation (Rejas, 1965;

Bauch, 1982; this study); (b) basal beds of the Whiskey Canyon Formation (Thompson, 1942; Rejas, 1965; Bauch, 1982; this study); (c) Amado Limestone (Rejas, 1965; Bauch, 1982; this study), or the upper, massive limestone beds of the Bolander Group (Thompson, 1942), or the cliff-forming limestone at the top of the Los Moyos Limestone (Myers, 1973); (d) Council Spring Limestone (Thompson, 1942; Rejas, 1965; Bauch, 1982; this study); (e) calcareous arkoses and carbonate conglomerates of the Del Cuerto Formation (Thompson, 1942; Rejas, 1965; this study) or Pine Shadow Member of the Wild Cow Formation (Myers, 1973); and (f) Bursum Formation (Rejas, 1965; Myers, 1973; Bauch, 1982; this study).

Sandia Formation. Basal Pennsylvanian strata in Navajo Gap are of the Sandia Formation. Kelley and Wood (1946) mapped the Sandia Formation in this area with a lower limestone member and an upper clastic member. Siemers (1978) recognized only the upper clastic member in his description of the Sandia Formation.

Like Siemers, I only recognize the upper clastic member. The measured thickness is 78.5 m (257.5 ft) compared to 123.0 m (403.5 ft) measured by Siemers' (1978). Because these sections were measured at the same location, the great difference in thickness may be due to placement of the Sandia Formation's upper boundary.

Sandia Formation consists of brown, orangish-brown, and brownish-purple, fine- to coarse-grained sandstone and conglomeratic sandstone, gray carbonate mudstone, and covered intervals of shale, limestone, and/or sandstone. Basal Sandia Formation is a thick bed of brown quartzose sandstone with lenses of rounded quartz-pebble conglomerate. This bed overlies the Caloso Formation with an angular unconformity and Proterozoic granite with a nonconformity. At the foot of Mesa Sarca, this bed is a conglomerate containing chert cobbles and small boulders, and quartz pebbles. Overlying the basal sandstone and

conglomerate are thin to very thick beds of brown and white quartzose sandstone. Three of these beds contain a few well-rounded sandstone pebbles. A very thick and prominent brownish-purple sandstone bed exhibits large-scale, wedge-shaped cross-beds in its lower half and planar-parallel bedding in its upper half.

Above this prominent sandstone bed are medium beds of sandstone underlying a medium bed of gray, fossiliferous carbonate mudstone. Small solitary rugose corals and brachiopods are visible on weathered surfaces of the limestone. Most of the remainder of the Sandia Formation is covered by colluvium accept for small outcrops of grayish black shale and two successions of sandstone beds.

Two exposures of medium- to thick-bedded, brown sandstone crop out near the middle of the Sandia Formation and at its upper boundary. Both outcrops contain subrounded to subangular, fine- to coarse-grained quartz and minor feldspar sand, and exhibit large-scale, trough- and wedge-shaped cross-bedding.

Elephant Butte Formation. The Elephant Butte Formation overlies the Sandia Formation. Thompson (1942) proposed this name for 25.0 m (82 ft) of thick-bedded fossiliferous limestone, and calcareous silty and micaceous shales with one conglomeratic sandstone 6.7 m (22 ft) above the base. Bauch (1982) described 53.8 m (176 ft) of Elephant Butte Formation as medium- to thick-bedded carbonate mudstone and wackestone with one coarse-grained quartz arenite 33.0 m (108 ft) above the base.

I measured 83.5 m (273.9 ft) of Elephant Butte Formation. The contact between Elephant Butte and the underlying Sandia Formation is covered and assumed to be gradational. I placed the lower boundary of Elephant Butte Formation at the bottom of a short covered slope below the first occurrence of carbonate wackestone and packstone.

In the study area, Elephant Butte Formation generally consists of thin- to mostly thick-bedded, gray, brownish-gray, and brown carbonate mudstones,

wackestones, and packstones, and gray, brown, and black coarse-grained quartzose sandstones. The Elephant Butte Formation is more clastic in the Navajo Gap area than at the type section in northern Mud Springs Mountains, southern Socorro County (Thompson, 1942), and in the Lomas de las Cañas quadrangle, eastern Socorro County (Bauch, 1982).

A unit of medium- to thick-bedded, fine- to very coarse-grained quartzose and feldspathic sandstone with planar-parallel bedding and low-angle, wedge-shaped cross-beds crops out 13.5 m (44.3 ft) above the base of Elephant Butte Formation. Thin, coarse-grained sandstone layers occur within a limestone unit 52.0 m (170.6 ft) above the base. At the top of the formation are medium to very thick beds of coarse-grained sandstone with large-scale, trough- and wedge-shaped cross-beds. This upper sandstone bed does not appear in previous descriptions of the formation and sandstones have not been described in the overlying Whiskey Canyon Formation. Therefore, I include it in the Elephant Butte Formation.

Limestone is gray and brownish-gray, thin- to very thick-bedded wackestone. Wavy shale interbeds occur in the lower half of the formation. Fauna include Chaetetes, solitary rugose corals, branching corals, brachiopods, fusulinids, crinoid columnals, and branching bryozoans.

Chaetetes changes its growth characteristics upwards within the formation. In lower beds, it is not present. In middle beds, colonies are up to 8 cm high and 20 cm wide, form a half-circular shape, and lie on wavy surfaces. In upper beds the colonies become elongate and thin (~1 cm), and define wavy surfaces.

Whiskey Canyon Limestone. The Whiskey Canyon Formation conformably overlies the Elephant Butte Formation. Thompson (1942) proposed this name for 50.0 m (163 ft) of massive and cherty limestone. Bauch (1982) described 41.5 m (136 ft) of Whiskey Canyon Formation as medium-bedded, cherty carbonate mudstones and wackestones.

In Navajo Gap, I measured 57.3 m (188.0 ft) of Whiskey Canyon Formation. Its base was placed at the bottom of the lowest limestone succession that contains an abundance of bedded chert.

Whiskey Canyon Formation consists of very thin to thick beds of gray and brown, cherty carbonate mudstones, wackestones, and packstone, and covered intervals of shale or very thinly-bedded limestone and shale. Wackestone is the most common type of carbonate. Fauna include solitary rugose corals, brachiopods, branching corals, branching bryozoans, and fusulinids.

Garcia Formation. The Garcia Formation conformably overlies the Whiskey Canyon Formation. Thompson (1942) proposed this name for 65.0 m (213 ft) of essentially pure and highly fossiliferous limestones, argillaceous to slightly arenaceous and cherty limestones, several thin shales and a 15.2 m (50 ft) thick bed of conglomeratic sandstone at its base. Bauch (1982) described 91.4 m (300 ft) of Garcia Formation as largely thin- to medium-bedded carbonate mudstones, wackestones and a few packstones, a couple units of coarse-grained subarkose and pebbly quartzarenite, and some presumed shales. Rejas (1965) divided the Garcia Formation into two members, a lower clastic member and an upper limestone. The lower clastic unit (38.5 m; 126 ft thick) consists of calcareous shales, sandstone, and minor limestone. The upper limestone unit (23.0 m; 75 ft thick) consists of limestone and thin calcareous shales.

In Navajo Gap I measured 36.8 m (120.7 ft) of Garcia Formation. Its lower boundary was placed at a change from thick-bedded cherty limestones to thin- to thick-bedded, cherty and non-cherty limestones with wavy shale interbeds and an increase in faunal diversity.

The Garcia Formation consists of gray, brownish-gray , and brown cherty and non-cherty carbonate wackestones and packstones. The lower half consists of thin to very thick beds with and without nodular chert, wavy shale interbeds, and

short covered intervals. Above a middle covered interval, the upper half consists of thick to very thick beds with and without nodular chert. Although no sandstone beds are present, these two successions may be laterally related to the lower clastic and upper limestone units proposed in the Garcia Formation by Rejas (1965). Fauna include rugose corals, fusulinids, crinoid columnals, branching and fenestrate bryozoans, brachiopods, and branching corals.

Bartolo Formation. The Bartolo Formation conformably overlies the Garcia Formation. Rejas (1965) proposed this name for a lower formation in his Socorro Group (Bolander Group of Thompson, 1942). Rejas described 67.0 m (220 ft) of calcareous shale, sandstones, and carbonate mudstone overlying the Garcia Formation. Bauch (1982) described the Bartolo Formation as 75 m (246 ft) consisting of "greenish gray shales and siltstones interbedded with fossiliferous sandstones" and one bed of carbonate grainstone.

In the Navajo Gap area, the Bartolo Formation was measured at 34.9 m (114.5 ft) thick. Its lower boundary is presumed conformable and was placed at the base of a covered interval with scattered outcrops of shale.

The Bartolo Formation consists of gray and brown, non-cherty and cherty carbonate wackestones and packstones, covered slopes (presumed to be shales), calcareous shales, and thin-bedded limestones. Limestones are thin- to very thick-bedded. In the middle of the formation, limestone beds have wavy laminae and shale interbeds. The upper beds contain discontinuously bedded and nodular chert. Fauna include solitary rugose corals, branching corals, crinoid columnals, fusulinids, and brachiopods.

Amado Limestone. The Amado Limestone conformably overlies the Bartolo Formation. Rejas (1965) proposed this name for the upper formation in the Socorro Group. Rejas described the Amado Limestone as 10.7 m (35 ft) of

cherty limestone. Bauch (1982) described it as 18.3 m (60 ft) of carbonate wackestone.

This limestone is the prominent cliff, 11.5 m (37.7 ft) thick, at the top of the southern portion of Saiz ridge (northwest-extending cuesta of the Ladron Mountains). The massive character of the limestone separates it from the overlying and underlying formations.

Amado Limestone consists of thin beds grading upwards to very thick and massive beds of carbonate grainstone. Basal thin beds have wavy surfaces. Fauna include microfossils and crinoid columnals.

Coane Formation. The Coane Formation conformably overlies the Amado Limestone. The Coane Formation was named by Thompson (1942) for 30.5 m (100 ft) of cherty limestone, shales and sandstones. Rejas (1965) and Bauch (1982) described the Coane Formation as undifferentiated with the overlying Adobe Formation, they found no distinct lithologic boundary.

In Navajo Gap, the Coane Formation was measured at 25.5 m (83.7 ft) thick. Its lower boundary was placed at the top of the massive beds of Amado Limestone.

The Coane Formation consists of thin to very thick beds of brown to gray carbonate wackestone and packstone and a central interval of argillaceous limestone. Fauna include fusulinids, solitary rugose corals, crinoid columnals, branching bryozoans, brachiopods, phylloid algae, and gastropods.

At the base of this formation is a meter-thick series of thin- to medium-bedded solitary rugose coral packstone. The corals are disposed from an upright growth position to a flat lying position and are packed in a matrix of argillaceous carbonate mudstone. Flat lying disposition suggests that these beds are death assemblages of solitary rugose corals. At the top of this formation is a thick-bedded series of limestones which contain very large solitary rugose corals. The

largest one measured was 10 cm in diameter and 20 cm in length. Some specimens are found in a disposed flat lying position and others are found in an upright growth position. Both these accumulations of rugose coral are laterally continuous south of the graded road passing through Navajo Gap. On Mesa Sarca these rugose corals are not recognized.

Adobe Formation. The Adobe Formation conformably overlies the Coane Formation. Adobe Formation was named by Thompson (1942) for 61.0 m (200 ft) of non-cherty to cherty limestone, calcareous shale and arkosic sandstone.

In Navajo Gap, the Adobe Formation was measured at 27.9 m (91.5 ft) thick. The base was placed at the bottom of thin to medium beds of silty limestones cropping out above the very large rugose coral unit.

The Adobe Formation consists of non-cherty and cherty, brown to gray carbonate mudstone, wackestone and packstone, and reddish-brown and gray calcareous shale and calcareous siltstone. Limestones are mostly mudstone, very thin- to thick-bedded, and contain small amounts of bedded and nodular chert. A diverse fauna includes small brachiopods, crinoid columnals, branching bryozoans, fusulinids, solitary rugose corals, Chaetetes, and Syringopora.

Calcareous shales and siltstones occur mostly in the middle and upper intervals of the formation. Siltstones show wavy laminae.

Council Spring Limestone. The Council Spring Limestone conformably overlies the Adobe Formation. Thompson (1942) proposed this name for 5.5 m (18 ft) of massive light gray to white limestone. Bauch (1982) described Council Spring limestone as 10.4 m (34 ft) of carbonate mudstone and packstone. Rejas (1965) described it as 6.1 m (20 ft) of thin to irregular-bedded, gray biomicrosparite, micrite and dismicrite.

In Navajo Gap, I measured 14.9 m (48.9 ft) of Council Spring Limestone. The

base was placed at the bottom of a very thick-bedded algal wackestone overlying a calcareous shale of the Adobe Formation.

Council Spring Limestone consists of thin to very thick beds of gray and whitish-gray wackestone. Wavy laminae appear in the very thick basal bed. The lower half is a very thick-bedded, prominent ridge. Fauna include phylloid algae (by itself in the lower half), crinoid columnals, and fusulinids.

Burrego Formation. The Burrego Formation conformably overlies the Council Spring Limestone. Thompson (1942) proposed this name for 15.8 m (52 ft) of massive-bedded and nodular limestones, thick sandstones, and thick shales. Bauch (1965) described the Burrego Formation as 60 m (197 ft) of subarkoses, siltstones and claystones.

In Navajo Gap, I measured 52.0 m (170.6 ft) of Burrego Formation. The base was placed at the bottom of a cherty carbonate wackestone showing wavy laminae.

The Burrego Formation consists of calcareous shales, thin- to thick-bedded and nodular carbonate mudstones, wackestones and packstones, and a thick covered interval. Gray calcareous shales occur in thick units and are interbedded with nodular and bedded carbonate mudstone. One silty limestone changes to a calcareous sandstone and back to a silty limestone laterally over a distance of approximately 1.0 km. Two very thick, lenticular (channel)-shaped, coarse-grained arkosic sandstones crop out north of Coyote Draw in NE/16 section 4, T3N. R3W., and SE/16 section 33, T4N. R3W..

Limestones are dark gray, gray and brown, thin- to thick-bedded and mostly carbonate mudstone. Fauna include brachiopods, branching bryozoans, crinoid columnals, phylloid algae, and gastropods.

Story Formation. The Story Formation conformably overlies the Burrego Formation. Thompson (1942) proposed the name Story Formation for 17.8 m (58.5 ft) of basal, reddish-brown and gray shales, sandstone and upper, massive-bedded, fossiliferous limestone. Rejas (1965) described the Story Formation as a lower clastic member and an upper limestone member 7.0 m (23 ft) and 4.9 m (16 ft) thick, respectively. The lower clastic member consists of gray arkose and grayish-red calcareous shale, and the upper limestone member consists of gray, thin- to medium-bedded, crinoidal wackestone and carbonate mudstone.

In Navajo Gap, I measured 70.6 m (231.6 ft) of Story Formation. The lower clastic and upper carbonate members are recognizable. The base of the formation was placed at the bottom of a mixed limestone and calcareous shale unit.

The lower clastic member (43.6 m; 143.0 ft thick) consists of medium beds and one very thick (19.5 m; 64.0 ft) bed, of reddish-brown and gray calcareous shales interbedded with thin- to thick-bedded, brown and gray carbonate wackestones and mudstones. Reddish-brown shales show planar-parallel bedding, and small-scale, trough-shaped cross-bedding. Fauna include brachiopods, phylloid algae, crinoid columnals, and gastropods. At the top of the very thick unit of gray calcareous shale is a fossiliferous zone containing an abundance of large brachiopods, including Composita and species of productids, strophomenids, spirifers and unidentified species.

The upper limestone member (27.0 m; 88.6 ft) consists of thin- to very thick-bedded, gray and brown carbonate packstone, wackestone and mudstone. Fauna include fusulinids, brachiopods, phylloid algae, crinoid columnals, and gastropods. One bed of distinctive fusulinid packstone, about 23.0 m (75.5 ft) below the top of the formation (fusulinids up to 1.5 $\times$ 5 mm in size), is laterally continuous across all of Navajo Gap.

Del Cuerto Formation. The Del Cuerto Formation conformably overlies the Story Formation. Thompson (1942) proposed this name for 24.7 m (81 ft) of irregular-bedded and nodular limestone, arkosic sandstone, limestone conglomerate, and gray and red shale. Rejas (1965) described three members of the Del Cuerto Formation totalling 17.4 m (57 ft) thick. Rejas' lower member consists of calcareous arkose and calcareous shale. The middle member consists of slightly crinoidal biosparite, and the upper member consists of sandy micrite and arkose.

In Navajo Gap, I measured 31.8 m (104.3 ft) of Del Cuerto Formation. The base was placed at the bottom of a calcareous arkose. Rejas' (1965) three members were not recognized.

The Del Cuerto Formation consists of light to medium gray and brown carbonate packstones, wackestones and mudstones, plus two carbonate conglomerates, a calcareous shale and a calcareous arkose. The basal calcareous arkose is medium-bedded, gray, fossiliferous, and medium-grained. Clastic grains include quartz, lithics, and feldspars. Biota include crinoid columnals, branching bryozoans and brachiopods. Carbonate-pebble conglomerates occur at 10.9 m (36 ft) and 19 m (62 ft) above the base of the formation.

Limestones are thin- to thick-bedded, mostly wackestones and packstones, locally arenaceous, and argillaceous in the upper unit. Fauna include crinoid columnals, phylloid algae, fusulinids, brachiopods, branching and fenestrate bryozoans, and gastropods. A distinct packstone containing the longest fusulinid found in Paleozoic strata of Navajo Gap (fusulinids up to $2 \times 8$ mm in size) occurs 4.2 m (13.8 ft) above the base of the formation. This bed is laterally continuous across the study area.

Moya Formation. The Moya Formation overlies the Del Cuerto Formation. Thompson (1942) proposed this name for 15.5 m (51 ft) of massive-

and irregular-bedded and nodular limestones, and interbedded sandstones and shales. Bauch (1982) described the Moya Formation as 42.8 m (140.4 ft) of carbonate mudstones with a basal cherty packstone.

In the Navajo Gap area, the Moya Formation has a thickness of 48.2 m (158 ft). The lower boundary is presumed to be conformable and was placed at the base of a covered slope showing scattered outcrops of gray shale.

The Moya Formation consists of light to medium shades of gray and brown, non-cherty and cherty carbonate grainstones, packstones, wackestones, and mudstones plus gray shales. One very thick covered slope contains scattered outcrops of shale. Another very thick covered slope contains scattered outcrops of shale and very thin to thin beds of limestone. These covered slopes are presumed to be mostly shale.

Limestones are very thin- to very thick-bedded and occasionally contain nodular or bedded chert and wavy shale interbeds. Fauna include crinoid columnals, phylloid algae, brachiopods, fusulinids, branching and fenestrate bryozoans, solitary rugose corals, and rare Syringopora.

At the top of the Moya Formation is very thick bedded crinoidal grainstone grading upwards into medium bedded phylloid algal packstone. The grainstone thickness ranges from <1 to 6 m laterally over a distance of about 70 m.

## Permian Strata

Bursum Formation. Bursum Formation and Red Tanks Member of the Madera Limestone are two names for the succession of strata that overlie Pennsylvanian limestones of the Moya Formation and underlie Permian sandstones of the Abo Formation. The strata represent an interfingering transitional relationship between underlying marine and overlying continental sediments. Kelley and Wood (1946) named this unit Red Tanks Member of the

Madera Limestone, at a type location northwest of the Ladron Mountains at Red Tanks Arroyo (Coyote Draw). They described 71.0-91.4 m (200-300 ft) of limestone, conglomeratic sandstone, shale and siltstone overlying the Atrasado Member of the Madera Limestone and underlying the Abo Formation. North of Navajo Gap at Mesa Lucero, Kues and Kietzke (1976) described approximately 137.2 m (~450 ft) of Red Tanks Member of the Madera Formation consisting of red, green, black and gray claystone with less siltstone, sandstone, limestone, and limestone-pebble conglomerate.

Wilpolt and others (1946) named the Bursum Formation for 8.5-71.3 m (28-234 ft) of shale, arkose, arkosic conglomerate, and limestone in approximately the same stratigraphic position as the Red Tanks Member of the Madera Limestone of Kelley and Wood (1946). Following Wilpolt and others (1946), Rejas (1965) described 71.0 m (200 ft) of Bursum Formation consisting of arkose, arkosic conglomerate, calcareous shale, calcareous mudstone, and limestone.

I measured and described these strata in the same area as Kelley and Wood's (1946) type locality for the Red Tanks Member of the Madera Limestone. This type locality is strongly faulted. Due to the greater similarity of my section (see following) to that described by Wilpolt and others (1946) for the Bursum Formation, more common usage of the name Bursum Formation, and the poor quality of Kelley and Wood's (1946) type locality, I recommend dropping use of the name Red Tanks Member of the Madera Limestone.

I measured 31 to 41 m (102 to 134.5 ft) of Bursum Formation. An absolute thickness is unknown due to faulting and lateral changes in bed thickness. The base of the formation is at the bottom of the first brownish-red shale overlying the limestone beds of Moya Formation.

Bursum Formation consists of reddish-brown, brownish-red, gray, and lavender shales and calcareous shales, mottled gray and brown carbonate

mudstones, wackestones, and packstones, carbonate-pebble conglomerates, and arkoses. A blackish-brown, medium-bedded (30 cm), fine- to medium-grained micaceous arkose occurs 11.4 m (37.4 ft) above the base. Locally, this bed swells to more than 2 m thick and beds below it disappear. A gray and brown, medium-bedded, coarse-grained calcareous arkose occurs approximately 18.6 m (61.0 ft) above the base of the formation, a couple of meters below a thick sequence of carbonate conglomerates.

Above the middle of the formation a 3.6 m (11.8 ft) thick sequence of gray and brown, medium-bedded conglomerate consisting of well-rounded, siltstone- and carbonate-pebbles with a medium-grained calcareous sand matrix occurs. Locally, this conglomerate pinches to less than 50 cm thick.

Most limestones occur at the bottom and top of the formation with one bed in the middle. At the base, these limestones are abundantly fossiliferous, nodular and medium-bedded packstone and wackestone. Fauna include crinoid columnals, brachiopods, fenestrate and branching bryozoans, and fusulinids. The middle limestone is packstone with a wackestone top. Fauna are distinctive coated microfossils and skeletal fragments. The upper limestone beds are purplish-gray, gray, and brown, nodular and thin- to medium-bedded, mudstones and wackestones. Fauna include gastropods and brachiopods.

Between the limestone, conglomerate, and arkose beds are thin to very thick intervals of shale and calcareous shale. Shales at the middle and base of Bursum Formation are mostly brownish-red. Those in the upper part are gray, purple, and lavender.

There is some disagreement over the age of the Bursum Formation. The problem is in part a difficulty in establishing the horizon between Moya and Bursum Formations. The Bursum Formation has been described as upper Pennsylvanian (Kelley and Wood, 1946; Wilpolt and Wanek, 1951), lower

Permian (Wilpolt and others, 1946; Rejas, 1965; Maulsby, 1981; Bauch, 1982), and overlapping Pennsylvanian and Permian (Kues and Kietzke, 1976). A detailed paleontologic study by Kues and Kietzke (1976) indicates that the Red Tanks Member (Bursum Formation) overlaps the Pennsylvanian-Permian boundary. Rejas (1965) described a fusulinid association of Schwagerina with a very obese Triticites in the Bursum Formation. In Navajo Gap, an obese species of fusulinid (up to 3 × 7.5 mm in size) occurs at the base of the Bursum Formation.

Abo Formation. The name Abo Sandstone was proposed by Lee (1909) for 198.1 m (650 ft) of dark-red and purple, coarse-grained sandstone and shale in Abo Canyon, Torrance County, New Mexico. Regional and local studies and observations redefined the Abo Formation (Needham and Bates, 1943) as variably thick (91.4-248.4 m, 300-815 ft; Anonymous I, 1963) red shales and sandstones, with less arkoses and conglomerates.

In Navajo Gap, the incomplete Abo Formation is approximately 150-160 m (492-525 ft) thick with its upper contact faulted out. Its lower contact is gradational and placed at the top of the uppermost limestone in the underlying Bursum Formation. The lower Abo Formation is considered Wolfcampian age in Joyita Hills, Socorro County, New Mexico (Kottlowski and Stewart, 1970) and the upper is considered Leonardin age in Sacramento Mountains, Otero County, New Mexico (Wilpolt and Wanek, 1951).

The Abo Formation consists predominantly of brownish-red shales with lesser very fine-grained sandstones and minor siltstones and conglomerates. The lower 80 m (~262.5 ft) consists almost entirely of shale and calcareous shale. Interbedded in the shale are a few very thin- to medium-bedded, very fine-grained sandstones and one medium-bedded, medium- to very coarse-grained sandstone containing less than 5% sandstone and limestone pebbles.

The upper 80-90 m (~262.5-295.3 ft) consists of thick successions of brownish-red shale interbedded with thick successions of brownish-red, very fine-grained sandstones and two medium-bedded, gray, carbonate-pebble conglomerates. Sandstones locally show abundant reduction spots, climbing-ripple and small-scale, trough-shaped cross-bedding, and discontinuous wavy-parallel bedding. Bedding surfaces often reveal ripple marks, mud cracks, burrows, and fern-like leaf and stem impressions.

Yeso Formation. The name Yeso Formation was proposed by Lee (1909) for a succession of sandstones, shales, limestones, and gypsum exposed on Mesa del Yeso, Socorro County, New Mexico. Needham and Bates (1943) recognized and described four members in the Yeso Formation. Incomplete sections of the lower two members crop out in Navajo Gap around the old Saladito homestead (NW/16, Section 3, T3N. R3W.) in Coyote Draw. The Yeso Formation was previously mapped as undifferentiated in Navajo Gap (Kelley and Wood, 1946).

*Meseta Blanca Member.* Wood and Northrop (1946) named the lowest member of the Yeso Formation the Meseta Blanca Sandstone. Near Cañon, Sandoval County, New Mexico, they described this member as light orange and red, cross-bedded sandstone that weathers to a rounded form. Rejas (1965) described an estimated 97.5 m (320 ft) of the Meseta Blanca Member of the Yeso Formation consisting of sandstones and siltstones with mudstone and shale. He also indicated that nodular limestones occur near the top of the member and salt casts, found in siltstone beds, occur in the lower beds. Bauch (1982) noted the lower Meseta Blanca Member consists of interbedded sandstone and limestone.

Exposure of Meseta Blanca Member of the Yeso Formation in Navajo Gap is incomplete due to faulting. I measured 100.6 m (330 ft) of very fine-grained sandstone. Sandstones are medium- to mostly thick-bedded, indurated to well-

indurated, reddish-brown, very fine-grained, and have planar-parallel bedding and small-scale, trough-shaped cross-bedding. Reduction spots are common in the upper beds. One medium-bedded, carbonate-sandstone pebble conglomerate with a very fine- to medium-grained sand matrix crops out approximately 28 m (92 ft) above the base of the measured section. Exposures do not reveal interbeds of other lithologies. Although described as weathering to a rounded shape by Wood and Northrop (1946) and Rejas (1965), these sandstones have a moderately angular weathering characteristic.

*Torres Member.* The Torres Member of the Yeso Formation conformably overlies the Meseta Blanca Member. Torres Member was named by Wilpolt and others (1946) at a type locality 11.3 km (7 mi) south of Black Butte, Socorro County, New Mexico. They described 182.9 m (600 ft) consisting of alternating beds of orange-red sandstone, siltstone, gray limestone, and gypsum. Rejas (1965) and Bauch (1982) both described similar characteristics for the Torres Member, although their sections are faulted and not as thick. Bauch (1982) described the sandstones as yellow, yellow-orange and red, friable, and very fine-grained.

Exposure of Torres Member of the Yeso Formation in Navajo Gap is incomplete due to faulting. Not all of this is measurable and much of it is highly brecciated. I measured 75.5 m (247.7 ft) of sandstone and alternating sandstone and limestone. Both the basal and upper contacts are faulted out. The lower 42.0 m (137.8 ft) of the section consist of banded yellowish-brown, reddish-brown, buff, and pinkish-white, thin to thick beds of friable, fine-grained sandstone. Sandstones occasionally show small- to medium-scale, low-angle, trough-shaped cross beds and wavy parallel bedding. The upper 33.5 m (109.9 ft) of the section consist of alternating sandstone and limestone or shaley limestone. Upper sandstones are poorly exposed and presumed the same as in the lower 42.0 m. Limestones are thin- to medium-bedded carbonate mudstones with wavy bedding

surfaces.

*Yeso Undifferentiated.* Small outcrops of the Yeso Formation are exposed northwest and southeast of the old Saladito homestead and Coyote Draw (Plate 1). Very poor exposures, limited thicknesses, and structural deformation render these outcrops undifferentiable.

## CRETACEOUS ROCK

A small exposure of quartzite-chert-pebble conglomerate crops out on, or within folded and faulted strata of the Permian Yeso Formation in SE/4 section 33, T4N. R3W.. The conglomerate consists of very well-rounded, clast- and matrix-supported pebbles of black, light gray, and reddish-brown chert and pinkish-gray, dark-gray, and brown quartzite. The matrix is brownish-yellow, subrounded to subangular, medium-grained, siliceous, quartz sandstone. Alignment of elongate pebbles indicates that bedding is moderately tilted eastward. The contact with the underlying Yeso Formation is not exposed and presumed faulted.

In the surrounding region, conglomerates occur in Eocene, Cretaceous, upper Paleozoic, and Proterozoic rocks. Source of the quartzite pebbles could be quartzites in local Proterozoic rocks (P.W. Bauer, personal communication 1986). But chert pebbles are not a constituent in Proterozoic conglomerates (P.W. Bauer, personal communication 1986).

In local Paleozoic strata, conglomerates occur within basal and upper Pennsylvanian and Permian beds. Basal Pennsylvanian conglomerates contain chert, quartz, and feldspar clasts and have a coarse-grained arkose matrix. Upper Pennsylvanian and lower Permian conglomerates contain carbonate clasts.

The quartz sand matrix of the quartzite-chert-pebble conglomerate resembles late Cretaceous sandstone (O.P. Anderson, personal communication 1986). Osburn (1984) mapped the Dakota Sandstone west of Navajo Gap in the Pueblo Viejo Mesa quadrangle, Socorro and Cibola Counties. Osburn (1984) described a basal conglomerate containing well-rounded quartzite and chert pebbles. In the local area around Navajo Gap, Cretaceous strata have been eroded or are not exposed. Rift-related faulting (to be discussed in a later section) could have

placed these strata in their present location.

Eocene structural deformation resulted in deposition of the Baca Formation and abundant conglomeratic sediments in the Socorro area (Cather and Johnson, 1984). During Eocene time, the Navajo Gap area was subjected to severe structural deformation (to be discussed in a later section). Any conglomerates deposited in the area would probably consist predominantly of carbonates, chert, and sandstones.

Through a process of elimination, the most likely age for this quartzite-chert-pebble conglomerate is late Cretaceous. It is most likely a conglomerate lense in the base of the Dakota Sandstone. This outcrop of basal Dakota Sandstone has not been previously recorded.

# CENOZOIC ROCKS AND SEDIMENTS

## Intrusions

Mafic dikes are exposed throughout Navajo Gap. Sporadic in the southern part along the Ladron fault and other faults, mafic dikes occur in abundance and commonly in swarms in the low hills at the base of Mesa Sarca. Dike thickness ranges from 0.20 m to 2.20 m. Trend of dikes is from NS to N10°E. These dikes approximately follow the same trend as, and are probably related to mafic dike swarms in the Riley area to the southwest. The dikes in the Riley area are considered to be related to the La Jara Peak Basaltic Andesite of late Oligocene-early Miocene age (Chamberlin and others, 1982).

In hand specimen, the dike rocks are medium to dark gray and greenish-gray, aphanitic, porphyritic, and vesicular to massive. Some specimens have phenocrysts of olivine less than 1.0 mm in size, while other specimens have phenocrysts of plagioclase less than 3.0 mm in length. Rarely are both phenocrysts seen in the same sample. Secondary calcite often forms amygdules. Many of these dikes are partially or completely metasomatized to a granular mass of biotite and unrecognized whitish-gray material.

## Santa Fe Group

Introduction. Santa Fe Group deposits include cemented gravels, Riley travertine, and alluvial gravels. The alluvial gravels are a complex intertonguing sequence of poorly to moderately cemented, pediment/alluvial fan and paleostream gravels. Clast compositions in these gravels reflect a minimum of three local sources. Travertine and carbonate cemented gravels occur within and upon these gravels. Travertine and carbonate cemented gravels are separated into

two deposits east and west of the Comanche (Saiz) fault zone. The Riley travertine crops out on the west side of the study area.

Cemented Gravels and Associated Gravels. Well cemented gravels crop out along Coyote Draw east of the Comanche (Saiz) fault (Plate 1). The deposit has a thickness of approximately 2.5 m (8.2 ft; possibly greater) and consists of carbonate-cemented pebbles and cobbles of Pennsylvanian limestone and sandstone, Permian sandstone, basalt, and an igneous intrusion. Clasts are supported by a very poorly sorted matrix of sand and gravel. Moderately defined bedding dips very gently eastward. Unconsolidated paleostream gravel (discussed below) overlies this cemented gravel.

Similarly composed cemented gravel lies beneath the well cemented gravel with an undulatory erosional contact. Bedding dips 16 degrees northeastward and is characterized by alternating sand and gravel.

In hand specimen, the intrusive rock is dark green, white and yellow and porphyritic. Phenocrysts consist of feldspars, biotite, and an amphibole. Biotite and amphibole phenocrysts are less than 4.0 mm in length and feldspars are less than 1.5 mm in length. This intrusive appears to be a diorite, monzonite, or monzodiorite. A possible source for this clast is a monzonitic-cored mafic dike approximately 6 km (~9.5 mi) southwest of Navajo Gap in western section 32, T3N. R3W. (Duschatko and Poldervat, 1955; Chamberlin and others, 1982).

Banded travertine crops out northeast of the old Saladito homestead approximately 0.8 km (1.3 mi) outside of the field area. This travertine is approximately 1 m (~3.3 ft) thick and overlies cemented gravels and underlies pediment/alluvial fan gravels.

Riley Travertine. On the western side of the study area, isolated erosional remnants of banded travertine and travertine cemented gravels occur

(Plate 1). Bachman mapped these deposits as Riley travertine (Barker, 1983). The deposits range from a banded and vuggy travertine to calcareous-cemented gravels. Calcareous-cemented gravels contain rounded to angular pebbles and cobbles of Pennsylvanian limestone, Permian sandstone, Proterozoic granite, and Tertiary monzodiorite. The clasts are supported by a sandy matrix. Thin bands of travertine are interbedded in the cemented gravel. Bedding dips very gently westward. Northernmost exposures thin eastward.

Pediment/Alluvial Fan and Paleostream Gravels. Covering bedrock and other Santa Fe Group deposits is a veneer of gravel (Plate 1). This deposit is approximately 4-5 m (13.1-16.4 ft) thick, possibly greater close to topographic highs. These gravels form three deposits based on clast types: northeastern, northwestern, and southern. On aerial photographs, the northwestern and southern deposits look very much like alluvial fans. Kelley (1977) suggests that the "high cut surface north" of the Ladron Mountains is Pliocene-Pleistocene in age. This "surface" represents part of the southern pediment/alluvial fan deposit in the Navajo Gap area.

In the southern half of the field area, the gravels consist of sand to very large boulders of predominantly Proterozoic granite and metavolcanic rocks, and Pennsylvanian limestone. Chamberlin and others (1982) indicate this deposit to be an alluvial fan of Pleistocene age. The source of this southern deposit is steep-sided canyons in the Ladron Mountains. The sediments were deposited on a gently north- to west-dipping bedrock surface.

In the northern part of the field area, the gravels consist of sand to medium-boulders of predominantly Pennsylvanian limestone and lesser sandstone and Permian sandstone. The source of this northwestern deposit is Mesa Sarca. Here the sediments were deposited on a gently east-dipping bedrock surface.

Northwest of Coyote Draw and the old Saladito homestead, in the area of

east-central to north-central section 33, T4N. R3W., the gravels (northeastern) consist of sand to large-boulders of predominantly Pennsylvanian limestone and sandstone, and Permian sandstone, with lesser quartzite-chert-pebble conglomerate (Dakota Sandstone), basalt, monzodiorite, and ash-flow tuff. The largest boulders are monzodiorite. The ash-flow tuff clasts are Hells Mesa and La Jencia Tuffs and have a source to the southwest in the Bear Mountains (C.E. Chapin, personal communication 1986). This northeastern deposit has both a local and a southwestern source. Deposition was on top of, and possibly contemporaneously with the cemented gravels and associated gravels discussed previously.

The southwest source of the monzodiorite and ash-flow tuff clasts in the northeastern deposit indicates a similarity to Tertiary gravel deposits described about 40 km (25 mi) west (Osburn, 1984) and 61 km (38 mi) northwest (Maxwell, 1976) of Navajo Gap. In these areas, the gravels consist predominantly of Oligocene volcanic rocks and have a northward transport direction (Maxwell, 1976; Osburn, 1984). This northward transport was terminated by the incision of Rio Salado (Osburn, 1984). This similarity in transport direction, along with the lack of Proterozoic clasts in the northeastern deposit, suggest the presence of a northeast-flowing drainage prior to deposition of the southern and northwestern gravels. Therefore, Navajo Gap was the location of a northeast-draining, late Tertiary valley prior to the incision of Rio Salado.

### Terrace Gravels

A terrace deposit of very poorly-sorted, reddish-brown gravel occurs within Coyote Draw in NE/16 section 3, and N/4 section 4, T3N. R3W. This deposit is approximately 3.1 m (10.2 ft) thick "upstream" from the old Saladito homestead (section 3, T3N. R3W). Clasts consist of boulders to pebbles of Pennsylvanian limestone and Permian sandstone. A meter-thick layer of subangular boulders lies

on bedrock and is covered by a sandy matrix-supported, subrounded pebble-cobble gravel. These terrace gravels are calcareous-cemented in the area of the old Saladito homestead downstream from the perennial saline spring Ojo Saladito.

Landslide Debris

Landslide deposits, consisting of jumbled boulders, occur in SW/4 section 29, T4N. R3W., and NE/4 section 26, T3N. R3W. These deposits occur on strata of the Bartolo, Amado, Coane, and Adobe Formations.

Colluvium, Alluvium and Alluvial Channels

Recent deposits of unconsolidated sand and gravel occur as thin cover in valleys, intermittent stream channels, isolated areas on gentle slopes, and thin alluvial fan deposits at the base of steep topography. Alluvial gravels in Coyote Draw, near the old Saladito homestead, have undergone recent and present cementation due to carbonate-saturated waters welling up at Ojo Saladito.

# STRUCTURE

## Regional Structural Setting

The Navajo Gap area straddles southeastern Lucero uplift and northwestern Ladron uplift (Fig. 4). These uplifts lie within the transitional zone separating the Colorado Plateau and Rio Grande rift. The study area overlaps part of a border fault of the Albuquerque basin and includes other less prominent faults related to the Rio Grande rift. These tectonic provinces, as they relate to the Navajo Gap area, are reviewed in the following sections.

Colorado Plateau. The Colorado Plateau is a broad area of relative structural stability within the Cordillera of North America (Kelley and Clinton, 1960). Principle structural elements of the plateau are Laramide and younger in age (Kelley, 1955). Bordering the Colorado Plateau on the east and southeast are the southern Rocky Mountains and the Rio Grande rift, respectively (Kelley, 1955). The Navajo Gap area lies within two tectonic subdivisions of southeastern Colorado Plateau, the Lucero and Ladron uplifts (Fig. 4).

*Lucero Uplift.* Callender and Zilinski (1976) describe the Lucero uplift as "a westward-tilted fault block" about 50 km long and 20 km wide (Fig. 4). During the Laramide orogeny (late Cretaceous to middle Eocene), the Lucero area was uplifted (Chapin and Cather, 1981) and folded (Zilinski, 1976) as the southern segment of a right-lateral wrench zone (Slack and Campbell, 1976). Major structures in the Lucero uplift trend northward and include "an east-facing monocline, an eastward-yielding thrust, and several high-angle normal faults with easterly dips" (Callender and Zilinski, 1976). The eastern margin is complexly folded and faulted and marks the intersection between the Colorado Plateau and the Rio Grande rift (Zilinski, 1976). Along the northern half of the Lucero uplift,

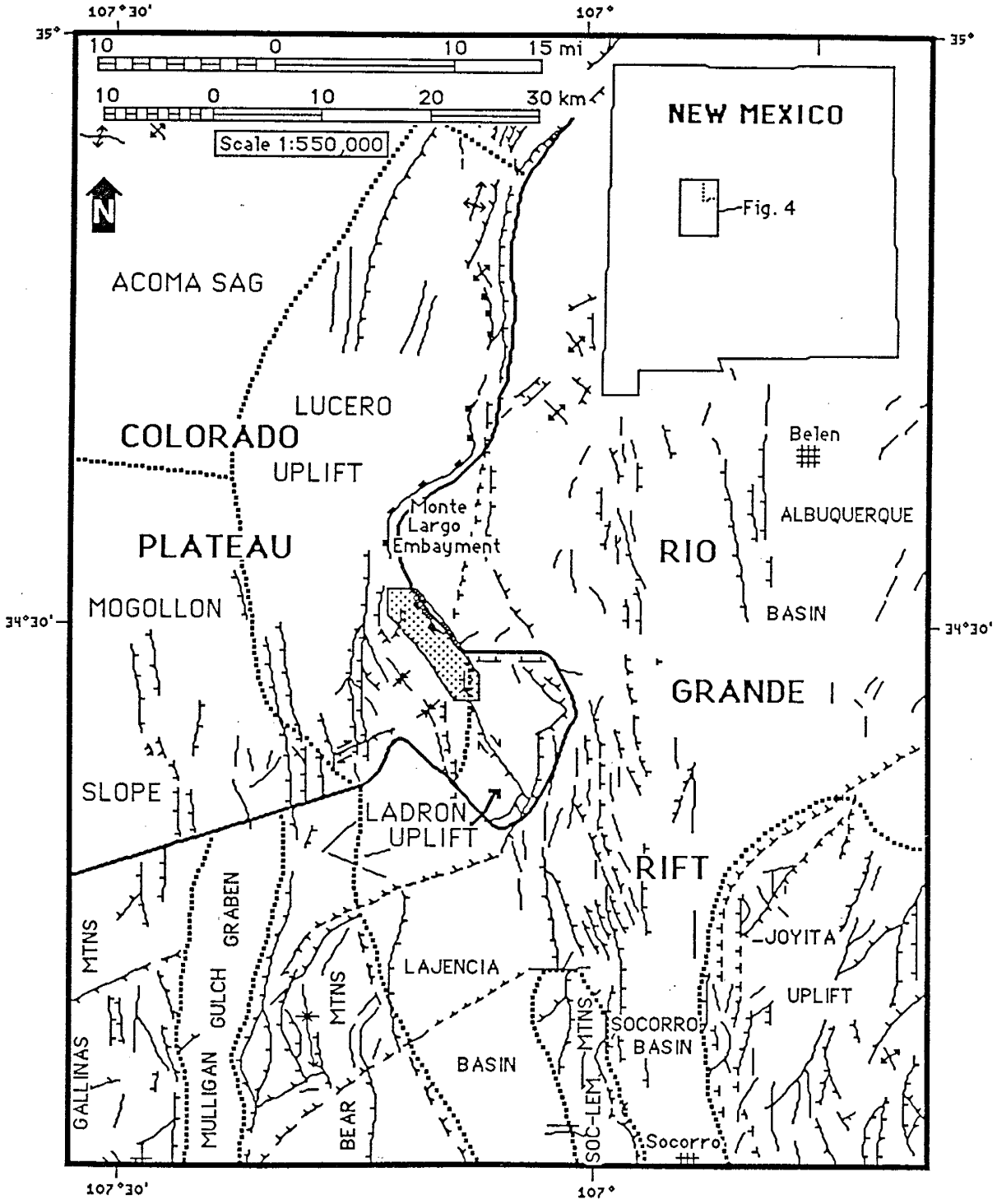


Figure 4. Location of Navajo Gap area (stippled) on tectonic map of central New Mexico (after Woodward and others, 1975). Tectonic provinces are outlined (after Chapin, 1971; Zilinski, 1973). Colorado Plateau boundary: ———; province boundary:·····; normal fault:–·–·–; reverse fault:– – – –; folds: ⌇ ⌇.

this complex zone includes Laramide, east-facing monoclinal folds and east-yielding thrusts (Comanche fault zone) and younger gravity slides (Carrizo fault), followed by high-angle normal faults (Santa Fe fault) (Callender and Zilinski, 1976).

Tracing the Comanche fault zone southward into the Navajo Gap area, Kelley and Wood (1946) interpreted it as an east-yielding thrust. Duschatko (1953) interpreted this structural zone as a steep west-facing monocline cut by the downdropping of the uplifted eastern block into the Rio Grande rift. In this study, I present structural evidence suggesting that this fault zone should not be considered the same as the Comanche fault zone, along the east edge of the Lucero uplift, to the north. The name Comanche was wrongly extended southward to this structural zone in Navajo Gap. Therefore, I informally name it Saiz fault zone after Saiz Ranch on which it crops out. In the study area, the Saiz fault zone includes tight to gentle folds, strike-slip faults, and east and west-yielding thrusts, and younger Tertiary high- and low-angle, east-dipping normal faults (Plate 1 and Fig. 5). Mesa Sarca, a separately uplifted southeastern section of Lucero uplift lies in northwestern Navajo Gap (Fig. 5).

*Ladron Uplift.* The Ladron uplift is a westward-tilted and block-faulted massif of Proterozoic crystalline rocks (Chamberlin and others, 1982). The uplift was part of the northern end of the Laramide, Precambrian-cored Sierra uplift (Chapin and Cathers, 1981, fig. 1). Since early Miocene time, the Ladron Mountains have been episodically uplifted (Denney, 1940; Bruning, 1973) and have formed an intrarift horst. Chamberlin and others (1982) indicate that the uplift has rotated no more than 25 degrees to the west during rift-related extension. They also suggest that the Ladron Mountains "represent a resistant prong of the Colorado Plateau block that juts into the western side of the [Rio Grande] rift".

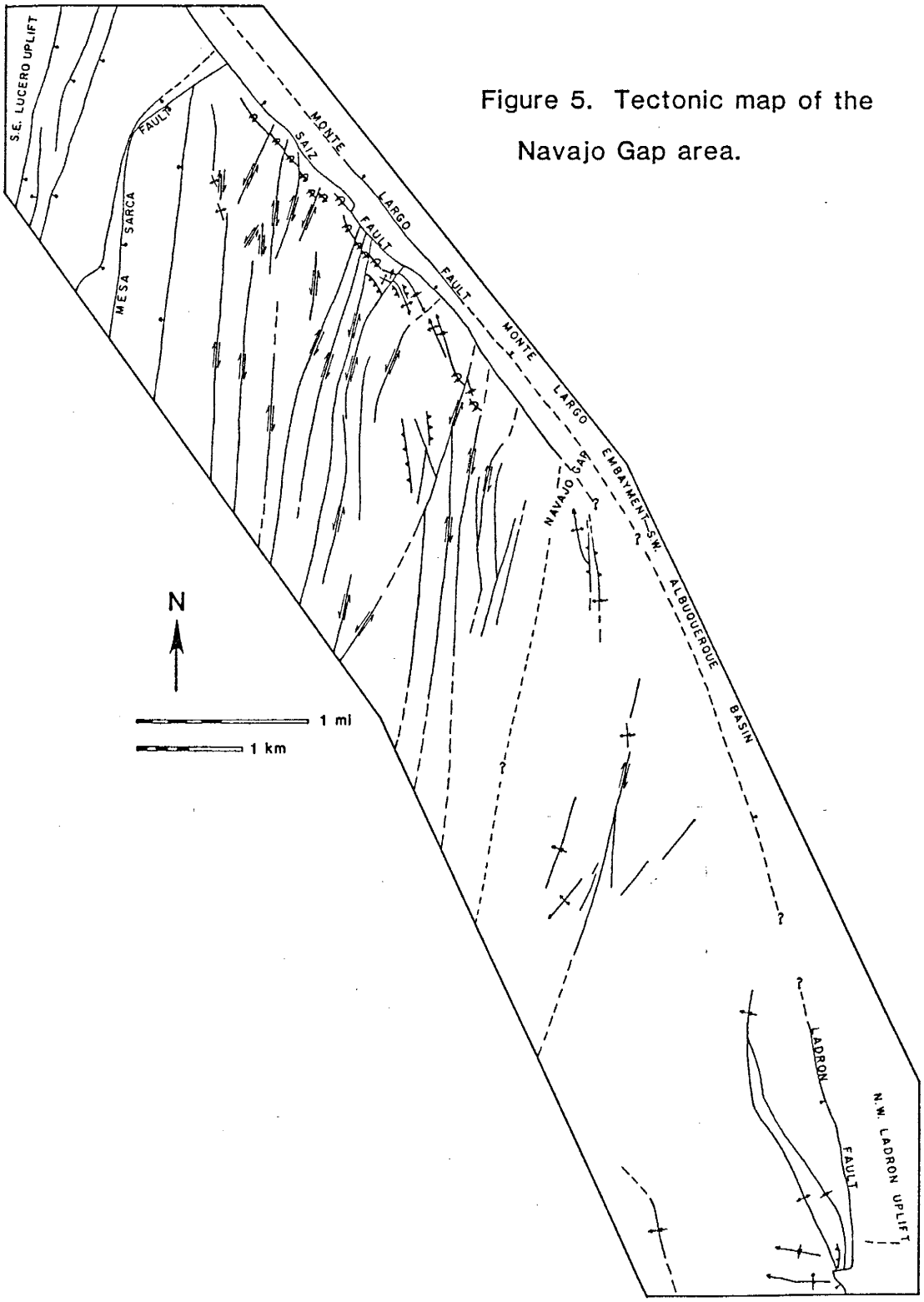


Figure 5. Tectonic map of the Navajo Gap area.

Strata that have been subjected to rift-related extensional faulting are in normal fault contact with the Ladron block along its north, east, and southeast margins. On its western margin, Proterozoic rocks of the Ladron block are nonconformably overlain by upper Paleozoic rocks, and are apparently in normal fault contact, along the Ladron fault, with faulted and folded but non-extended strata. The southern Navajo Gap area extends into the northwestern side of the Ladron uplift and includes the northern quarter of the Ladron fault (Fig. 4 and 5).

Rio Grande Rift. The Rio Grande rift formed as east-west regional tension (Aldrich and others, 1986) eased the Colorado Plateau away from the High Plains. The rift is composed of a series of north-trending en echelon basins, intrarift horsts, and marginal uplifts. These structures extend from central Colorado to southern New Mexico and western Texas, and possibly northernmost Mexico (Chapin, 1971). In the Socorro area, rifting began between 31 and 28 m.y. ago and is continuing today (Chapin and Seager, 1975).

Within the Rio Grande rift, Navajo Gap is in a transitional area between a dominantly axial-basin rift to the north and a broader multiple-basin rift to the south (Chapin, 1971, fig. 2). North of the study area, the Rio Grande rift trends north-northeasterly between the Ladron Mountains and Taos. North of Taos, the rift trends north-northwesterly (Chapin, 1971).

North of the Ladron Mountains, the rift is composed of four en echelon axial basins and marginal uplifts with four eastern subsidiary basins (Chapin, 1971). South of the Ladron Mountains, the rift is more similar to the Basin and Range province (Olsen and others, 1984). The southern part of the Rio Grande rift is composed of at least three north-trending, parallel basins with intrarift horsts and one northeast-trending set of basins along the Plains of San Agustin (Chapin, 1971). The San Agustin arm of the rift lies to the southwest of Ladron

Mountains.

The rift basins formed in an en echelon pattern as they developed between "a series of northeast- and west-northwest-trending.... lineaments in the basement terrane of the southern Rocky Mountains" (Chapin, 1979; Chapin and others, 1978, fig. 1). Basins with opposing asymmetries, hinged on the west side and deeper on the east side, contrary to being hinged on the east side and deeper on the west side, developed on opposite sides of the lineaments (Chapin, 1979). Extensional fault types in the Rio Grande rift include: (a) early-rift low-angle normal faults and high-angle domino-style faults (Seager, 1981; Chamberlin, 1983); and (b) listric normal faults (Brocher, 1981; Cape and others, 1983; De Voogd, 1986). The main rift basins, or grabens have "vertical structural offsets of as much as 6 km" (Olsen and others, 1984).

The southern most of the northern singular-basins, Albuquerque basin, borders the map area (Fig. 4 and 5). Studies concerning the COCORP Seismic reflection profiles across the southern Albuquerque basin reveal complex basinal and basement structures, including an intrarift horst (Brown and others, 1979; Brown and others, 1980; Jurdy and Brocher, 1980; Brocher, 1981; Cape and others, 1983; de Voogd, 1986). Shallow structures within the east side of the southern Albuquerque basin include down-to-west listric faults (Cape and others, 1983; De Voogd, 1986) superimposed over Laramide eastward verging thrust faults (Cape and others, 1983; Pascal Cabezas, personal communication, 1986). Basinal west-side structures of the southern Albuquerque basin are separated from the main basin by a buried northeast-plunging extension of the Ladron uplift (Brown and others, 1979). West-side basinal structures include either high-angle normal (Brown and others, 1979; 1980) or listric faults (Cape and others, 1983). Albuquerque basin and the Plains of San Agustin wrap around the southeastern edge of the Colorado Plateau.

The study area includes a southwestern marginal fault of the Albuquerque basin. Trending northwestward in the Navajo Gap area, this fault is part of the Saiz fault zone (Plate 1 and Fig. 5). East of Saiz fault zone is Monte Largo embayment, the west side of the southern Albuquerque basin. Monte Largo embayment is a northeast-plunging trough within, but partially separated from the main Albuquerque basin by the buried northeast extension of the Ladron uplift. Other extensional faults in the study area occur along the east base of Mesa Sarca.

## Discussion of Major Structures

General Statement. Navajo Gap lies in a zone transitional to the Rio Grande rift and the Colorado Plateau (Fig. 4). Major structures in the area include the Saiz fault zone, Ladron fault, and Monte de Belen (Mesa Sarca) fault (Plate 1 and Fig. 5). Field work has revealed complex structures within these zones and across the study area.

Strata dip moderately to gently westward in the direction of local tilting. Lateral shear zones and faults are very abundant. Fault types include low- to high-angle normal, reverse, thrust, strike-slip, oblique-slip, and bedding-slip. Most are strike-slip faults trending approximately N10 ° E. Many are discontinuous and do not cross the study area. Some strike-slip faults laterally change into fault zones or shear zones.

The east side of Mesa Sarca is cut by normal faults. The topographically low area in the middle of Navajo Gap is shattered by strike-slip faults and a few gentle folds. Normal faulting occurs along the west side of the Ladron Mountains. Stratigraphic displacements range from 600 m or more in the three major fault(s) zones mentioned above, and 20 m or less on the multitude of faults across the area. Most faults have less than 4 m of stratigraphic throw. Some faulting and

brittle shearing is apparent within Proterozoic rocks of the northwest Ladron Mountains. I did not analyze the metamorphic fabric in the foliated Proterozoic rocks.

Folded strata crop out sporadically over the whole area, but are concentrated along the west sides of the Saiz and Ladron faults. Small-scale folds verging northeastward and large-scale folds verging southwestward crop out in abundance along the west side of the Saiz fault zone. Strata are strongly sheared within the Saiz fault zone. West of the Ladron Mountains, east-verging anticlinal and synclinal folds, and west and north-verging monoclinal folds crop out.

Saiz Fault Zone. In northern Navajo Gap, the Saiz fault zone includes two styles of structural deformation. Relative motion was first up to the northeast, with southwest vergence, along an apparent northeast-dipping reverse fault. Following northeast uplift, relative motion was down to northeast as low- to moderate-angle normal faulting. This fault zone is the southwest border of Monte Largo embayment, southwest Albuquerque basin. Saiz ridge is the eroded escarpment of the fault zone. Exposed in the northern Navajo Gap area, the fault zone is buried as it trends northwestward out of the study area. It is also buried to the southeast as it trends towards or joins with the Ladron fault.

About 1 km of the Saiz fault zone is moderately to well exposed in the northern Navajo Gap area at Coyote Draw and the old Saladito homestead (Plate 1). The fault zone ranges from about 100 to 200 meters wide. Occurring from west to east across the Saiz fault zone are: (a) steeply northeast dipping and overturned middle Pennsylvanian limestones, shales, and channel sands; (b) the Saiz fault proper striking N40 ° E and dipping 20-50 ° NE; (c) strongly deformed (gently to tightly folded, strongly faulted and sheared, moderately to steeply northeast-dipping, and steeply southwest-dipping overturned) sandstones and shales of the Permian Yeso Formation; (d) an extensional fault striking

approximately N40 ° E with a presumed steep northeast dip and relative dip-slip motion; and (e) synrift sediments of Monte Largo embayment (Plate 1).

Striking nearly parallel to the Saiz fault proper, on its west side, are steeply northeast-dipping overturned strata of the middle Pennsylvanian Burrego Formation and Veredas Group. These strata, and gently westward-dipping strata further to the west, form the limbs of large-scale, symmetric, synclinal folds (Plate 1). Fold axes trend chiefly N40 ° E and plunge gently northwest and southeast. Axial planes dip moderately northeast. Within the hinge zone of the synclines are abundant, small-scale, gentle to tight asymmetric folds. These folds range from about 2 to 8 m in amplitude and about 2 to 10 m in half-wavelength where measurable. Axes have the same trend and plunge as the larger synclines. However, their axial planes are vertical or steeply dipping west and east.

Figure 6 looks southeastward across Coyote draw and along Saiz ridge on the southwest side of Saiz fault zone. Ladron Mountains are in the background. This synclinal fold suggests northeast uplift along a reverse fault at apparently the location of Saiz fault (Fig. 6 overleaf). Dip of this fault is indeterminate and presumed to be moderate to steep (steep at the location of Fig. 6). Displacement along this fault is indeterminate, and estimated to be approximately 40 m. The small-scale asymmetric folds and reverse faults (Fig. 6 overleaf) suggest that northeast-directed compression occurred, along with secondary folding, within the synclinal hinge zone on the down side of the Saiz reverse fault.

Locally, right and left-slip faults trend N5-10 ° E into the synclinal hinge zone and displace small-scale folds (Plate 1 and Fig. 5). As the strike-slip faults penetrate into the synclinal hinge zone, displacement decreases until the fault becomes a lateral shear refolding the hinge zone folds. Locally, these strike-slip faults completely penetrate the folds, but do not extend beyond the Saiz fault proper.

Figure 6. Photograph collage looking southeastward across Coyote Draw and along Saiz Ridge. The Ladron Mountains are in the background. Map units, folded strata, and faults are shown with the overleaf. Small arrows on bedding traces show stratigraphic up. Map symbols show motion on faults. PPhb: Pennsylvanian Burrego Fm; PPhs: Pennsylvanian Story Fm; PPdc: Pennsylvanian Del Cuerto Fm; PPm: Pennsylvanian Moya Fm.

In summary, these folds, strike-slip faults, and lateral shear zones on the southwest side of Saiz fault zone suggest northeast uplift along a northwest-striking, northeast-dipping reverse fault at the location of Saiz fault. Reverse faulting was contemporaneous with folding and northeast-directed compression into the fault plane within the footwall syncline. Reverse faulting and folding was followed by continued folding and N5-10 ° E trending right- and left-slip faulting and shearing.

Field evidence suggests that the most recent relative motion along the Saiz fault was down to the northeast, low- to moderate-angle normal faulting. Normal faulting is presumed to have occurred either along the previously developed reverse fault plane or below it, displacing the uplifted northeast side and part of the footwall syncline into Monte Largo embayment.

Figure 7 shows a low-angle Saiz normal fault with near vertical limestone strata of the Pennsylvanian Veredas Group in the foot wall, nnand gently southwest-dipping, drag-faulted strata of the Permian Yeso Formation in the hanging wall. At least 425 m (~1,394 ft) of upper Pennsylvanian and lower Permian strata is missing at this fault outcrop. But, the northeast side moved up prior to this motion. Therefore, down to northeast displacement along Saiz normal fault was greater than the amount of strata missing.

East of the Saiz fault, strongly deformed strata of the Yeso Formation crop out. Strata occur in three sliver blocks that are separated by presumed extensional faults (Plate 1). Low- to moderate-angle normal faulting along the Saiz fault placed these blocks into their present positions. Two of the sliver blocks consist of strata of the Torres Member of the Yeso Formation. Between the Torres Member blocks, is a block consisting of strata of the Meseta Blanca Member of the Yeso Formation. The Torres blocks were apparently downdropped against the Meseta Blanca block during extensional faulting.

Figure 7. Photograph of a low-angle section of Saiz fault. Map units, Saiz fault, and drag faults within the hanging wall are shown with the overleaf. Small arrows on bedding traces show stratigraphic up. PPv: Pennsylvanian Veredas Group; and Py: Permian Yeso Fm undifferentiated.


Pv

The northern of the Torres Member sliver blocks is strongly sheared, faulted, and folded. The southern Torres block is synclinally folded. This synclinal fold trends parallel to the Saiz fault and is slightly overturned northeastward. Overall, the dominant dip of strata in both Torres blocks is northeastward. The Meseta Blanca block is overturned and dips very steeply northeast. This block of strata is strongly sheared, tilted, and folded, but not as strongly folded as the other blocks.

Two opposing verges are recorded in the sliver blocks. Torres blocks verge northeastward and the Meseta Blanca block verges southwestward. Strata of the Meseta Blanca Member consist of thick units of thickly bedded, fine-grained sandstones with little shale. Strata of the Torres Member consists of friable sandstones, shales and limestone. So, the Meseta Blanca block is structurally more competent. Therefore, the southwest-verging Meseta Blanca block is most likely dominant. Southwest-verging would be expected in strata on the northeast side of the Saiz reverse fault. Strata in this position would be folded in a southwest-verging anticlinal structure. Northeast-verging in the less competent Torres strata is most likely secondary and may record the direction of extensional faulting.

Separating these deformed Yeso strata from synrift sediments of the Albuquerque basin is an extensional fault that apparently subparallels the Saiz fault (Plate 1). This fault marks the east edge of the Saiz fault zone, and in the study area it is the main border fault to Monte Largo embayment and the southwestern Albuquerque basin. This fault is here informally named Monte Largo fault after Monte Largo embayment. Monte Largo fault is very poorly exposed in the sides of Coyote draw approximately 160 m (~525 ft) east of the old Saladito homestead. This fault does not displace the well-cemented gravels forming the rim of Coyote draw. But it does form the contact between cemented

gravels, lying below the well-cemented gravels, to the northeast and deformed strata of the Yeso Formation to the southwest. Both the cemented and well-cemented gravels are within the Santa Fe Group. Monte Largo fault strikes approximately N40 ° W and the dip is indeterminate but presumed to be steep eastward. Bedding in the cemented gravel dips 16 degrees northeastward.

South of Coyote draw, folded strata crop out within and at the base of Saiz ridge. An anticline crops out immediately north of a small drainage through Saiz ridge (north of where the gravel road passes through Navajo Gap) and south of Coyote draw (Plate 1). The anticline occurs east of gently west-dipping strata and west of small-scale folds (Plate 1). This anticline has an amplitude of approximately 50 m (~160 ft) and a halfwavelength of approximately 200 m (~655 ft). Its axial trace ends to the north at a strike-slip fault and plunges southward below alluvial sediments (Plate 1). Both limbs of the anticline are cut by small thrusts directed towards the fold apex. The thrust planes have steeper dips than the fold limbs and contain striations that indicate an east-northeast--west-southwest axis of compression.

A north-northeast-trending asymmetric anticline (Plate 1) occurs immediately south of the pass through Navajo Gap. Asymmetry indicates it verges eastward. Its axial trace plunges northward below alluvial fan sediments. Southward its axial trace bends into and terminates at a north-trending, west-dipping apparent reverse fault. Northward this fault displaces the anticlines east limb and southward it trends into a shear zone. The shear zone eventually disappears over approximately 200 m (~656 ft). Approximately 10 m (~33 ft) east of this fault is a similar trending but east-dipping apparent reverse fault. Southward this fault trends into a right-shear zone, also disappearing like the fault to the west. These two faults form the hinge zone of a synclinal structure. The anticline and the faulted and sheared synclinal structure suggest a slightly north of east axis of

compression plus high-angle reverse faulting and right-shearing. The Saiz fault zone is buried by recent sediments to the east of these structures.

Ladron Fault. In the southern Navajo Gap area, the Ladron fault borders the west side of the Ladron uplift (Fig. 5). The Ladron fault strikes north to north-northwest and dips vertical to 74 ° E. This fault is the boundary between Proterozoic rocks of the Ladron Mountains to the east and lower Pennsylvanian limestones, sandstones and shales to the west. For two and one half kilometers the Ladron fault is poorly to very well exposed in the study area (Plate 1). Northward this fault is buried by synrift sediments and southward it trends out of the study area. Tertiary mafic dikes intrude the fault plane at two locations (Plate 1).

In northern exposures of the fault plane, sandstones of the lower Pennsylvanian Sandia Formation dip moderately west (Plate 1 and Fig. 8). In middle exposures of the fault plane, lower Pennsylvanian limestones of the Bartolo Formation dip very steeply west, become vertical, and then dip very steeply east (overturned) along the west side of the fault. To the south, the fault makes an abrupt ninety degree clockwise bend before continuing southward out of the study area. In this fault bend, lower Pennsylvanian strata of the Socorro (Bolander) and Veredas Groups are strongly deformed.

Nearly paralleling the Ladron fault 100 to 600 m (328 to 1,968 ft) to the west are folded strata. From north to south, these folds include (a) a west-facing monocline, trending into (b) a paralleling set of centrally plunging asymmetric folds (an anticline to the west and a syncline to the east), (c) the southern termination of the paralleling folds at the bend in the Ladron fault, and (d) a north-facing monocline (Plate 1 and Fig. 5).

The west-facing, east-verging monocline (Fig. 8) is exposed for approximately 250 m of its length and has an amplitude of up to 15 m. Amplitude decreases to

Figure 8. Photograph collage looking southeastward at the north-northwest-trending Ladron fault (left photo) and south-southwestward to a north-trending and west-facing monocline (right photo) within Saiz Ridge. Ladron Peak is in the background. Map units and the Ladron fault are shown with the overleaf. pЄm: Proterozoic metavolcanics; pЄg: Proterozoic Capriote granite; ℙs: Pennsylvanian Sandia Fm; ℙa: Pennsylvanian Armendaris Group; ℙb: Pennsylvania Socorro (Bolander) Group; and ℙv: Pennsylvanian Veredas Group.

zero as one traces the steeply east-dipping axial plane downward (down the east face of Saiz ridge) to Proterozoic rocks. This decrease in amplitude is indicative of bedding-slip and flexural folding. Locally, the monocline's anticlinal hinge contains two gently to moderately northwest-dipping, intra-bed thrust faults. Thrust faults lie one atop the other, each displacing a limestone bed 6 to 8 meters southeastward. Striations parallel the dip of the thrust plane and point directly to Ladron Peak, the highest point of the Ladron Mountains. The occurrence of this flexural fold, and the intra-bed thrust and striations suggests (1) a possible northwest-directed gravity slide of lower Pennsylvanian strata away from the Ladron Mountains, (2) east-west compression contemporaneous with uplift of the Ladron block followed by gravity sliding, or (3) east-west compression contemporaneous with uplift of the Ladron block at a lateral change in the orientation and nature of the Ladron fault (not revealed in exposures) causing thrusting to occur in the monocline.

To the south, the west-facing monocline trends into paralleling asymmetric folds (Plate 1). Paralleling folds are an anticline to the west and a syncline to the east (Fig. 9). These folds verge eastward, are centrally plunging, and are centrally increasing in amplitude from 0 to approximately 60 m (~187 ft). Axes trend north to north-northwest and axial planes dip steeply west. Two, moderately west-dipping, north-south-striking, intra-bed thrust faults, with displacements of 2 to 3 m directed eastward, occur locally in the hinge of the syncline and on the west limb of the anticline. These paralleling folds and the two intra-bed thrust faults suggest east to east-northeast directed compression.

In the southern field area, the Ladron fault bends nearly ninety degrees and trends east-west for approximately 200 m (~656 ft) before it bends back to a north-northwest strike (Plate 1). This sharp bend in the Ladron fault is the southern termination of the paralleling syncline and anticline. Plunging

Figure 9. Photograph looking northward along the limb between the anticline and syncline west of the Ladron fault. The amplitude of these folds decreases to zero within the Saiz Ridge in the background. The far side of Saiz Ridge is the monocline shown in the right photograph of Figure 8. Map units are shown with the overleaf. Pb: Pennsylvanian Socorro (Bolander) Group; and Pv: Pennsylvanian Veredas Group.

northward from this location, the folds have an amplitude of approximately 5 m (~16.5 ft). Between the folds, strata are strongly sheared along a steeply west-dipping thrust. East-directed displacement along this thrust is from 20 to 30 m (~66 to 98 ft).

Proterozoic granite is brittlely sheared (Plate 1) east of the bend in the Ladron fault. Sense of shear was not determined. Further to the east, the granite is apparently folded along with metavolcanic rocks (Plate 1). Northeast of the bend in the Ladron fault, within Proterozoic granite, occurs an east-west-trending, very steeply north-dipping fault (Plate 1). Amount of displacement and direction of throw is indeterminate. West of the Ladron fault bend, Pennsylvanian strata is folded in a gently west-plunging, north-facing monocline. Amplitude of this fold is approximately 170 m (~560 ft). Amplitude rapidly decreases to zero westward over approximately 800 m (~2,625 ft). This monocline is interpreted to be a drape fold.

Relative down-to-north motion in an east-west-trending structural zone is suggested by the occurrences of the north-facing monocline, the east-northeast-trending segment of Ladron fault, and the steeply north-dipping fault in Proterozoic granite. Amount of displacement along this structural zone is interpreted to be the amplitude of the monocline, a minimum of approximately 170 m (~560 ft). This structural zone is within the northeast-trending Alamito shear zone, proposed by Chamberlin and others (1982). They suggested that possible Precambrian deformation occurred along this shear zone. From the present study, evidence indicates that deformation was at least as young as the monoclinally folded middle Pennsylvanian strata.

With the monocline's amplitude fading westward to zero, rocks on the northern side of this zone moved down and rotated eastward relative to rocks on the south side. During Tertiary extensional faulting, could westward rotation of

the Ladron block be greater to the south of the Alamito shear zone than to the north? Could the Alamito shear zone separate greater block rotation and rift extension to the south and less to the north? No evidence was found to suggest that deformation along this zone was as young as Tertiary.

Exposures of the Ladron fault in the study area reveal only relative throw. However, one northern exposure does show fault breccia containing a limestone boulder that has a striated side facing the Ladron uplift. The breccia suggests down-to-west motion and the striations trend parallel to the fault and plunge 30 ° N. This exposure suggests down-to-west, right-oblique motion.

Monte de Belen (Mesa Sarca) Fault. In the northwestern Navajo Gap area, Mesa Sarca fault was the site of relative down-to-east, high-angle normal faulting. This fault could be considered the southeastern border fault of the Colorado Plateau as it is the east margin of the separately uplifted southeastern part of Lucero uplift. The trace of Mesa Sarca fault bends from north-south in southern exposures to northeast-southwest in limited northern exposures (Plate 1). The fault plane dips 60 to 80 ° east and locally contains striations that indicate dip-slip displacement. Relative down-to-east throw on Mesa Sarca fault is approximately 840 m (~2,756 ft). Displacement decreases rapidly southward to zero where the fault apparently ends about 1 km (~0.6 mi) outside of the study area.

Strata of the Permian Abo Formation crop out east of Mesa Sarca fault. These strata dip chiefly 15 to 30 ° west. Synclinal folds, interpreted to be due to drag along the fault plane, occur at three locations along the east side of Mesa Sarca fault (Plate 1). Axial traces of these synclinal folds are concave towards Mesa Sarca fault.

Approximately 475 m (~1,560 ft) east of Mesa Sarca fault, a north-south-striking, down-to-west, vertical fault crops out (Plate 1). Formed in an earlier

zone of lateral shear or strike-slip faulting, most recent motion along this fault is apparently antithetic to Mesa Sarca fault. This fault trends northward into the northeast-southwest trending segment of Mesa Sarca fault. Relative down-to-west throw on the antithetic fault is 20 to 40 m (65 to 130 ft), greater to the north than to the south. East of this antithetic fault strata dip chiefly 6 to 15 ° west. Other extensional faults occur east of Mesa Sarca fault. But most of these contain very minor displacements.

Locally, mafic dikes intrude along the antithetic fault and within a few of the minor extensional faults. Some of these faults are most likely reactivated strike-slip faults and dikes could have intruded along them prior to extension. One of the dikes is sheared. Therefore, the intruded extensional faults are probably younger than the late Oligocene-early Miocene mafic dikes.

Strata of the lower Pennsylvanian middle Elephant Butte Formation crop out immediately west of Mesa Sarca fault. These strata dip moderately to very steeply east. A synthetic fault to Mesa Sarca fault crops out 20 to 375 m (65 to 1,230 ft) to the west of it (Plate 1). Poorly exposed in most of the study area, one good southern exposure of the synthetic fault plane indicates that it strikes northsouth and dips 56 ° E. On the fault plane are striations that trend N54W and plunge 50 ° E, indicative of relative down to east, oblique-right-slip motion. Relative throw along this synthetic fault is approximately 105 m (~344 ft). At the fault contact, strata of the Elephant Butte formation to the east are in contact with lower Pennsylvanian sandstones of the Sandia Formation and Proterozoic granitic gneiss to the west. Immediately west of this synthetic fault is an anticlinal fold (Plate 1). This anticlinal structure parallels the synthetic fault and appears to be a large drag fold in the foot wall of the synthetic fault.

Further to the west, Mesa Sarca's east face is cut by extensional faults. Most of these faults dip steeply east with overall down-to-east relative motion (Plate 1).

Throw across these faults is minor and negligible when compared to that along Mesa Sarca fault (Plate 1).

Southward, the strata between Mesa Sarca fault and its synthetic fault are strongly deformed. Deformation includes synclinal folding, strong eastward-tilting, and apparent normal faulting. I am unable to put definite constraints on this deformation. Outside of the study area, Kelley and Wood (1946) mapped the southern termination of the Monte de Belen (Mesa Sarca) fault to the south and a southeast-dipping "ramp like" structure of southern Monte de Belen (Mesa Sarca) to the southwest.

Relative to Mesa Sarca, the Navajo Gap area was downdropped to the east along Mesa Sarca fault zone (Mesa Sarca fault and its synthetic fault) approximately 945 m (~3,100 ft). Or Mesa Sarca was uplifted as a horst block (Kelley and Wood, 1946) in the southeastern Lucero uplift. With this uplift, a normal fault occurred on its eastern margin and a south-dipping ramp structure occurred on its southern margin.

Other Unnamed Structures. Between the Saiz fault zone, Ladron fault, and Mesa Sarca fault, nearly 40 strike-slip faults and lateral shear zones occur (Plate 1). Lateral slip on these structures is interpreted to be minor; less than 30 m on the main faults. Many smaller faults and shears occur secondary to the strike-slip faults and lateral shear zones. Faults and shear zones are nearly perpendicular to bedding.

East of, and paralleling, the antithetic fault to Mesa Sarca, occurs a classic north-south-trending right-slip fault and shear zone (Plate 1). The northern exposure of this structure is a shear zone with relative down-to-east motion across it. This zone is made up of two left-echelon jumps of a right-slip fault and anticlinal structures (restraining bends) trending north-northwestward between the echelon faults. The right-shear zone trends southward into a right-slip fault

that has relative down-to-west motion. The fault splays into shears as it extends southward out of the study area.

East of this fault, an approximate kilometer wide right-shear zone occurs. This shear zone is made up of right-slip faults and lateral shears. Exposed limestone beds contain strong jointing that parallels the faults. To the east of this right-shear zone occurs a 500 to 1,000 m wide left-shear zone. This left-shear zone is also made up of left- and right-slip faults and lateral shears. Most of the strata in which these shear zones occur dip very gently westward. Uplift and thrusting occurs at the northern end of the zone between these two opposing shear zones (immediately south of the old Saladito Ranch in Coyote Draw). Strata dip gently southwestward at the southern end of these shear zones. Shears trend southward, from strata dipping gently westward, through these gently southwestward dipping strata without any change in shear strike or dip. This indicates that a gently southwest-plunging, gentle anticline was present before the shears developed.

Another approximate kilometer-wide right-shear zone occurs east and south of the left-shear zone. This right-shear zone is made up of right- and left-slip faults and lateral shears. The eastern edge of this right-shear zone is the pass (Navajo Gap) where a through-going gravel road crosses the study area. No faulting was recognized in this pass, but the similar trend of it to other structures in the area suggests the possibility of structures beneath the veneer of sediments.

East of the pass about one kilometer, a relatively narrow right-slip shear zone occurs (Plate 1). Northern exposures of the shear zone contain left-echelon, west-dipping reverse faults. Southward, the left-echelon reverse faults trend into a right-slip fault. This right-slip fault splays southward into northeast-southwest trending faults and a shear zone with folded strata between. This splaying occurs as the fault trends southward through a south dipping "ramp like" structure.

Strata dip gently to moderately west on the north, east, and west sides of this south-dipping ramp. The ramp forms the limb between two gently southwest-plunging low-amplitude folds, an anticline to the northwest and a syncline. Because the right-shear zone structures splay southward, as the shear trends through the ramp structure, and does not change its strike or dip, I interpret that the ramp structure was present before the right-shear developed. This relatively narrow right-shear zone separates strata that dip moderately west on the east side from strata that dip gently west on the west side. In the southwestern study area, a north- to north-northwest-trending anticlinal structure separates very gently dipping strata to the east from steeply dipping strata to the west.

Most of the strata in the area between the three major structures (Saiz fault zone, Ladron fault, and Mesa Sarca fault zone) dip gently to very gently westward. Exceptions are the gently southwestward dipping strata in central-west Navajo Gap and the steep westward dipping strata in southwest Navajo Gap.

Summary. Styles of structural deformation in the Navajo Gap area are compressional, strike-slip, and extensional. Interrelationships between folds, thrusts, and strike-slip faults suggest that east-northeast to northeast-directed compression developed folds, reverse faults, and thrust faults. Folding was followed by continued folding and strike-slip faulting. Strike-slip deformation was dominated by right-slip faults trending N5-10 °E. During deformation, relative uplift occurred on the east sides of faults at the locations of the Ladron and Saiz faults. The relative motion along these faults suggests that they may have been connected. However, the nature of relative east uplift changed with a change in fault strike. Relative east uplift of the Ladron block along a north- to north-northwest-trending vertical fault (at the location of the Ladron fault) changed to reverse faulting as the fault strike changed to northwest (along the

location of the Saiz fault). The changing nature of folds west of the fault at the location of the Ladron fault, from east-verging parallel folds northward to a west-verging monocline, may reflect the initial change in fault orientation and vertical uplift to reverse faulting.

Extension in the area was northeast-southwest and east-west. Main extensional faults include high-angle normal (Mesa Sarca fault) and low to moderate-angle normal (Saiz fault). The study area was downdropped relative to Mesa Sarca, or Mesa Sarca was uplifted relative to the study area, as much as 945 m (~3,100 ft) along Mesa Sarca fault zone. The study area was also downdropped relative to the Ladron Mountains an indeterminate amount. The eastern uplifted side of the reverse fault at the location of the Saiz fault was downdropped into Monte Largo embayment. Gently dipping strata in central Navajo Gap, and the perpendicular relationship of strike-slip faults to bedding suggest that the study area was tilted approximately 5 to 10 degrees westward.

# STRUCTURAL ANALYSIS

## Extension and Shear Veins, and Faults and Striations.

Extension and shear veins, and faults and striations are macro and mesostructures useful as kinematic indicators. These structures are abundant in the Navajo Gap area. Plotting these structures on lower hemisphere equal-area stereographic nets and contouring reveals their most common orientation. Using techniques of stereonet analysis (Ragan, 1985; Suppe, 1985), I have found the approximate stress orientations responsible for strike-slip faulting, lateral shearing, and normal faulting in the Navajo Gap area.

Introduction. In an extensional regime, the maximum principal stress axis is vertical and the intermediate and minimum stress axes are horizontal; intermediate axis lies parallel to fault planes and minimum axis is the trend of extension. In a strike-slip stress regime, the maximum and minimum principal stress axes are horizontal and the intermediate principal stress axis is vertical; maximum axis is the trend of compression and minimum axis is the trend of tension. Figure 10 is a summary of en echelon structures characteristic of strike-slip fault zones superimposed on a shear ellipse. All of the structures shown on this diagram are not necessarily found in every strike-slip, shear, or wrench zone. Structures developed in a wrench zone are dependent on the orientations of principal stresses to the shear zone and the stage of deformation (early, late) in which wrenching ceased.

The angular relationships between these structures and the shear zone is variable. Angular relationships are governed by the shear strength, or shear modulus of the rocks in the shear zone, the amount of compression and shear across the zone, and orientations of preexisting structures in the shear zone. In an

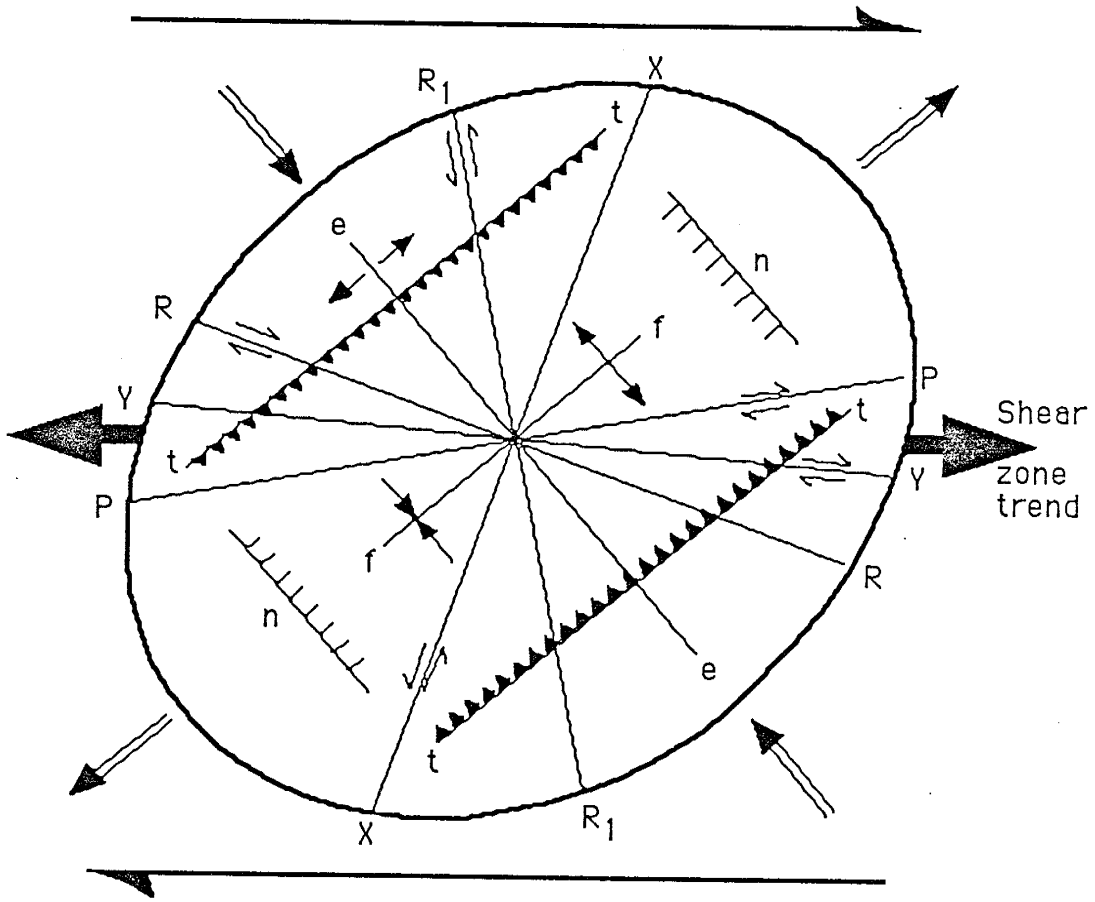


Figure 10. Summary of en echelon structures characteristic of wrench fault zones superimposed over a shear ellipse. R and $R_1$, Riedel and conjugate riedel shears; P, X, and Y shears; e, extension joint, fissure, or veins; f, fold; n, normal fault; t, thrust. Modified from Hancock (1985).

ideal homogeneous system, a high shear modulus, or increased horizontal compression (transpression), initiates folds and thrusts at smaller angles to the shear zone and tensional structures at larger angles to the shear zone (Sanderson and Marchini, 1984; Jaroszewski, 1984). Shears rotate along with the compressional and tensional structures (Hancock, 1985; Sanderson and Marchini, 1984; Jaroszewski, 1984). With a low shear modulus, decreased transpression, or shear with horizontal extension (transtension), the opposite occurs (Hancock, 1985; Jaroszewski, 1984).

In a wrench zone, there is sequential development of the structures shown in Figure 10 (Wilcox and others, 1973). "Folds form early in the deformation and are accompanied or followed by conjugate strike-slip, reverse, or normal faulting. Deformation may cease at any stage or may continue until strike-slip along the wrench zone produces a [main] wrench fault...." (Wilcox and others, 1973). "Riedel shears occur just before the peak shear strength is reached.... P-shears form during the post-peak [shear strength] period as the Riedel shears are extended and rotated.... The Y-shears [main wrench fault] form just prior to the residual shear strength and as total movement is continued; the Y-shears gradually accommodate most of the displacement." (Bartlett and others, 1981; Fig. 10).

Analysis. In the field, I classified extension veins as linear or en echelon (Fig. 11). Linear veins are first-order and crop out singularly, but most often in sets of subparallel veins (Fig. 12a). Linear veins are at least 1 m in length, usually much longer, and typically less than 1 cm in width. The depth of a linear vein is usually not measurable because they are often only visible as traces on outcrop surfaces. Where this third dimension is visible, veins extend to a depth of 3 m or more. Quite often, linear veins are associated with second- and third-order en echelon and pinnate veins, and vein "steps" (Fig. 11a).

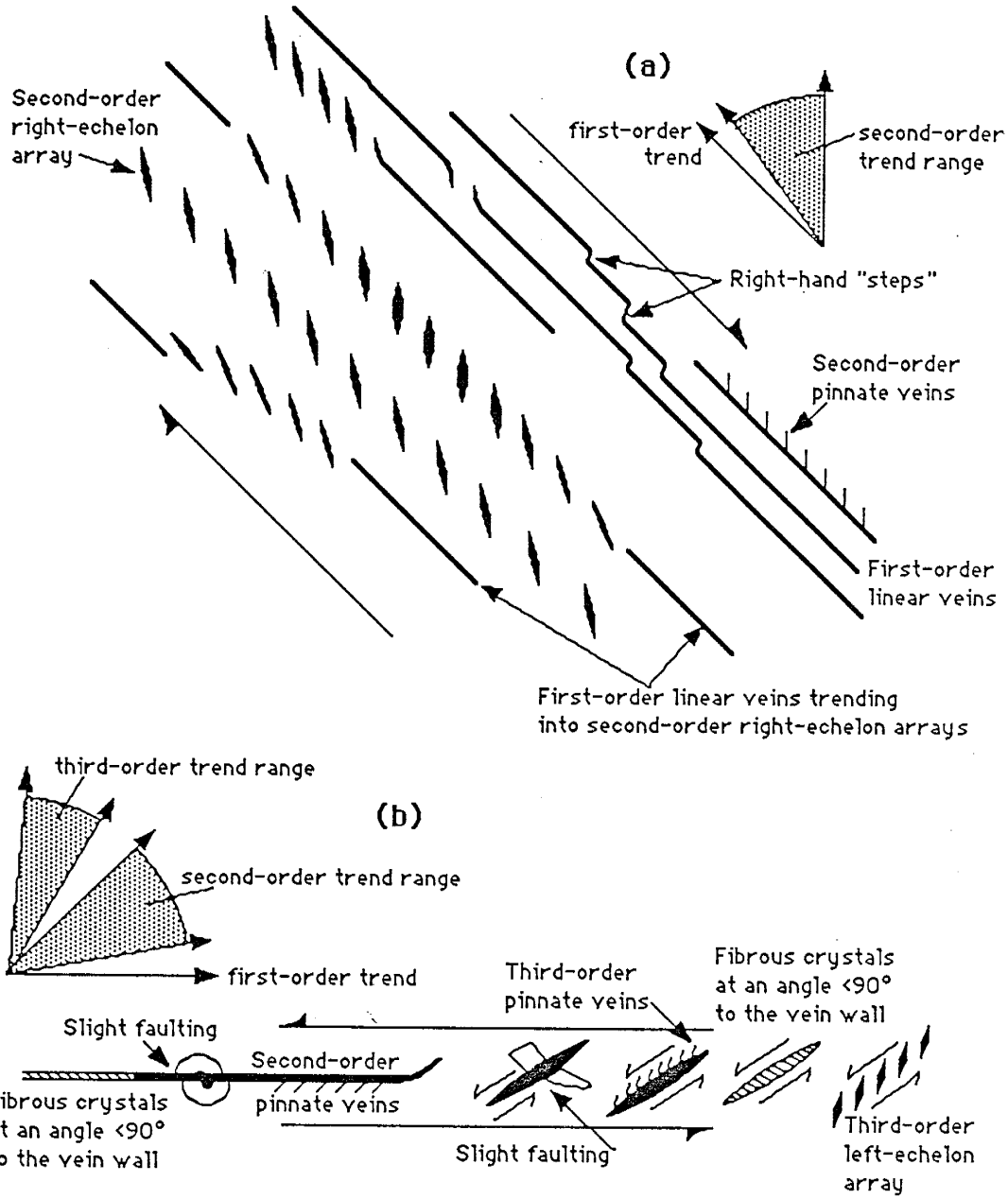


Figure 11. Relationship of veins to shear direction. (a) Schematic plan view showing linear, left-echelon, and pinnate veins, and right-hand "steps" in a right-shear zone. (b) Schematic plan view showing kinemataic indicators on veins in a left-shear zone. Modified from Hancock (1972, fig. 1).

Figure 12. Photographs of extension veins.

(a) Linear vein swarm with right-hand "steps" and left-echelon vein arrays within a right-shear zone.

(b) Right-echelon vein arrays, a left-echelon vein array, and a linear vein.

Figure 12 (continued).

(c) A left-echelon vein array.

(d) A short linear vein with right-echelon pinnate veins.

En echelon veins (Fig. 12b and 12c) are second- or third-order; the trend of an en echelon array of second-order veins is the first-order shear zone (Fig. 11a). En echelon veins are typically less than 30 cm in length, less than 2 cm in thickness, and may be 30 cm or greater in depth. The depth of an en echelon vein is often not measurable and is the longest orientation (Nicholson and Ejiofor, 1987). Pinnate veins form in an en echelon array along one or both sides of, and in contact with, a linear or an en echelon vein (Fig. 12d, and Fig. 11a and 11b). The orientation of en echelon and pinnate veins ranges form about eight to 65 degrees to the array. Most often their orientation is about 15 degrees to the array, near the Riedel shear. Vein "steps" are abrupt lateral jumps, or skips in the trend of a linear vein (Fig. 11a). "Steps" are third-order fractures apparently in a conjugate Riedel shear orientation.

For the analysis of crystal fiber systems in extension veins, en echelon and linear veins were further categorized as shear or extension. In field analysis of crystal fibers, only extension veins were used. Extension veins contain fibrous crystals at angles greater than 45 ° (most commonly greater than 60 ° ) to the vein wall (Fig. 13a), in spite of an often occurring large component of shear. Shear veins contain fibrous crystals at angles of less than 45 ° (commonly less than 15 ° ) to the vein wall (Fig. 13b).

En echelon veins, pinnate veins, and vein "steps" are kinematic indicators which reveal the sense of slip in a shear zone. En echelon and pinnate veins "face against the sense of slip along a shear zone" (Hancock, 1972; Fig. 11b). Right-echelon arrays indicate left-slip, and left-echelon arrays indicate right-slip. Vein "steps" with a left-hand lateral shift indicates left-slip, and a right-hand lateral shift indicates right-slip (Fig. 11b).

Field measurements of extension and shear veins consisted of (a) vein type (linear, en echelon, shear), (b) sense of slip (right, left), and (c) vein strike and

Figure 13. Field photographs of fibrous crystals.

(a) Fibrous calcite in extension veins. Fibers are nearly perpendicular to vein walls.

(b) Fibrous calcite in left-shear veins. Fibers are nearly parallel to vein walls.

dip. Thirty five left-echelon veins, 42 right-echelon veins, 59 right-slip linear extension and shear veins, 31 left-slip linear extension and shear veins, and 166 linear veins with indeterminate slip were analyzed. All data from these structures were measured on veins found in gently dipping strata. No data was analyzed from extension veins in folded strata. The dip of strata containing the measured veins was not removed during stereonet analysis.

Faults are abundant in the Navajo Gap area. They are found singularly or in sets forming fault zones. Sense of fault displacement is revealed by extension-vein kinematic indicators alongside faults or within fault zones, or can be solved geometrically using striation trend and plunge and direction of relative throw.

Striations and slickensides indicate the latest displacement along a fault. However, striations may not indicate the overall, or dominant motion. If this is the case, post deformational relaxation, or tension would develop near-vertical striations in established fault planes. In Navajo Gap the majority of striations are sub-horizontal (Fig. 14a). Therefore, the sub-horizontal striations are relicts of strike-slip, the dominant nature of faulting. High-angle thrusts, reverse faults, and normal faults are not as common as strike-slip faults. These structures contain near-vertical striations (Fig. 14b).

Throw is determined through close scrutiny of the stratigraphy. This is a problem in the Navajo Gap area due to the difficulties in determining the stratigraphy of the seemingly repetitive upper Paleozoic limestones, the most common strata cropping out. Once stratigraphic throw is determined, the sense of fault displacement is easily determined.

Measurements of faults and striations consisted of (a) fault strike and dip, (b) striation trend and plunge, and (c) sense of displacement (right-slip, left-slip, normal, reverse, thrust). Oblique-slip faults were analyzed as right- or left-slip. Thirty three right-slip faults, 30 left-slip faults, 13 normal faults, four reverse

Figure 14. Photographs of friction striations in fault planes.

(a) Horizontal striations in a strike-slip fault plane.

(b) Near-vertical striations in a normal fault plane.

faults, ten thrust faults, and 114 faults with indeterminate displacement were analyzed. Twenty six striations in right-slip faults, 27 striations in left-slip faults, 13 striations in normal faults, six striations in reverse faults, eight striations in thrust faults, and 57 striations in faults with indeterminate displacements were analyzed. Data collected on these structures were measured on faults in gently dipping Pennsylvanian and lower Permian strata. The dip of the strata containing the measured faults and striations was not removed during stereonet analysis.

Data points were plotted using a computer program for lower hemisphere equal-area stereonets (Schmidt equal-area projection). Data points were counted using a Kalsbeek counting net. Contouring was done by hand.

Extension and Shear Veins. Appendix H includes the lower hemisphere equal-area stereographic point plots for extension and shear veins. Figure 15 includes the contoured lower hemisphere equal-area plots of the diagrams in Appendix H. Also included with the plots of Figure 15 are the modal orientations of extension veins (solid lines) and, where appropriate, less typical orientations (dashed lines). Figure 15a is the contoured lower hemisphere equal-area plot of poles to extension veins in left-echelon arrays (right-shear). The modal orientation of extension veins in left-echelon arrays is N36 ° E and vertical. The modal right-shear zone is inferred to be 30 ° counterclockwise from the strike of the modal left-echelon extension vein. Therefore, the modal right-shear zone trends N6 ° E. Less typical extension veins in left-echelon arrays have strikes and dips of N60 ° E and 87 ° SE with a right shear zone striking N30 ° E and dipping 87 ° E. Figure 15b is the contoured plot of poles to extension veins in right-echelon arrays (left-shear). The modal orientation of extension veins in left-echelon arrays is N9 ° E and vertical. The modal left-shear zone is inferred to be 30 ° clockwise from the strike of the modal right-echelon extension vein.

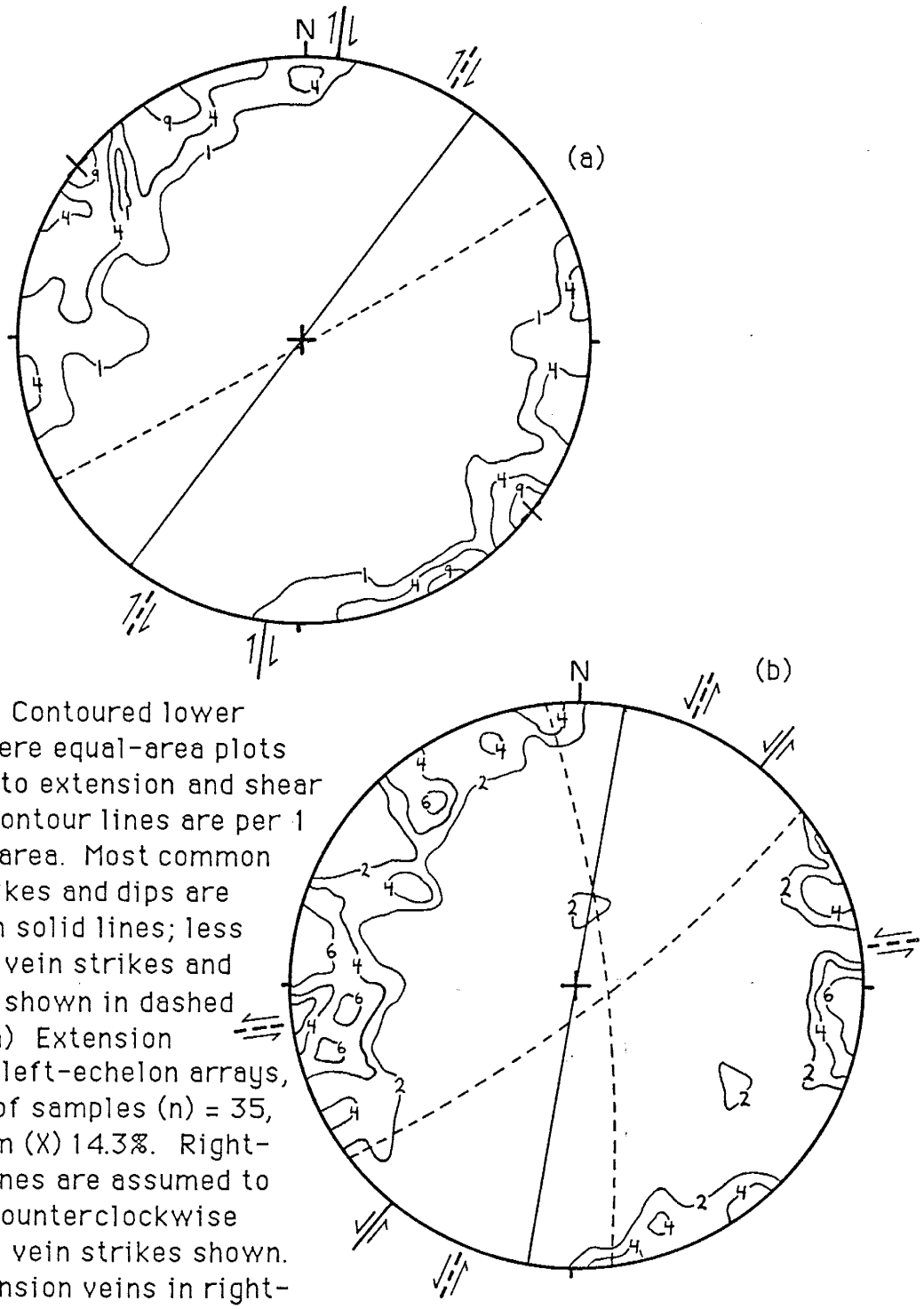


Figure 15. Contoured lower hemisphere equal-area plots of poles to extension and shear veins. Contour lines are per 1 percent area. Most common vein strikes and dips are shown in solid lines; less common vein strikes and dips are shown in dashed lines. (a) Extension veins in left-echelon arrays, number of samples (n) = 35, maximum (X) 14.3%. Right-shear zones are assumed to be 30° counterclockwise from the vein strikes shown. (b) Extension veins in right-echelon arrays, n = 42. Left-shear zones are assumed to be 30° clockwise from the vein strikes shown.

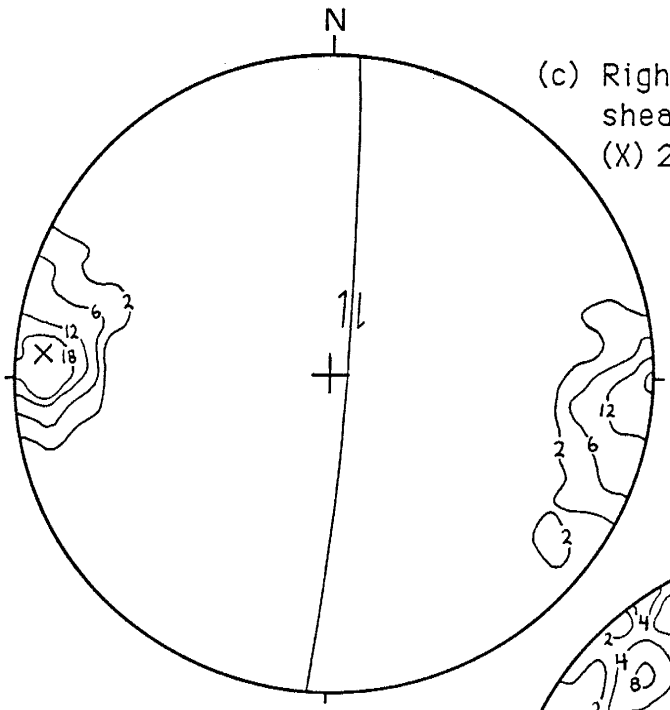


(c) Right-slip linear extension and shear veins, n = 59, maximum (X) 27.1%.

(d) Left-slip linear extension and shear veins, n = 31, maximum (X) 19.4%.

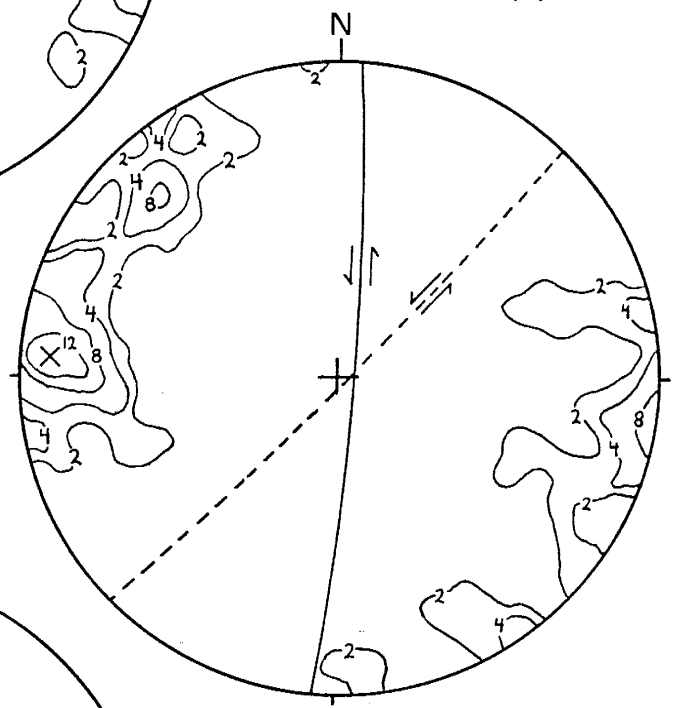


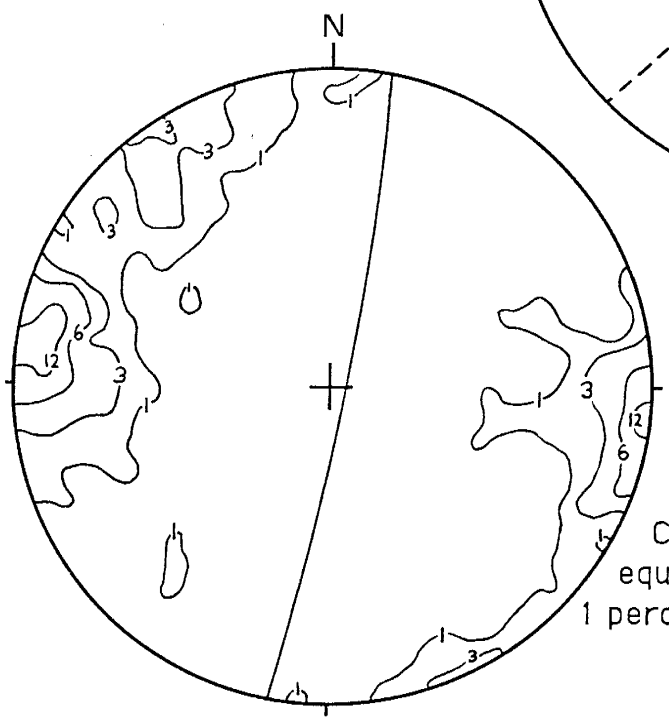


(e) Veins with indeterminate slip, n = 166.

Figure 15. (continued) Contoured lower hemisphere equal-area plots. Contours per 1 percent area.

Therefore, the modal left-shear zone trends N39 ° E. Slightly less typical extension veins in left-echelon arrays have strikes and dips of N7 ° W and 78 ° E, and N52 ° E and 79 ° SE. These less typical veins form right-shears with strikes and dips of N23 ° E and 78 ° E, and N82 ° E and 79 ° S, respectively. Figure 15c is the contoured plot of poles to right-slip linear extension and shear veins. The modal orientation of right-slip linear veins is N4 ° E and 84 ° E. Figure 15d is the contoured plot of poles to left-slip linear extension and shear veins. The modal orientation of left-slip linear veins is N4 ° E and 83 ° E. Less typical linear left-slip veins have strikes and dips of N44 ° E and 86 ° SE. Figure 15e is the contoured plot of poles to linear veins with indeterminate slip. The modal orientation of linear veins with indeterminate slip is N10 ° E and 83 ° E.

Shear zones of the modal veins in en echelon arrays, shear zones of the less typical veins in en echelon arrays, and the modal right- and left-slip linear extension and shear veins are summarized in the synoptic diagrams of Figure 16. Figure 16a shows a N22 ° E-trending axis of compression bisecting conjugate modal shears. These shears are interpreted to be Riedel (right-shear) and conjugate Riedel shears (left-shear). The acute angle between these conjugate shear structures is arbitrary, due to the inferred 30 ° angle in determining the orientation of the shear.

Figure 16b shows a N51 ° E trending axis of compression bisecting a conjugate set of less typical shears. A second less typical left-shear is interpreted to be secondary, possibly related to the modal right-shear. Again, the acute angle between these conjugate shear structures is arbitrary, due to the inferred 30 ° angle in determining the orientation of the shear. However, if the less typical shears (Fig. 16b) and the modal shears (Fig. 16a) form two separate conjugate sets, the difference in their acute angles may reflect a difference in stress. The wider acute angle of the less typical conjugate shears is interpreted to be due to

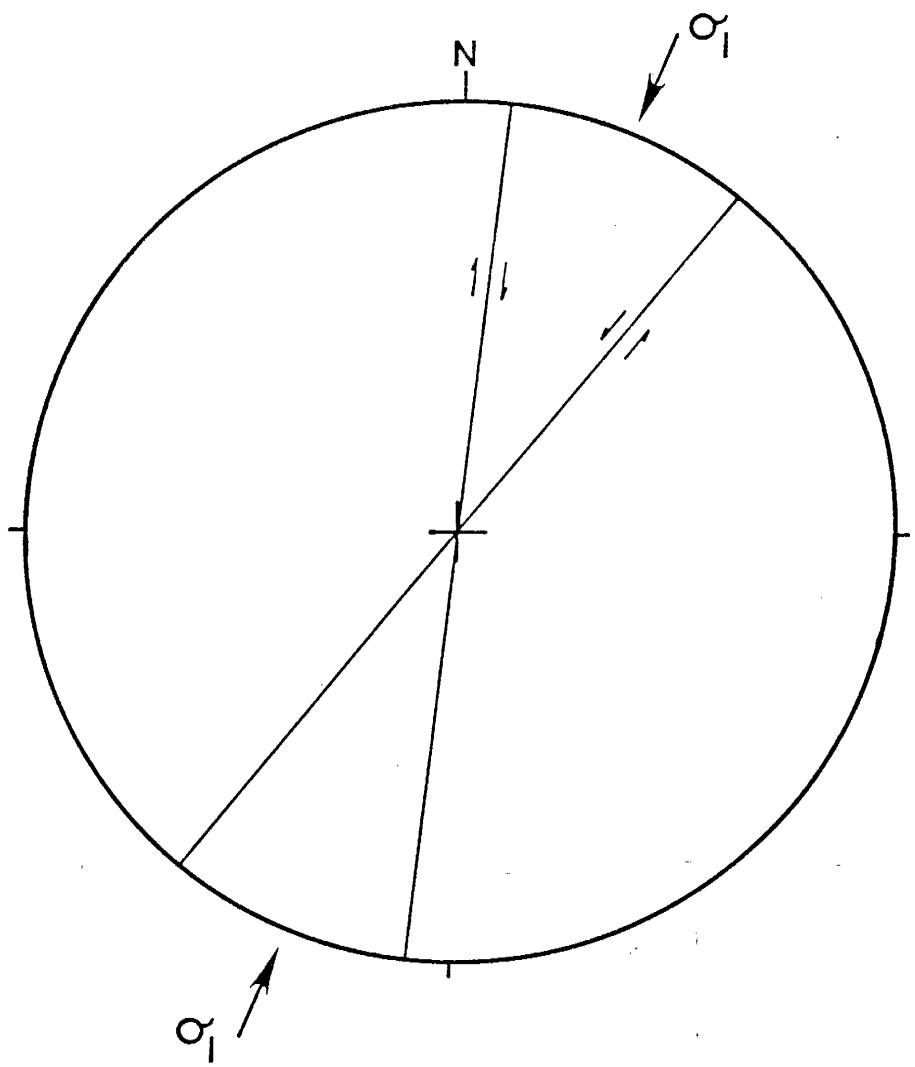


Figure 16a. Synoptic diagram of right- and left-shear zones deduced from the most common orientations of extension veins in right- and left-echelon arrays. Maximum principal horizontal stress (sigma one) from conjugate shears trends N22°E.

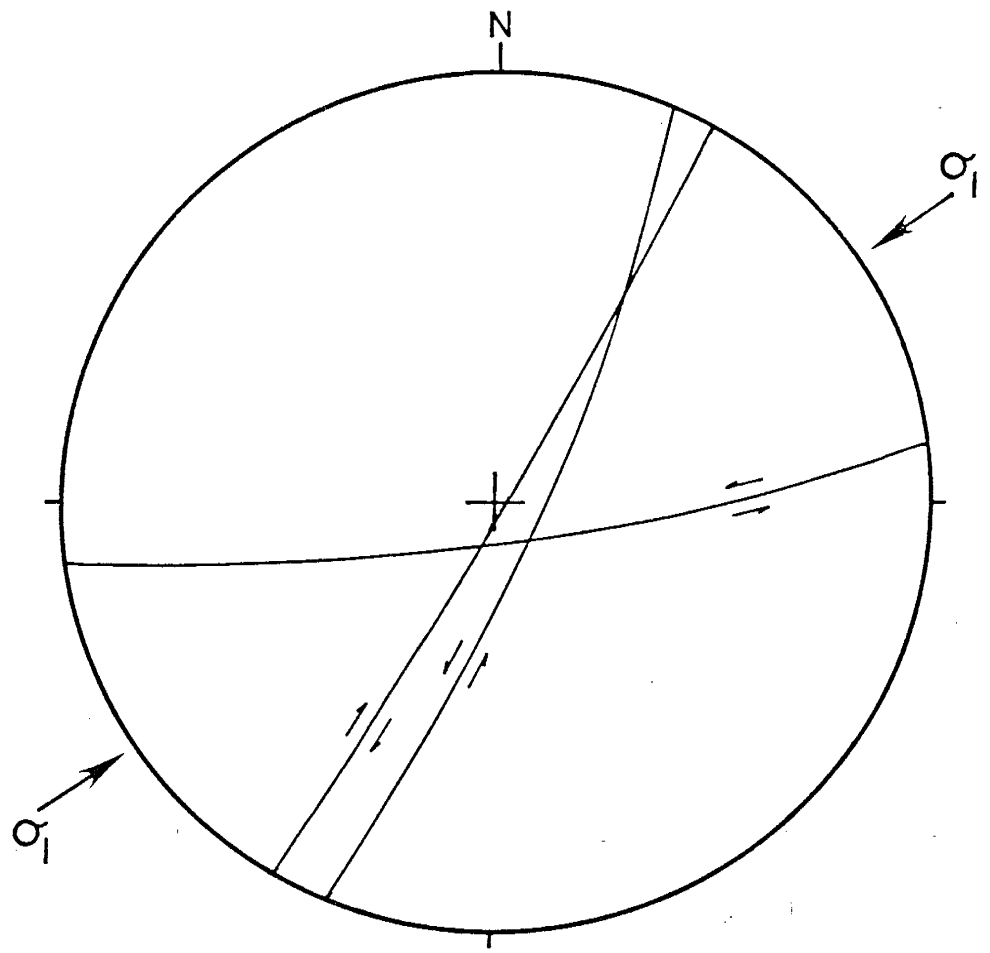


Figure 16b. Synoptic diagram of right- and left-shear zones deduced from the less typical orientations of extension veins in right- and left-echelon arrays. Sigma one from conjugate shears trends N56°E.

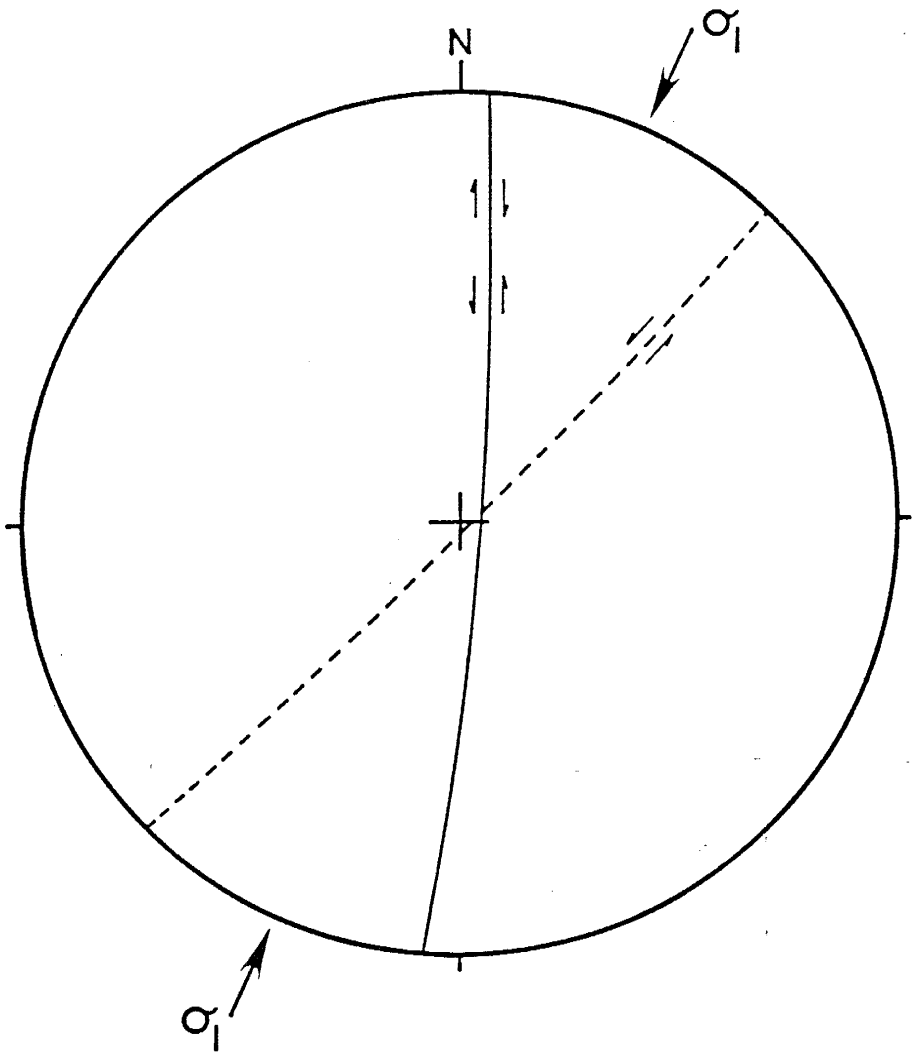


Figure 16c. Synoptic diagram of the most common orientations of right- and left-slip linear extension and shear veins. Solid line represents modal orientations and dashed line represents less typical orientations. Sigma one from conjugate shears trends N25°E.

greater compressional stress, with less compression during development of the modal conjugate shears.

Figure 16c shows a N25 ° E trending axis of compression bisecting a conjugate set of linear extension and shear veins. However, the modal right- and left-slip linear extension and shear veins are in the same orientation. This occurrence is interpreted to be due to jostling of sliver blocks between faults and shear zones experiencing different amounts, or directions, of motion within a wrench zone.

In summary, stereonet analysis of extension and shear veins in the Navajo Gap area reveals a prominent axis of compression trending N22 ° E. This analysis may also reveal a second axis of greater compressional stress trending N51 ° E. The orientations of the shears that reveal these axes of compression are inferred representations of en echelon extension vein arrays and not actual field measurements. However, the stress axis trends are directly related to field measurements and would not change if a different angle (between 15 ° and 45 °) was used to infer shear orientations from en echelon extension veins.

Time-relationships of extensional and shear vein structures may be indicated by transecting, or crosscutting relationships between extension veins (Fig. 17). Intersecting veins were measured in gently dipping strata predominantly in the northern half of the field area. Figures 17a and 17b show the trend relationships between sets of veins with opposing directions of slip and the revealed shear zones on strain ellipses. Veins in Figure 17a crosscut veins in Figure 17b. In Figure 17a, trend mean and standard deviation of right-slip veins are N2 ° W and 10.9 degrees, respectively. The trend mean and standard deviation of left-slip veins are N83 ° E and 12.8 degrees, respectively. Structures in the strain ellipse of Figure 17a are interpreted to be conjugate shears, even though the acute angle is 85 °. The bisecting axis of the acute angle trends N40 ° E. This is interpreted to be the apparent axis of compression that produced these shears.

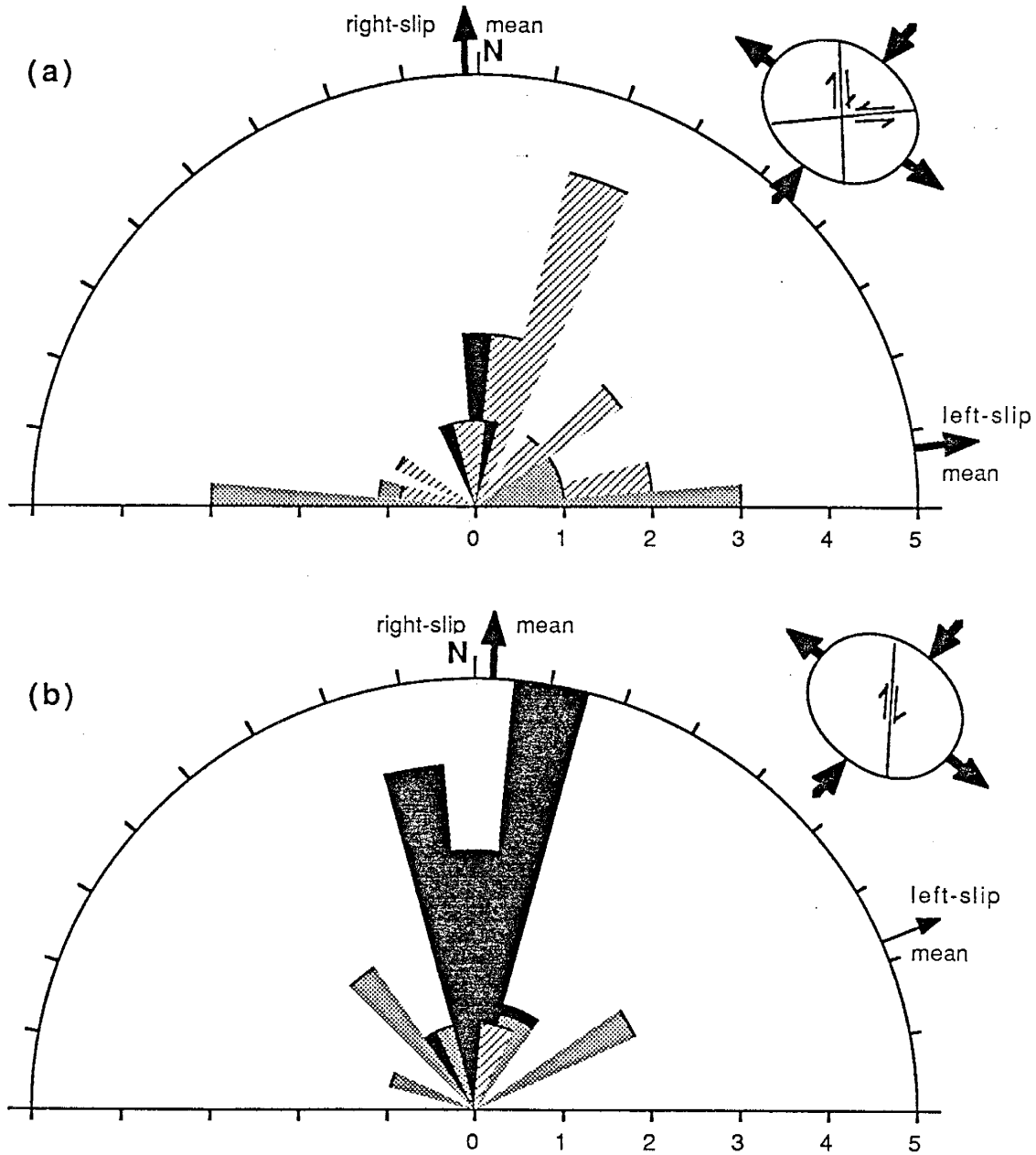


Figure 17. Trend relationships between vein styles. Veins in set (b) crosscut veins in set (a).

Right-slip (R-linear, L-echelon array), (a) number of samples, n = 4, trend mean = N2°W, standard deviation, s.d. = 10.9°. (b) n = 15, trend mean = N3°E, s.d. = 14.2°.

Left-slip (L-linear, R-echelon array), (a) n = 7, trend mean = N83°E, s.d. = 12.8°. (b) n = 8, trend mean = N68°E, s.d. = 54.5°.

Linear w/ unknown shear, (a) n = 15, (b) n = 2.

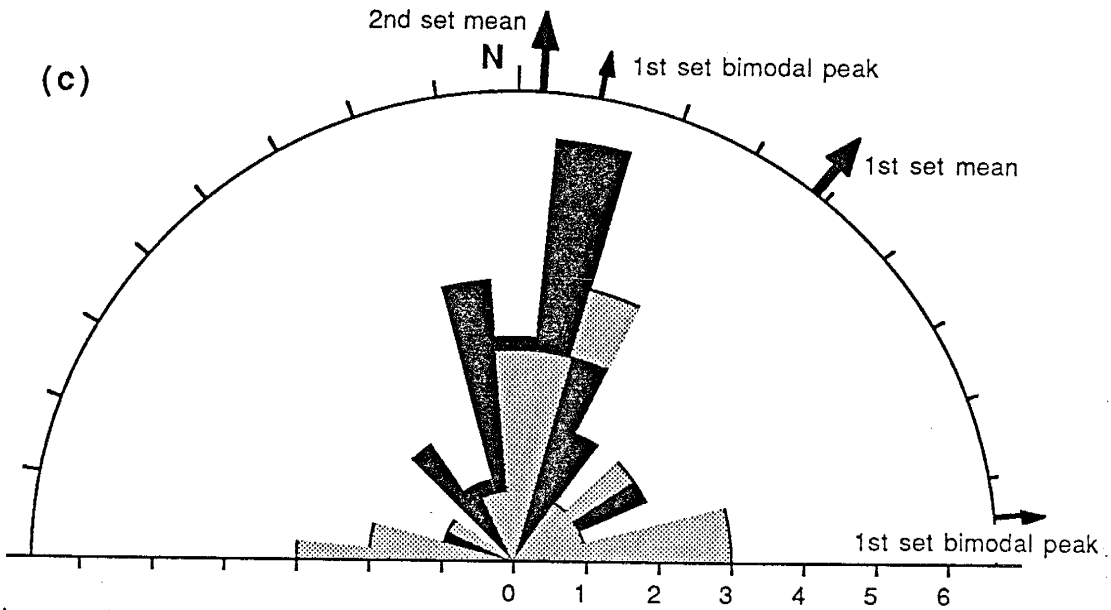


Figure 17. (c) Time-trend relationship between crosscutting veins.
First vein set, n = 26, trend mean = N38°E, s.d. = 42.1°.
Bimodal peaks at ~N10 and 85°E.
Second vein set, n = 25, trend mean = N2°E, s.d. = 28.6°.

In Figure 17b, trend mean and standard deviation of right-slip veins are N2 ° E and 14.2 degrees, respectively. The trend mean and standard deviation of left-slip veins are N68 ° E and 54.5 degrees, respectively. The major structure on the strain ellipse in Figure 17b is interpreted to be a Y-shear, possibly the final shear zone in a wrench fault system. The structures in Figures 17a and 17b were formed in either two unrelated periods of deformation or in two stages of a deformational event.

Figure 17c shows the time-trend relationship between the sets of intersecting veins. In Figure 17c, trend mean and standard deviation of the first vein set are N38 ° E and 42.1 degrees, respectively. This large standard deviation is due to the bimodal nature of the veins in this first set. Bimodal peaks are at trends of approximately N10 ° and 85 ° E. The trend mean and standard deviation of the second vein set are N2 ° E and 28.6 degrees, respectively.

In summary, analysis of crosscuttting extension and shear veins in Navajo Gap reveals two deformation events, or stages within an event, which produced different structural styles. The first event or stage of deformation developed conjugate shears around an axis of compression trending N40 ° E. The right-shear trends N2 ° W and the left-shear trends N83 ° E. The second event or stage of deformation developed right-shears trending N2 ° E. The trend in the axis of compression during the first event or stage is apparent at this point of the study. Through analysis discussed in a later section I have located this axis of compression with greater precision. Incorporation of the summary deduced from the stereonet analysis of extension and shear veins suggests that most of these vein structures in Navajo Gap were formed during the second event or stage of deformation.

Faults and Striations. Appendix I includes the lower hemisphere equal-area stereographic point plots for faults and striations. Figure 18 includes the

contoured lower hemisphere equal-area plots of the diagrams in Appendix I. Included in the contoured plots of Figure 18 are the modal orientations of faults (solid lines) and trend and plunges of striations and, where appropriate, less typical orientations of faults (dashed lines). Figure 18a is the contoured lower hemisphere equal-area plot of poles to right-slip faults. The modal orientation of right-slip faults is N3 ° E and 82 ° E. Figure 18b is the contoured plot of striations in right-slip faults. The modal trends and plunges of striations in right-slip faults are N1 ° W and 12 ° N and S22 ° W and 11 ° S. Figure 18c is the contoured plot of poles to left-slip faults. The modal orientation of left-slip faults is N30 ° E and 85 ° SE. Figure 18d is the contoured plot of striations in left-slip faults. The modal trend and plunge of striations in left-slip faults is N17 ° E and 20 ° N. Figure 18e is the contoured plot of poles to thrust faults. The modal orientation of thrust faults is N20 ° W and 34 ° W. Figure 18f is the contoured plot of striations in thrust faults. The modal trend and plunge of striations in thrust faults is S84 ° W and 8 ° N. Figure 18g is the contoured plot of poles to normal faults. The modal orientation of normal faults is N7 ° E and 82 ° E. A slightly less typical normal fault strike and dip is N7 ° W and 77 ° W. Figure 18h is the contoured plot of striations in normal faults. The modal trends and plunges of striations in normal faults are N87 ° E and 67 ° E and approximately N73 ° W and 84 ° W. Figure 18i is the contoured plot of poles to reverse faults. The small amount of data on reverse faults does not reveal a modal orientation for these structures except possibly N19 ° E and steeply east and west. Figure 18j is the contoured plot of striations in reverse faults. The modal trends and plunges of striations in reverse faults are N78 ° E and 51 ° E, and N78 ° E and vertical. Figure 18k is the contoured plot of poles to faults with indeterminate motion. The modal orientation of these faults is N6 ° E and vertical. Figure 18l is the contoured plot of striations in faults with indeterminate motion. Common trends

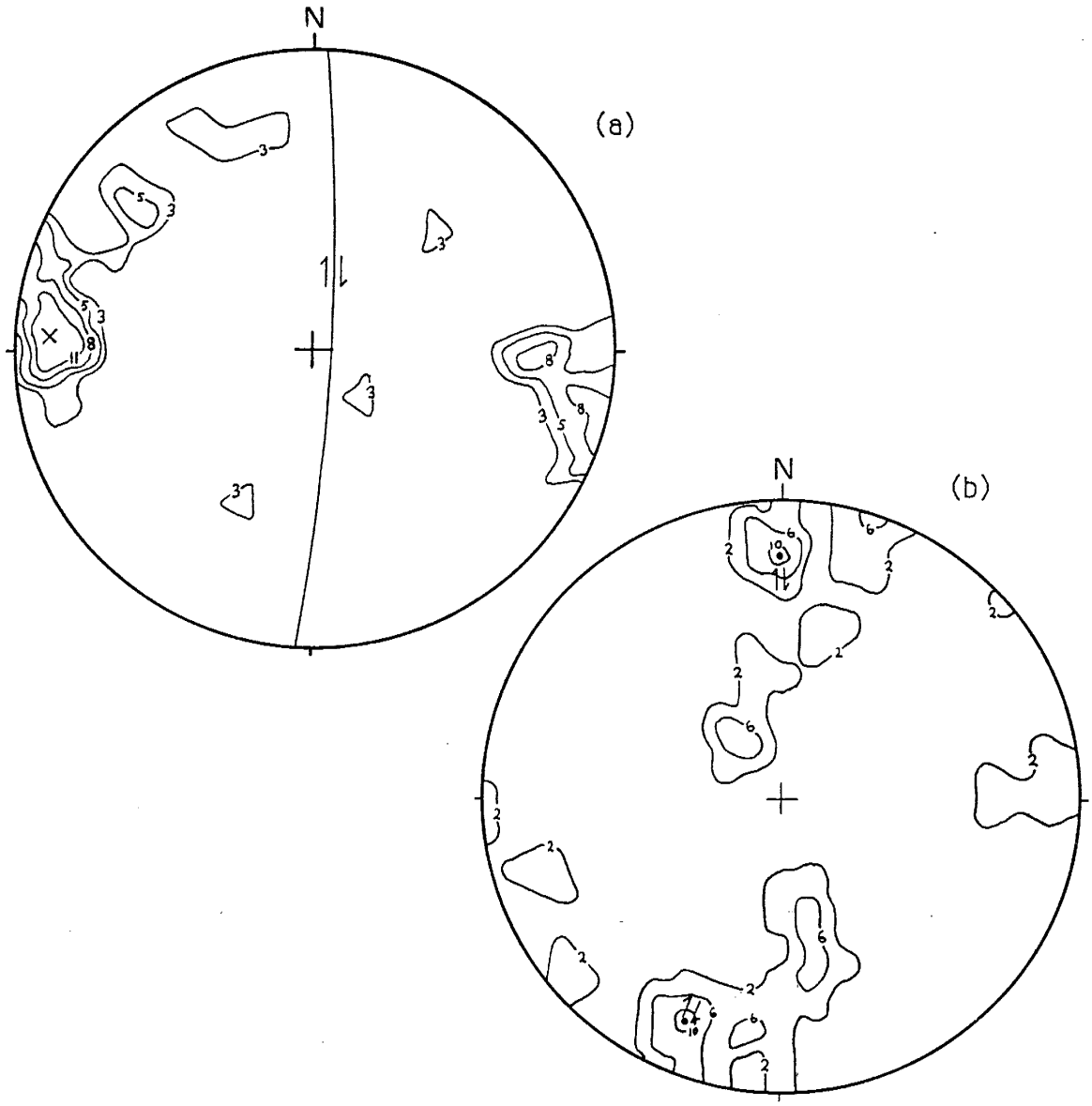


Figure 18. Contoured lower hemisphere equal-area plots of poles to faults, and striation trends and plunges. Contours per 1 percent area.

(a) Poles to right-slip faults, number of samples (n) = 33, maximum (X) 15.2%.

(b) Striations in right-slip faults, n = 26.

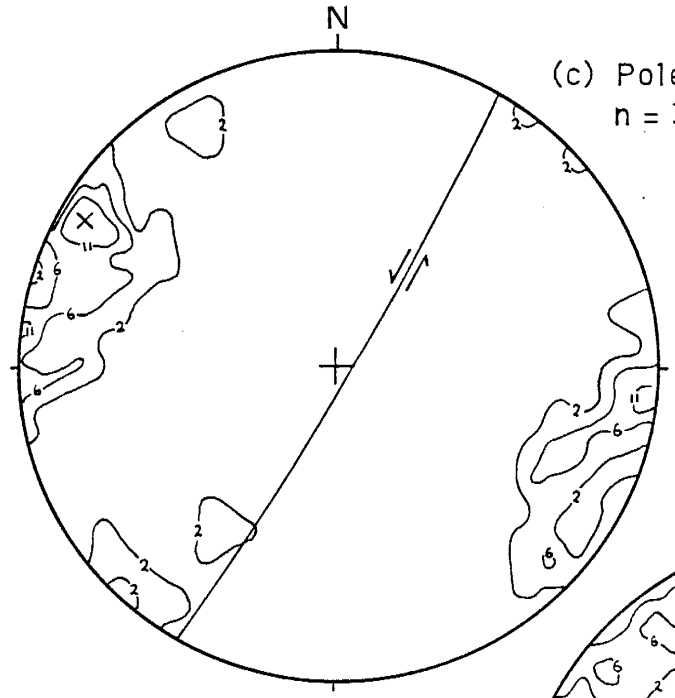


(c) Poles to left-slip faults, n = 30, maximum (X) 20%.

(d) Striations in left-slip faults, n = 27.

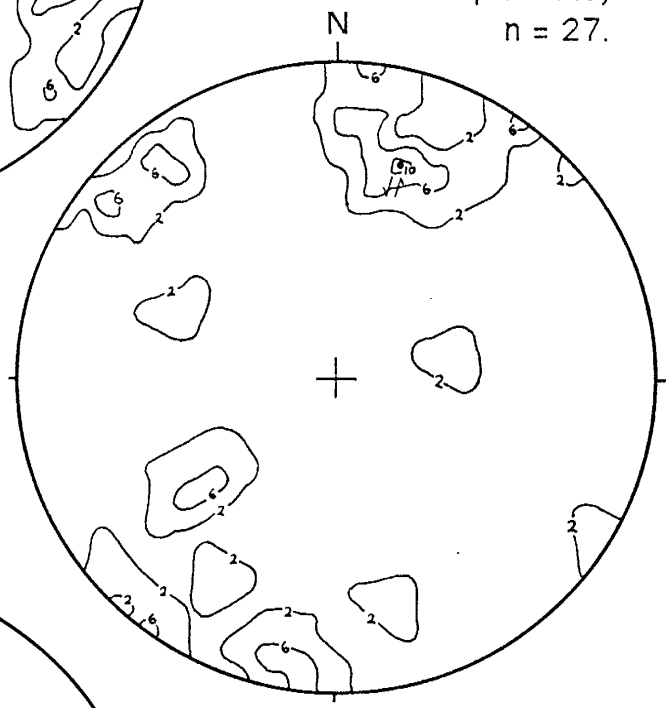


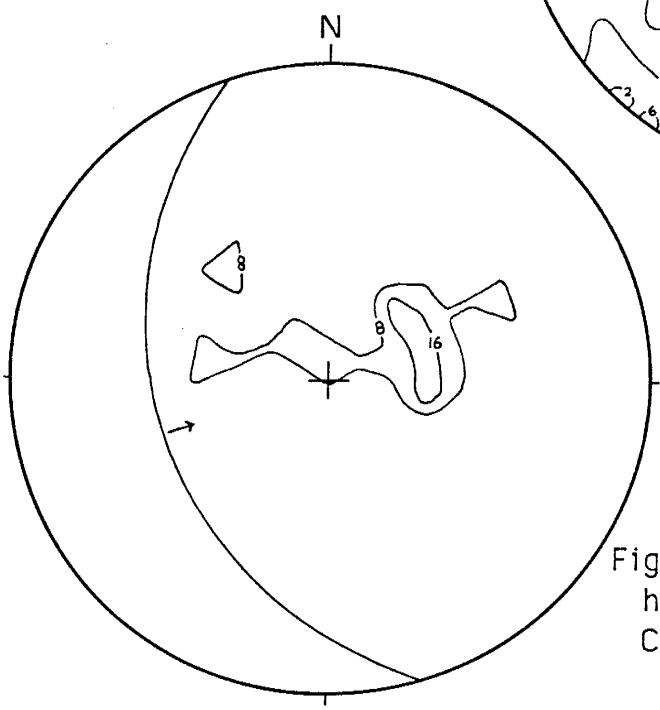


(e) Poles to thrust faults, n = 10.

Figure 18 (continued). Lower hemisphere equal-area plots. Contours per 1 percent area.

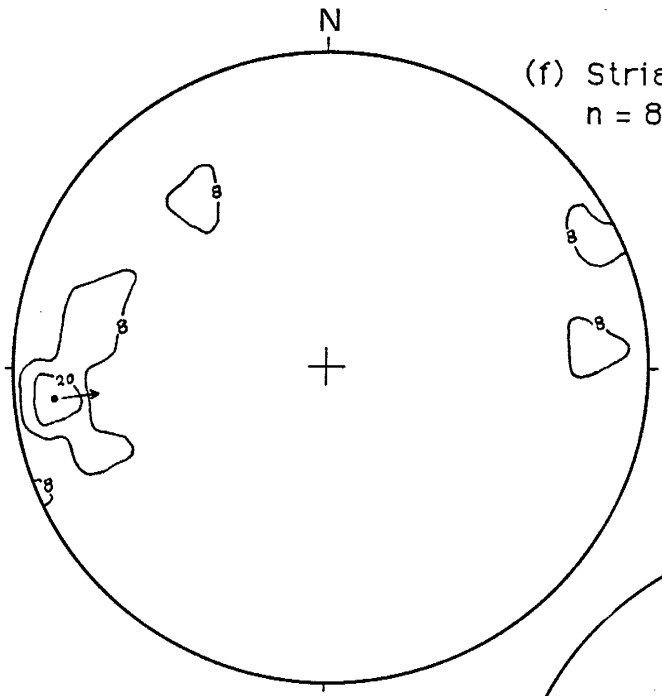


(f) Striations in thrust faults, n = 8.

(g) Poles to normal faults, n = 13. Maximum (X) 23.1%

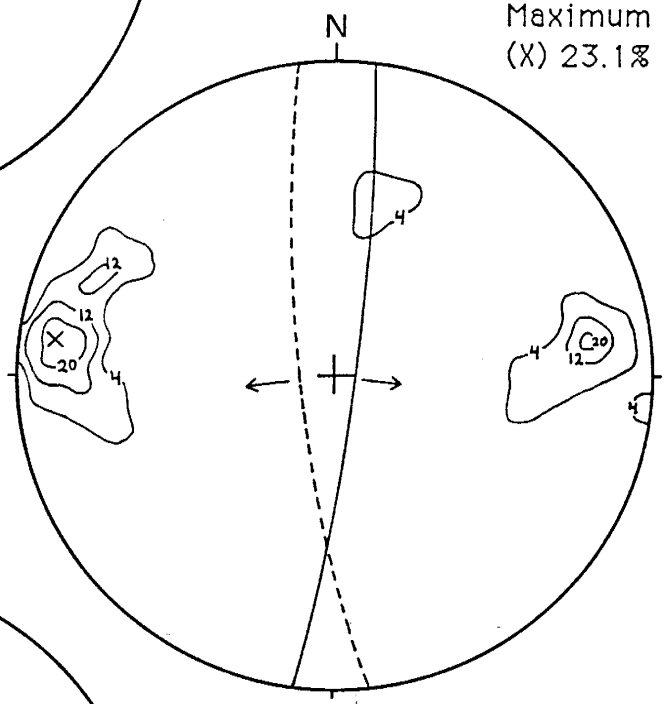


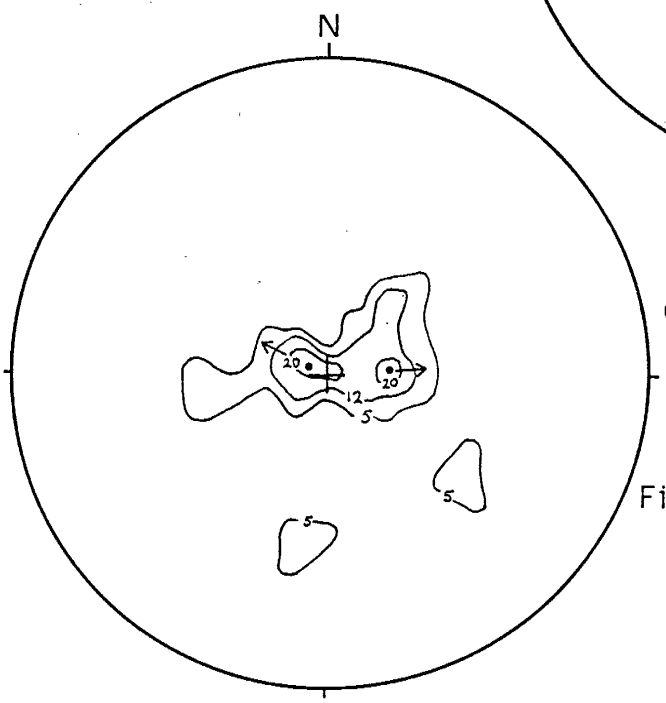


(h) Striations in normal faults, n = 13.

Figure 18 (continued). Lower hemisphere equal-area plots. Contours per 1 percent area.

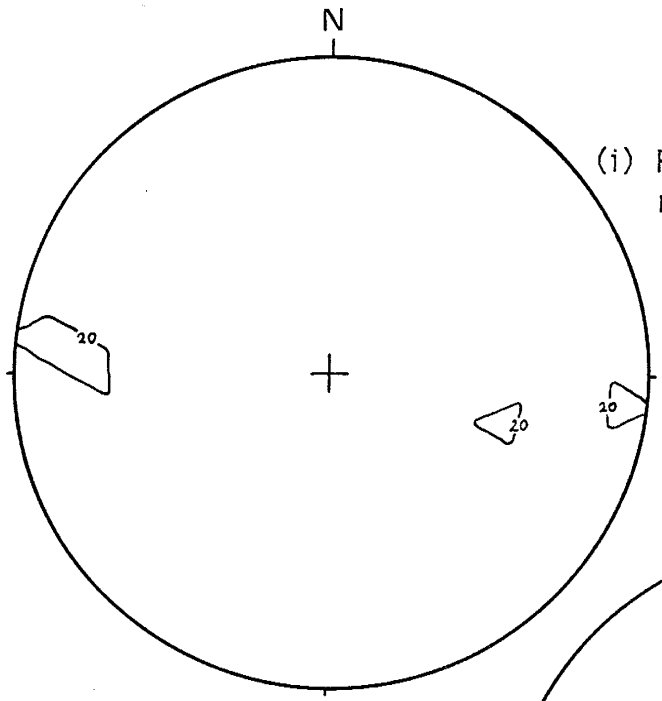


(i) Poles to reverse faults, n = 4.

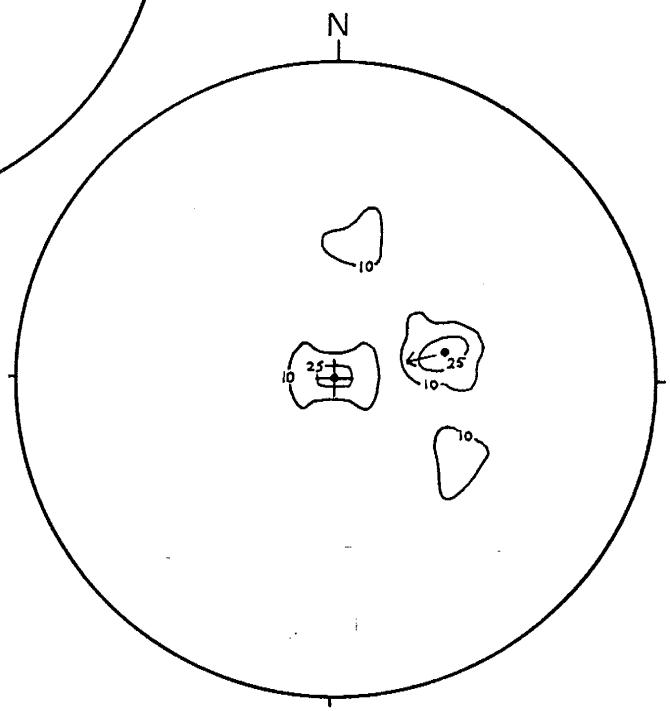


(j) Striations in reverse faults, n = 6.

Figure 18 (continued). Lower hemisphere equal-area plots. Contours per 1 percent area.

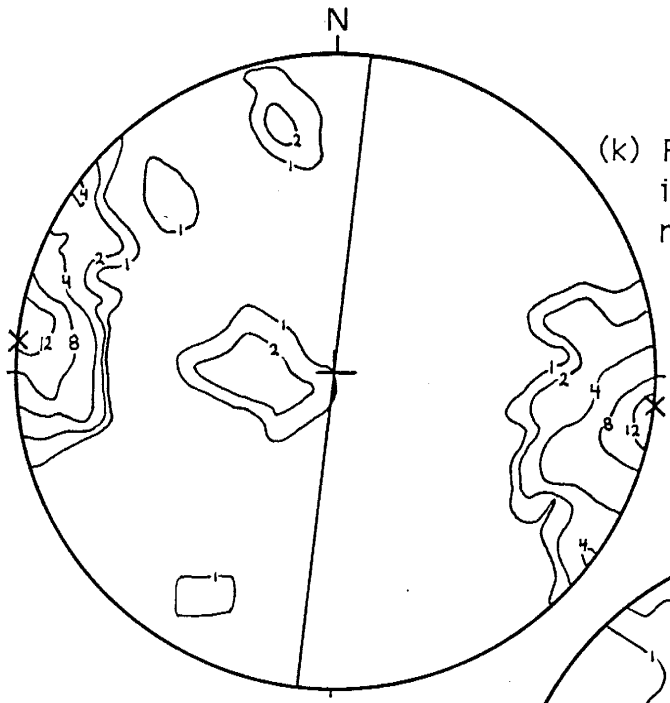


(k) Poles to faults with indeterminate motion, n = 114. Maximum (x) 14%.

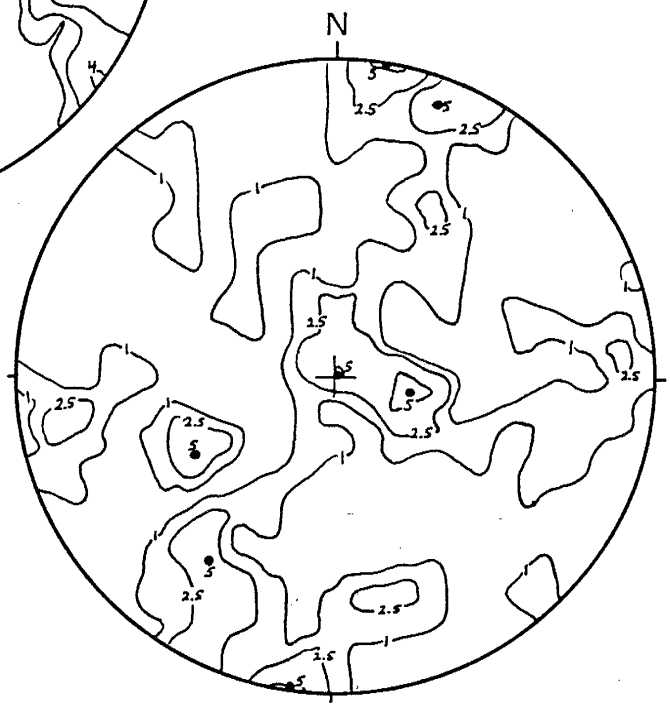


(l) Striations in faults with indeterminate motion, n = 57.

Figure 18 (continued). Lower hemisphere equal-area plots. Contours per 1 percent area.

and plunges of striations in these faults are N9 ° E and horizontal, N21 ° E and 5 ° N, and approximately N55 ° E and 88 ° NE, S79 ° E and 62 ° E, S34 ° W and 19 ° S, and S61 ° W and 36 ° SW.

Summarized on a synoptic diagram (Fig. 19) are the modal orientations of strike-slip and thrust faults, and trends and plunges of striations in these faults. Right- and left-slip faults appear to fall in Riedel and conjugate Riedel shear orientations. Chapin (1987) shows that minor left-slip faulting is expected during rift-related extension. In Navajo Gap, left-slip faulting and lateral shearing has the same nature of deformation as right-slip. Also, in three field locations right- and left-slip faults form interdependent conjugate pairs. Therefore, the right- and left-slip faults shown in Figure 19 are interpreted to form a conjugate set.

An axis of compression trends N17 ° E bisecting these conjugate strike-slip faults. The modal thrust fault strike and dip suggests an axis of compression with an orientation of approximately N73 ° E. Field analysis indicates thrust faults and reverse faults, along with folds, initiated first. With continued thrusting and folding, strike-slip faults developed. Therefore, the interpreted axis of compression from thrust faults occurred before the axis of compression interpreted from conjugate strike-slip faults. The maximum stress axis apparently rotated 56 ° counterclockwise between initial thrust faulting and later strike-slip faulting.

In summary, stereonet analysis of faults and striations indicates a dominance in strike-slip faulting within the Navajo Gap area. Field relationships between right- and left-slip faults, thrust faults, and folds indicates deformation initiated with folding and thrust faulting. Deformation continued with an apparent counterclockwise rotation in the axis of compression from east-northeast to north-northeast. Conjugate strike-slip faults developed with this counterclockwise rotation.

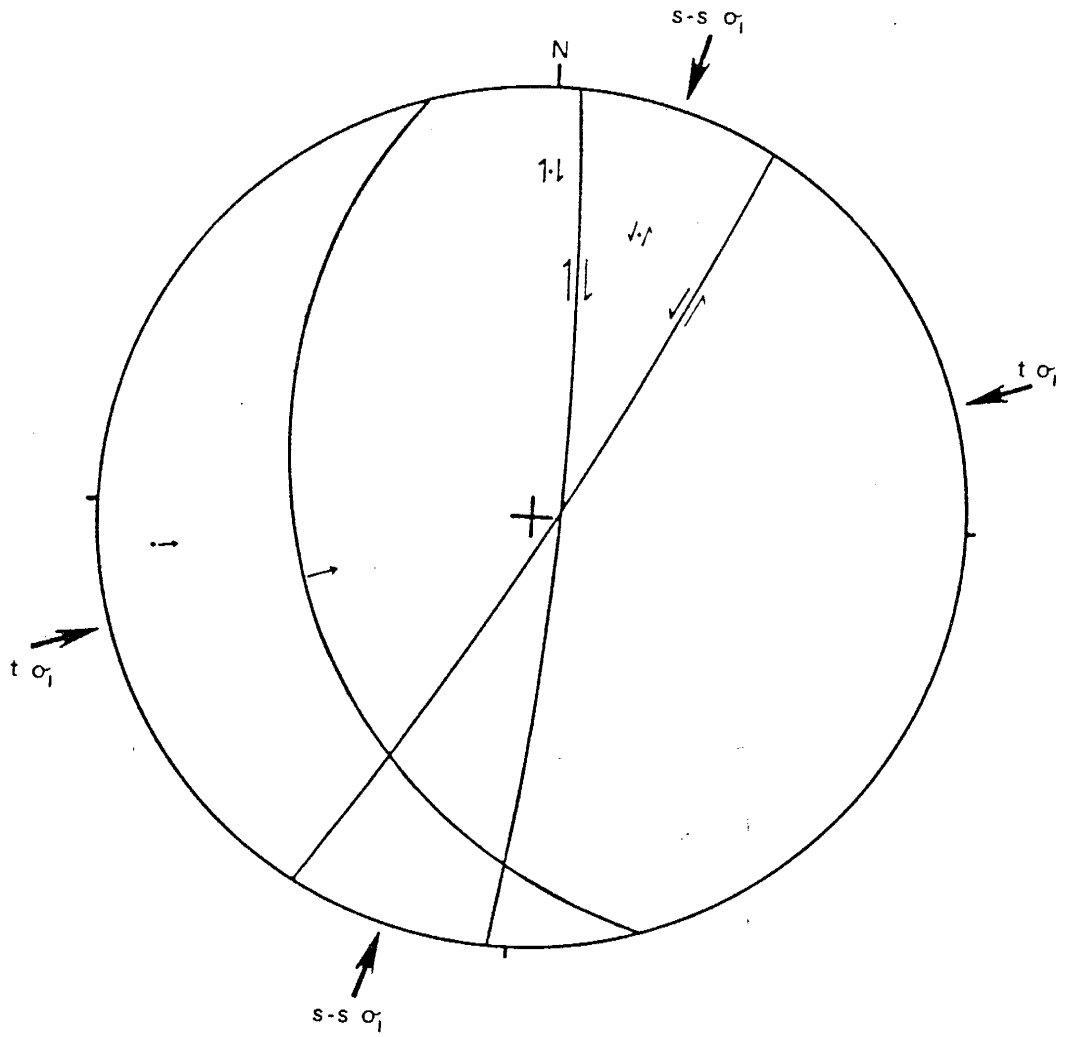


Figure 19. Synoptic diagram of the most common strike-slip faults, thrust faults, and striations in these faults. Maximum principal horizontal stress (sigma one) from thrust faults (t $\sigma_1$) trends N73°E. Sigma one from conjugate strike-slip faults (s-s $\sigma_1$) trends N17°E.

Contoured lower hemisphere equal-area diagrams of normal and reverse faults (Figs. 18g, 18h, 18i, and 18j) suggest a nearly east-west- (N83 ° W) trending axis of minimum principal stress during extensional faulting in the Navajo Gap area. Aldrich and others (1986) indicate that east-west tension occurred throughout rift extension.

Extensional faulting in the Navajo Gap area appears to have been three-stage. In one stage, north- to north-northeast trending mafic dikes were emplaced. In another stage, east-west regional tension produced north-south striking and steeply east and west-dipping extensional faults. These faults are represented in Figure 18g. In a third stage, northeast-southwest local tension formed a northwest-southeast striking fault zone (Saiz fault zone) dipping gently to moderately northeastward.

Seager (1981), Chamberlin (1983), and Morgan and others (1986) suggest that early-rift extensional faults rotated to low-angles during rifting. They also suggest that late-rift extensional faulting is high-angle. The stages of extensional faulting in the Navajo Gap area can not be described as early or late-rift by the dip of the faults.

The high-angle, north- to north-northeast-striking tension faults are locally buried by upper Santa Fe Group gravels. This suggests that these extensional faults are late-rift (Pliocene-Pleistocene). But these faults appear to be intruded locally by mafic dikes, suggesting an early-rift (late Oligocene-early Miocene) age. However, one of these dikes is brittlely fractured and both the dikes and extensional faults are presumed to follow previously established structural trends. Therefore, the dikes record early-rift, west-northwest--east-southeast extension and the faults are most recently late-rift.

No striations were found on the Saiz fault proper. This major fault cuts strike-slip-related structures. Field evidence does not show the Saiz fault

displacing other extension faults. The approximate strike of Saiz fault, N40 ° E, suggests an extension orientation of northeast-southwest. However, this orientation reflects the control of preexisting structures and can not be interpreted as a rift-related stress.

Normal faults may also occur in wrench zones parallel to the axis of compression (Fig. 10). In Navajo Gap, most of the normal faults are oriented counterclockwise from the interpreted axis of compression. Therefore, these normal faults are not tension induced structures within a wrench zone and the Navajo Gap area was extended in an east-west direction.

In summary, the mafic dikes record early-rift (late Oligocene-early Miocene) extension. The north-south-striking tension faults are interpreted to be late-rift (Pliocene-Pleistocene). The northwest-striking Saiz fault is interpreted to have developed sometime between early- and late-rift.

Problems. A number of problems and difficulties developed during the above analyses. One problem that could prove to be major is that the analyzed structures may have been produced by secondary stresses, not primary or principal stresses. Secondary, and even tertiary stresses, may have developed in overlying strata as weaknesses in basement structure were reactivated during deformation. If a planar zone of weakness in the basement is oriented within 60 ° of the direction of compression, shearing will probably occur along it. This shearing sets up local stresses in the overlying strata secondary to the principal stress. Secondary stresses produce second-order structures. Structural weaknesses underlying upper Paleozoic strata in the study area are not exposed. However, structures in the Proterozoic rock of the Ladron Mountains trend north-northeast (Taylor, 1986) while other structures trend northwest and east-west (Condie, 1976).

During my analyses, I assume that the extension and shear veins, and faults

and striations in the Navajo Gap area were produced by primary stress and that the basement is homogeneous and isotropic. I know, however, that the Proterozoic basement is heterogeneous and anisotropic. Therefore, the analyzed structures may be second-order, produced as reactivated basement structures developed local secondary stresses in the overlying upper Paleozoic strata.

Age of the deformation that produced most of these structures is uncertain. In the field, the only relative-time relationships I found in structures were between extension veins (Fig. 17). By comparing the stresses suggested from the analyses of extension veins and faults and striations to previously documented, or theoretical, tectonic stress regimes for the regional area, one may be able to indicate an approximate age of deformation. These problems are addressed in the discussion following analysis of fibrous crystals in extension veins.

## Fibrous Crystals in Extension Veins

Within faults, fault zones, and shear zones are meso and microstructures useful as kinematic indicators. These indicators are extension veins, shear veins, and the fibrous crystal systems in these veins. From the orientations of fibrous crystals in extension veins it is possible to calculate principal stress directions, progressive strain or strain sequences, and incremental strain at the time the vein formed (Ramsay and Huber, 1983). Using techniques for analysis of fibrous crystal systems (Hancock, 1972; Ramsay, 1980; Ramsay and Huber, 1983), I have found relicts of principal stresses produced locally during strike-slip and lateral shear deformation in the Navajo Gap area.

Introduction. Mechanical cracking initiates perpendicular to maximum incremental strain at the time of initial deformation (Ramsay and Huber, 1983). Cracks continue to open in a direction normal or oblique to their walls. They

open in an oblique direction if a change in the orientation of progressive incremental strain occurs (Ramsay and Huber, 1983). Two points, in contact before crack development, move away from each other in the direction of maximum longitudinal strain. With continued rotation in progressive incremental strain, initial cracks may propagate in a different orientation, or new cracks may form cutting across older ruptures (Ramsay and Huber, 1983, fig. 13.1). Intersecting cracks may delineate a progressive change in stress orientation or represent unrelated periods of deformation (Ramsay and Huber, 1983).

Cracks develop into veins as crystalline material is precipitated within them from aqueous solution. As an extension crack opens, fibrous crystals grow parallel to the displacement direction of the crack surfaces (Wickham, 1973). In other words, a fibrous crystal grows in the direction of vein wall movement, the direction of extension. Fibrous crystals connect points on the vein wall that were initially in contact (Ramsay and Huber, 1983; Fig. 20a and 20b). Therefore, the orientation of a fibrous crystal is a relict of the orientation of maximum longitudinal strain at the time that crystal grew. If the plane containing the vein is vertical and the fibrous crystals are horizontal, then the longitudinal normal to the fibrous crystal trend is the minimum longitudinal strain, or the orientation of maximum principal horizontal stress (Fig. 21). Linking a progression of stress directions, derived from cross-cutting veins or curved fibrous crystals, leads to the development of a progressive strain sequence.

Fibrous crystals are straight or curved. During progressive deformation, crystal fibers are curved if strain orientations rotate during crystal growth (Ramsay and Huber, 1983). A constant crystallographic orientation throughout the curved fiber indicates that the curving was not a result of mechanical deformation (Ramsay and Huber, 1983). A fiber that is curved due to mechanical deformation does not have constant crystallography throughout the fiber length

Figure 20. Photomicrographs of extension veins containing "stretched" fibrous crystals.

(a) Fibrous crystals under polarized light. Crystallographic continuity of fibers is best seen where the "wide" oblique vein cuts two other "wide" veins. Long axis of photograph is 6 mm in length.

(b) Fibrous crystals under nonpolarized light. Extension vein cuts a fusulinid. Long axis of photograph is 1.3 mm in length.

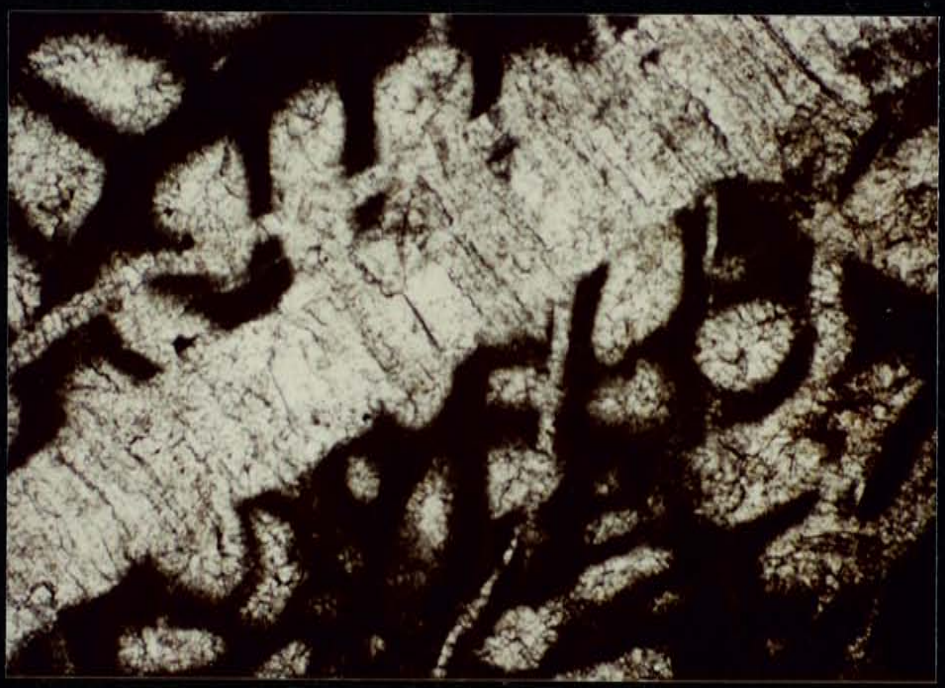

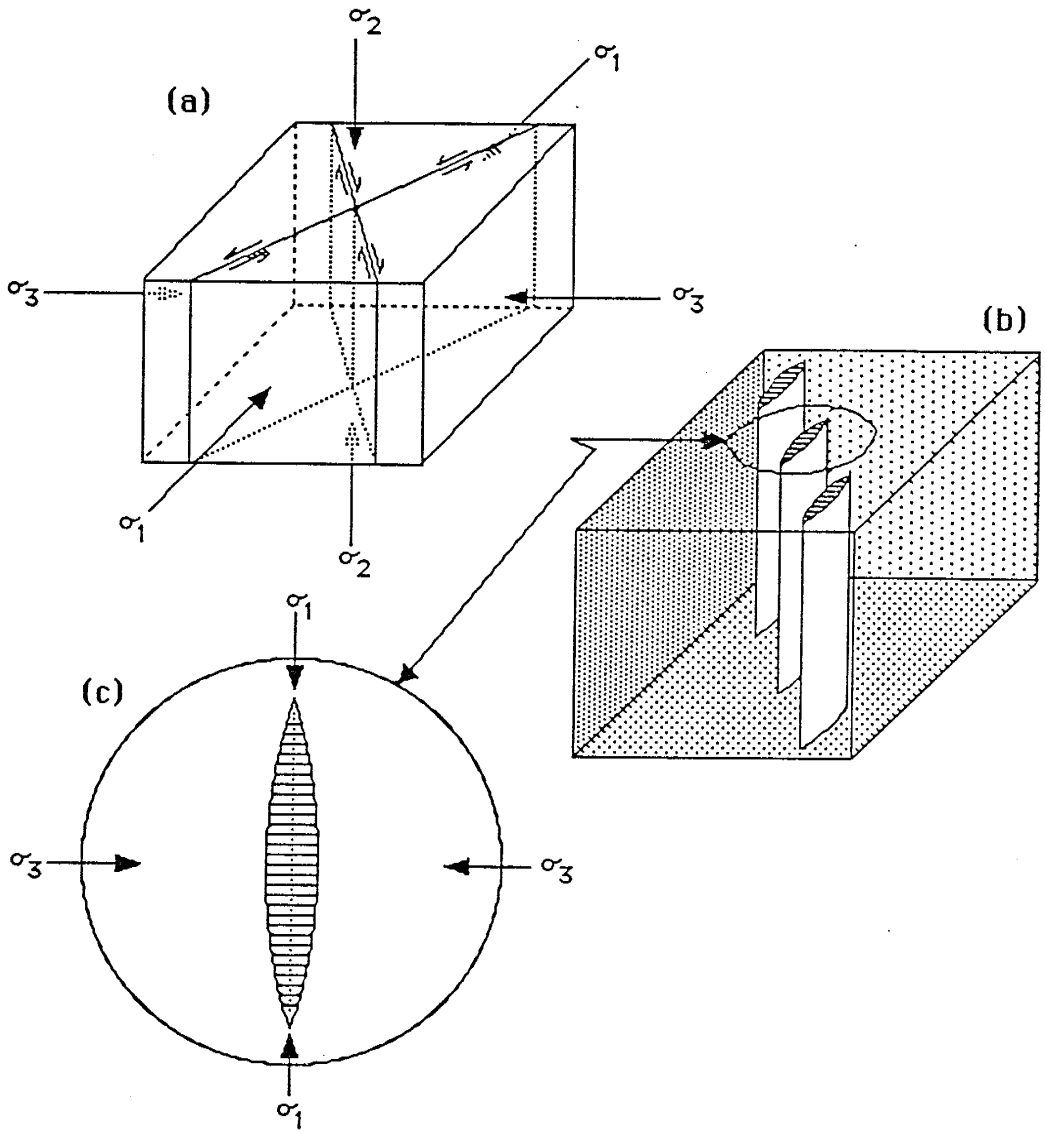


Figure 21. (a) Block diagram of strike-slip stress system with relationship between principal stresses ( $\sigma_1 > \sigma_2 > \sigma_3$ ) and conjugate shears. (b) Block diagram of Left-echelon vein array. (c) Schematic plan view of extension vein with intermal fibrous crystals and relationships to maximum and minimum principal stress orientations.

(Ramsay and Huber, 1983). The orientation of a section of a curved fiber represents an increment of growth, and also an increment of strain during progressive deformation.

Ramsay and Huber (1983) describe four types of vein-filling fibrous crystal systems: syntaxial, antitaxial, composite, and "stretched" (Fig. 22). Briefly, syntaxial crystal fibers grow from vein wall to center of veins and are compositionally similar to the vein wall. Antitaxial crystal fibers grow from vein center to vein wall and are compositionally different than the vein wall. Composite fibrous crystal systems incorporate syntaxial and antitaxial crystal fibers in separate zones within one vein. "Stretched" crystal fibers have an irregular growth location and are compositionally similar to the vein wall (Ramsay and Huber, 1983). The growth progression of "stretched" crystal fibers is indeterminate (Ramsay and Huber, 1983). In Navajo Gap, data was collected from veins in limestone; the fibrous crystals consist of calcite. All vein fibers are in the "stretched" crystal systems. Most veins contain straight crystal fibers and cross-cutting relationships indicate increments. Where crystal fibers are curved, the direction of crystal growth is seen with an increase in fiber width. The increase in width is the result of a more favorable crystallographic orientation for growth at the expense of neighboring crystal fibers. A section of a curved fiber represents an increment of strain. However, because all fibers collected in Navajo Gap were found to be in the "stretched" system, increments of growth cannot be determined from curved fibers (Ramsay and Huber, 1983).

Direct measurement of strain increments, from fibrous crystal systems in extension veins, is based on a method described by Ramsay and Huber (1983, pp. 250-251, fig. 13.24; Fig. 23). Incremental strain relates fiber orientation to the amount of strain for different fiber orientations in a sample. Amount of strain is simply the longer the crystal fiber, the greater the strain.

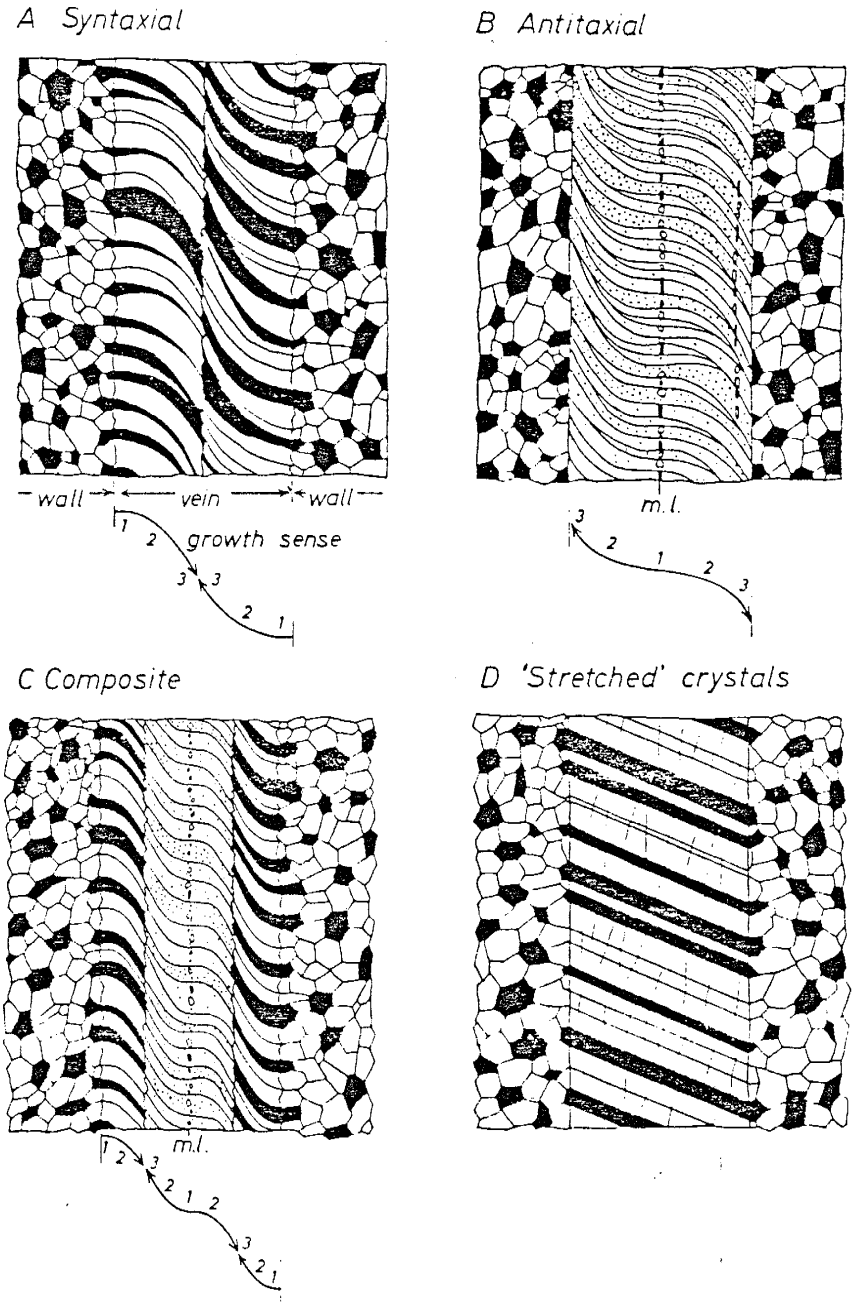


Figure 22. Schematic representations of the four fibrous crystal systems. The black and white areas are crystals with the same mineralogy but with different crystallographic orientations. Stippled crystals are of a different mineralogy with stipple intensity indicating their crystallographic orientations. From Ramsay and Huber (1983).

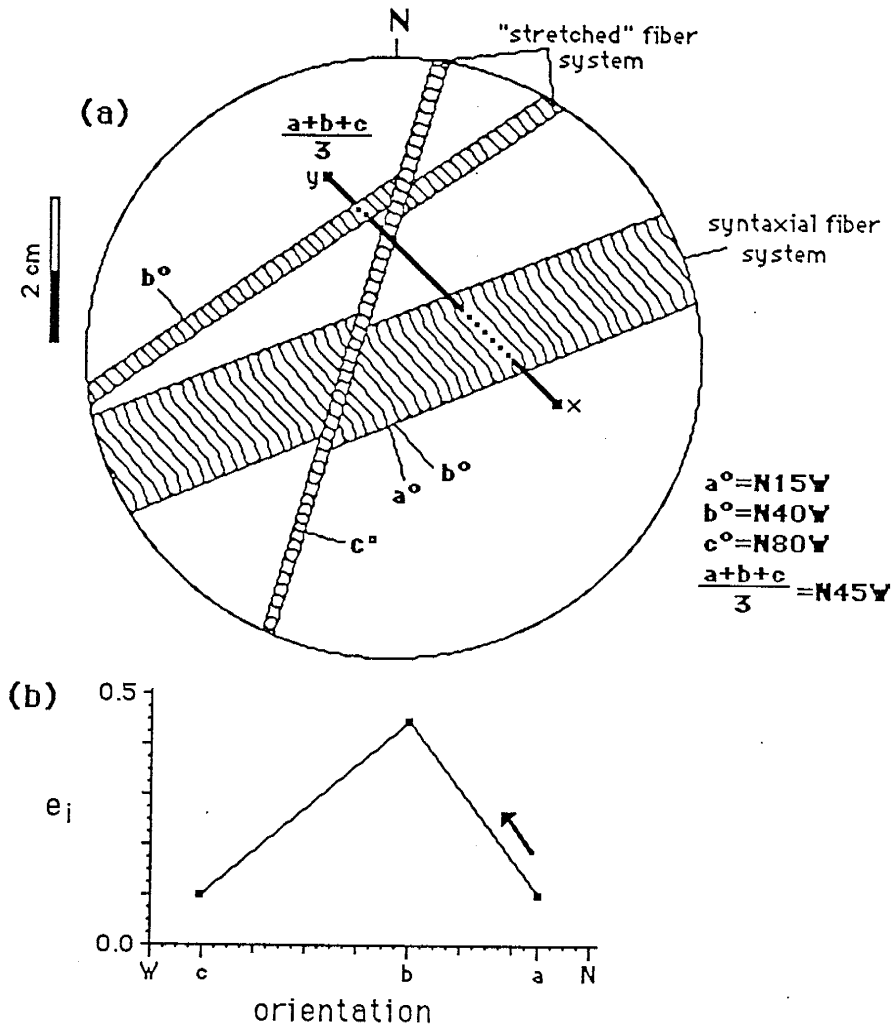


Figure 23. (a) Schematic representation of a vein sample and the techniques for the measurement of incremental strain. The fixed line (x-y) is oriented in the average trend of the three sets of crystal fibers. For the crystal fibers with trend **b°**, incremental length ($\delta L$) is measured along the dotted segments of line x-y. The existing length (l), or length of wall rock and any vein fibers formed before the increment being measured, is measured along the solid segment of line x-y.

(b) Graph showing strain history of the schematic sample, where Incremental strain; $e_i = \frac{\Sigma \delta L}{\Sigma l}$. Based on Ramsay and Huber (1983, pg. 250-251, fig. 13.24).

Analysis. Classification of extension veins (Fig. 11) was discussed for the previous structural analysis. For petrographic analysis of fibrous crystals in extension veins, extension veins were the major component of analysis with shear veins aiding in the understanding of progressive strain rotation.

A few oriented samples were collected by hand, but most were collected with a rock drill. Only veins found in non-folded areas were studied. Dip of strata containing the veins is equal to or less than 12°. The dip of strata was not removed during analysis. The long axes of veins in en echelon arrays, and the planes containing linear veins, are nearly perpendicular to bedding. Thirteen oriented thin sections were prepared for analysis. Three were not used due to duplication of vein sampled or poor quality. Data measurements from each vein in a sample include: (a) vein trend; (b) vein type (extension, shear); (c) sense of slip (right, left, normal (no slip)); (d) fibrous crystal trend; (e) normal to fibrous crystal trend; and (f) timing determined by cross-cutting relationships, progression in growth of curved crystals, or logical development during a rotating stress regime (Appendix J). For study of incremental strain measurements were taken on (a) the length of a crystal fiber increment measured along a fixed line oriented parallel to the average trend of all crystal fibers in a sample ($\Sigma dl$), and (b) the length of wall rock and any previously measured fibers along the fixed line ($\Sigma L$).

Each thin section contains three to nine separate veins. Veins are described as right- or left-shear, and right-, left-, or normal-extension. Due to the scale of thin sections, no distinction was made between linear and en echelon patterns. A total of twenty one extension veins with right-slip (right-extension), twenty five extension veins with left-slip (left-extension), four normal-extension veins, five right-shear veins, and four left-shear veins were analyzed in the ten thin sections.

Appendix J includes thin section data and sample drawings. Appendix K

includes a series of half-circle trend diagrams depicting the data collected in Appendix J. For each thin section, the two half-circle trend diagrams show: (a) vein types, vein trends, and vein timing; and (aa) the progression in trends of maximum principal stress derived from the extension veins. By viewing together the two diagrams of one sample, one can recognize how a rotating stress regime causes new veins to form in different orientations and/or with different natures of slip.

Appendix L includes summaries of the relationships between vein trends and fibrous crystal trends. Compiled on half-rose diagrams, the summaries show the relationships between the trends of fibrous crystals and the trends of (a) right-extension veins, (b) left- extension veins, (c) normal-extension veins, (d) right-shear veins, and (e) left-shear veins.

Incremental strain analysis involves drawing a line across the veins, on the surface, or a picture of the sample to be analyzed, in the average orientation of all crystal fiber trends (Ramsay and Huber, 1983). Strain during an increment of growth (ei) is measured along this line by dividing the sum of the lengths of similar trending fiber increments ($\Sigma dl$) by the sum of the lengths of wall rock and any previously measured fiber increments ($\Sigma L$) (Ramsay and Huber, 1983; Fig. 23). Plotting incremental strain versus increment orientation can reveal increasing, decreasing, or no change in amount of strain during the vein development (Appendix L). Incremental strains are relative only to other veins in a sample. Rates of strain in a sample are not relative to rates of strain in another sample.

Field measurements of fibrous crystals in extension veins consisted of (a) trend of veins, (b) trend of en echelon arrays, and (c) trend of fibrous crystals. Twenty two linear right-extension veins, seven linear left-extension veins, six left-echelon veins, and two right-echelon veins, all containing fibrous crystals, were

analyzed. Appendix M is four half-rose diagrams displaying the above data. Only veins found in non-folded areas were studied. Dip of strata containing the veins is equal to or less than 12 degrees. The dip of strata was not removed during analysis. All veins are nearly perpendicular to bedding.

Stress Regime From Thin Sections. From earlier discussion, the longitudinal normal to fibrous crystals, in extension veins collected in vertically oriented shear zones, is taken to be the direction of maximum principal horizontal stress (sigma one). Figure 24 summarizes all the sigma one's observed in thin section. Mean trend of this stress is N49 ° E with a standard deviation of 34.0 degrees. Since there are two or more increments of strain observed in each sample, I compiled a summary of only the first and final increments observed in all samples (Fig. 25). In Figure 25, mean trend and standard deviation of the initial sigma one's are N60 ° E and 30.3 degrees, respectively. Mean trend and standard deviation of the final sigma one's are N21 ° E and 15.8 degrees, respectively. From Figure 25, I see that the deformational event that produced these vein structures initiated with the direction of maximum principal horizontal stress oriented N60 ° E. This episode of deformation ended with the direction of maximum principal horizontal stress oriented N21 ° E. This 39 ° counterclockwise rotation was apparently progressive and not an immediate shift in maximum principal stress. This is suggested in Appendix K where the maximum principal horizontal stress diagrams include stress axes between the end members. Some samples show a counterclockwise rotation of 20 to 45 ° followed by clockwise rotation of 2 to 10 ° and continued counterclockwise rotation. Scatter in the data is believed to be due to mechanical rotation of veins and crystal fibers in strongly deformed shear zones. Thin sections 8a, 9a, and 13e are from samples collected in strongly sheared areas and are the samples that produced the scatter.

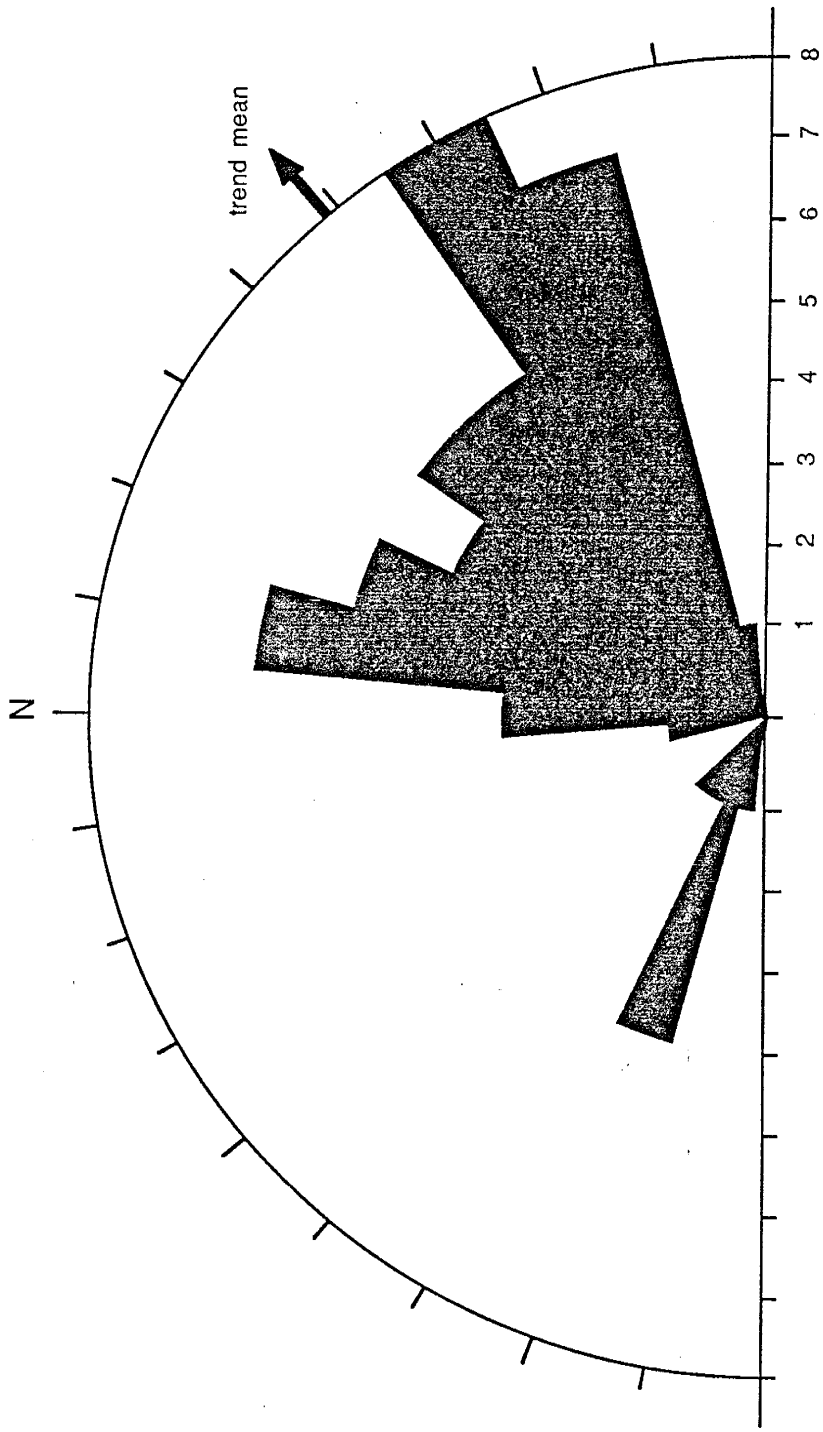


Figure 24. Summary of maximum principal stresses observed in thin sections.
Number of samples = 52, trend mean = N49°E, standard deviation = 34.0°

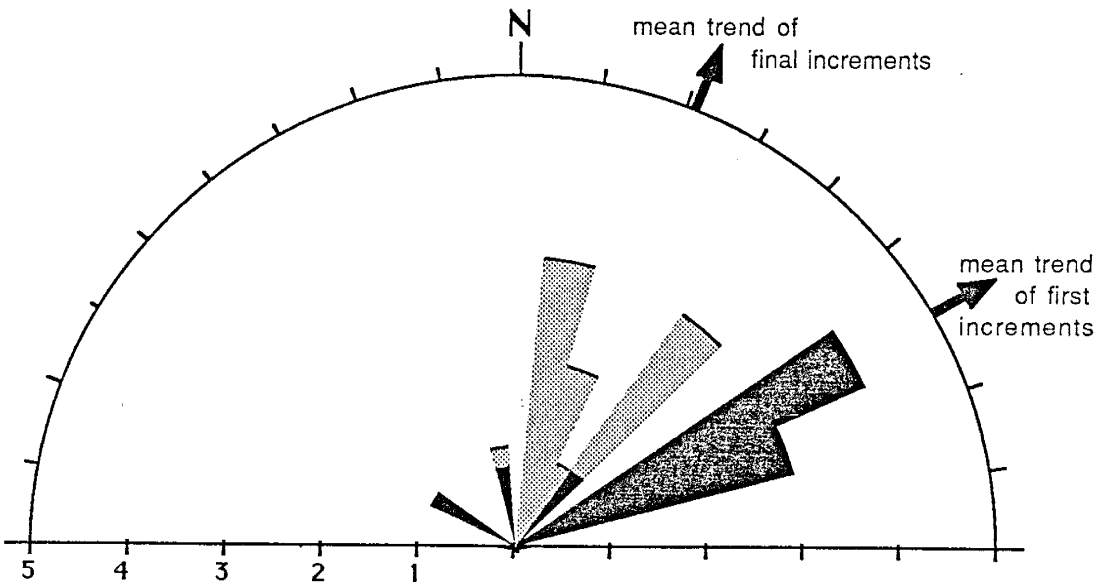


Figure 25. Summary of the first and final trends in maximum principal stress observed in thin sections.

First maximum principal stress increments. Number of samples = 10, trend mean = N60°E, standard deviation = 30.3°.

Final maximum principal stress increments. Number of samples = 10, trend mean = N21°E, standard deviation = 15.8°.

In summary, thin section analysis of fibrous crystal systems in extension veins in the Navajo Gap area indicates that the deformation that produced these structures initiated with the direction of maximum principal horizontal stress oriented N60 ° E. Deformation continued during a 39 ° counterclockwise rotation of the maximum principal horizontal stress.

Incremental Strain. The measurement of data for the analysis of incremental strain was discussed briefly in a previous section. Appendix N includes the plots of incremental strain versus orientation of crystal fibers for each thin section and accompanying sets if necessary. These graphs show an increase or decrease in amount of strain and any change in the orientation of the strain axes during a rotating stress regime for a sample. Although vague similarities exist between two or more samples, I don't think a summary of this small collection of data would reveal any general trends other than the counterclockwise rotation of strain axes. Also, I constructed the graphs in Appendix N before I recognized that all the crystal fibers are in the "stretched" crystal fiber systems. Therefore, the graphs for thin sections 1a, 3a, and 9a may not be correct because these contain measurements of curved crystal fibers.

Stress Regime from Field Data. Figure 26, a summary of field data on extension veins and fibrous crystals (Appendix M), shows the longitudinal normal to fibrous crystals measured in the field. Maximum principal horizontal stress has a mean trend of N15 ° E and a standard deviation of 20.1 degrees in this diagram.

Problems. A number of problems and difficulties developed during the above analyses. Discussed in the previous structural analysis is the major problem concerning the possibility that some, or all, of the analyzed structures were produced by stresses secondary to the principal stress. Similar problems of dating the deformational event that produced these structures occurs.

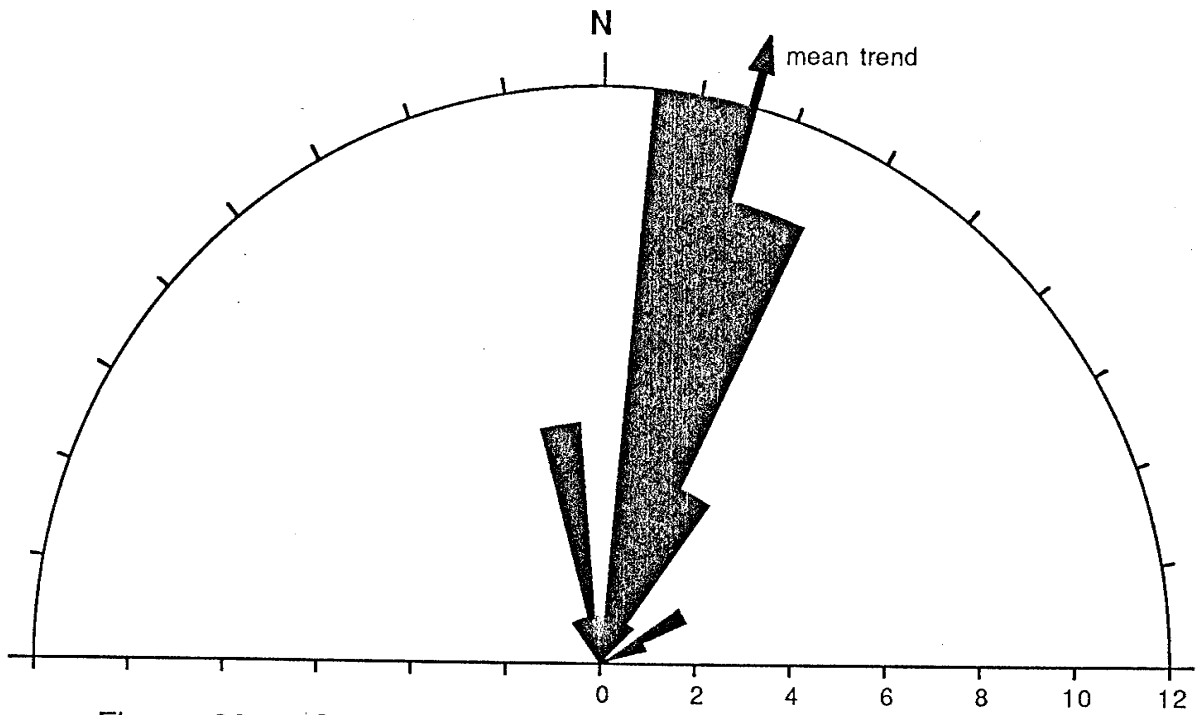


Figure 26. Summary of maximum principal stresses observed in the field. Number of samples = 38, mean trend = N15°E, standard deviation = 20.4°.

Concerning fibrous crystal systems in extension veins, a problem occurs when one considers if these structures develop in an extensional normal faulting regime. Assuming they do, then one must account for the nature of deformation in which the vein formed, i.e. was the deformation strike-slip or extensional faulting? The nature of deformation is revealed in the field.

What is the rate of crack opening and the rate of crystal growth within the resulting pore? Rapid crack opening and influx of hydrothermal or meteoric fluids can result in development of drusy or equant mineral crystals (Nicholson and Ejiofor, 1987). A large majority of veins in the field are filled with equant calcite crystals. But I did not determine if these crystals were primary or secondary. Fibrous crystals may also fill a rapidly opened crack (C.M. Cather, personal communication, 1987). However, a medial line indicating the end of crystal growth would occur in more or less the central plane of the vein. Medial lines were not found in the samples analyzed. Slow crack opening may allow minerals to precipitate repeatedly at the same location forming an accicular habit.

Analysis of petrographic data is limited because there are few samples. Sampling did not uniformly cover the map area, and few third-dimension observations were made of the veins.

## Discussion

Since extension veins and faults in the upper Paleozoic strata of Navajo Gap are probably influenced by Proterozoic basement structures, I will assume that the prominent north- to north-northeast-trending extensional faults, strike-slip faults, and lateral shears in Navajo Gap are related to planes of structural weakness in the basement. If a N60 $^{\circ}$ E directed horizontal compression is imposed across the assumed trend (north to north-northeast) in basement weakness, structures that would most likely be produced in overlying, and presumed previously undeformed

strata would probably be (a) N40 ° W trending folds and thrust, (b) N30 ° E trending Riedel shears, (c) east-west-trending conjugate Riedel shears, and (d) possibly north to north-northeast-trending right-slip faults and shears as basement weaknesses are reactivated. Other than the possible north to north-northeast-trending right-slip faults and shears, the orientations of these structures are primary to the N60 ° E trending maximum principal stress. These structures are very close to what I have interpreted, from field and structural analyses, as early compression-structures, except most thrust faults strike N10-20 ° W (Fig. 19) and most Riedel shears trend nearly north-south (Fig. 17a). These north-south-trending Riedel shears are either primary P-shears and not Riedel shears (Fig. 10), or are second-order shears caused by secondary stresses set up in overlying strata as the assumed basement structures were reactivated.

As the N60 ° E axis of compression rotates counterclockwise to N21 ° E, the stress regimes Riedel shear crosses the inferred north- to north-northeast-trending basement weakness. When this occurs, basement structures are reactivated setting up secondary stresses in the overlying strata. Therefore, the north-northeast-trending, right-slip, late-structures may be second-order, while the conjugate shear, early-compression structures may be first-order.

Assuming that the structures in Navajo Gap were not influenced by basement weaknesses, both early and late structures may be interpreted as first-order. Early-compression structures (conjugate shears, folds, and thrust faults) are first-order as interpreted above. Late-strike-slip structures may be interpreted as "Riedel within Riedel" structures as described by Tchalenko (1970). However, the Proterozoic basement is heterogeneous and structurally anisotropic. Therefore, I assume that basement structures influenced the structures in Navajo Gap.

Dating the age of deformation that produced many of the analyzed structures (infilling fibrous crystal systems, extension veins, shear veins, faults, striations) is

uncertain. Reviewing previously documented, or theoretical tectonic stress regimes in the regional area should reveal the probable age of these structures.

Most recent tectonism in the area is regional extension that produced the Rio Grande rift. Late Oligocene-early Miocene regional extension in central New Mexico west of the Rio Grande rift was east-northeast--west-southwest (Aldrich and others, 1986). East-west extension within the rift during this time was controlled by preexisting structures (Aldrich and others, 1986). Middle to late Miocene regional extension in New Mexico rotated clockwise from east-northeast--west-southwest to east-west (Aldrich and others, 1986). Latest (Pliocene to present) regional extension in New Mexico east of the rift was north-northeast to northeast (Aldrich and others, 1986). Throughout Tertiary regional extension, the least principal horizontal stress within the Rio Grande rift has been consistently east-west (Aldrich and others, 1986).

During tensional normal faulting, I assume that it is possible for vertically oriented veins to develop. In this case, linear extension veins may develop subparallel to normal faults with en echelon vein arrays oblique to normal faults, in tear zones between blocks of strata subjected to different degrees of extension. Horizontally oriented en echelon veins may form in drag zones along normal faults. However, field evidence indicates that the majority of extension veins in the Navajo Gap area are not a result of extensional normal faulting. Extension veins occur in association with lateral shear zones and strike-slip faults. Coincidentally, right-extension linear veins (Appendix M(a)) are oriented such that they fit into the stress regime of more recent rifting. But, the majority of these veins trend into strike-slip faults!

Prior to rifting, the compressive stress-regime of the Laramide orogeny resulted in the formation of the Rocky Mountains. The Laramide orogeny began in late Cretaceous and ended in early Tertiary (Tweto, 1975). Structures in the

Rocky Mountains reveal east-west to north-south directed Laramide compression (Gries, 1983). Seager (1983, 1986) has mapped Laramide structures revealing a north-northeast-trending maximum principal stress in southern New Mexico. Keith (Chapin and Cather, 1981) records a northwest-trending belt of southwest-verging thrust faults along the southern border of the Colorado Plateau. A northeast-trending axis of compression is suggested for these structures. From a study of faults and folds along the western border of the Colorado Plateau, Anderson and Barnhard (1986) reveal a Laramide maximum principal stress oriented northeast-southwest. Looking closer at this axis of compression, Chapin and Cather (1981) discussed the controls of Eocene sedimentation in the Rocky Mountain-Colorado Plateau area and reviewed the orientations of igneous dikes emplaced during the Laramide orogeny.

Chapin and Cather (1981) indicate an east-northeast-directed axis of compression occurring during early Laramide (72-56 m.y.B.P.; Liviccari and Keith, 1984). Younger Laramide (56-43 m.y.B.P.; Liviccari and Keith, 1984) structures suggest a counterclockwise rotation in the Laramide axis of compression from east-northeast to more northeasterly (Chapin and Cather, 1981). From Figures 24 and 25, one can see how the trends, and rotation, of the maximum principal stress in the Navajo Gap area closely match predicted trends in Laramide maximum principal stresses. Therefore, based on the presumption that the rotation in the maximum principal stress found in Navajo Gap is the same as that indicated by Chapin and Cather (1981), I interpret that the shear structures in Navajo Gap are of Laramide age. If this is a correct presumption, Figure 25 may indicate a more northerly north-northeast trend, rather than a northeast trend in the late Laramide axis of compression. Or, this north-northeast trend is a secondary axis of compression developed by the reactivation of assumed basement structures.

Prior to the Laramide orogeny, and after the formation of the Ancestral

Rocky Mountains, central New Mexico was in a period of relative quiescence with erosion of Ancestral Rocky highlands and deposition of dominantly continental sediments (Rascoe and Baars, 1972; MacLachlan, 1972; Peterson, 1972; McGookey and others, 1972). The Ancestral Rockies were late Paleozoic "large fault-block mountains" (Kluth and Coney, 1981). Chamberlin (1982) mapped an early Mississippian to middle Pennsylvanian high-angle reverse fault, originally striking northwest, in the Lemitar Mountains approximately 25 miles south-southeast of the Navajo Gap area. Armstrong (1958) observed folds, a high-angle normal fault, and stream channels in Mississippian strata of the Ladron Mountain area. He did not show any trends to the structures, but his figures 9 and 10 suggest uplift of the Ladron Mountain area during early Pennsylvanian with erosion and deformation of Mississippian strata. Kluth and Coney (1981, fig. 2) indicate that late Paleozoic structures have a northwest to north-northwest trend in central New Mexico. Baars (1982) suggests that extensional Paleozoic basement structures in the Albuquerque basin area trend north-south.

Kluth and Coney (1981) reviewed plate tectonics responsible for the Ancestral Rocky Mountains. They suggest that the uplift of the Ancestral Rockies was the result of northwest-directed compression, along the Ouachita-Marathon region, as North America and South America-Africa collided. This plate interaction would have imparted a north-northwest to north-directed maximum principal stress across much of the southwestern and southern interior of the North American continent (Scotese and others, 1979). In Navajo Gap, no evidence was found for maximum principal stresses oriented in this direction.

If late Paleozoic structures occur in the Navajo Gap area, they are assumed to be recognized as folds and growth faults. Growth faults would be visible as abrupt thickness variations in faunal zones or facies changes. Field work did not reveal any major late Paleozoic structures. No growth faults were observed in

Mississippian, Pennsylvanian, or Permian strata in the Navajo Gap area. However, I observed gentle folds in poor outcrops of Mississippian strata unconformably underlying Pennsylvanian strata in south-central Navajo Gap.

In summary, besides the Tertiary extensional structures, most of the structures in Navajo Gap are Laramide in age. Initial Laramide maximum principal stress trended approximately N60°E. Tectonism continued with the maximum principal stress rotating counterclockwise to approximately N21°E. Figure 25 shows the trends of maximum principal stress responsible for the first and final increments of extension vein development.

# TECTONICS

Central New Mexico, including the Navajo Gap area, has been subjected to three Phanerozoic structural deformation events. The first event occurred during late Paleozoic. The nature of this deformation in Navajo Gap is indeterminate. The second deformation event was Laramide. The nature of Laramide deformation in Navajo Gap was compression followed by strike-slip. The final deformation event was middle to late Tertiary extension.

## Limitations and Interpretations

Structure and stratigraphy provide limitations to interpretations of tectonism in the Navajo Gap area. Structural guides consist of styles of structural deformation, orientations of structures, and timing between deformational events. Stratigraphic guides assist in bracketing the timing of deformation events or stages.

Late Paleozoic. Folded Mississippian strata, at the eastern foot of Saiz Ridge and west of Ladron fault, lie nonconformbly upon Proterozoic rocks and are unconformably overlain by basal Pennsylvanian strata. These folded strata suggest the occurence of late Paleozoic deformation in the study area. Analysis indicates that prior to Laramide deformation, these gentle, open folds had a trend of approximately N80 ° E and a plunge of approximately 5-10 ° E.

During late Paleozoic, the Navajo Gap area lay in the southern portion of Acoma sag (Baars, 1983, fig. 2), a north-trending basin. If displacement occurred in the area of the Ladron fault, the asymmetric, deepening to the east nature of the Acoma Sag (Baars,1983, fig. 4) suggests that it may have been relative down-to-east. The gentle east plunge of folds in Mississippian strata also suggests that

one component of deformation was down-to-east. The approximate N80 ° E axial trend of these folds suggests north-northwest--south-southeast compression.

Laramide. During late Laramide, a north-trending, right-wrench zone developed in New Mexico (Chapin and Cather, 1981). The interpreted Laramide maximum principal horizontal stress rotated counterclockwise from early Laramide east-northeast--west-southwest to late Laramide northeast-southwest (Chapin and Cather, 1981). A right-wrench zone is suggested to have developed as the first-order shear (Riedel shear) of this counterclockwise rotating stress regime lined up in near parallelism to the structural grain of the southern Rocky Mountains (Chapin and Cather, 1981). This wrench zone is 100 to 200 km wide (C.E. Chapin, personal communication, 1985) and stretches north-south from southeastern Wyoming to south-central New Mexico (Chapin and Cather, 1981). Chapin (1983) suggests that approximately 100 km of right-slip displacement occurred along this zone.

A right-wrench zone consists of anastamosing faults and fold belts, and uplifts and basins (Dibble, 1977). Prominent strike-slip faults would be right-slip. Extensional faults would border pull-apart basins. Fold belts would tend to occur at restraining bends that border uplifts, and along compressional strike-slip (transpressional) faults. "Wrench faults cutting stratified sequences of well-lithified sedimentary rocks tend to be expressed by zones of sharp upturning and complex folding of strata" (Chapin, 1983).

Thin section analyses of extension and shear veins in the Navajo Gap area indicate that a deformational event occurred during a rotating stress regime. Maximum principal horizontal stress rotated a maximum of 39 ° counterclockwise from N60 ° E to N21 ° E. The N21 ° E-trending maximum principal horizontal stress may be secondary, developed as the Riedel shears reactivated basement structures. Therefore, the counterclockwise rotation may have been less than 39 °.

Stereonet analyses of extension and shear veins and faults and striations, plus field analysis of vein intersections and the relationships of veins and faults to folds suggests that these structures developed during a two-stage deformation event. These two stages are related to the counterclockwise rotation in the maximum principal horizontal stress. First-stage structures were compressional. They consist of folds, minor thrust faults, reverse faults, and conjugate shears (Fig. 27a). Folds, thrusts, and reverse faults trend between N10 ° W and N40 ° W. The average trend of right-shears is N3 ° E and left-shears have an average trend of east-west. These structures were controlled by an approximately N60 ° E-trending maximum principal horizontal stress.

The second stage of deformation occurred during and after, or after, the stress regime rotated counterclockwise. Folds, reverse faults, and minor thrusts most likely continued to develop, but conjugate strike-slip faulting and lateral shearing became predominant (Fig. 27b). Most right-slip faults and right and left-shears trend N3 ° E. Most left-slip faults trend N30 ° E. The conjugate strike-slip faults were controlled by a N17 ° E-trending maximum principal horizontal stress, or they are second-order structures overlying reactivated basement structures.

These two stages of deformation are interpreted to be early and late Laramide. During early Laramide, the fold belt in the Navajo Gap area is interpreted to have developed on the western side of a northwest-striking, northeast-dipping, apparent reverse fault (at the location of the Saiz fault) and a north- to north-northwest-striking, vertical to east-dipping, down-to-west fault (at the location of the Ladron fault). During late Laramide, the Navajo Gap area is interpreted to have developed as a compressional strike-slip (transpressional) zone within the right-wrench zone proposed by Chapin and Cather (1981; Fig. 28). North- to north-northeast-trending strike-slip faults developed trending into and displacing structures within the fold belt that paralleled the reverse fault at the location of

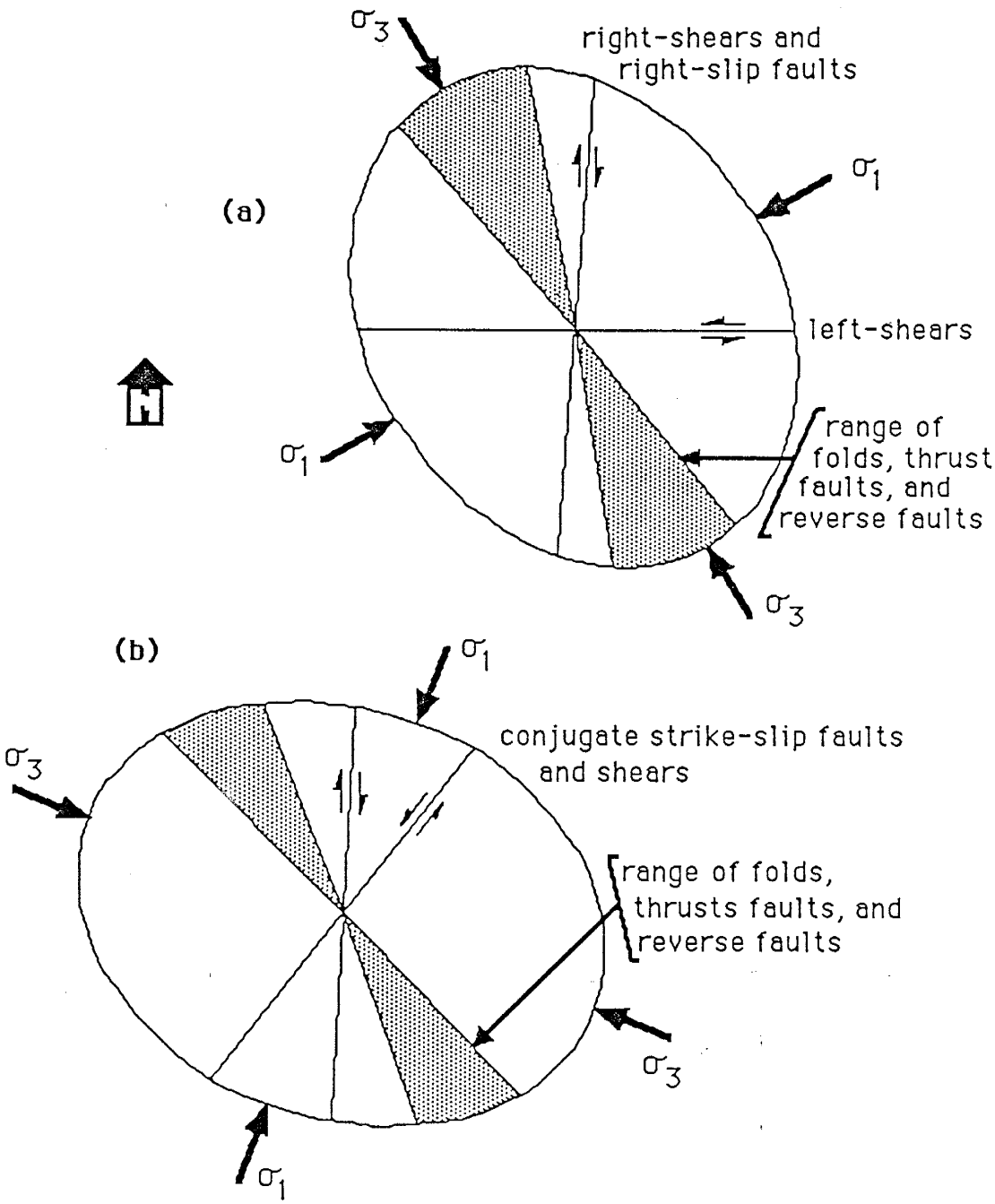


Figure 27. (a) Early-Laramide stress and strain in the Navajo Gap area. Left-shears, folds, thrusts, and reverse faults are first-order. Right-shears and right-slip faults are either first-order or second-order. (b) Late-Laramide stress and strain in the Navajo Gap area. All structures including the stress axes are most likely second-order.

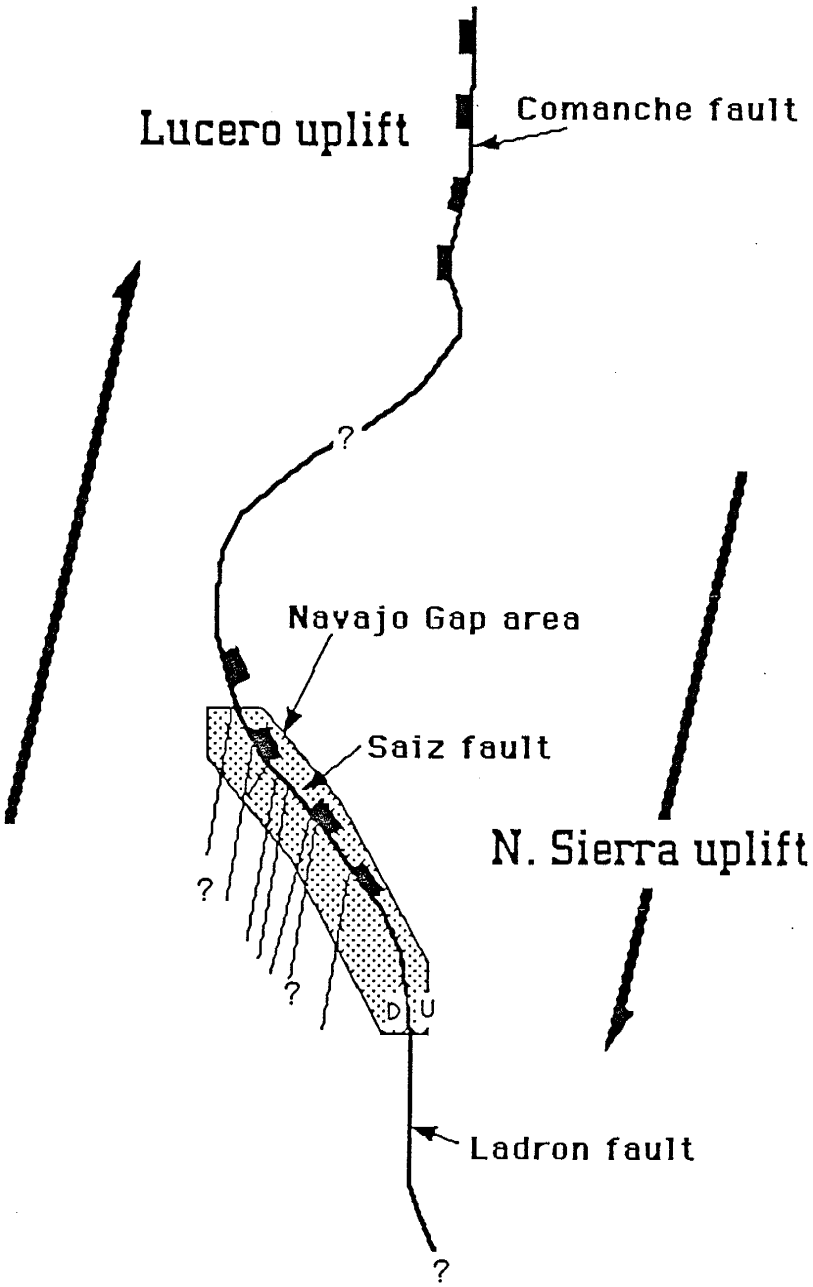


Figure 28. Schematic illustration showing an interpreted late Laramide tectonic setting for the Navajo Gap area.

the Saiz fault. Folding continued to develop during late Laramide. Therefore, the fold belt is both early and late Laramide while the strike-slip faults are late Laramide.

Middle to Late Tertiary Extension. Following compression and wrench tectonics of the Laramide orogeny, regional tension eased the Colorado Plateau away from the southern Great Plains. This formed the Rio Grande rift, a break in the continental lithosphere (Chapin, 1987).

The Navajo Gap area straddles part of a border fault zone (Saiz fault zone) of the southwestern Albuquerque basin and many other rift-related faults. This border trends northwest and includes a moderate- to low-angle normal fault (Saiz fault) and an apparent high-angle normal fault (Monte Largo fault). Other rift-related faults are high-angle, and include the Ladron and Mesa Sarca faults, and other normal faults that parallel, and are interpreted to be related to, Mesa Sarca fault.

Stereonet and field analyses of these structures suggests that they formed during three stages of extension. During one stage, a normal fault zone developed parallel to the Laramide reverse fault at the location of the Saiz fault. During another stage, north- to north-northeast-trending, high-angle normal faults developed. During a third stage of extension, north- to north-northeast trending mafic dikes were emplaced.

High-angle normal faults trend approximately N7 ° E and locally appear to have been intruded by mafic dikes. These faults and dikes indicate a west-northwest--east-southeast least principal horizontal stress in Navajo Gap. The dikes are probably related to the late Oligocene-early Miocene mafic dike swarm that extends for at least 30 km to the southwest through the Riley area. Mafic dikes in the Riley area range in age from 29 to 22 Ma (Chapin and others, 1978). These dikes record the first stage of extension in the Navajo Gap area (Fig. 29a).

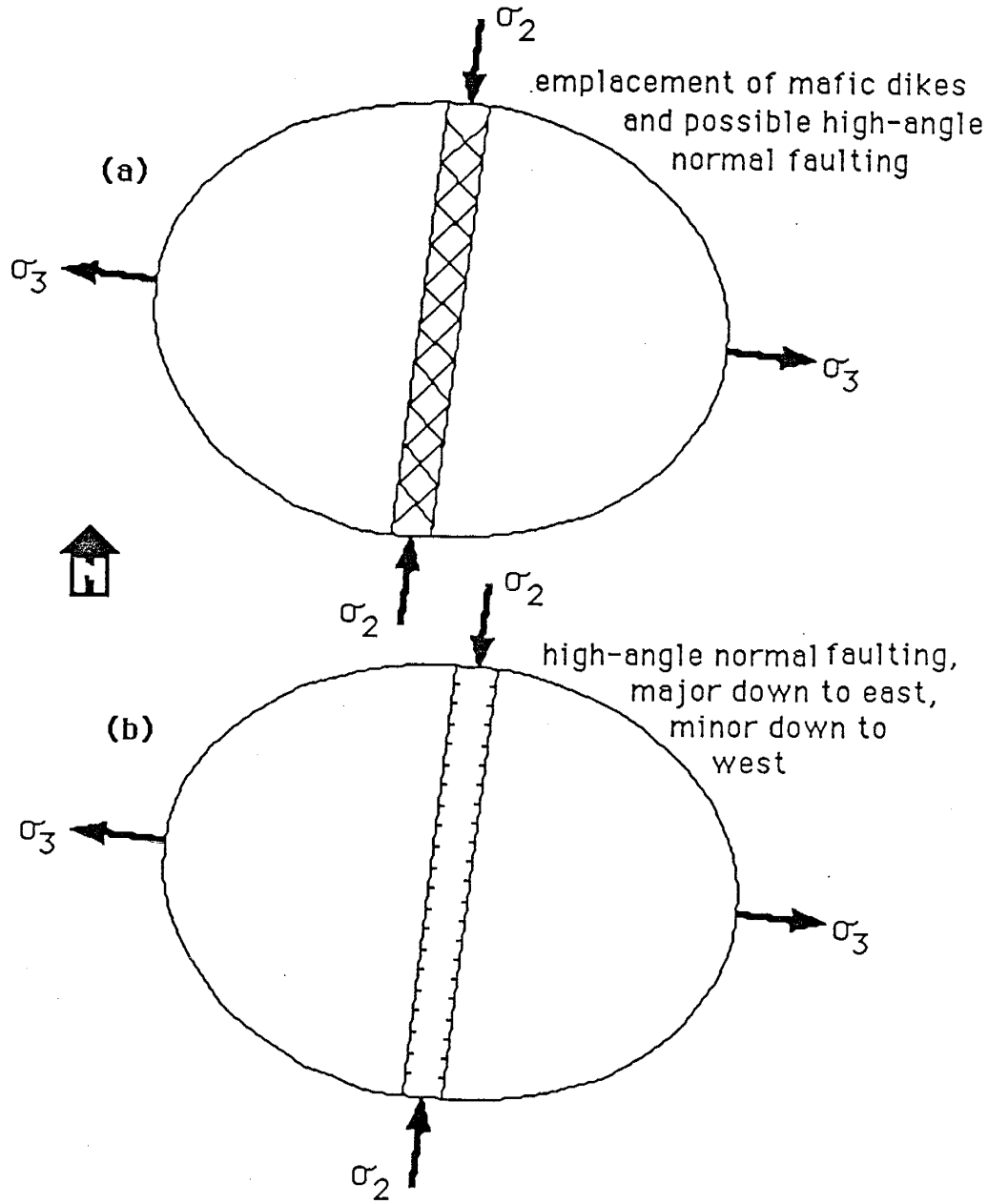


Figure 29. (a) Late Oligocene-early Miocene stress and strain in the Navajo Gap area. (b) Pliocene-Pleistocene stress and strain in the Navajo Gap area. Includes approximately seven rd degrees of westward rotation.

The major boundary fault zone (Saiz fault zone) strikes N40 ° W. This fault zone includes the Saiz fault and the Monte Largo fault. Both these faults are interpreted to reflect control by a preexisting Laramide reverse fault. Sales (1983) proposed that major normal faults "back down" the root zones of reverse faults. The Tertiary Saiz normal fault dips 20-50 ° NE and is interpreted to have developed more or less at the location of an upper level Laramide reverse fault. Monte Largo fault has a presumed steep northeast dip and is interpreted to be rooted in the deeper level of a Laramide reverse fault.

A thin veneer of unconsolidated Upper Santa Fe Group gravel overlies all extensional faults in the Navajo Gap area. This gravel is probably Pliocene-Pleistocene in age. On the down-to-east side of the Tertiary Saiz fault zone, cemented gravels underlie this thin veneer. Within the cemented gravel, a bedding contact shows evidence of erosion. The upper Santa Fe Group cemented gravels underlying the thin veneer east of the Tertiary Saiz fault zone suggests that this fault zone is older than the latest motion on the north-trending normal faults. Therefore, the Saiz fault zone developed during the second stage of extension in the Navajo Gap area.

The upper Santa Fe gravel consists of three deposits classified by clast composition. Two gravel deposits are interpreted to have been deposited in response to uplift along Mesa Sarca and Ladron faults. The third deposit reveals that Navajo Gap was a throughgoing, northeast-draining valley during late Pliocene-Pleistocene. Drainage was northeastward and clasts up to cobble and boulder size were transported from sources as far to the southwest as the Bear Mountains (~25 km, ~16.5 mi). The approximately N7 ° E trending normal faults, including Mesa Sarca and Ladron faults, are interpreted to be late rift (Pliocene-Pleistocene), the third stage of extension in the Navajo Gap area (Fig. 29b).

The nature and timing of deformation along the northeast-southwest-trending

Alamito shear zone (Chamberlin and others, 1982) is indeterminate. Field analysis suggests that north of this zone, rocks moved down and rotated eastward relative to rocks to the south. Structures are younger than the middle Pennsylvanian Veredas Group.

Models

During late Paleozoic, the Navajo Gap area lay in the southern portion of the north-trending Acoma sag (Baars, 1983, fig. 2). Deformation occurred along, or near, the Ladron fault during latest Mississippian or earliest Pennsylvanian. This deformation may have resulted in relative down-to-east motion

During early Laramide, east-dipping reverse faults formed at the locations of the Ladron and Saiz faults. These faults developed (Fig. 30a and 30b) during horizontal compression, possibly as an older late Paleozoic structural zone was reactivated. The early Laramide maximum principal horizontal stress trended N60 ° E. Fold belts developed on the west sides of the Ladron and Saiz faults. Minor thrust and reverse faulting occurred within the fold belts. Conjugate shears developed west of the fold belts.

The Laramide faults at the locations of the Ladron and Saiz faults may be parts of the same fault zone. Due to limited exposures, the relationship between these faults can only be inferred. However, both developed along the west edge of the northern, Laramide Sierra uplift, or an uplift between the Sierra uplift and Lucero uplift (Cather and Johnson, 1984, fig. 2). A down-to-west fault is inferred within the basement in the southwest field area (Fig. 30b).

Between early and late Laramide, the maximum principal horizontal stress rotated 39 ° counterclockwise. With this rotation, strike-slip faults and lateral shears developed (Fig. 30c and 30d) forming conjugate sets that trend into the fold belt on the west side of the Laramide Saiz reverse fault. Folding, thrust

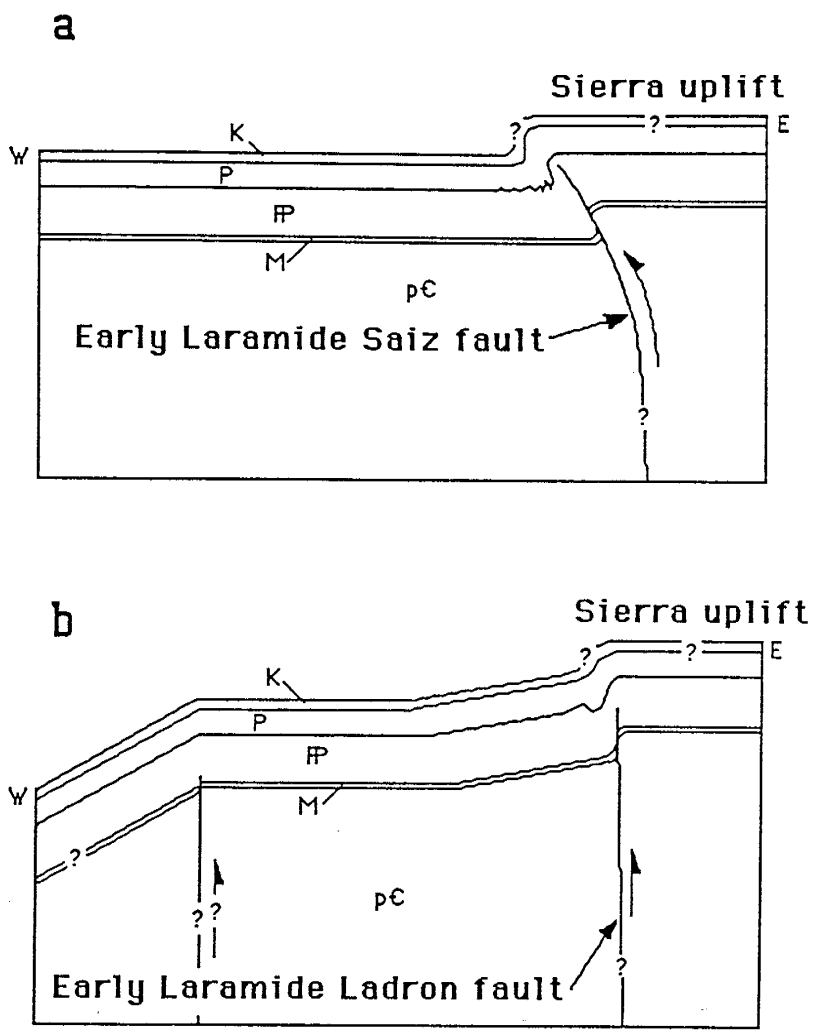


Figure 30. Early Laramide structural interpretations of east-west cross-sections through the Navajo Gap area (not to scale). (a) is the approximate location of cross-section BB' on Plate 1, and (b) is the approximate location of cross-section FF' on Plate 1. pC = Precambrian rocks, M = Mississippian strata, PP = Pennsylvanian strata, P = Permian strata, and K = Cretaceous strata.

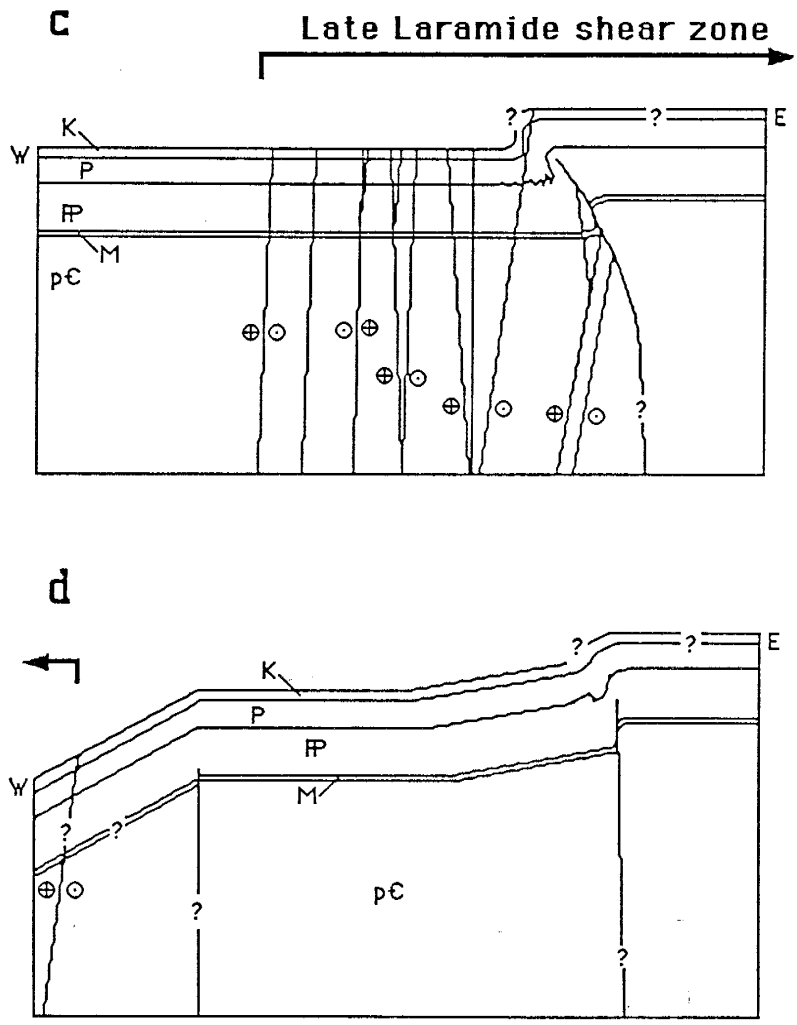


Figure 30 (continued). Late Laramide structural interpretations of east-west cross-sections through the Navajo Gap area (not to scale). (c) is the approximate location of cross-section BB' on Plate 1, and (d) is the approximate location of cross-section FF' on Plate 1.

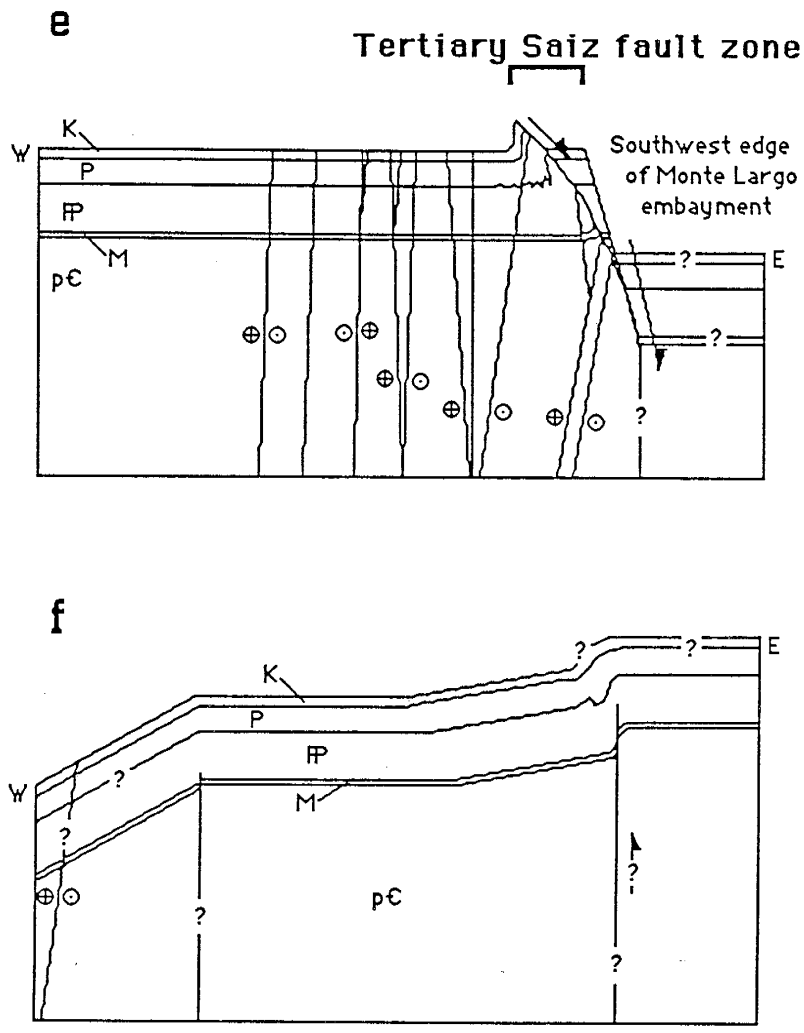


Figure 30 (continued). Structural interpretations of east-west cross-sections through the Navajo Gap area during mid-rift (?) extension (not to scale). (e) is the approximate location of cross-section BB' on Plate 1, and (f) is the approximate location of cross-section FF' on Plate 1.

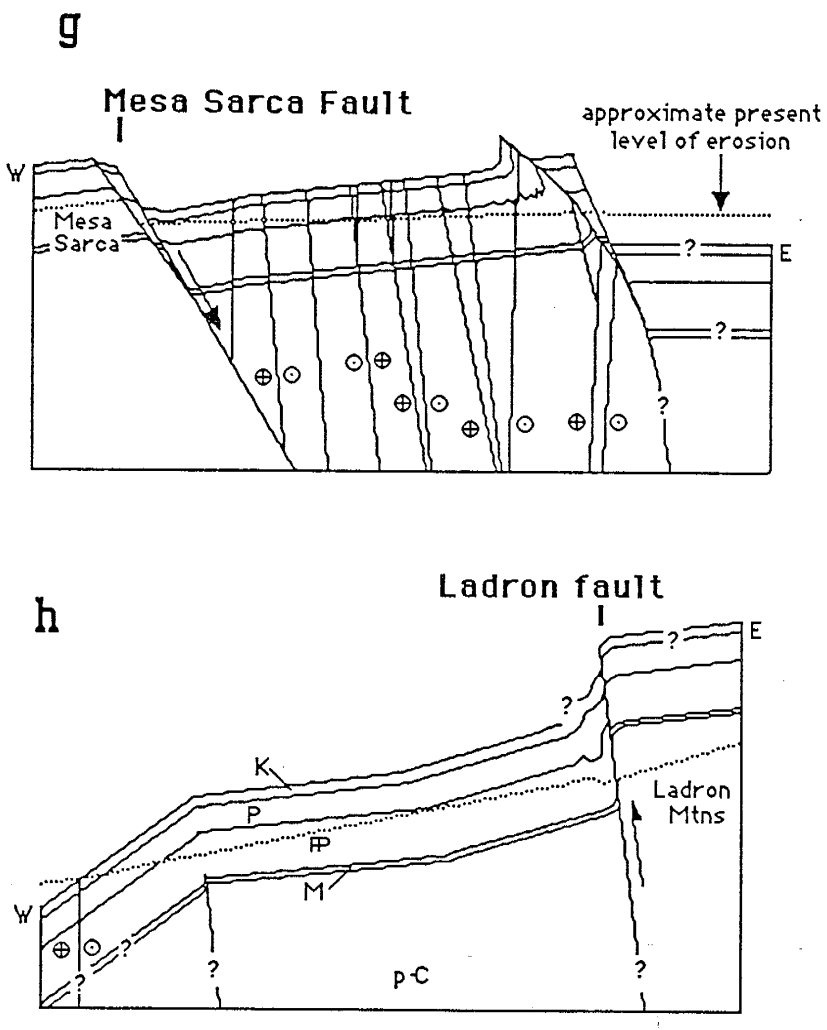


Figure 30 (continued). Pleistocene-Pliocene structural interpretations of east-west cross-sections through the Navajo Gap area (not to scale). (g) is the approximate location of cross-section BB' of Plate 1, and (h) is the approximate location of cross-section FF' on Plate 1.

faulting, and reverse faulting continued to occur within the fold belt. With the development of the strike-slip faults and lateral shears, the Navajo Gap area developed as a zone of compressional strike-sip within the late Laramide right-wrench zone.

The late Tertiary Saiz fault zone is interpreted to have developed at the location of an early Laramide reverse fault (Fig. 30e) as an Eocene uplift collapsed into the Albuquerque basin. The west edge of this fault zone (Saiz fault) is interpreted to have developed along the reactivated upper level Laramide reverse fault. The east edge of this fault zone (Monte Largo fault) forms the structural border to the southwestern Albuquerque basin and is interpreted to be rooted in the deeper level of the Laramide reverse fault.

Prior to the development of the Tertiary Saiz fault zone, late Oligocene-early Miocene mafic dikes indicate west-northwest--east-southeast-oriented early rift extension. After development of the Tertiary Saiz fault zone, high-angle normal faults, interpreted to be late rift (Pliocene-Pleistocene), also indicate a west-northwest--east-southeast oriented least principal horizontal stress. During this tension, Navajo Gap was downdropped to the east approximately 945 m (~3,100 ft) relative to Mesa Sarca (Fig. 30f), and to the west relative to the Ladron Mountains (Fig. 30g). Other tensional faults exhibiting minor displacements occur paralleling Mesa Sarca fault to the east and west. During this stage of extensional faulting, the Navajo Gap area is presumed to have tilted approximately 7 degrees westward (Fig. 30f and 30g). Due to this rotation, the downdropping of the study area, and the close-spaced shearing of the bedrock, Navajo Gap became a northeast-trending paleovalley draining into the Albuquerque basin.

# CONCLUSIONS

1. Thompson's (1942) Pennsylvanian lithostratigraphic nomenclature, as modified by Rejas (1965), can be applied to the Navajo Gap area. But the formations in Navajo Gap may not be coeval with Thompson's (1942) because of facies changes between this study area and Thompson's type locations.

2. A previously unrecorded small outcrop of Proterozoic, foliated, granitic gneiss overlain by Mississippian strata is exposed at the western foot of Mesa Sarca in the western SE/4 of section 32, T4N. R3W..

3. A previously unrecorded small outcrop of quartzite-chert-pebble conglomerate, interpreted as basal Dakota Sandstone, is exposed in the SE/4 of section 33, T4N. R3W..

4. Earliest preserved Phanerozoic deformation in the study area was late Paleozoic. Late Paleozoic structures include gently folded Mississippian strata exposed at the east foot of Saiz Ridge in SW/4 Section 24, T3N. R3W.. Prior to later deformation, these folds had a trend of approximately N80 ° E and a plunge of approximately 5-10 ° E.

5. Late Paleozoic deformation was apparently down-to-east in the area of the Ladron fault. The nature of deformation, and the orientation of the structural zone is indeterminate. Gentle open folds suggest a maximum principal horizontal stress oriented approximately N10 ° W.

6. A second deformation event in the Navajo Gap area consisted of two stages. The style of deformation during the early stage was compressional. The style of deformation during the later stage was strike-slip faulting. These stages of deformation are interpreted to be early and late Laramide, respectively. This interpretation is based on the presumption that the stress regime responsible for the development of the brittle shear zone found in Navajo Gap is the same stress regime suggested for the Laramide by Chapin and Cather (1981).

7. The two-stage Laramide deformation was due to a 39° counterclockwise rotation in the maximum principal horizontal stress. Early Laramide maximum principal horizontal stress trended N60°E. Late Laramide maximum principal horizontal stress rotated to approximately N21°E.

8. Early Laramide structures developed during compression and include north-northwest- to northwest-trending folds, reverse faults, and minor thrusts, and north to north-northeast- and east-trending conjugate lateral shears. Major reverse faults developed at the present locations of the Saiz and Ladron faults. The relationship between these two faults is indeterminate. A fold belt, including minor reverse and thrust faults, developed on the west side, paralleling these major reverse faults. Early Laramide structures are primary to the N60°E-trending maximum principal horizontal stress.

9. Major early Laramide reverse faults at the locations of the Ladron and Saiz faults are interpreted to form the west side of the northern Sierra uplift of Eocene age, or an uplift between the Sierra uplift and Lucero uplift. The Eocene Sierra uplift was proposed by Cather and Johnson (1984).

10. Late Laramide structures developed during right-slip faulting and include: folds and minor thrusts, and north-south- to north-northeast--south-southwest-trending conjugate strike-slip faults and lateral shears. Folding and thrust faulting continued to occur in the fold belt. Conjugate strike-slip faults and lateral shears developed trending into, and displacing, structures in the fold belt. North-trending right-slip faults were the most common. Total offset during strike-slip faulting is indeterminate but believed to be minor. These late Laramide structures are most likely secondary to the N21°E-trending maximum principal horizontal stress.

11. Late Laramide structures are interpreted to have developed in a zone of compressional strike-slip within the late Laramide right-wrench zone proposed by

Chapin and Cather (1981).

12. A third deformation event in the Navajo Gap area includes three stages of Rio Grande rift-related extensional faulting. Early rift extension (late Oliogocene-early Miocene) was recorded by the emplacement of mafic dikes. The tensional Saiz fault zone developed during the next stage of rift extension. High-angle normal faults developed during late rift (Pliocene-Pleistocene) extension.

13. Throughout middle to late Tertiary extension, the least principal horizontal stress in the Navajo Gap area was oriented west-northeast--east-southeast.

14. The northwest-trending and northeast-dipping Saiz fault zone developed during Laramide compression as a high-angle reverse fault was reactivated as a normal fault during extension. This structural zone includes, from west to east, the moderate- to low-angle Saiz fault, strongly deformed strata of the Permian Yeso Formation, and a normal fault (Monte Largo falt) marking the border of Monte Largo embayment, southwestern Albuquerque basin.

15. The Saiz normal fault is presumed to have developed at the location of the shallow level Laramide reverse fault. At least 425 m (~1,394 ft) of relative down-to-northeast throw occurred along this fault. The dip of the border fault to Monte Largo embayment (Monte Largo fault) is indeterminate and presumed to be high-angle. This fault is interpreted to be rooted in the Laramide reverse fault at a deeper level than the Saiz normal fault. Throw on this fault is indeterminate and presumed greater than 945 m (~3,100 ft).

16. Approximately north-south-trending, high-angle normal faults developed during late Tertiary extensional faulting. These include Mesa Sarca fault, faults paralleling Mesa Sarca fault to the east and west, and the Ladron fault.

17. Mesa Sarca fault marks the southeast edge of the Lucero uplift. The Navajo Gap area was downdropped approximately 945 m (~3,100ft) to the east along this fault and a synthetic fault that parallels it. A normal fault east of

Mesa Sarca fault, interpreted to be antithetic, contains 20 to 40 m (65 to 130 ft) of relative down-to-west throw. Other normal faults paralleling Mesa Sarca fault contain minor amounts of throw (less than 8 m; ~24 ft).

18. The Ladron fault marks the west edge of the Ladron uplift. The Navajo Gap area was downdropped to the west along this fault. The amount of throw is indeterminate. Some displacement occurred during Laramide reverse faulting and some is inferred to have occurred during late Tertiary extension.

19. The Navajo Gap area tilted approximately 7 degrees westward during late Tertiary (Pliocene-Pleistocene) extensional faulting.

20. Due to late Tertiary downdropping of the study area between the Ladron Mountains and Mesa Sarca, westward tilting, and the close-spaced shearing of the upper Paleozoic bedrock, Navajo Gap became a northeast-trending paleovalley occupied by a stream that drained into the Albuquerque basin. Incision of Rio Salado south of this valley most likely captured the throughgoing drainage.

## REFERENCES

Aldrich, M.J., Jr., Chapin, C.E., and Laughlin, A.W., 1986, Stress history and tectonic development of the Rio Grande rift, New Mexico: Journal of Geophysical Research, v. 91, no. B6, pp. 6199-6211.

Anderson, R.E., and Barnhard, T.P., 1986, Genetic relationships between faults and folds and determination of Laramide and neotectonic paleostress, western Colorado Plateau-transition zone, central Utah: Tectonics, v. 5, no. 2, pp. 335-357.

Anonoymous, I, 1963, The Abo formation in the area around Socorro, New Mexico: New Mexico Geological Society, Guidebook to 14th Field Conference, pp. 98-99.

Armstrong, A.K., 1958, The Mississippian of west-central New Mexico: New Mexico Bureau of Mines and Mineral Resources Memoir 5, 49 pp.

Armstrong, A.K., Kottlowski, F.E., Stewart, W.J., Mamet, B.L., Baltz, E.H., Jr., Siemers, W.T., and Thompson, S., III, 1979, The Mississippian and Pennsylvanian (Carboniferous) systems in the United States--New Mexico: U.S. Geological Society, Professional Paper 110-W, 27 pp.

Baars, D.L., 1982, Paleozoic history of the Albuquerque trough: Implications of basement control on the Rio Grande rift: New Mexico Geological Society, Guidebook to 33rd Field Conference, pp. 153-157.

Bachman, G.O., 1975, Paleotectonic investigations of the Pennsylvanian system in the United States, Part I: Introduction and regional analyses of the Pennsylvanian system: U.S. Geological Survey Professional Paper 853, pp. 232-243.

Barker, J.M., 1983, Preliminary investigation of the origin of the Riley travertine, Socorro County, New Mexico: New Mexico Geologic Society, Guidebook to 34th Field Conference, pp. 269-276.

Bartlett, W.L., Friedman, M., and Logan, J.M., 1981, Experimental folding and fracturing of rocks under confining pressure, Part IX. Wrench faults in limestone layers: Tectonophysics, v. 79, no. 3-4, pp. 255-277.

Bauch, J.H.A., 1982, Geology of the central area of the Lomas de las Cañas Quadrangle [M.S. thesis]: New Mexico Institute of Mining and Technology, Socorro, 116 pp.

Black, B.A., 1964, The geology of the northern and eastern parts of the Ladron Mountains, Socorro County, New Mexico [M.S. thesis]: University of New Mexico, Albuquerque, 117 pp.

Bowring, S.A., Kent, S.C., and Summer, W., 1983, Geology and U-Pb geochronology of Proterozoic rocks in the vicinity of Socorro, New Mexico: New Mexico Geologic Society, Guidebook to 34th Field Conference, pp. 137-143.

Brocher, T.M., 1981, Shallow velocity structure of the Rio Grande rift north of Socorro, New Mexico: A reinterpretation: Journal of Geophysical Research, v. 86, no. B6, pp. 4960-4970.

Brown, L.D., Krumhansl, P.A., Chapin, C.E., Sanford, A.R., Cook, F.A., Kaufman, S., Oliver, J.E., and Schilt, F.S., 1979, COCORP seismic reflection studies of the Rio Grande rift: in Riecker, R.E. (ed.), Rio Grande Rift: Tectonics and Magmatism: American Geophysical Union, Washington, D.C., pp. 1-5.

Brown, L.D., Chapin, C.E., Sanford, A.R., Kaufman, S., Oliver, J.E., 1980, Deep structure of the Rio Grande rift from seismic reflection profiling: Journal of Geophysical Research, v. 85, no. B9, pp. 4773-4800.

Callender, J.F., and Zilinski, R.E., 1976, Kinematics of Tertiary and Quaternary deformation along the eastern edge of the Lucero uplift, central New Mexico: in Woodward, L.A. and Northrup, S.A. (eds.), Tectonics and Mineral Resources of Southwestern North America, New Mexico Geological Society, Special Publication 6, pp. 53-61.

Campbell, C.V., 1967, Lamina, laminaset, bed and bedset: Sedimentology, v. 8, no. 1, pp. 7-26.

Cather, S.M., and Johnson, B.D., 1984, Eocene tectonics and depositional setting of west-central New Mexico and eastern Arizona: New Mexico Bureau of Mines and Mineral Resources, Circular 192, 33 pp.

Cape, C.D., McGeary, S., and Thompson, G.A., 1983, Cenozoic normal faulting and the shallow structure of Rio Grande rift near Socorro, New Mexico: Geological Society of America Bulletin, v. 94, p. 3-14.

Chamberlin, R.M., 1982, Geologic map, cross sections, and map units of the Lemitar Mountains, Socorro County, New Mexico: New Mexico Bureau of Mines and Mineral Resources Open-file Report No. 169, 3 plates, scale 1:12,000.

Chamberlin, R.M., 1983, Cenozoic domino-style crustal extension in the Lemitar Mountains, New Mexico: A Summary: New Mexico Geological Society, Guidebook to 34th Field Conference, pp. 111-118.

Chamberlin, R.M., Lodson, M.J., Eveleth, R.W., Bieberman, R.A., Roybal, G.H., Osburn, J.C., North, R.M., McLemore, V.T., and Weber, R.H., 1982, Preliminary evaluation of the mineral resourse potential of the Sierra Ladrones Wilderness Study area, Socorro County, New Mexico: New Mexico Bureau of Mines and Mineral Resources Open-file Report No. 179, 141 pp, 6 sheets, scale 1:100,000.

Chapin, C.E., 1971, The Rio Grande rift, part I: Modifications and additions: New Mexico Geological Society, Guidebook to 22th Field Conference, pp. 191-201.

Chapin, C.E., 1979, Evolution of the Rio Grande rift - a summary: in Riecker, R.E. (ed.), Rio Grande Rift: Tectonics and Magmatism: American Geophysical Union, Washington, D.C., pp. 1-5.

Chapin, C.E., 1987, Axial basins of the northern and central Rio Grande rift: in Sloss, L.L., Vail, P.R., and Mankin, C.J. (eds.), Sedimentary Cover--North American Craton: Geological Society of America, Decade of North American Geology, v. D-2, Chap. 17, Rocky Mountain Region (in press).

Chapin, C.E., Chamberlin, R.M., Osburn, G.R., Sanford, A.R., and White, D.W., 1978, Exploration framework of the Socorro geothermal area, New Mexico, in Chapin, C.E. and Elston, W.E. (eds.), Field Guide to Selected Cauldrons and Mining Districits of the Datil-Mogollon Volcanic Field, New Mexico: New Mexico Geological Society, Pub. No. 7, pp. 115-130.

Chapin, C.E., and Cather, S.M., 1981, Eocene tectonics and sedimentation in the Colorado Plateau-Rocky Mountains area, in Dickinson, W.R. and Payne, W.D. (eds.), Relations of Tectonics to Ore Deposits in the Southern Cordillera: Arizona Geological Society Digest, v. 14, pp. 173-198.

Chapin, C.E., and Seager, W.R., 1975, Evolution of the Rio Grande rift in the Socorro and Las Cruces areas: New Mexico Geological Society, Guidebook to 26th Field Conference, pp. 297-321.

Condie, K.C., 1976, Precambrian rocks of Ladron Mountains, Socorro County, New Mexico: New Mexico Bureau of Mines and Mineral Resources, Geologic Map 38, scale 1:24,000.

Denney, C.S., 1940, Tertiary geology of the San Acacia area, New Mexico: Journal of Geology, v. 48, no. 1, pp. 73-106, map scale 1:200,000.

de Voogd, B., Brown, L.D., and Merey, C., 1986, Nature of the eastern boundary of the Rio Grande rift from COCORP surveys in the Albuquerque basin, New Mexico: Journal of Geophysical Research, v. 91, no. B6, pp. 6305-6320.

Dibble, T.W., Jr., 1977, Strike-slip tectonics of the San Andreas Fault and its role in Cenozoic basin evolvement: in Sylvester, A.G. (ed.), Wrench Rault Tectonics, American Association of Petroleum Geologists Reprint Series No. 28, pp. 159-172.

Dunham, R.J., 1962, Classification of carbonte rocks according to depositional texture, in Ham, W.E. (ed.), Classification of Carbonte Rocks: American Association of Petroleum Geologists, Memoir 1, pp. 108-121.

Duschatko, R.W., 1953, Fracture studies in the Lucero uplift, New Mexico: U.S. Atomic Energy Commission, RMW 3072, Technical Information Service, 49 pp.

Duschatko, R.W., and Poldervat, A., 1955, Spilitic intrusion near Ladron Peak, Socorro County, New Mexico: Geological Society of America Bulletin, v. 66, no. 9, pp. 1097-1108, map scale 1:7,800.

Folk, R.L., 1968, Petrology of Sedimentary Rocks: Hemphill's, Austin, Texas, 170 pp.

Gries, R., 1983, North-south compression of Rocky Mountain foreland structures, in Lowel, J.D. (ed.), Rocky Mountain Foreland Basins and Uplifts: Denver, Rocky Mountain Association fo Geologists, pp. 9-32.

Hancock, P.L., 1972, Brittle microtectonics: Principles and practice: Journal of Structural Geology, v. 7, no. 3/4, pp. 437-457.

Ingram, R.L., 1954, Terminology for the thickness of stratification and parting units in sedimentary rocks: Geological Society of America Bulletin, v. 65, pp. 937-938.

Jaroszewski, W., 1984, Fault and Fold Tectonics: John Wiley and Sons, New York, 565 pp.

Jurdy, D.M., and Brocher, T.M., 1980, Shallow velocity model of the Rio Grande rift near Socorro, New Mexico: Geology, v. 8, no. 4, pp. 185-189.

Kelley, V.C., 1955, Regional tectonics of the Colorado Plateau and relationships to the origin and distribution of uranium: University of New Mexico Publications in Geology No. 5, 120 pp.

Kelley, V.C., 1977, Geology of the Albuquerque Basin, New Mexico: New Mexico Bureau of Mines and Mineral Resources, Memoir 33, 59 pp, scale 1:190,000.

Kelley, V.C., and Clinton, N.J., 1960, Fracture systems and tectonic elements of the Colorado Plateau: University of New Mexico Publications in Geology No. 6, 104 pp.

Kelley, V.C., and Wood, G.H., 1946, Geology of the Lucero uplift, Valencia, Socorro, and Bernalillo Counties, New Mexico: U.S. Geological Survery, Oil and Gas Investigations, Preliminary Map 47, scale 1:62,500.

Kluth C.F., and Coney, P.J., 1981, Plate tectonics of the Ancestral Rocky Mountains: Geology, v. 9, no. 1, pp. 10-15.

Kottlowski, F.E., 1960, Summary of Pennsylvanian section in southwestern New Mexico and southeastern Arizona: New Mexico Bureau of Mines and Mineral Resources, Bulletin 66, 187 pp.

Kottlowski, F.E., 1963, Paleozoic and Mesozoic strata of southwestern and south-central New Mexico: New Mexico Bureau of Mines and Mineral Resources, Bulletin 79, 93 pp.

Kottlowski, F.E., and Stewart, W.J., 1970, The Wolcampian Joyita uplift in central New Mexico: New Mexico Bureau of Mines and Mineral Resources, Memoir 23, (Part I), pp. 1-31.

Kues, B.S., and Kietzke, K.K., 1976, Paleontology and stratigraphy of the Red Tanks Member, Madera Formation (Pennsylvanian) near Lucero Mesa, New Mexico: in Woodward, L.A. and Northrup, S.A. (eds.), Tectonics and Mineral Resources of Southwestern North America, New Mexico Geological Society, Special Publication 6, pp. 102-108.

Lee, W.T., 1909, The Manzano Group of the Rio Grande valley, New Mexico: U.S. Geological Survey, Bulletin 389, pp. 1-40.

Liviccari, R.F., and Kieth, S.B., 1984, Tectonic evolution of Seiver-Laramide foreland structures from latest Jurrasic through the Eocene [abst]: American Association of Petroleum Geologists Bulletin, v. 68, no. 4, pp. 501.

MacLachlan, M.M., 1972, Triassic System: in Mallory, W.W. (ed.), Geologic Atlas of the Rocky Mountain Region: Rocky Mountain Association of Geologists, Denver, pp. 166-176.

Maulsby, J., 1981, Geology of the Rancho de Lopez area [M.S. thesis]: New Mexico Institute of Mining and Technology, Socorro, 85 pp.

Maxwell, C.H., 1976, Stratigraphy and structure of the Acoma Region, New Mexico: in Woodward, L.A. and Northrup, S.A. (eds.), Tectonics and Mineral Resources of Southwestern North America, New Mexico Geological Society, Special Publication 6, pp. 95-101.

McGookey, D.P., Haun, J.D., Hale, L.A., Goodel, H.G., McCubbin, D.G., Weimer, R.J., and Wulf, G.R., 1972, Cretaceous System: in Mallory, W.W. (ed.), Geologic Atlas of the Rocky Mountain Region: Rocky Mountain Association of Geologists, Denver, pp. 190-228.

McKee, E.D., and Weir, G.H., 1953, Terminology for stratification and cross-stratification in sedimentary rocks: Geological Society of America Bulletin, v. 64, pp. 381-390.

Morgan, P., Seager, W.R., and Golombek, M.P., 1986, Cenozoic thermal, mechanical and tectonic evolution of the Rio Grande rift: Journal of Geophysical Research, v. 91, no. B6, pp. 6263-6276.

Myers, D.A., 1973, The upper Paleozoic Madera Group in the Manzano Mountains, New Mexico: U.S. Geological Survey, Bulletin 1372-F, 13 pp.

Needham, C.E., and Bates, R.L., 1943, Permian type section in central New Mexico: Geological Society of America Bulletin, v. 54, pp. 1653-1668.

Nicholson, R., and Ejiofor, I.B., 1987, The three-dimensional morphology of arrays of echelon and sigmoidal, mineral-filled fractures: data from north Cornwall: Journal of the Geological Society, London, v. 144, pp. 79-83.

Olsen, K.H., Baldridge, W.S., and Callender, J.F., 1984, Rio Grande rift: An overview: unpublished (?).

Osburn, J.C., 1984, Geology of Pueblo Viejo Mesa quadrangle, Socorro and Cibola Counties, New Mexico: New Mexico Bureau of Mines and Minerals Resources, Geologic Map 55, scale 1:24,000.

Peterson, J.A., 1972, Jurrasic System: in Mallory, W.W. (ed.), Geologic Atlas of the Rocky Mountain Region: Rocky Mountain Association of Geologists, Denver, pp. 177-189.

Pettijohn, F.S., Potter, P.E., and Siever, R., 1973, Sand and Sandstone: Springer-Verlag, New York, 618 pp.

Ragan, D.M., 1985, Structural Geology: An Introduction to Geometrical Techniques, 3rd Edition: John Wiley and Sons, New York, 393 pp.

Ramsay, J.G., 1980, The crack-seal mechanism of rock deformation: Nature, v. 284, pp. 135-139.

Ramsay, J.G., and Huber, M.I., 1983, The Techniques of Modern Structural Geology, Volume 1: Strain Analysis: Academic Press, Inc., London, 307 pp.

Rascoe, B., Jr., and Baars, D.L., 1972, Permian System: in Mallory, W.W. (ed.), Geologic Atlas of the Rocky Mountain Region: Rocky Mountain Association of Geologists, Denver, pp. 143-165.

Read, C.B., and Wood, G.H., 1947, Distribution and correlation of Pennsylvanian rocks in late Paleozoic sedimentary basins of northern New Mexico: Journal of Geology, v. 55, p. 220-236.

Rejas, A., 1965, Geology of the Cerros de Amado area, Socorro County, New Mexico [M.S. thesis]: New Mexico Institute of Mining and Technology, Socorro, 128 pp.

Sales, J.K., 1983, Collapse of Rocky Mountain basement uplifts, in Lowell, J.D. (ed.), Rocky Mountain Foreland Basins and Uplifts: Denver, Rocky Mountain Association of Geologists, pp. 79-97.

Sanderson, D.J., and Marchini, W.R.D., 1984, Transpression: Journal of Structural Geology, v. 6. no. 5, pp. 449-458.

Scotese, C., Bambach, R.K., Barton, C., Van der Voo, R., and Siegler, A.M., 1979, Paleozoic base maps: Journal of Geology, v. 87, no. 3, pp. 217-277.

Seager, W.R., 1981, Geology of the Organ Mountains and southern San Andres Mountains, New Mexico: New Mexico Bureau of Mines and Mineral Resources, Memoir 36, 97 pp.

Seager, W.R., 1983, Laramide wrench faults, basement-cored uplifts, and complimentary basins in southern New Meixco: New Mexico Geology, v. 5, no. 4, pp. 69-76.

Seager, W.R., Mack, G.H., Raimonde, M.S., and Ryan, R.G., 1986, Laramide basement-cored uplift and basins in south-central New Mexico: New Mexico Geologic Society, Guidebook to 37th Field Conference, pp. 123-130.

Siemers, W.T., 1978, Stratigraphy, petrology, and paleoenvironments of the Pennsylvanian system of the Socorro Region, west-central New Mexico: [Ph.D. dissertation], New Mexico Institute of Mining and Technology, Socorro, 165 pp.

Slack, P.B., and Campbell, J.A., 1976, Structural geology of the Rio Puerco fault zone and its relationships to central New Mexico tectonics: in Woodward, L.A. and Northrup, S.A. (eds.), Tectonics and Mineral Resources of Southwestern North America, New Mexico Geological Society, Special Publication 6, pp. 46-52.

Suppe, J., 1985, Principles of Structural Geology: Prentice-Hall, Inc., New Jersey, 537 pp.

Taylor, K.R., 1986, Structural and stratigraphic analysis of Precambrian rocks in the Ladron Mountains, Socorro County, New Mexico [abst]: New Mexico Geology, v. 8, no. 4, pp. 97.

Tchalenko, J.S., 1970, Similarities between shear zones of different magnitudes: Geological Society of America Bulletin, v. 81, pp. 1625-1649.

Thompson, M.L., 1942, Pennsylvanian system in New Mexico: State Bureau of Mines and Mineral Resources, Bulletin 17, 85 pp.

Tweto, O., 1975, Laramide (late Cretaceous-early Tertiary) Orogeny in the southern Rocky Mountains: Geological Society of America, Memoir 144, 44 pp.

Wickham, J.S., 1973, An estimate of strain increments in a naturally deformed carbonate rock: American Journal of Science, v. 273, no. 1, pp. 23-47.

Wilcox, R.E., Harding, T.P., and Seely, D.R., 1973, Basic wrench tectonics: American Association of Petroleum Geologists Bulletin, v. 57, no. 1, pp. 74-86.

Wilpolt, R.H., McAlpin, A.J., Bates, R.L., and Vorbe, G., 1946, Geologic map and stratigraphic section of Paleozoic rocks of the Joyita Hills, Los Pinos Mountains, and northern Chupadera Mesa, Valencia, Torrance, and Socorro Counties, New Mexico: U.S. Geological Survey, Oil and Gas Investigations, Preliminary Map 61, scale 1:62,500.

Wilpolt, R.H., and Wanek, A.A., 1951, Geology of the region from Socorro and San Antonio east to Chupadera Mesa, Socorro County, New Mexico: U.S. Geological Survey, Oil and Gas Investigations, Preliminary Map OM-121.

Wood, G.H., and Northrop, S.A., 1946, Geology of Nacimiento Mountains, San Pedro Mountains, and adjacent plateaus in parts of Sandoval and Rio Arriba Counties, New Mexico: U.S. Geological Survey, Oil and Gas Investigations, Preliminary Map 57.

Zilinski, R.E., 1976, Geology of the central part of the Lucero uplif

# APPENDIX A

## *NOMENCLATURE IN STRATIGRAPHIC SECTIONS*

Limestone classification: Dunham, 1962.

Sandstone classification: Pettijohn, Potter, and Siever, 1973.

Grain size: Wentworth, 1922.

Sorting: Folk, 1968.

Roundness: Pettijohn, Potter, and Siever, 1973.

Bed thickness: based on Ingram, 1954; Campbell, 1967.

| | |
|---|---|
| very thick | >1 meter |
| thick | 30 - 100 centimeters |
| medium | 10 - 30 centimeters |
| thin | 3 - 10 centimeters |
| very thin | <3 centimeter |

Bed internal structure, modified from: Campbell, 1967; McKee and Weir, 1953; Pettijohn, Potter, and Siever, 1972.

laminae:

| | | |
|---|---|---|
| shape: | planar parallel | laminae surfaces lie in one plane |
| | wavy | laminae surfaces are undulatory |

cross-bedding:

| | | |
|---|---|---|
| shape: | wedge | planar bounding surfaces |
| | trough | curved bounding surfaces |
| size: | small-scale | <25 centimeters |
| | large-scale | >25 centimeters |
| dip: | low-angle | <15 degrees |
| | (no mention) | >15 degrees |

massive: no laminae

APPENDIX A (continued)

*UNIT DESCRIPTION FORMAT*

| Unit No. | Thickness(m) (unit) | (cum) | |
|---|---|---|---|
| - | -- | --- | Rock type, classification; weathered color; fresh color; allochemical and/or terrigenous materials; bedding; internal bed structure; other; topographic expression. |

# APPENDIX B

## *MISSISSIPPIAN MEASURED SECTION ONE*

Mississippian section is located in the SW/4 section 24, T3N. R3W. (Plate 1). Measured strata is exposed west of a small hill of Proterozoic granitoid.

TOP CALOSO FORMATION (4.5 m thick)

| Unit No. | Thickness(m) (unit) | (cum) | |
|---|---|---|---|
| | ---------- angular unconformity ---------- | | |
| 2 | 2.5 | 4.5 | LIMESTONE, arenaceous mudstone; brownish-orange and gray weathered; dark gray fresh; coarse-grained sand (<15% of volume), few crinoid columnals and small brachiopods; medium beds. |
| 1 | 2.0 | 2.0 | SANDSTONE quartzose; brownish-white weathered; white fresh; thick beds; medium-grained; small-scale, low-angle, wedge-shaped cross-bedding. |
| | ---------- nonconformity ---------- | | |
| PRECAMBRIAN | | | GRANITOID; redish-brownish-orange weathered; dark pink fresh; coarse-grained. |

# APPENDIX C

## *COMPOSITE PENNSYLVANIAN MEASURED SECTIONS TWO AND THREE*

### PENNSYLVANIAN MEASURED SECTION TWO

Section two is located in the SW/4 section 24, and SE section 23, T3N. R3W. (Plate 1). Measured Section Two begins at the top of the Mississippian measured strata (Appendix B), and continues westward up to the top of Saiz Ridge and the Amado Limestone. Following Amado limestone along strike northward across a small pass in the ridge, the section continues westward up and over Saiz Ridge, then along an eastwest-trending ridge (Plates 4 and 5. Section two ends east of a faulted zone.

### PENNSYLVANIAN MEASURED SECTION THREE

Section three is located in the northern section 4, T3N. R3W. (see Plate 1). Measured Section Three begins in strongly tilted strata on the north side of Coyote draw, west of a series of tight folds. The section-line trends southwestward along the north side of the arroyo. From the incised bend in Coyote Draw, the section-line continues northwestward over a series of low cuesta-like ridges.

TOP MEASURED SECTION THREE

| Unit No. | Thickness(m) (unit) | (cum) | |
|---|---|---|---|
| Top Moya Limestone (48.2 m thick) | | | |
| 92 | 2.2 | 573.4 | LIMESTONE, packstone; light and dark gray weathered; dark gray fresh; phylloid algae, crinoid columnals, and microfossils; medium beds; bioturbated algal packstone; small ledge and dip-slope former. |
| 91 | 4.8 | 571.2 | LIMESTONE, grainstone with packstone; light gray weathered; whitish-gray fresh; crinoid columnals, phylloid algae, and microfossils; very thick beds; crinoid packstone lower half; large ledge and cliff former. |
| 90 | 6.6 | 566.4 | LIMESTONE, mudstone and wackestone with packstone; light to dark gray and browns weathered; dark gray fresh; crinoid columnals, brachiopods, and chert; thin to thick beds; discontinuous bedded chert; wavy partings between beds; stepped slope and small ledge former. |
| 89 | 6.2 | 559.8 | covered slope, small outcrops of laminated mudstone at base and packstone at top. |
| ---------- | FAULT, down-to-west ~1.5 m | | |
| 88 | 3.6 | 553.6 | LIMESTONE, packstone and wackestone; light brown, gray and mottled light and medium gray weathered; dark gray fresh; crinoid columnals, brachiopods (small and large), branching and fenestrate bryozoans, microfossils, rare rugose corals, and Syringopora; thin to medium beds; small ledges and slope former. |
| 87 | 1.8 | 550.0 | covered slope |
| ---------- | FAULT, down-to-west ~1.0 m | | |
| 86 | 2.6 | 548.2 | LIMESTONE, wackestone; light gray and light brown weathered; light brownish-gray fresh; microfossils; medium beds; rounded slope former. |
| 85 | 3.3 | 545.6 | LIMESTONE, packstone and wackestone, brown (base) and gray (upper) weathered; brownish-gray (base) and dark gray (upper) fresh; brachiopods, crinoid columnals, phylloid algae, rare rugose corals, and chert nodules; thin to thick beds; chert nodules and wackestone in upper beds on dip-slope; small stepped ledge and dip-slope former; |
| 84 | 3.4 | 542.3 | LIMESTONE, mudstone and grainstone; shades of brown and gray weathered; light brownish-gray and gray fresh; microfossils; thin (nodular) and thick beds; medium ledge former. NOTE--appears as a cherty limestone, or a |

| | | | |
|---|---|---|---|
| | | | lime-cobble conglomerate with silt matrix, but is most likely a bioturbated carbonate mudstone (appears as brown chert or silt) with grainstone filled burrows (appears as lime cobbles). |
| 83 | 2.1 | 538.9 | LIMESTONE, packstone and wackestone; light to medium gray and brown weathered; dark and light gray fresh; phylloid algae, microfossils, brachiopods, and unidentied skeletal material; medium beds; base is wackestone, middle is algal packstone, and upper is packstone; medium ledge former. |
| 82 | 6.3 | 536.8 | covered slope, with poor outcrops of shale and argillaceous carbonate packstone with crinoid columnals and bryozoans. |
| 81 | 0.4 | 530.5 | LIMESTONE, wackestone; shades of gray and brown weathered; dark gray fresh; fusulinids; medium bed; slope former. |
| 80 | 4.9 | 530.1 | covered slope, with poor outcrops of light gray shale. |

---

Top Del Cuerto Formation (31.8 m thick)

---------- FAULT, down-to-east ~2 m

| | | | |
|---|---|---|---|
| 79 | 0.7 | 525.2 | LIMESTONE, wackestone; shades of gray and brown weathered; brownish-gray fresh; brachiopods, crinoid columnals, and unidentified skeletal material; medium bed; base of slope. |

---------- SHEAR ZONE

| | | | |
|---|---|---|---|
| 78 | 4.9 | 524.5 | LIMESTONE, packstone and wackestone, arenaceous and argillaceous; shades of brown with gray weathered; brownish-gray fresh; crinoid columnals, fenestrate (very abundant) and branching bryozoans, brachiopods, microfossils, silt and coarse-grained quartz (<1% in basal brachiopod packstone); thin to medium beds; wavy laminae; rounded slope and dip-slope former. |
| 77 | 2.4 | 519.6 | LIMESTONE, wackestone; light gray weathered; light brownish-gray fresh; brachiopods (large), microfossils, and unidentified skeletal material; thin to medium beds; stepped small ledge and dip-slope former. |
| 76 | 1.0 | 517.2 | covered slope, with small outcrops of brownish, abundantly fossiliferous, calcareous shale; very abundant brachiopods. |
| 75 | 2.8 | 516.2 | LIMESTONE, packstone with wackestone; light brown and grays weathered; medium brownish-gray fresh; fusulinids, brachiopods, and gastropods; thin to medium |

beds; small stepped ledge and dip-slope former.

| | | | |
|---|---|---|---|
| 74 | 1.0 | 513.4 | SILTSTONE, calcareous, and CONGLOMERATE, lime pebble (at base); conglomerate--speckled blackish-gray on shades of gray weathered; very well-rounded pebbles of carbonate mudstone, wackestone, packstone, and grainstone, with calcareous siltstone matrix; siltstone--yellowish-orangish-brown and gray weathered; dark gray fresh; thin beds; low-angle, wedge-shaped cross-beds, and planar parallel laminae; increasing carbonate content upwards; slope former. |
| 73 | 1.7 | 512.4 | covered slope |
| 72 | 6.0 | 510.7 | LIMESTONE, packstone, wackestone and mudstone; gray and light brown, and mottled gray weathered; medium gray fresh; phylloid algae, fusulinids, brachiopods, crinoid columnals, and microfossils; thin to thick beds; capped by phylloid algae packstone and fusulinid packstone. |
| 71 | 0.4 | 504.7 | CONGLOMERATE, lime pebble; speckled grays weathered and fresh; well-rounded to very well-rounded, medium to very coarse-grained sand, and pebbles of limestone with skeletal material; crinoid columnals and brachiopods; medium bed; slope former. |
| 70 | 5.7 | 504.3 | LIMESTONE, wackestone, packstone, and grainstone; light to medium gray weathered; light brownish-gray fresh; phylloid algae, brachiopods, and rare gastropods; medium and very thick (base) beds; upper medium beds are grainstone; cliff and dip-slope former. |
| 69 | 4.5 | 498.6 | LIMESTONE, packstone; grayish-white to dark gray weathered; dark gray fresh; crinoid columnals, branching bryozoans, brachiopods (small), fusulinids, microfossils, and silt; very thin (nodular) to thick beds (increasing in thickness upwards); fusulinid packstone at top (fusulinids 2 × 8 mm in size); slope and ledge former below cliff. |
| 68 | 0.7 | 494.1 | SANDSTONE, calcareous; light to dark gray weathered; dark gray and speckled white fresh; medium beds; moderately-sorted, indurated, well-rounded to subangular medium-grained quartz, lithic, and feldspar sand, with limestone and a few quartz and feldspar pebbles; crinoid columnals, branching bryozoans, and brachiopods; medium beds. |

---

Top Story Formation (70.6 m thick), upper limestone member

| | | | |
|---|---|---|---|
| 67 | 2.0 | 493.4 | LIMESTONE, mudstone; mottled light and medium gray weathered; brownish-gray fresh; medium beds; slope former, partially covered. |
| 66 | 3.9 | 491.4 | LIMESTONE, packstone and wackestone; light and |

| | | | |
|---|---|---|---|
| | | | medium gray weathered; light brownish-gray fresh; unidentified skeletal fragments, brachiopods (large); thin- to thick-bedded and nodular; wavy partings between beds; slope and small ledge former. |
| 65 | 3.2 | 487.5 | covered slope; carbonate mudstone crops out at base. |
| 64 | 9.8 | 484.3 | LIMESTONE, packstone; brown and light to medium gray weathered; light brownish-gray fresh; phylloid algae, brachiopods (small), and crinoid columnals; medium (base) and very thick (top) beds; slope and moderate ledge former. |
| 63 | 8.1 | 474.5 | LIMESTONE, packstone and wackestone; shades of gray and brown weathered; medium brownish-gray fresh; fusulinids (1.5 × 5 mm in size), phylloid algae, brachiopods (small and large), gastropods; medium beds, layered packstone and wackestone; phylloid algae packstone at top; slope former. |
| 62 | 2.4 | 466.4 | covered slope |

BOTTOM MEASURED SECTION THREE

::::::::::::::::::::::::::::::::::::::::::::::::::::::::::::::::::::::::::::::

TOP MEASURED SECTION TWO

| | | | |
|---|---|---|---|
| 61 | 1.6 | 464.0 | LIMESTONE, mudstone, argillaceous; shades of gray and reddish-brown weathered; light gray and light brown fresh; silt and clay; thin to medium beds; small-scale, trough-shaped cross-beds and planar parallel laminae; easily recognized bioturbation; small ledge former. |
| 60 | 1.8 | 462.4 | LIMESTONE, wackestone; shades of gray and brown weathered; mottled dark brownish-gray and blackish-gray fresh; silt and brachiopods; thick beds; medium ledge former. |

---

Top lower clastic member of Story Formation

| | | | |
|---|---|---|---|
| 59 | 19.5 | 460.6 | SHALE, calcareous; whitish-gray to gray weathered; light gray to blackish-gray fresh; silt, clay, and brachiopods (productids, spirifers, strophomenids, and other unidentified species); very thin to thin beds; slope former; abundant brachiopods near top. |
| 58 | 9.5 | 441.1 | LIMESTONE, wackestone; light gray weathered; light brownish-gray and grayish white fresh; intraclasts, phylloid algae, crinoid columnals, and silt; medium to thick beds; small ledge former. |
| 57 | 8.8 | 431.6 | LIMESTONE, wackestone and mudstone and SHALE, calcareous; light gray, brownish-gray, light brown, and reddish-brown weathered; dark gray and brownish-gray fresh; silt, and minor gastropods, crinoid columnals, and |

| | | | |
|---|---|---|---|
| | | | brachiopods; very thin to thick beds; small-scale, trough-shaped cross-beds and parallel laminated; wavy partings, slope and small ledge former. |
| | | | --- |
| | | | Top Burrego Formation (52.0 m thick) |
| 56 | 5.8 | 422.8 | LIMESTONE, wackestone and packstone; gray weathered; gray fresh; brachiopods, phylloid algae, and gastropods; medium to very thick beds; large ledge former. |
| 55 | 7.4 | 417.0 | SHALE, calcareous and LIMESTONE, mudstone; shades of gray and brown weathered; silt and clay; very thin to medium beds; one bed changes laterally into a sandstone ~0.5 km from section; wavy laminae and bed surfaces; slope former. |
| 54 | 5.5 | 409.6 | LIMESTONE, mudstone and wackestone; dark gray weathered; blackish-gray fresh; crinoid columnals; thin to medium beds; medium ledge former. |
| 53 | 12.7 | 404.1 | covered slope |
| 52 | 2.9 | 391.4 | LIMESTONE, wackestone, mudstone and packstone, argillaceous; variable grays, brown-grays, browns, red-browns weathered; grayish-brown to dark brown fresh; brachiopods (packstone at top), bryozoans and unidentified skeletal material; thin to thick beds; small slope and ledge former. |
| 51 | 14.4 | 388.5 | SHALE, calcareous and LIMESTONE, nodular mudstone; gray and grayish-white weathered; very thin beds. |
| 50 | 3.3 | 374.1 | LIMESTONE, wackestone; shades of gray and brown weathered; dark grayish-brown fresh; brachiopods, bryozoans, crinoid columnals, rugose corals, and chert in very small nodules and elongate nodules; thin to thick beds; wavy laminae, small ledge former. |
| | | | --- |
| | | | Top Council Spring Limestone (14.9 m thick) |
| 49 | 8.4 | 370.8 | LIMESTONE, wackestone; shades of gray and brown weathered; grayish-brown and brownish-gray fresh; phylloid algae, crinoid columnals (concentrated at base), and fusulinids; thin to very thick beds; medium ledge former. |
| 48 | 6.5 | 362.4 | LIMESTONE, wackestone; light gray weathered; grayish-white fresh; phylloid algae; very thick bed; wavy laminae at base; large ledge former. |
| | | | --- |
| | | | Top Adobe Formation (27.9 m thick) |
| 47 | 5.9 | 355.9 | SHALE, calcareous and LIMESTONE, mudstone and |

wackestone; reddish-brown and gray weathered; small brachiopods (productids), Syringopora, bryozoans, crinoid columnals, silt and clay; very thin to thin beds; slope former.

| | | | |
|---|---|---|---|
| 46 | 3.0 | 350.0 | LIMESTONE, mudstone and wackestone; mottled shades of brown and gray weathered; dark gray fresh; crinoid columnals, and small chert nodules; thick beds; |
| 45 | 6.4 | 347.0 | LIMESTONE and SILTSTONE; rare rugose corals, and silt; thin to thick beds; mostly covered slope. |
| 44 | 6.9 | 340.6 | LIMESTONE, mudstone, wackestone and packstone; brown, reddish-brown, brownish-gray, and gray weathered; dark gray fresh; intraclasts, crinoid columnals, Chaetetes and rugose corals, and bedded and nodular chert; thin to thick beds; crinoid packstone at base; discontinuous wavy laminae; large ledge former. |
| 43 | 5.7 | 333.7 | LIMESTONE, mudstone and wackestone, argillaceous; light brown and gray weathered; gray fresh; small brachiopods, bryozoans, fusulinids, crinoid columnals, chert, and silt; thin to medium beds; chert bed at top; slope former. |

---

Top Coane Formation (25.5 m thick)

| | | | |
|---|---|---|---|
| 42 | 8.3 | 328.0 | LIMESTONE, wackestone; shades of gray and brown weathered; dark gray fresh; crinoid columnals, very large rugose corals, phylloid algae, brachiopods; medium to very thick beds; medium ledge former. |
| 41 | 12.2 | 319.7 | LIMESTONE, wackestone and packstone, argillaceous; brown, brownish-gray, and gray weathered; shades of dark gray fresh; fusulinids, crinoid columnals, bryozoans, rugose corals, and clay; medium to very thick beds; argillaceous upper beds; forms medium ledges and slope. |
| 40 | 5.0 | 307.5 | LIMESTONE, packstone and wackestone, argillaceous; brown, brownish-gray, and gray weathered; shades of gray fresh; rugose corals, fusulinids, bryozoans, crinoid columnals, brachiopods, silt and clay; thin to medium beds; slope former; easily distinguished by a rugose coral "death assemblage". |

---

Top Amado Limestone (11.5 m thick)

| | | | |
|---|---|---|---|
| 39 | 11.5 | 302.5 | LIMESTONE, grainstone; gray weathered; dark gray fresh; crinoid columnals, microfossils, and unidentified skeletal material; thin (base) and very thick beds (top); wavy partings in base; cliff former. |

---

Top Bartolo Formation (34.9 m thick)

| | | | |
|---|---|---|---|
| 38 | 11.4 | 291.0 | LIMESTONE, wackestone; shades of gray and brown weathered; shades of gray fresh; crinoid columnals, branching and rugose corals, brachiopods, and chert nodules; thin to very thick beds; forms large ledges. |
| 37 | 2.1 | 279.6 | covered slope |
| 36 | 12.4 | 277.5 | LIMESTONE, wackestone and packstone; shades of gray and brown with black weathered; gray and blackish-gray fresh; large brachiopods (productids), branching and rugose corals, fusulinids, lime mud, chert nodules, microfossils and clay; medium to very thick beds; wavy laminae and shale interbeds; forms large ledges with slopes. |
| 35 | 2.2 | 265.1 | covered slope |
| 34 | 1.8 | 262.9 | LIMESTONE, wackestone, argillaceous; gray, black and brown weathered; silt, and unidentified skeletal material; small ledge former. |
| 33 | 5.0 | 261.1 | covered slope (fissile shale on slope) |

---

Top Garcia Formation (36.8 m thick)

| | | | |
|---|---|---|---|
| 32 | 14.8 | 256.1 | LIMESTONE, packstone and wackestone; light to dark gray, brownish-gray, and light to dark gray weathered; medium gray to black fresh; crinoid columnals, fusulinids, branching bryozoans, brachiopods, and chert; thick to very thick beds; chert in elongate, irregular nodules; large ledge former. |
| 31 | 3.3 | 241.3 | covered slope |
| 30 | 18.7 | 238.0 | LIMESTONE, wackestone and packstone, argillaceous; mottled brownish-gray, gray, and brown weathered; dark brownish-gray fresh; fusulinids, branching and fenestrate bryozoans, brachiopods, rugose and branching corals, crinoid columnals, intraclasts, chert nodules, silt and clay; thin to very thick beds; wavy shale partings; forms medium ledges and slope. |

---

Top Whiskey Canyon Limestone (57.3 m thick)

| | | | |
|---|---|---|---|
| 29 | 16.2 | 219.3 | LIMESTONE, wackestone and packstone; light to dark brown and gray weathered; shades of gray and brown fresh; chert, brachiopods, rugose and branching corals, and fusulinids; thick to very thick beds; wavy laminae; abundant crenulated-chert in layers; forms large ledges. |
| 28 | 2.2 | 203.1 | LIMESTONE, mudstone and wackestone, argillaceous; light to dark gray and brown weathered; light to dark gray fresh; unidentified skeletal material; very thin to medium |

| | | | |
|---|---|---|---|
| | | | beds; wavy laminae and shaley partings; slope former. |
| 27 | 7.0 | 200.9 | covered slope |
| 26 | 9.7 | 193.9 | LIMESTONE, wackestone and packstone; gray, mottled gray, and dark brown weathered; dark gray and blackish gray fresh; rugose corals, brachiopods, bryozoans, and intraclasts; medium to very thick beds; forms partially covered small ledges. |
| 25 | 3.9 | 184.2 | covered slope |
| 24 | 11.6 | 172.6 | LIMESTONE, wackestone and packstone; shades of gray and brown weathered; dark gray and black fresh; chert, rugose corals, and brachiopods; medium to very thick beds; abundant crenulated-chert in layers; forms large ledges. |

---

Top Elephant Butte Formation (83.5 m thick)

| | | | |
|---|---|---|---|
| 23 | 3.8 | 162.0 | SANDSTONE; gray, brown, black, and weathered speckled white weathered; shades of gray, brown and white fresh; well-indurated, moderatly-sorted, subangular to angular, coarse-grained quartz and feldspar sand with very minor siltstone pebbles; medium to very thick beds; large-scale, wedge- and trough-shaped cross-beds; moderate ledge former. |
| 22 | 16.0 | 158.2 | LIMESTONE, wackestone and packstone; shades of gray and brown weathered; dark gray and black fresh; Chaetetes and rugose colonies, brachiopods, and intraclasts; medium to very thick beds; thin and very broad Chaetetes colonies on wavy surfaces; small cliff former. |
| 21 | 3.1 | 142.2 | covered slope |
| 20 | 8.6 | 139.1 | LIMESTONE, wackestone and packstone, arenaceous; shades of brown and gray weathered; dark gray fresh; brachiopods (Composita, spirifers), phylloid algae, Chaetetes and rugose corals, crinoid columnals, fusulinids, and medium- to coarse-grained quartz and minor feldspar sand; thin to thick beds; wavy shaley layers between beds; small-scale, wedge-shaped cross-beds in thin sand layers; small to moderate ledge formers. |
| 19 | 3.0 | 130.5 | covered slope |
| 18 | 4.7 | 127.5 | LIMESTONE, wackestone and packstone; brownish-gray weathered; dark gray fresh; Chaetetes and rugose corals, crinoid columnals, brachiopods, and phylloid algae; medium to very thick beds; wavy shaley layers between beds; Chaetetes colonies on wavy surfaces; moderate ledge former. |
| 17 | 1.4 | 122.8 | LIMESTONE, mudstone; shaley partings; poor |

exposure; mostly covered slope.

| | | | |
|---|---|---|---|
| 16 | 11.2 | 121.4 | LIMESTONE, wackestone and mudstone; brown, orangish- and reddish-brown, and light to blackish-gray weathered; dark gray and grayish-black fresh; brachiopods, phylloid algae, crinoid columnals, bryozoans, and rugose corals; thin to thick beds with shaley partings; forms small ledges with covered slope. |
| 15 | 3.2 | 110.2 | covered slope |
| 14 | 6.2 | 107.2 | LIMESTONE, wackestone and packstone; gray and orange-brown weathered; dark gray fresh; Chaetetes and rugose corals, branching bryozoans, brachiopods, phylloid algae, fusulinids, crinoid columnals, silt and clay; thin to thick beds; Chaetetes colonies on wavy surfaces; forms small ledges with covered slopes. |
| 13 | 3.0 | 100.8 | covered slope |
| 12 | 5.8 | 97.8 | SANDSTONE; brown, gray, black, and speckled white weathered; brown, gray, and speckled white fresh; very poorly-sorted, subrounded to subangular, well-indurated, fine- to very coarse-grained quartz and feldspar; very minor quartz pebbles; medium to thick beds; planar parallel laminae by color and grain size; vague, very low-angle, wedge-shaped cross-beds; small ledge former. |
| 11 | 7.7 | 92.0 | LIMESTONE, argillaceous; light gray and gray weathered; gray and dark gray fresh; silt; thin beds; slope former. |
| 10 | 2.6 | 84.3 | LIMESTONE, packstone and wackestone; brown and gray weathered; dark gray fresh; brachiopods, echinoid spines, crinoid columnals, fusulinids, and phylloid algae; medium to thick beds; shaley partings between beds; medium laminae by color; small ledge former. |
| 9 | 3.2 | 81.7 | covered slope |

---

Top Sandia Formation (78.5 m thick)

| | | | |
|---|---|---|---|
| 8 | 2.3 | 78.5 | SANDSTONE; brown weathered and fresh; moderately- (lower half) and well- (upper half) sorted, indurated, subrounded to subangular, fine- to coarse-grained quartz with minor feldspar; few chert nodules 1.5 × 6.0 cm in size; thick beds; large-scale, wedge- and trough-shaped cross-beds; small ledge former. |
| 7 | 24.9 | 76.2 | covered slope. |
| 6 | 6.9 | 51.3 | SANDSTONE, fossiliferous; yellow, orange-brown, and brownish-black weathered; red-brown to gray and white |

| | | | |
|---|---|---|---|
| | | | fresh; moderately sorted, indurated, subrounded to subangular, very fine to coarse-grained quartz with minor feldspar; brachiopods and skeletal material; medium beds; vague large-scale, low-angle, trough-shaped cross-beds; forms small ledges. |
| 5 | 20.0 | 44.4 | covered slope. |
| 4 | 0.9 | 24.4 | LIMESTONE, fossiliferous mudstone; gray weathered; brown-gray fresh; rugose corals, brachiopods. |
| 3 | 4.7 | 23.5 | SANDSTONE; brownish-purple weathered; pinkish-gray and white fresh; poorly sorted, well-indurated, subangular to angular, medium- to very coarse-grained quartz sand with minor feldspar; very thick beds; large-scale, wedge-shaped cross-beds at base, planar parallel laminated upper; large ledge former. |
| 2 | 12.8 | 18.8 | SANDSTONE; brown to white (variable) weathered; poorly- sorted, poorly- to well-indurated, very fine- to coarse-grained sand, sandstone pebbles (<5%) in upper beds; thin to medium beds; poor exposures on slope. |
| 1 | 6.0 | 6.0 | QUARTZ PEBBLE CONGLOMERATE; brown, white-speckled weathered; well-indurated, coarse-grained quartzose sand and rounded pebbles up to 2 cm in length; thick to very thick beds; conglomerate in lenses 10 to 120 cm thick. |

---------- nonconformity ----------

PRECAMBRIAN

GRANITOID; reddish-brownish-orange weathered; dark pink fresh; coarse-grained.

# APPENDIX D

*LOWER PERMIAN MEASURED SECTIONS FOUR-A (lower Bursum Formation) AND FOUR-B* (lower Abo and upper Bursum Formations).

## MEASURED SECTION FOUR-A: lower Bursum Formation

Section 4-A is located in the NW/4 section 4, T3N. R3W., and SW/16 section 33, T4N. R3W. (Plate 1). Measured Section Four-A is a composite section that begins at Coyote draw where the arroyo initiates a clockwise turn off a north-northeast-trending course. The section-line trends west-northwestward on the southern side of a low ridge and ends east of a down-to-the-east fault.

## MEASURED SECTION FOUR-B: lower Abo and upper Bursum Formations

Section 4-B is located in the SW/16 section 33 and SE/4 section 32, T4N. R3W. (Plate 1). Measured Section Four-B starts at the east end of an eastwest-trending, low, narrow ridge. East of this location, Measured Section Four-A is repeated. Section-line Four-B trends westward across a large down-to-the-west fault, where the top of Bursum and basal Abo Formations are faulted out. This section ends at Mesa Sarca fault.

SECTION FOUR-B, LOWER ABO FORMATION

| Unit No. | Thickness (unit) | Thickness (cum) | |
|---|---|---|---|
| | | | Top of Abo Formation is faulted out |
| 15 | 9.8 | 132.8 | SANDSTONE; brownish-red weathered; brown fresh; very fine-grained sand; thin- to medium-bedded with shale interbeds; massive and platy weathering; climbing rippled and trough-shaped cross-bedding, and planar parallel bedding; abundant reduction spots; abundant fern-like leaf impressions; forms small ledges and covered slopes. |
| 14 | 22.5 | 123.0 | covered slope, presumed similar to unit below. |
| 13 | 18.0 | 100.5 | SANDSTONE and SHALE; brownish-red and gray weathered; very fine-grained sand; very thin to medium beds; massive to platy weathering; climbing ripple and trough-shaped cross-bedding; few reduction spots; burrows on bedding surfaces; few thin bluish-white layers; forms small ledges and covered slope. |
| 12 | 5.3 | 82.5 | covered slope. |
| 11 | 3.3 | 77.2 | SANDSTONE; reddish-brown weathered; brown fresh; thin to thick beds; very fine-grained massive beds with medium-grained interbeds; climbing ripple and trough-shaped cross-bedding, and minor planar-parallel bedding; few reduction spots; ripple marks, burrows, and fern-like leaf and stem impressions on bedding surfaces; forms small ledges. |
| 10 | 0.7 | 73.9 | CONGLOMERATE and SANDSTONE; whitish-gray, gray and brown weathered; medium beds; carbonate pebble and cobble clasts with coarse-grained sand matrix base, coarse- to fine-grained sandstone upper; trough-shaped cross-bedding; forms at base of small ledges. |
| 9 | 4.4 | 73.2 | SANDSTONE and SHALE; brownish-red and gray weathered; fine silt to very fine-grained sand; very thin to thin beds; low-angle, trough-shaped cross-bedding; mud cracks and burrows on bedding surfaces; small ledge and slope former. |
| 8 | 0.80 | 68.8 | CONGLOMERATE; mottled gray, brown, and reddish-brown weathered; medium beds; lime pebble and cobble clasts with thin lenses of very fine-grained, cross-bedded sandstone; forms base of small ledge. |
| 7 | 5.0 | 68.0 | covered slope |
| 6 | 16.8 | 63.0 | SANDSTONE; reddish-brown weathered; brown and purplish-brown fresh; very thin to medium beds; platy and massive weathering; low-angle, trough-shaped cross-bedding, |

| | | | |
|---|---|---|---|
| | | | wavy parallel bedding; ripple marks, burrows, fern-like leaf and stem impressions on bedding surfaces; small ledge and slope former. |
| 5 | 13.6 | 46.2 | SHALE; reddish-brown weathered. |
| --- | ---- | ---- | MAFIC DIKE; highly altered; fine-grained groundmass with biotite; vesicular chill margins with plagioclase phenocrysts; 2.1 m thick. |
| 4 | 16.8 | 32.6 | SHALE; brownish-red and reddish-brown weathered; few very thin beds of brownish-red siltstone. |
| 3 | 1.1 | 15.8 | CARBONATE SANDSTONE; brown and reddish-brown weathered; medium beds; poorly sorted, poorly indurated, well-rounded, medium- to very coarse-grained carbonate sand and few very fine-grained sandstone and carbonate pebbles; vague wedge-shaped cross-bedding; forms small ledge. |
| 2 | 10.2 | 14.7 | covered slope, presumed similar to unit below. |
| 1 | 4.5 | 4.5 | SHALE; brownish-red weathered; scattered irregularly shaped calcareous nodules. |

Basal Abo Formation is faulted out

---------- FAULT, down-to-west 20-40 meters

SECTION FOUR-B, UPPER BURSUM FORMATION

Upper Bursum Formation is faulted out

| | | | |
|---|---|---|---|
| 13 | 3.4 | 31.0 | LIMESTONE, mudstone and wackestone; purplish-gray, gray and brown weathered; gray fresh; large brachiopods, gastropods, microfossils, and skeletal fragments; thin- to medium-bedded and nodular; wavy shale interbeds; stepped ledge former. |
| 12 | 2.8 | 27.6 | SHALE; purple base and gray upper; slope former. |
| 11 | 3.6 | 24.8 | CONGLOMERATE, carbonate-pebble; grays and browns weathered and fresh; medium beds; well-rounded pebbles and cobbles of limestone and siltstone; medium-grained calcareous sand matrix; ledge former. Note: this unit locally thins to 12 cm thick. |

---

SECTION FOUR-A, LOWER BURSUM FORMATION

| | | | |
|---|---|---|---|
| 10 | 2.2 | 21.2 | SHALE; purplish-brown; slope former. |
| 9 | 0.4 | 19.0 | ARKOSE, calcareous; speckled gray and brown |

| | | | |
|---|---|---|---|
| | | | weathered; speckled brown, gray, and pink fresh; medium beds; subrounded to subangular, coarse- to very coarse-grained sand of quartz, feldspar, and carbonate; small ledge former. |
| 8 | 0.8 | 18.6 | LIMESTONE, packstone and wackestone; mottled gray and brown weathered; light and dark gray fresh; coated microfossils and skeletal fragments; medium beds; medium- to very coarse-grained arkosic sand; forms small ledge. |
| 7 | 6.1 | 17.8 | covered slope, presumed gray and reddish-brown shale and calcareous shale. |
| 6 | 0.3 | 11.7 | ARKOSE, micaceous; blackish- and reddish-brown weathered; blackish-gray fresh; fine- to medium-grained quartz, feldspar, and mica; medium bed; forms very small ledge. Note: this bed locally thickens to >2 m and lower units may disappear. |
| 5 | 5.1 | 11.4 | covered slope, presumed reddish-brown shale and nodular limestone. |
| 4 | 1.7 | 6.3 | LIMESTONE, packstone and wackestone; mottled dark and light brown and grays weathered; dark gray fresh; crinoid columnals, fenestrate and branching bryozoans, brachiopods, and microfossils; medium beds and covered slope. |
| 3 | 1.4 | 4.6 | LIMESTONE, mudstone; mottled light brown and light gray weathered; gray fresh; brachiopods and crinoid columnals; nodular and medium-bedded; forms slope and small ledge. |
| 2 | 1.7 | 3.2 | LIMESTONE, packstone and wackestone (upper); mottled light brown and gray weathered; gray fresh; crinoid columnals, brachiopods, branching bryozoans, fusulinids, and microfossils; nodular and medium bedded; forms small ledge. |
| 1 | 1.5 | 1.5 | SHALE, calcareous; yellowish-reddish-brown; base of small ledge. |

Base of Bursum Formation

# APPENDIX E

*LOWER PERMIAN MEASURED SECTION FIVE: (basal Abo and upper Bursum Formations)*

Section 4 is located in central section 5, T3N. R3W. (Plate 1). Measured Section Five starts on the west side of a down-to-the-west fault (same fault which cuts out the contact between the Bursum and Abo Formations in Sections Four A an B). Section-line trends westward across a low area cut by dikes, small faults, and possible unrecognized faults, and covered by a thin veneer of alluvium. Section-line ends at Mesa Sarca fault.

BASAL PERMIAN ABO FORMATION

| Unit No. | Thickness(m) (unit) | (cum) | |
|---|---|---|---|
| Upper Abo Formation is faulted out | | | |
| 5 | 8.5 | 33.5 | SHALE; brownish-red weathered; interbedded, small, irregularly shaped, calcareous nodules; rare very thin beds of siltstone; slope and covered slope former. Note: measurement may be incorrect due to poor exposures and gently-folded and possibly faulted strata. |
| 4 | 11.5 | 25.0 | SHALE and SANDSTONE; reddish-brown weathered; thin to medium sandstone beds with very thin shale interbeds; low-angle, trough-shaped cross-bedding, and wavy parallel bedding; forms covered slope with poor exposures. MAFIC DIKES intrude strata. Note: measurement may be incorrect due to poor exposures and gently-folded and possibly faulted strata. |
| 3 | 0.8 | 13.5 | SANDSTONE; reddish-brown weathered; medium beds; very fine- to fine-grained sand. |
| 2 | 7.2 | 12.7 | covered slope, with scattered outcrops of very thinly-bedded shale and siltstone. |
| --- | ---- | ---- | MAFIC DIKE; high alteration; ~2 m wide. |
| 1 | 5.5 | 5.5 | SHALE; lavender and reddish-brown lower, brownish-red upper. |
| base Abo Formation | | | |

---

TOP PENNSYLVANIAN BURSUM FORMATION

| | | | |
|---|---|---|---|
| 7 | 0.3 | 18.6 | LIMESTONE, packstone; lavender and brown weathered; gray fresh; gastropods and brachiopods; carbonate mud matrix; slope former. |
| 6 | 5.8 | 18.3 | SHALE, CALCAREOUS SHALE, and CARBONATE SANDSTONE; gray, reddish-brown, and lavender weathered; very thin to thin beds; base consists of shale and calcareous shale; cap consists of coarse-grained carbonate sandstone with a very thin layer of carbonate mudstone; forms slope. |
| 5 | 1.8 | 12.5 | CALCAREOUS SANDSTONE and LIMESTONE, mudstone; light gray, lavender, and brown weathered; gray fresh; thin-bedded and nodular; wavy parallel bedding; forms very small ledge. |
| 4 | 4.7 | 10.7 | SHALE; lavender and reddish-brown weathered; forms slope. |

| | | | |
|---|---|---|---|
| 3 | 0.4 | 6.0 | SANDSTONE; brown and brownish-gray weathered; thin and medium beds; medium- to very coarse-grained carbonate, lithic, and quartz sand with calcareous, very fine-grained sand matrix; forms very small ledge. |
| 2 | 4.5 | 5.6 | SHALE; reddish-brown; forms slope. |
| 1 | 1.1 | 1.1 | CONGLOMERATE; grays and browns weathered and fresh; thin to medium beds; well-rounded carbonate and siltstone pebbles and cobbles, with fine- to medium-grained, calcareous sand matrix; forms small ledges. |

Base of Bursum Formation is faulted out

# APPENDIX F

## *PERMIAN MEASURED SECTIONS SIX-A (Yeso Formation, Meseta Blanca member) AND SIX-B (Yeso Formation, Torres member)*

### MEASURED SECTION SIX-A: Yeso Formation, Meseta Blanca member

Section 6-A is located in the NE/16 section 4, T3N. R3W., and SE/16 section 33, T4N. R3W. (see Plate 1). Measured Section Six-A trends northeastward and is fault bounded. Thicknesses may be inaccurate due to abundant small faults and brecciated zones.

### MEASURED SECTION SIX-B: Yeso Formation, Torres member

Section 6-B is located in the SE/16 section 33, T4N. R3W. (see Plate 1). Measured Section Six-B trends northward and is fault bounded. Thicknesses may be inaccurate due to abundant small faults and brecciated zones.

SECTION SIX-A: YESO FORMATION, MESETA BLANCA MEMBER

| Unit No. | Thickness(m) (unit) | (cum) | |
|---|---|---|---|
| Upper Meseta Blanca is faulted out | | | |
| 7 | 2.1 | 100.6 | SANDSTONE; brownish-red, pink and blackish-brown weathered; brown fresh; well-indurated, very fine-grained sand; brecciated; massive; medium to thick beds; planar parallel and small-scale cross-bedding; slope former. |
| 6 | 2.3 | 98.5 | SANDSTONE; reddish-brown weathered; well-indurated, very fine-grained sand; medium beds; abundant reduction spots; forms resistent ridges on slope. |
| 5 | 10.5 | 96.2 | SANDSTONE and SILTSTONE; reddish-brown, brown, and brownish-gray weathered; very coarse-grained silt to very fine-grained sand; brecciated; medium to thick beds; forms slope. |
| 4 | 27.0 | 85.7 | SANDSTONE; reddish-brown weathered; brown fresh; very fine-grained sand; thick beds; locally brecciated; planar parallel bedding, and climbing ripple and trough-shaped cross-beds; reduction spots; few bluish-gray interbeds (lower); forms resistant ridges. |
| 3 | 29.0 | 58.7 | covered slope, with scattered outcrops of siltstone and/or sandstone. |
| 2 | 1.2 | 29.7 | CONGLOMERATE; yellowish- and reddish-brown, brown, and gray weathered; browns and grays fresh; subrounded pebbles of very fine-grained sandstone and limestone; matrix of very fine- to medium-grained sandstone; crops out on slope. |
| 1 | 28.5 | 28.5 | SANDSTONE; reddish-brown (lower) and bluish-white and reddish-brown (upper) weathered; fine-grained sand; platy, thin to thick and massive beds; brecciated lower and middle sections; forms resistent ridges and slope. |
| Base of Meseta Blanca Member is faulted out | | | |

SECTION SIX-B: YESO FORMATION, TORRES MEMBER

| | | | |
|---|---|---|---|
| Upper Torres Member is faulted out | | | |
| --- | --- | --- | Some upper beds of Torres member are visible, but are too faulted and brecciated to measure with accuracy. They consist of friable sandstones and one bed of sandstone-carbonate pebble conglomerate. |
| 11 | 3.5 | 75.5 | LIMESTONE, mudstone; light brownish-gray and dark gray weathered; brownish-gray fresh; thin to medium beds; |

| | | | |
|---|---|---|---|
| | | | wavy bed surfaces; forms small ridge. |
| 10 | 5.2 | 72.0 | covered slope, with scattered outcrops of yellowish-, reddish-, and grayish-brown friable sandstone. |
| 9 | 1.3 | 66.8 | LIMESTONE, mudstone; dark gray weathered; light grayish-brown fresh; thin (lower) to thick (upper) beds; small resistant ridge former. |
| 8 | 6.0 | 65.5 | covered slope, with scattered outcrops of yellowish-brown and gray, fine- to medium-grained, friable sandstone. |
| 7 | 1.0 | 59.5 | SANDSTONE, calcareous; light grayish-brown weathered; light brown and gray fresh; fine-grained sand; medium beds; highly brecciated; forms small ridge. |
| 6 | 6.2 | 58.5 | covered slope, with scattered outcrops of reddish- and yellowish-brown friable sandstone. |
| 5 | 1.2 | 52.3 | LIMESTONE, mudstone; light brownish-gray weathered; gray fresh; thin to medium beds; brecciated; resistant ridge former. |
| 4 | 7.5 | 51.1 | SANDSTONE; brownish-red, gray, and yellowish-gray (upper) weathered; medium beds; friable; slope and covered slope former. |
| 3 | 1.9 | 43.6 | LIMESTONE, mudstone; light brownish-gray weathered; gray fresh; thin to medium beds; brecciated; wavy bed surfaces; resistant ridge former. |
| 2 | 2.2 | 41.7 | SANDSTONE; pinkish-brown weathered; fine-grained sand; medium beds; calcareous cement; forms base of resistant ridge. |
| 1 | 39.5 | 39.5 | SANDSTONE; banded yellowish-brown, reddish-brown, buff, and pinkish-white weathered; browns and grays fresh; fine-grained sand; very thin to thick (upper) beds; friable; calcareous cement; small- and medium-scale, low-angle, trough-shaped cross-beds, and wavy parallel bedding; slope former. |

Base of Torres member is faulted out

# APPENDIX G

# STRATIGRAPHIC COLUMNS

## EXPLANATION

### Stratigraphy

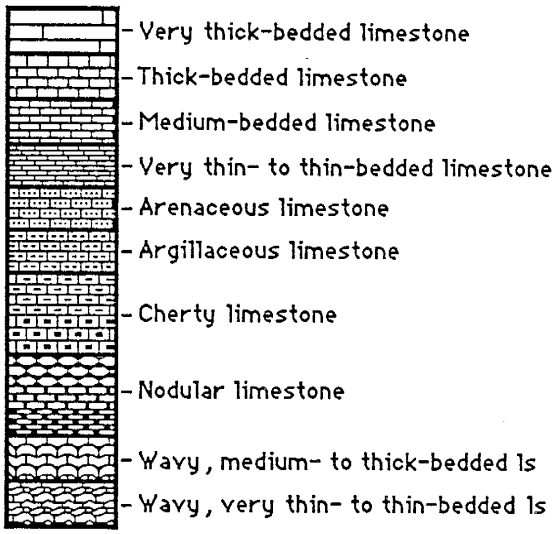


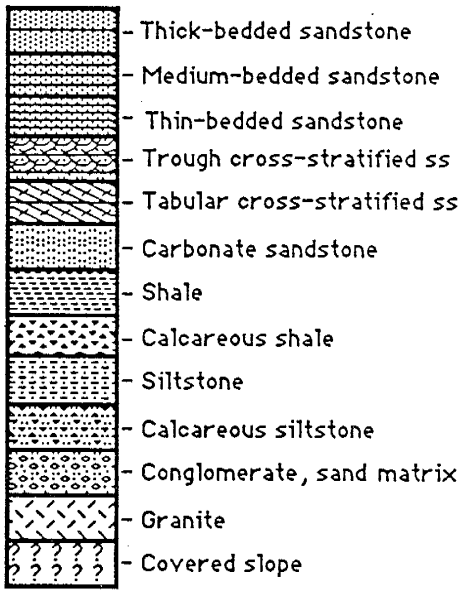


### Limestone Classification

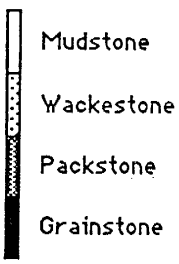


### Fossil Symbols

Symbols indicate fauna type. Placement of symbols reveal their relative abundance.

Example: ⊙ (1) ◇ (2) ⬭ (3) ▯ (4) ◠ (5) ✚ (6)

- ⊙ Crinoid Columnal
- ◇ Brachiopod
- ⬭ Fusulinid
- ▯ Rugose Coral
- ◠ Chaetetes
- ✚ Branching Coral
- Phylloid Algae
- Fenestrate Bryozoan
- Branching Bryozoan
- Gastropod
- Syringopora

APPENDIX G (cont.)

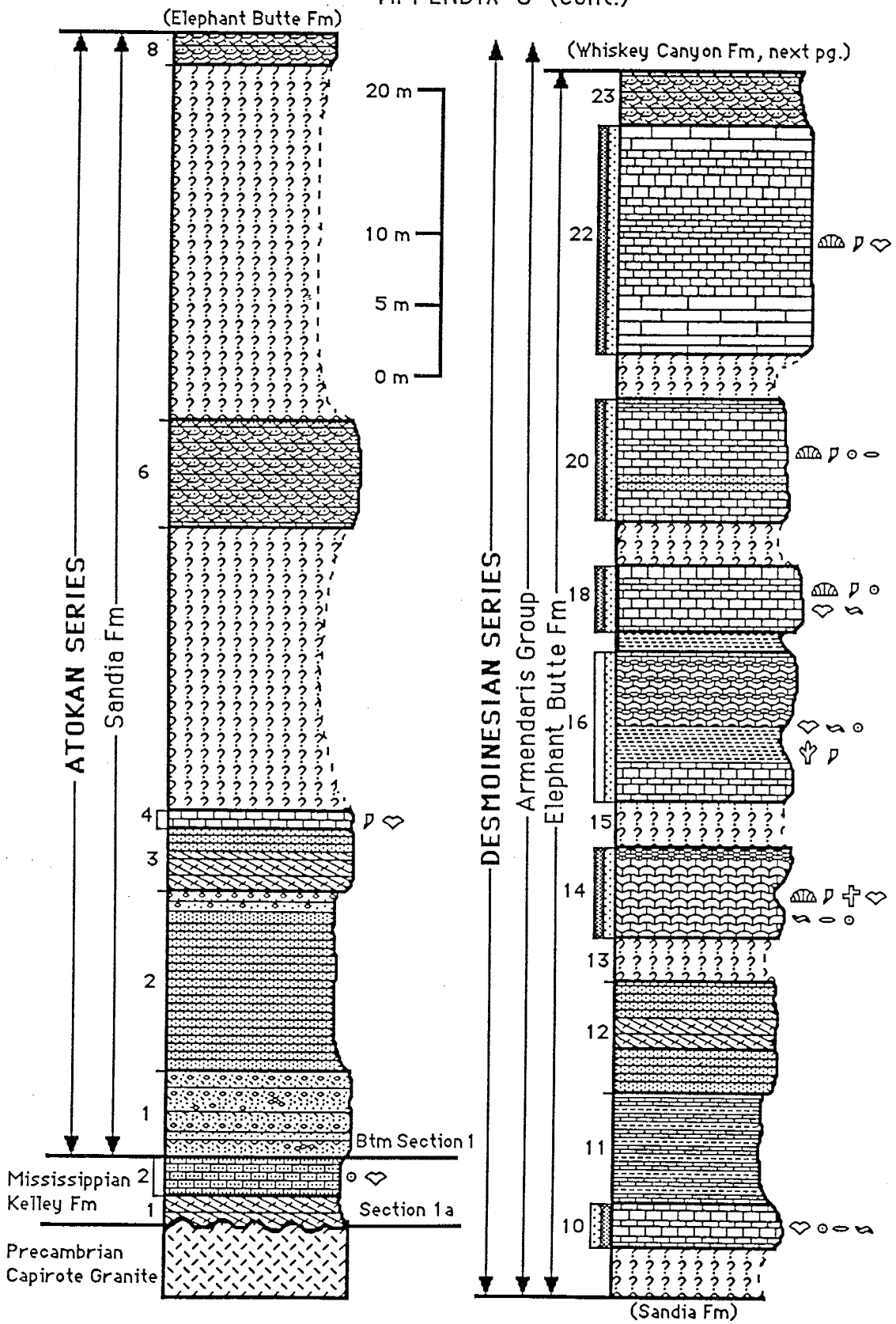

APPENDIX G (cont.)

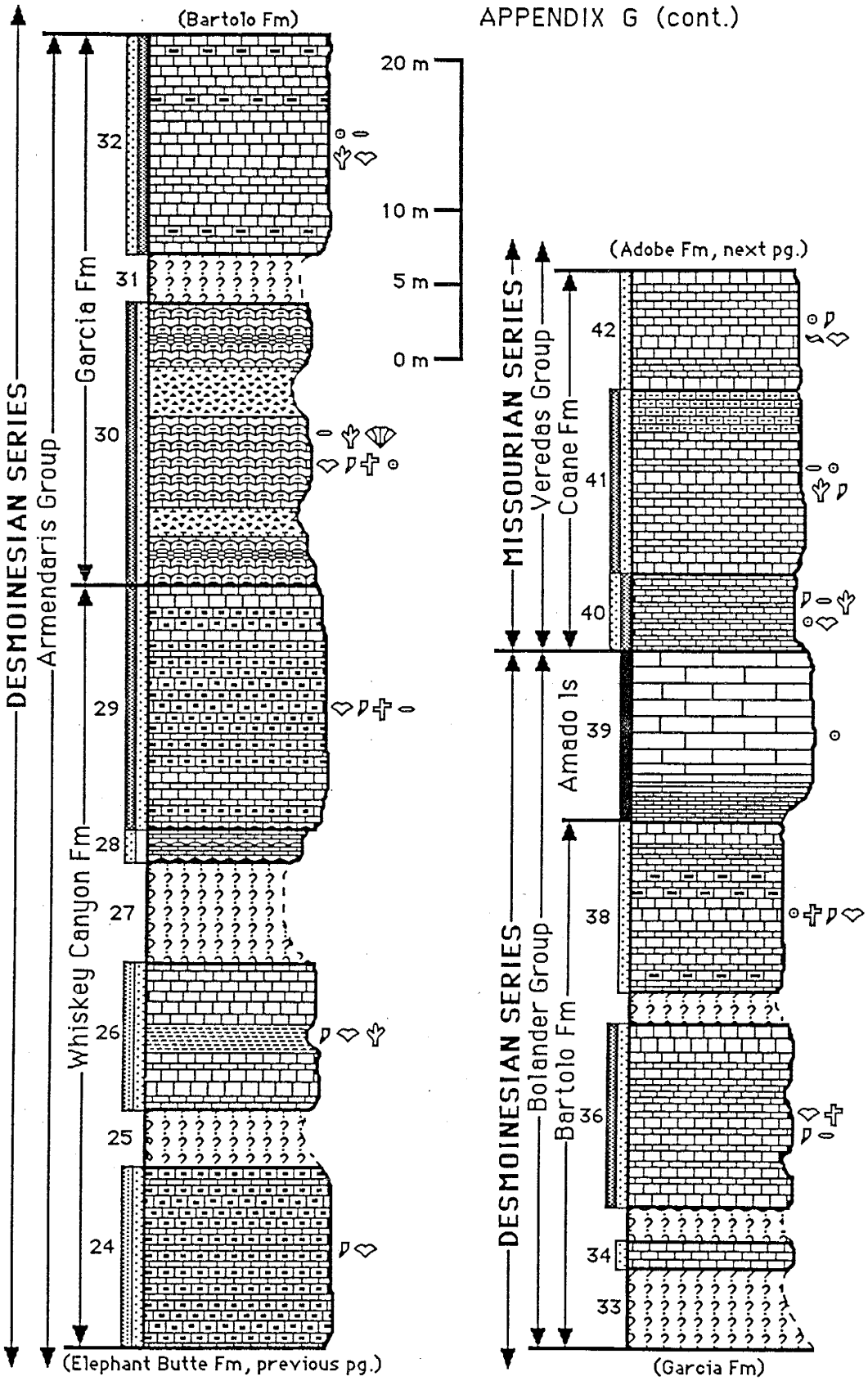

APPENDIX G (cont.)

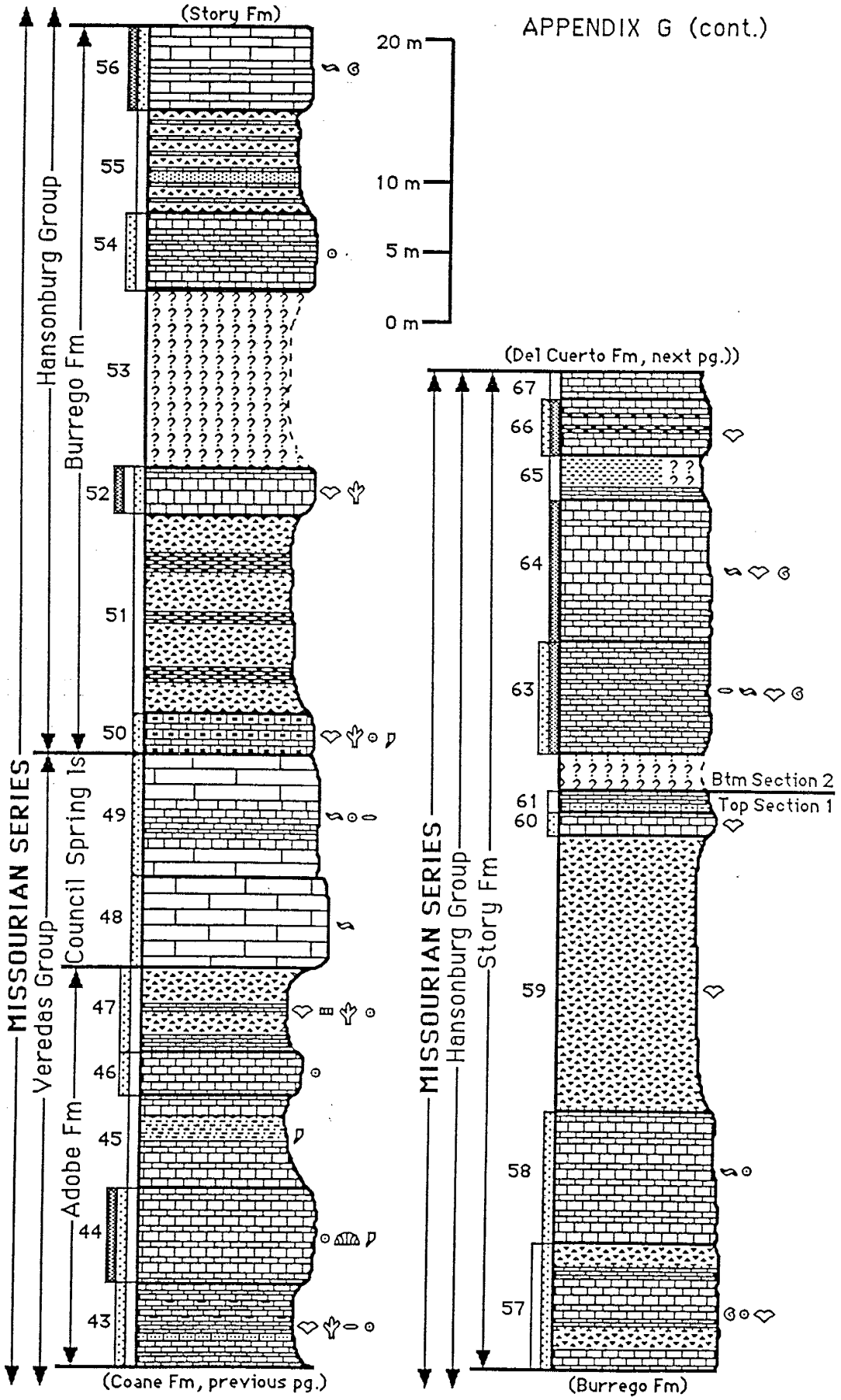

# APPENDIX G (cont.)

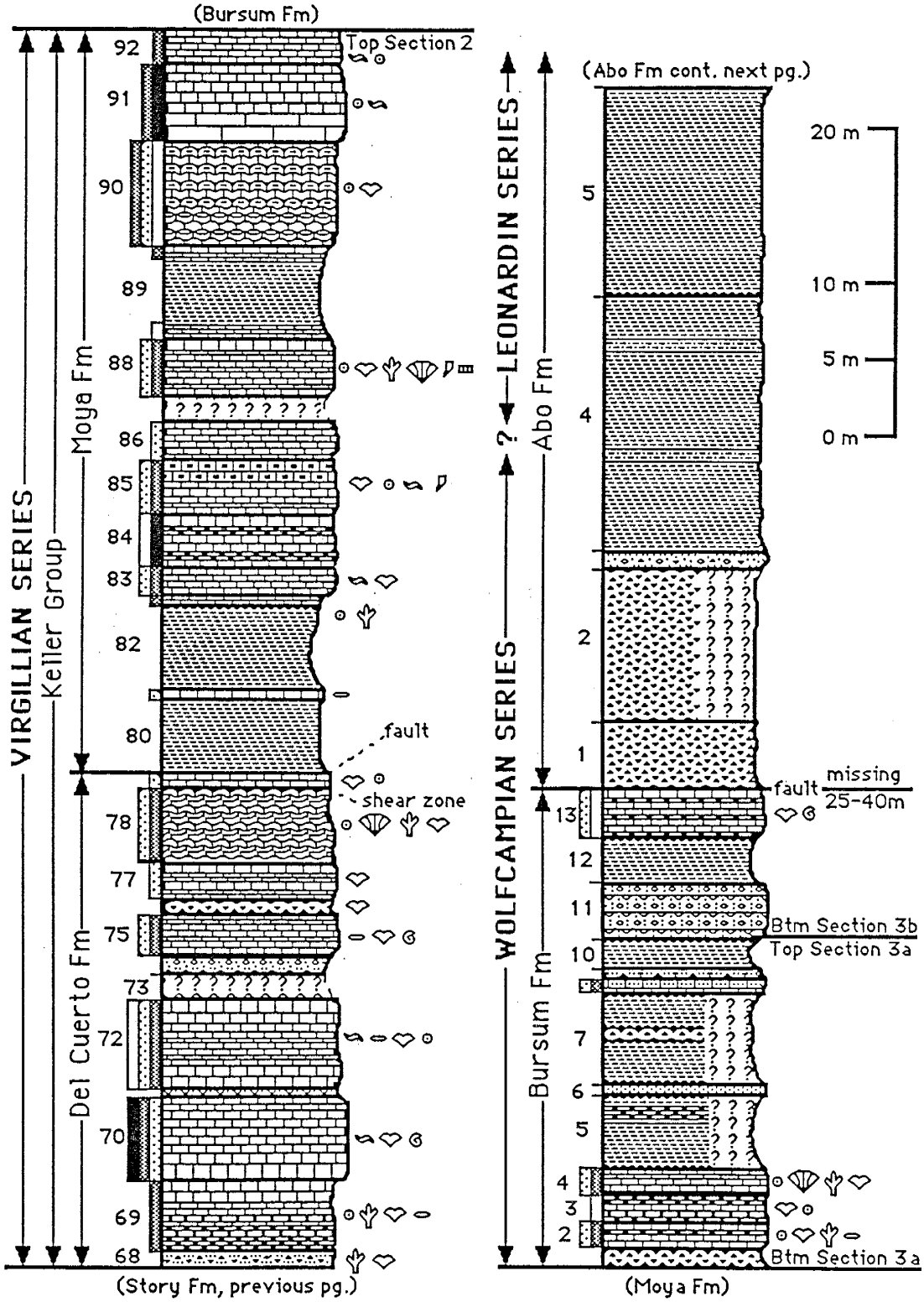

APPENDIX G (cont.)

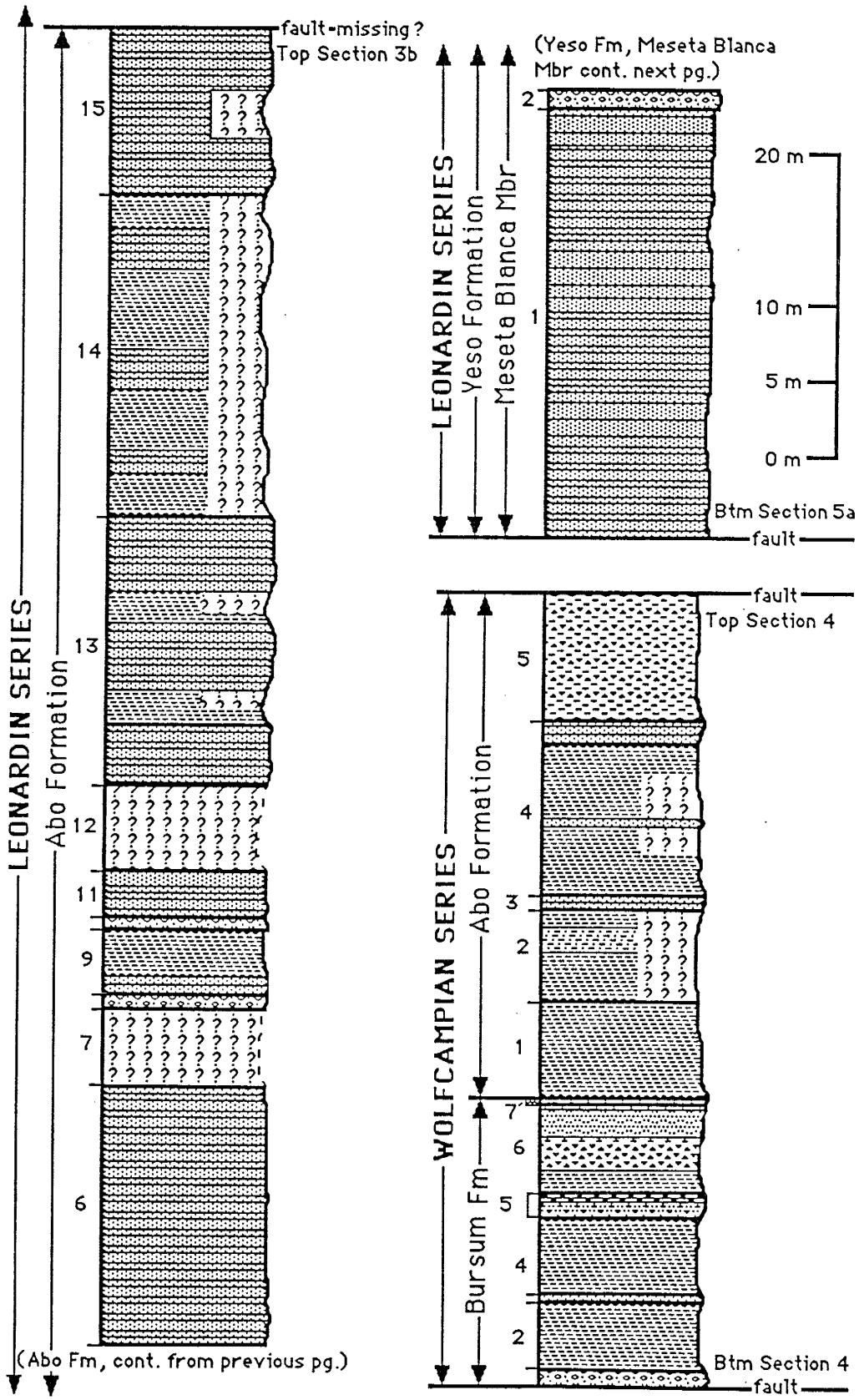

APPENDIX G (cont.)

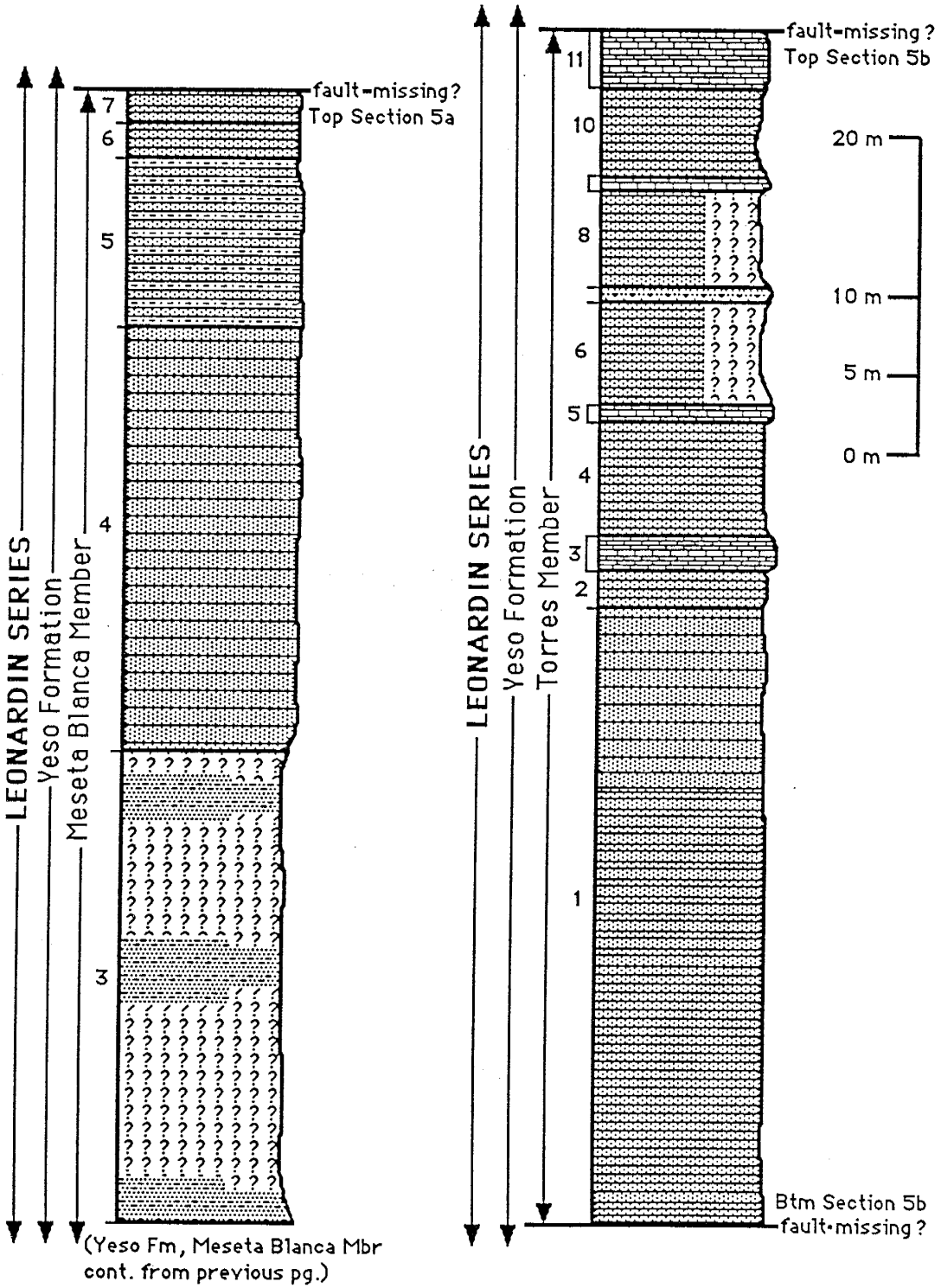

# APPENDIX H

Equal-area lower hemisphere stereographic projections for veins.

(a) Poles to extension veins in left-echelon arrays. Number of samples (N) = 35.

(b) Poles to extension veins in right-echelon arrays. N = 42.

(c) Poles to right-slip linear extension and shear veins. N = 59.

(d) Poles to left-slip linear extension and shear veins. N = 31.

(e) Poles to veins with indeterminate slip. N = 166.

APPENDIX H (continued)

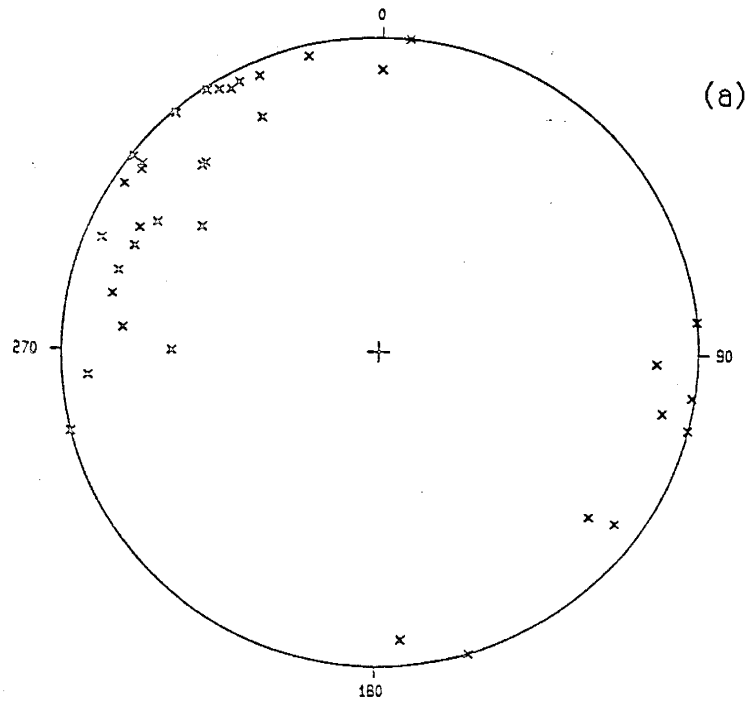


(a)

(b)

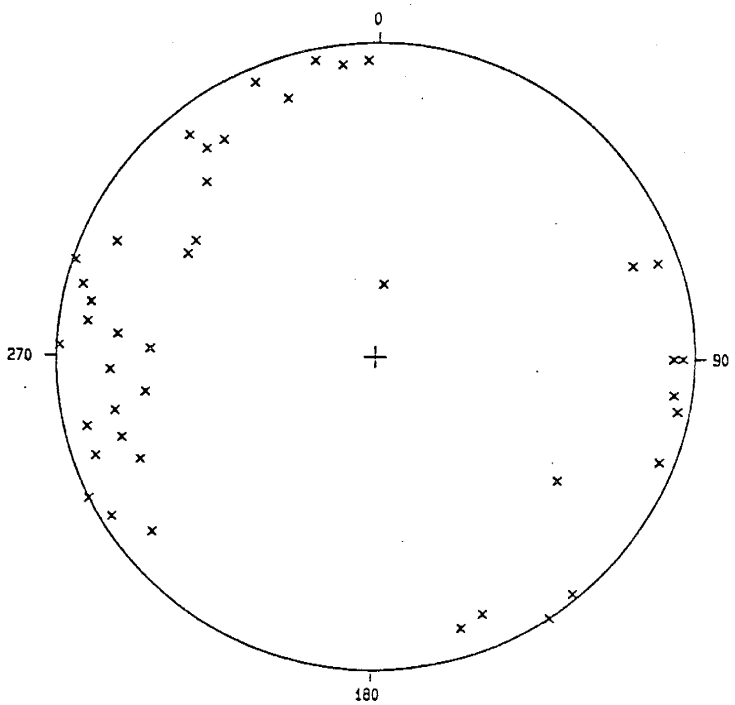

APPENDIX H (continued)

(c)

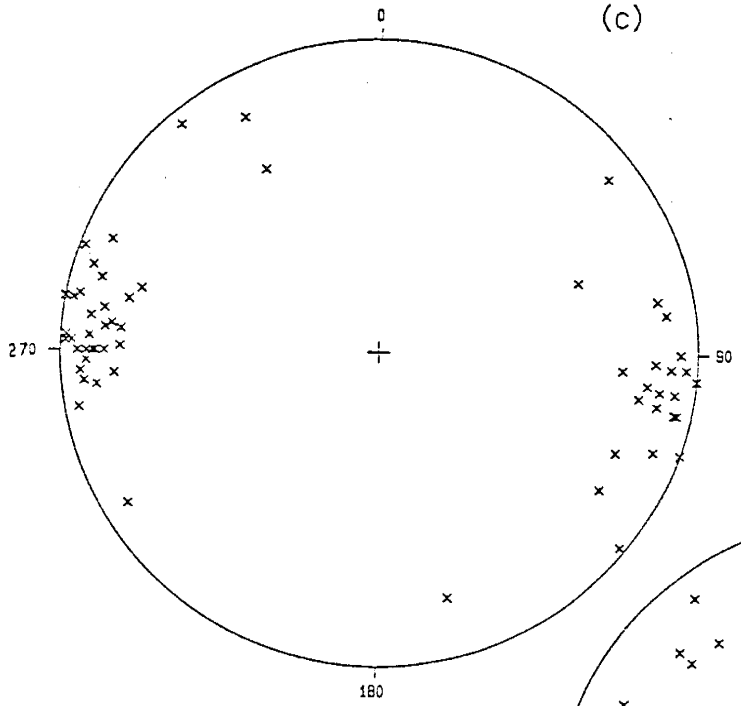


(d)

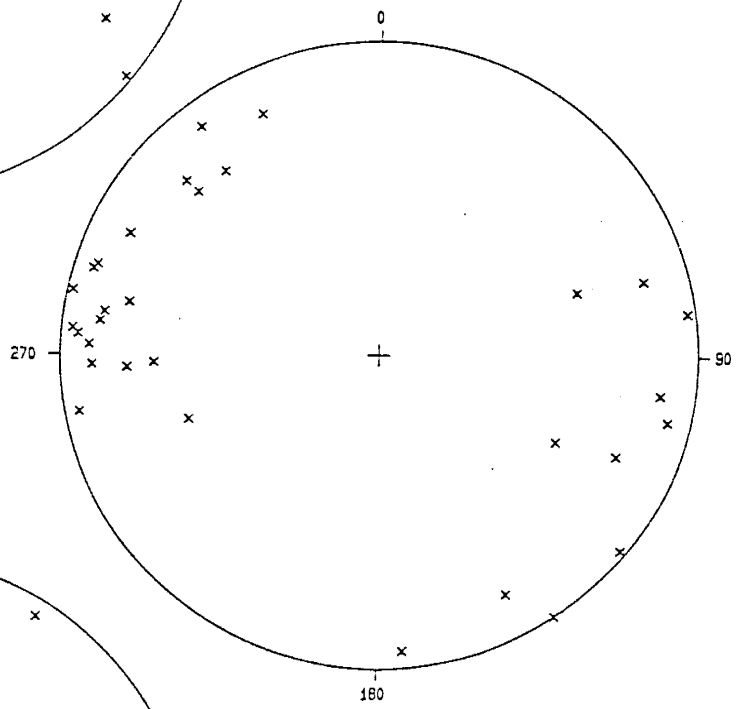


(e)

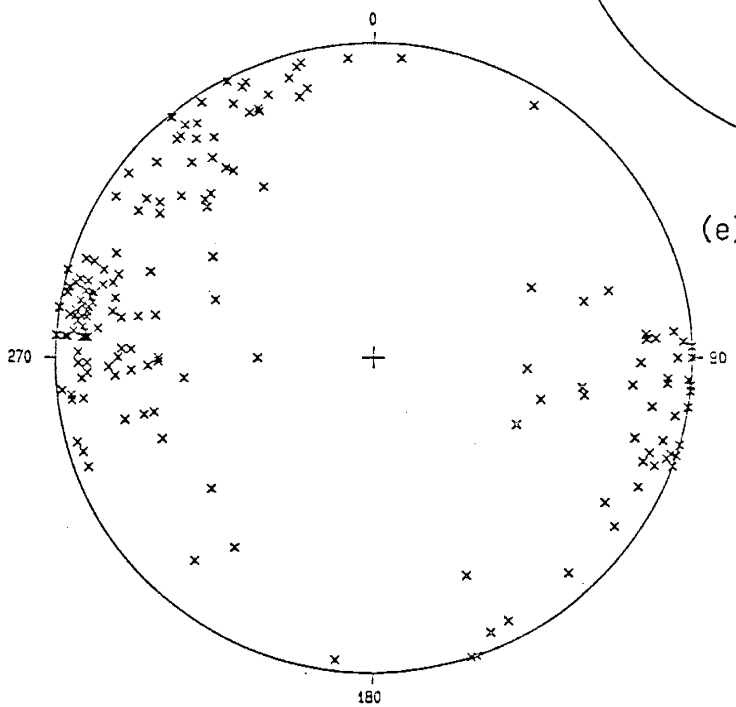

# APPENDIX I

Equal-area lower hemisphere stereographic projections for faults and striations.

(a) Poles to right-slip faults. Number of samples (N) = 33.

(b) Striations in right-slip faults. N = 26.

(c) Poles to left-slip faults. N = 30.

(d) Striations in left-slip faults. N = 27.

(e) Poles to thrust faults. N = 10.

(f) Striations in thrust faults. N = 8.

(g) Poles to normal faults. N = 13.

(h) Striations in normal faults. N = 13.

(i) Poles to reverse faults. N = 4.

(j) Striations in reverse faults. N = 6.

(k) Poles to faults with indeterminate motion. N = 114.

(l) Striations in faults with indeterminate motion. N = 57.

APPENDIX I (continued)

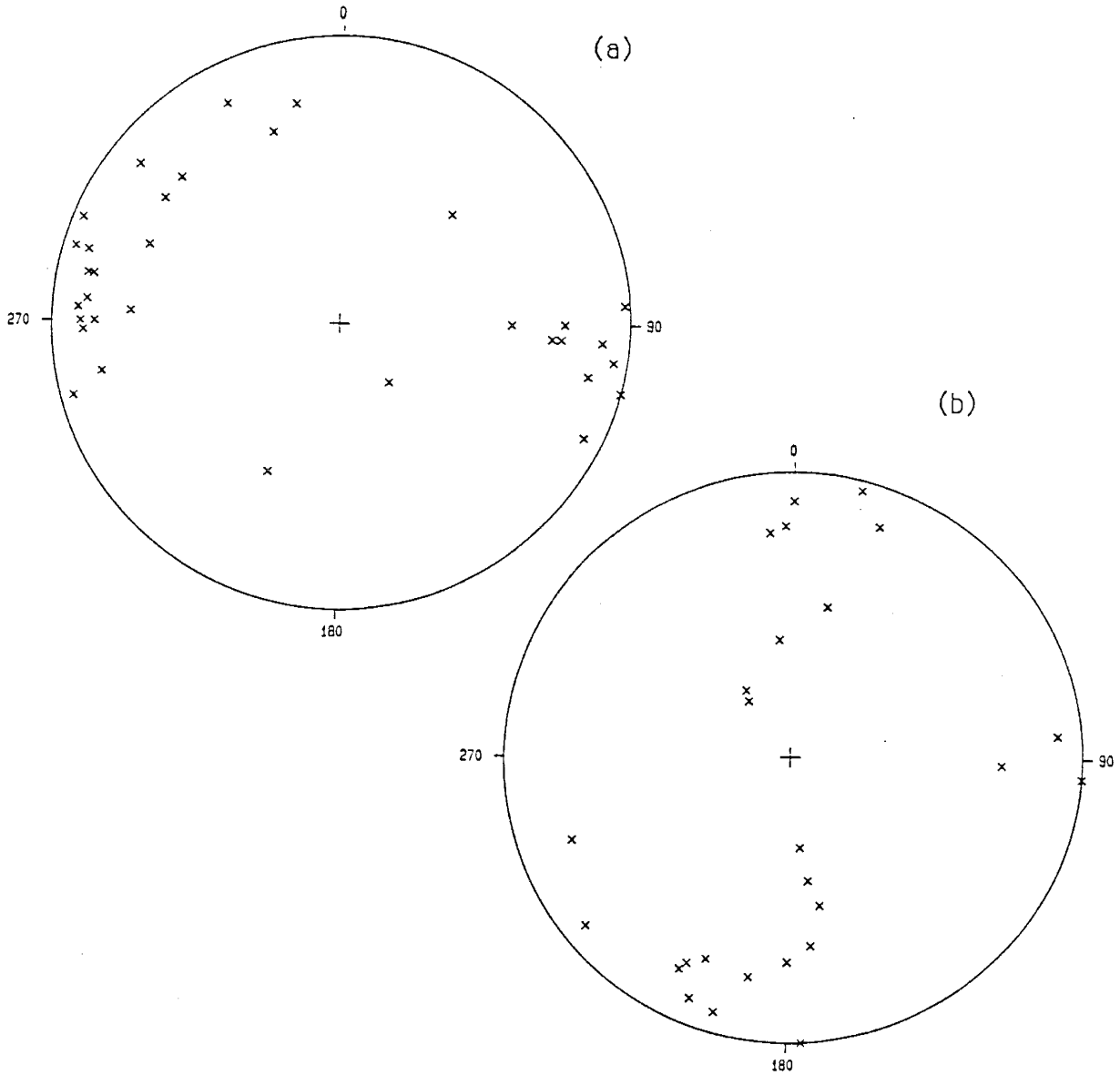

APPENDIX I (continued)

(c)

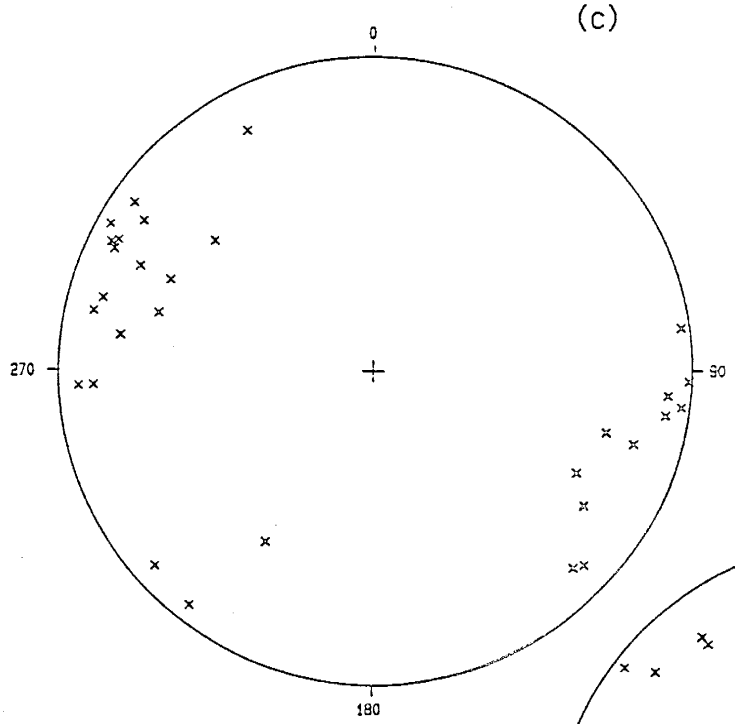


(d)

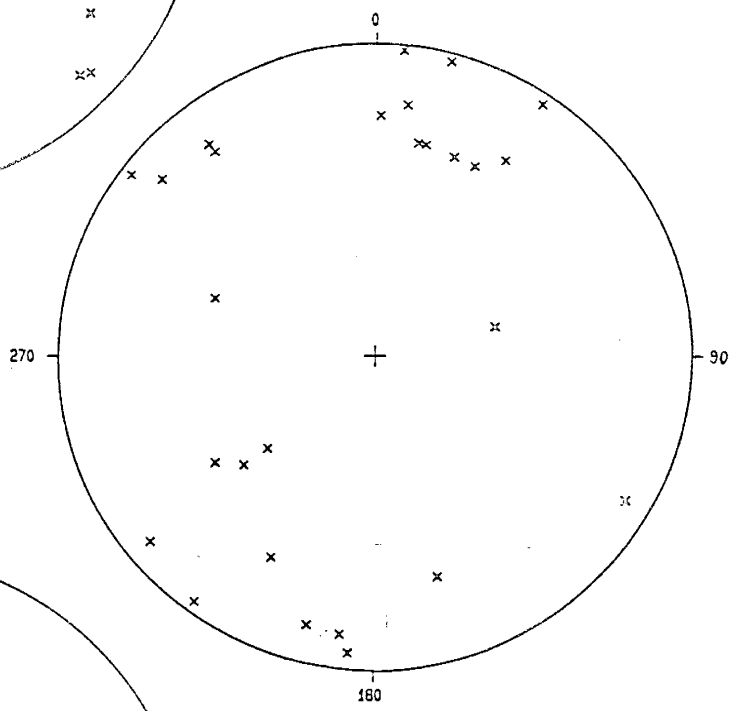


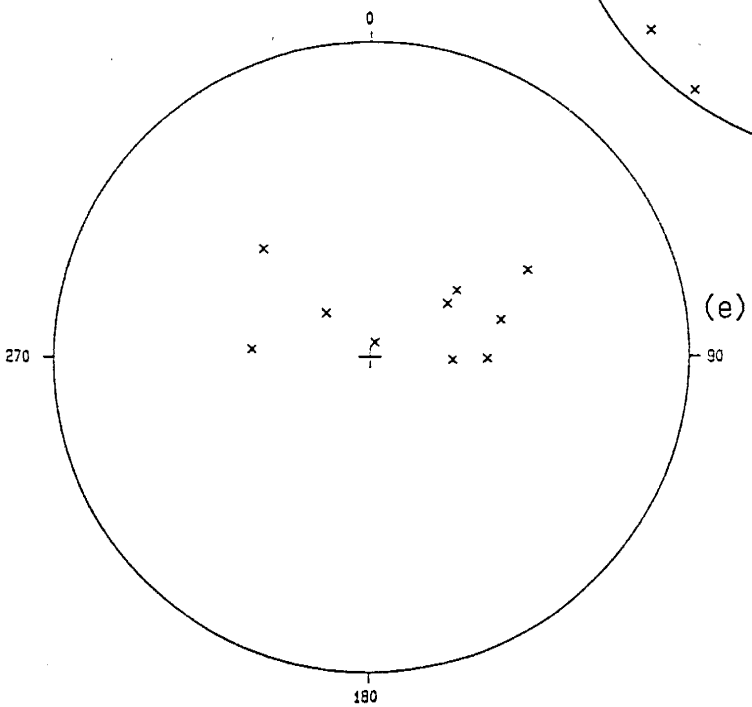


(e)

APPENDIX I (continued)

(f)

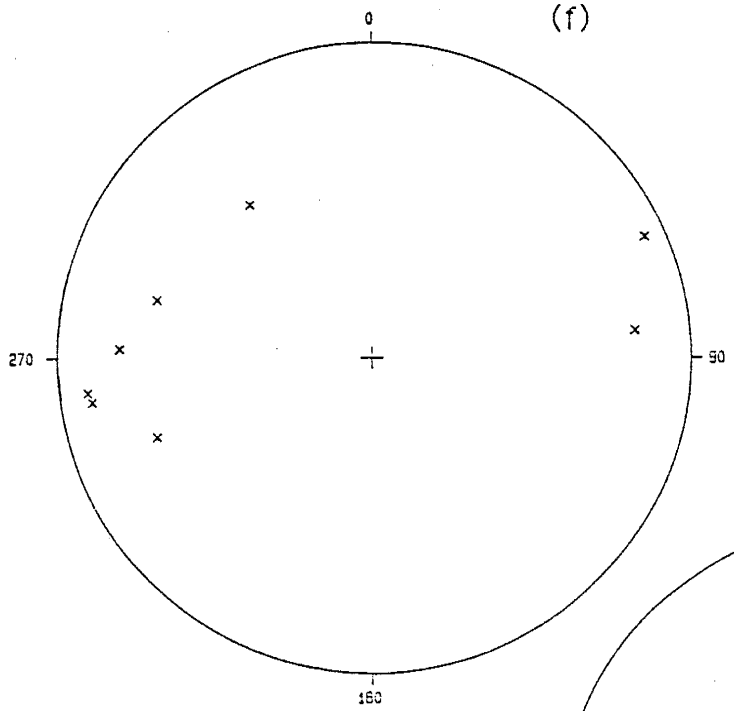


(g)

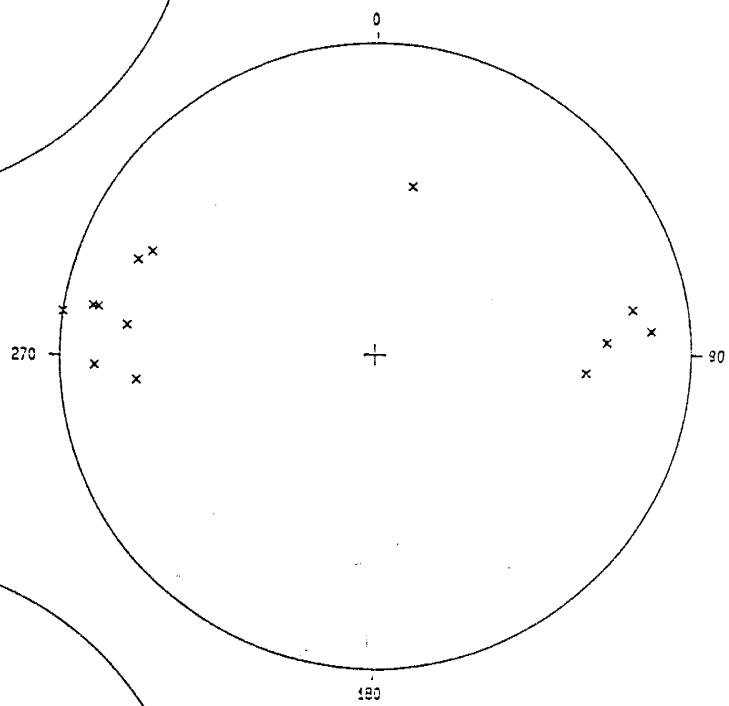


(h)

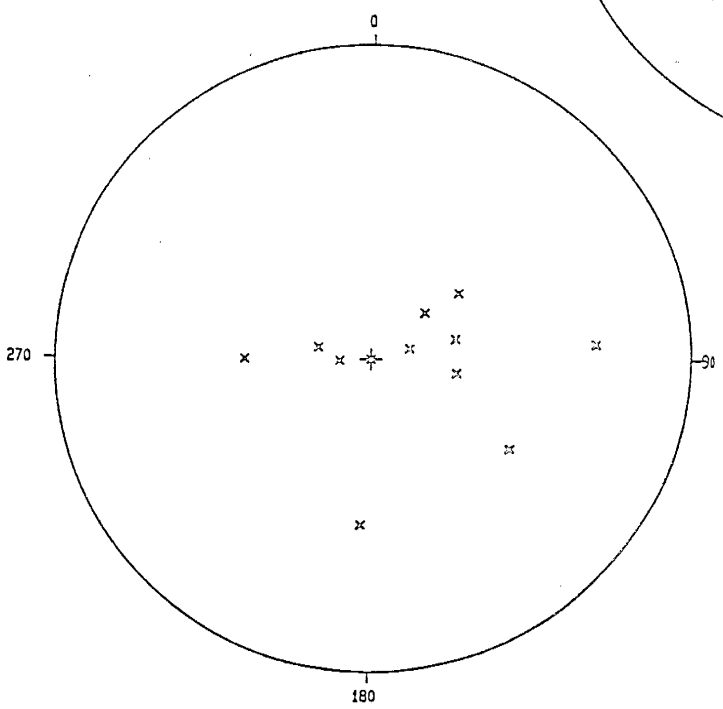

APPENDIX I (continued)

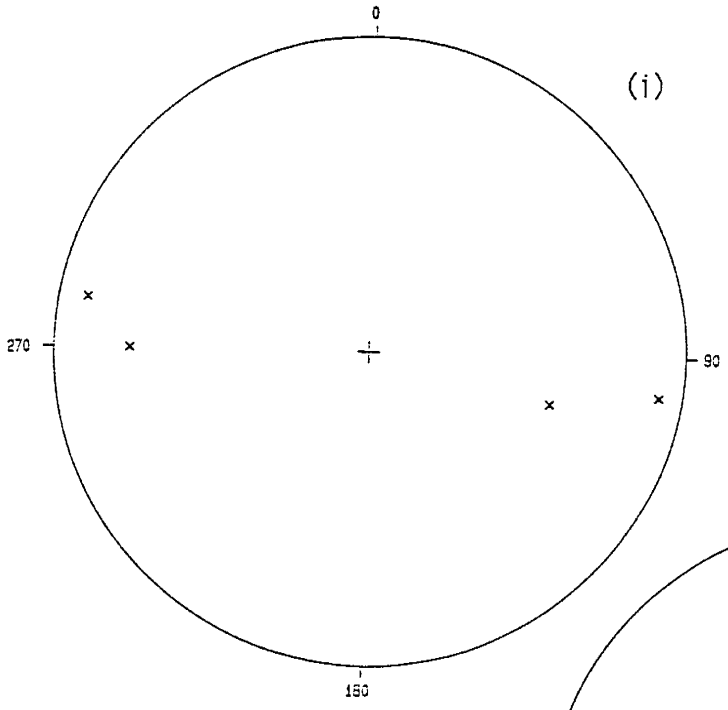


(i)

(j)

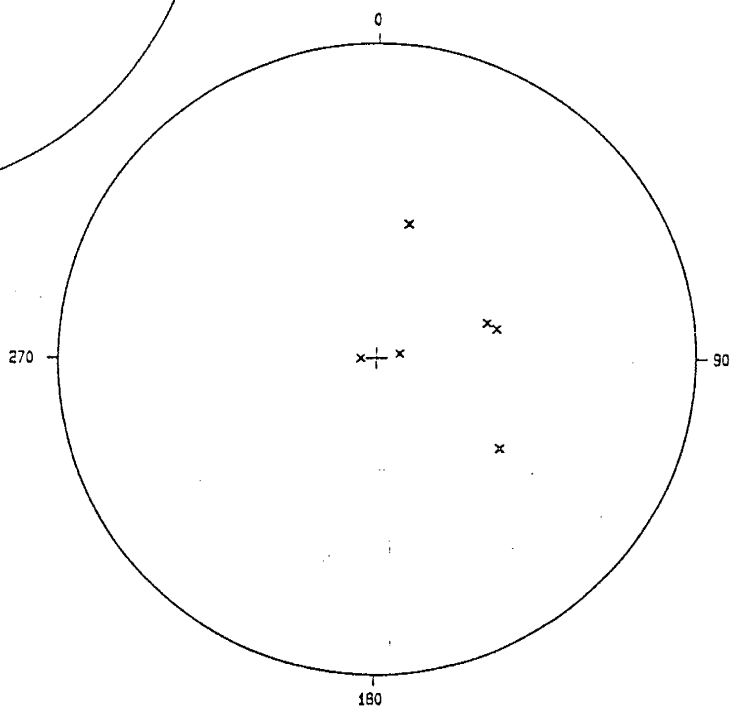

APPENDIX I (continued)

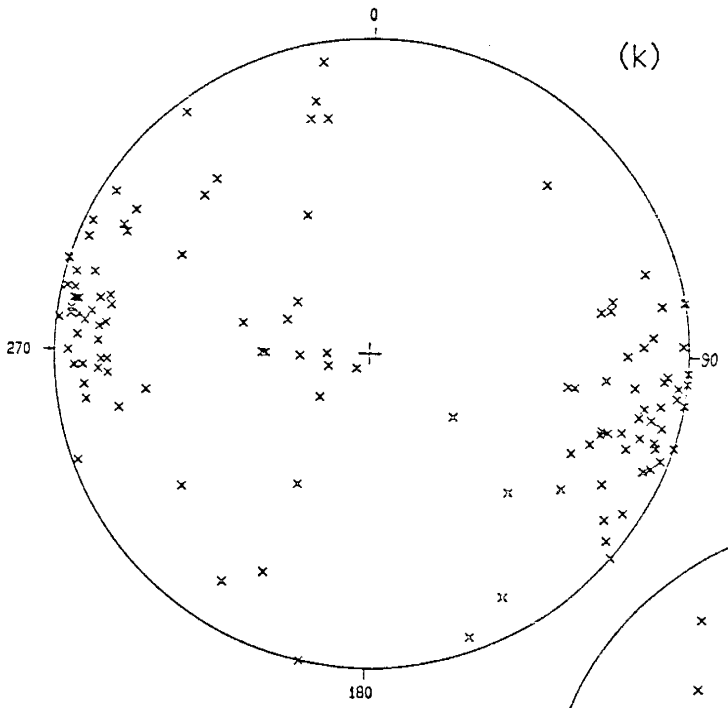


(k)

(l)

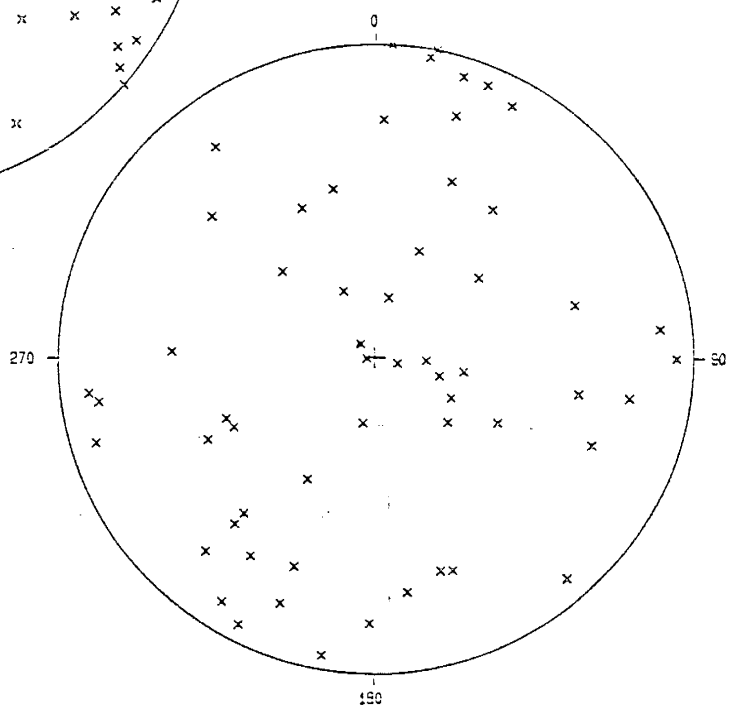

# APPENDIX J

Petrographic data collected from veins.

Data from a sample includes:

**Thin section label:** .....

Orientation of thin section: .....
Field location: .....
Photography: .....

**Drawing:** .....

## Vein Descriptions

Rock type: .....

label: of vein in drawing
time: of vein development relative to other veins in the sample. Veins may be split into time related 1st and 2nd sets, or sets A, B, and C when timing between sets is indeterminate.
style: or nature of vein separation during development
orientation: vein trend
contents: infilling crystalline material
system: fibrous crystal system, after Ramsay and Huber (1983).

crystal fiber measurements

°: trend of crystal fiber
$\Sigma\delta l$: length in centimeters of crystal fiber measured along a fixed line oriented parallel to the average trend of all crystal fibers in a sample
$\Sigma L$: length in centimeters of wall rock and previous vein crystal fibers measured along the fixed line
$e_i$: incremental strain; $e_i = \frac{\Sigma\delta l}{\Sigma L}$
$\sigma_1$: maximum stress trend, perpendicular to trend of crystal fiber

APPENDIX J (continued)

**Thin section label:** 1a
Orientation of thin section: horizontal, dot represents north.

Field Location: (x)4218
Photography: 6/9/86-A,1+2

**Drawing:**

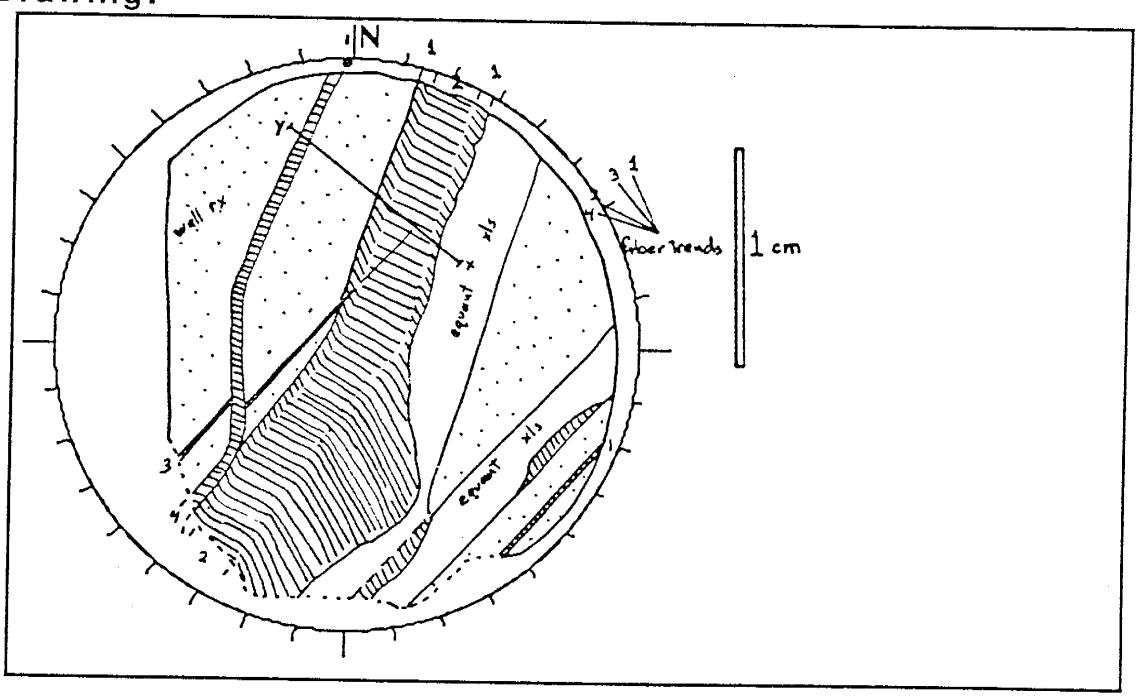


## Vein Descriptions

Rock type: Limestone-packstone, biomicrite

label: 1
time: first
style: right-extension
orientation: N18E and N39E
contents: fibrous calcite
system: stretched
crystal fiber measurements
°: N20W
$\Sigma\delta l$: 0.11
$\Sigma L$: 0.595
$e_j$: 0.185
$\sigma_1$: N70E

label: 2
time: second
style: normal-extension
orientation: N18E and N39E
contents: fibrous calcite
system: stretched
crystal fiber measurements
°: N72W
$\Sigma\delta l$: 0.25
$\Sigma L$: 0.705
$e_j$: 0.355
$\sigma_1$: N18E

APPENDIX J (continued)

**Thin section label:** 1a (cont.)

label: 3
time: third
style: right-extension
orientation: N48E
contents: fibrous calcite
system: stretched
crystal fiber measurements
°: N42W
$\Sigma\delta l$: 0.005
$\Sigma L$: 0.955
$e_j$: 0.005
$\sigma_1$: N46E

label: 4
time: fourth
style: L and R-extension
orientation: N5E(L)+N23E(R)
contents: fibrous calcite
system stretched
crystal fiber measurements
°: N78W
$\Sigma\delta l$: 0.04
$\Sigma L$: 0.96
$e_j$: 0.042
$\sigma_1$: N12E

label:
time:
style:
orientation:
contents:
system:
crystal fiber measruements
°:
$\Sigma\delta l$:
$\Sigma L$:
$e_j$:
$\sigma_1$:

label:
time:
style:
orientation:
contents:
system:
crystal fiber measurements
°:
$\Sigma\delta l$:
$\Sigma L$:
$e_j$:
$\sigma_1$:

label:
time:
style:
orientation:
contents:
system:
crystal fiber measurements
°:
$\Sigma\delta l$:
$\Sigma L$:
$e_j$:
$\sigma_1$:

label:
time:
style:
orientation:
contents:
system:
crystal fiber measurements
°:
$\Sigma\delta l$:
$\Sigma L$:
$e_j$:
$\sigma_1$:

APPENDIX J (continued)

**Thin section label:** 3a
Orientation of thin section: horizontal, dot represents north

Field Location: (x)4218
Photography: 6/9/86-A,1+2

**Drawing:**

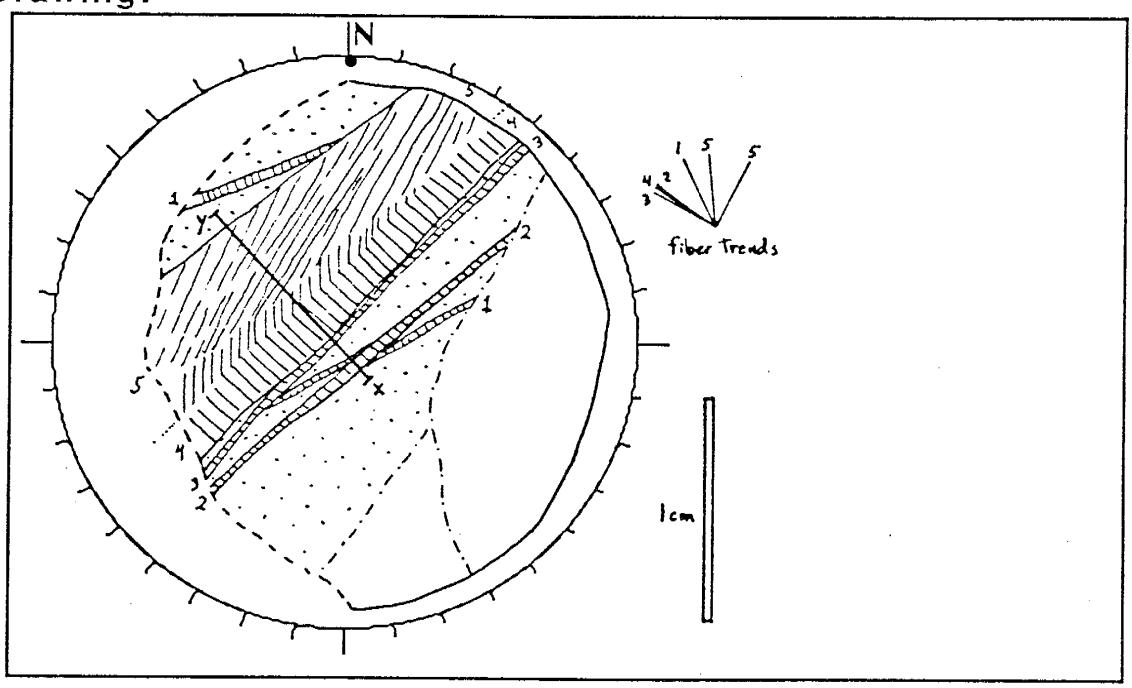


## Vein Descriptions

Rock type: limestone-wackestone, biomicrite

label: 1
time: first
style: right-extension
orientation: N64E
contents: fibrous calcite
system: stretched
crystal fiber measurements
°: N25W
$\Sigma\delta l$: 0.01
$\Sigma L$: 0.305
$e_j$: 0.033
$\sigma_1$: N65E

label: 2
time: second
style: left-extension
orientation: N50E
contents: fibrous calcite
system: stretched
crystal fiber measurements
°: N54W
$\Sigma\delta l$: 0.02
$\Sigma L$: 0.315
$e_j$: 0.062
$\sigma_1$: N36E

APPENDIX J (continued)

**Thin section label:** 3a (cont.)

label: 3
time: third
style: left-extension
orientation: N40E
contents: fibrous calcite
system: stretched
crystal fiber measurements
°: N60W
$\Sigma\delta l$: 0.035
$\Sigma L$: 0.335
$e_i$: 0.104
$\sigma_1$: N30E

label: 4
time: fourth
style: left-extension
orientation: N40E
contents: fibrous calcite
system stretched
crystal fiber measurements
°: N56W
$\Sigma\delta l$: 0.16
$\Sigma L$: 0.37
$e_i$: 0.432
$\sigma_1$: N34E

label: 5
time: fifth
style: right-shear
orientation: N40E
contents: fibrous calcite
system: stretched
crystal fiber measruements
°: N5W
$\Sigma\delta l$: 0.19
$\Sigma L$: 0.53
$e_i$:
$\sigma_1$:

label: 5
time: sixth
style: right-shear
orientation: N40E
contents: fibrous calcite
system: stretched
crystal fiber measurements
°: N26E
$\Sigma\delta l$: 0.28
$\Sigma L$: 0.72
$e_i$:
$\sigma_1$:

label:
time:
style:
orientation:
contents:
system:
crystal fiber measurements
°:
$\Sigma\delta l$:
$\Sigma L$:
$e_i$:
$\sigma_1$:

label:
time:
style:
orientation:
contents:
system:
crystal fiber measurements
°:
$\Sigma\delta l$:
$\Sigma L$:
$e_i$:
$\sigma_1$:

APPENDIX J (continued)

**Thin section label:** 6a

Orientation of thin section: dot represents 81,67 (inclination, declination). Thin section cut perpendicular to inclination.

Field Location: (x)4422

Photography: 4/22/96-8

**Drawing:**

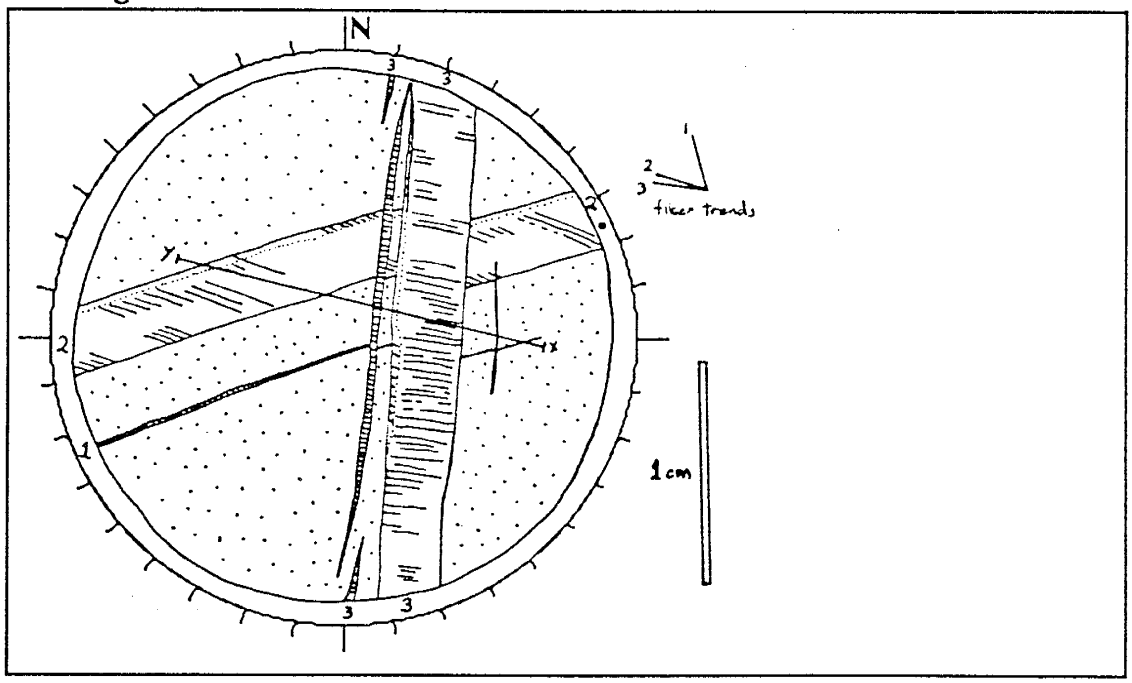


**Vein Descriptions**

Rock type: limestone-wackestone, biopelmicrite

label: 1
time: first
style: rifht-extension
orientation: N73E
contents: druse + eq' cal'
system: -

crystal fiber measurements

°: N15W
$\Sigma\delta$l: 0.01
$\Sigma$L: 0.785
$e_j$: 0.013
$\sigma_1$: N75E

label: 2
time: second
style: left-extension
orientation: N73E
contents: fibrous calcite
system: stretched

crystal fiber measurements

°: N72W
$\Sigma\delta$l: 0.4
$\Sigma$L: 0.795
$e_j$: 0.503
$\sigma_1$: N18E

APPENDIX J (continued)

**Thin section label:** 6a (cont.)

label: 3
time: third
style: right-extension
orientation: N5E
contents: fibrous calcite
system: stretched
crystal fiber measurements
°: N78W
$\Sigma\delta$l: 0.505
$\Sigma$L: 1.195
$e_i$: 0.423
$\sigma_1$: N12E

label:
time:
style:
orientation:
contents:
system
crystal fiber measurements
°:

$\Sigma$L:

label:
time:
style:
orientation:
contents:
system:
crystal fiber measrements
°:

$\Sigma$L:

label:
time:
style:
orientation:
contents:
system:
crystal fiber measurements
°:

$\Sigma$L:

label:
time:
style:
orientation:
contents:
system:
crystal fiber measurements
°:

$\Sigma$L:

label:
time:
style:
orientation:
contents:
system:
crystal fiber measurements
°:

$\Sigma$L:

APPENDIX J (continued)

**Thin section label:** 7a

Orientation of thin section: dot represents 80,332 (inclination, declination). Thin section cut perpendicular to inclination.

Field Location: (x)5422

Photography: 6/9/86-4,5+6

**Drawing:**

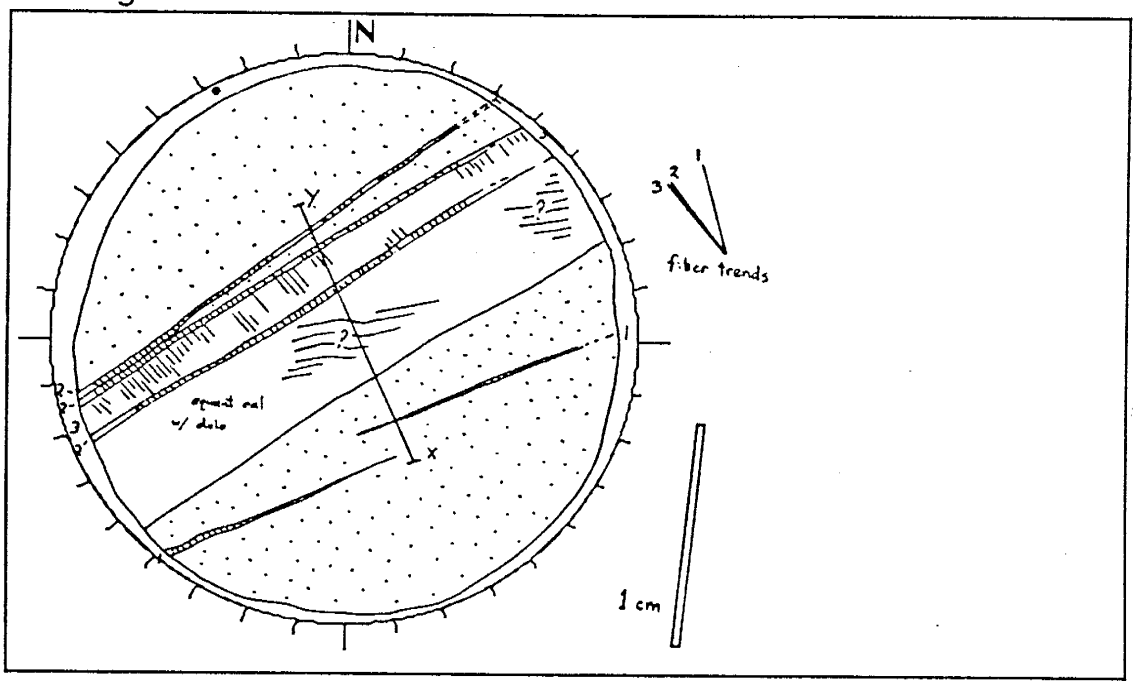


**Vein Descriptions**

Rock type:

label: 1
time: first
style: right-extension
orientation: N69E
contents: fibrous calcite
system: stretched

crystal fiber measurements

°: N20W
$\Sigma\delta$l: 0.01
$\Sigma$L: 0.3
$e_j$: 0.033
$\sigma_1$: N70E

label: 2
time: second
style: left-extension
orientation: N60E
contents: fibrous calcite
system: stretched

crystal fiber measurements

°: N43W
$\Sigma\delta$l: 0.08
$\Sigma$L: 0.31
$e_j$: 0.258
$\sigma_1$: N47E

APPENDIX J (continued)

**Thin section label:** 7a (cont.)

label: 3
time: third
style: left-extension
orientation: N60E
contents: fibrous calcite
system: stretched
crystal fiber measurements
°: N45W
$\Sigma\delta l$: 0.15
$\Sigma L$: 0.39
$e_i$: 0.385
$\sigma_1$: N45E

label: 4
time: fourth
style: left-shear
orientation: N60E
contents: fib calcite, dolo
system stretched
crystal fiber measurements
°: N74W
$\Sigma\delta l$: 0.66
$\Sigma L$: 0.54

label:
time:
style:
orientation:
contents:
system:
crystal fiber measruements
°:

$\Sigma L$:

label:
time:
style:
orientation:
contents:
system:
crystal fiber measurements
°:

$\Sigma L$:

label:
time:
style:
orientation:
contents:
system:
crystal fiber measurements
°:

$\Sigma L$:

label:
time:
style:
orientation:
contents:
system:
crystal fiber measurements
°:

$\Sigma L$:

APPENDIX J (continued)

**Thin section label:** 8a

Orientation of thin section: dot represents 82,305 (inclination, declination). Thin section cut perpendicular to inclination.

Field Location: (x)2-4711

Photography:

**Drawing:**

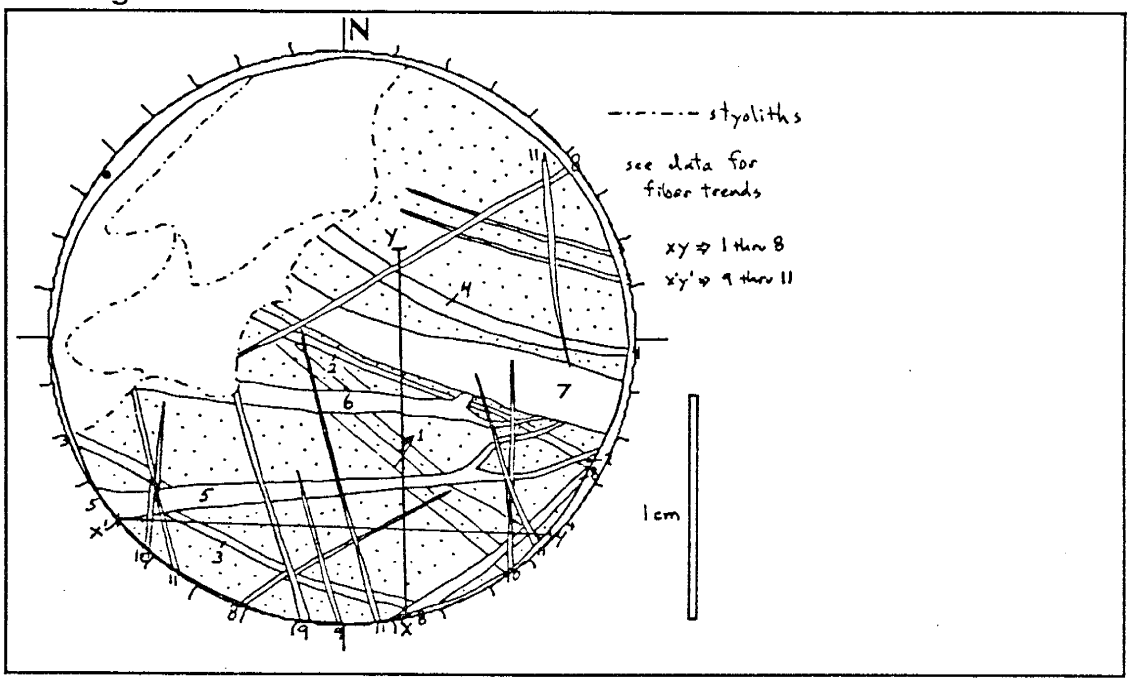


**Vein Descriptions**

Rock type:

label: 1
time: first
style: left-extension
orientation: N50W
contents: fibrous calcite
system: stretched

crystal fiber measurements

°: N30E
$\Sigma\delta$l: 0.015
$\Sigma$L: 0.9
$e_j$: 0.017
$\sigma_1$: N60W

label: 2
time: second
style: left-extension
orientation: N65W
contents: fibrous calcite
system: stretched

crystal fiber measurements

°: N23E
$\Sigma\delta$l: 0.03
$\Sigma$L: 0.915
$e_j$: 0.033
$\sigma_1$: N67W

APPENDIX J (continued)

**Thin section label:** 8a (cont.)

label: 3
time: third
style: right-extension
orientation: N75W
contents: fibrous calcite
system: stretched
crystal fiber measurements
°: N25E
$\Sigma\delta l$: 0.03
$\Sigma L$: 0.945
$e_i$: 0.032
$\sigma_1$: N65W

label: 4
time: fourth
style: left-extension
orientation: N64W
contents: fibrous calcite
system stretched
crystal fiber measurements
°: N18E
$\Sigma\delta l$: 0.025
$\Sigma L$: 0.975
$e_i$: 0.026
$\sigma_1$: N72W

label: 5
time: fifth
style: left-extension
orientation: N87E
contents: fibrous calcite
system: stretched
crystal fiber measruements
°: N15W
$\Sigma\delta l$: 0.06
$\Sigma L$: 1.045
$e_i$: 0.057
$\sigma_1$: N75E

label: 6
time: sixth
style: left-extension
orientation: N88W
contents: fibrous calcite
system: stretched
crystal fiber measurements
°: N41W
$\Sigma\delta l$: 0.05
$\Sigma L$: 1.105
$e_i$: 0.045
$\sigma_1$: N49E

label: 7
time: seventh
style: shear?
orientation: N65W
contents: fib' + equant cal'
system: stretched
crystal fiber measurements
°: ?
$\Sigma\delta l$: 0.3
$\Sigma L$: 1.155

label: 8
time: eighth
style: normal-extension
orientation: N56E
contents: fibrous calcite
system: stretched
crystal fiber measurements
°: N36W
$\Sigma\delta l$: 0.045
$\Sigma L$: 1.455
$e_i$: 0.031
$\sigma_1$: N54E

APPENDIX J (continued)

**Thin section label:** 8a (cont.)

label: 9
time: ninth
style: right-extension
orientation: N10W
contents: fibrous calcite
system: stretched
crystal fiber measurements
°: N80W
$\Sigma\delta l$: 0.03
$\Sigma L$: 1.6
$e_i$: 0.019
$\sigma_1$: N10E

label: 10
time: tenth
style: left-extension
orientation: N3W
contents: fibrous calcite
system stretched
crystal fiber measurements
°: N80E
$\Sigma\delta l$: 0.04
$\Sigma L$: 1.63
$e_i$: 0.025
$\sigma_1$: N10W

label: 11
time: eleventh
style: normal-extension
orientation: N10W
contents: fibrous calcite
system: stretched
crystal fiber measruements
°: N80E
$\Sigma\delta l$: 0.07
$\Sigma L$: 1.67
$e_i$: 0.042
$\sigma_1$: N10W

label:
time:
style:
orientation:
contents:
system:
crystal fiber measurements
°:

$\Sigma L$:

label:
time:
style:
orientation:
contents:
system:
crystal fiber measurements
°:

$\Sigma L$:

label:
time:
style:
orientation:
contents:
system:
crystal fiber measurements
°:

$\Sigma L$:

label:
time:
style:
orientation:
contents:
system:
crystal fiber measurements
°:

$\Sigma L$:

APPENDIX J (continued)

**Thin section label:** 9a

Orientation of thin section: dot represents 89,290. Thin section cut perpendicular to inclination.

Field Location: (x)2-4711

Photography:

**Drawing:**

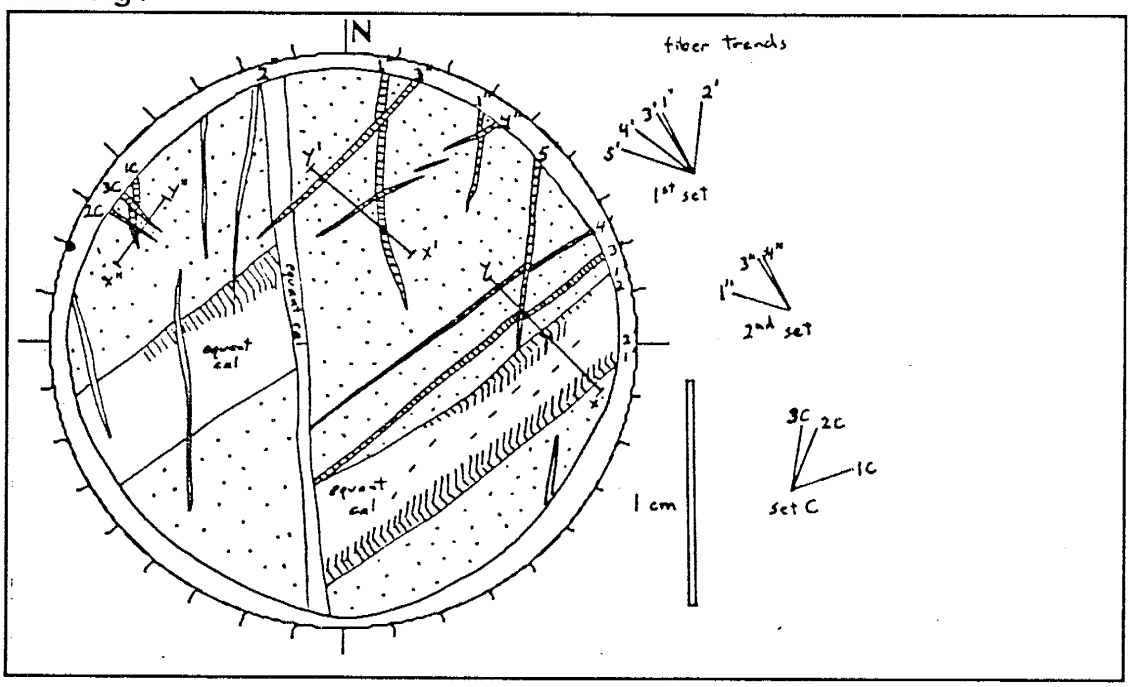


## Vein Descriptions

Rock type:

label: 1'
time: first of 1st set
style: right-extension
orientation: N55E
contents: fibrous calcite
system: stretched
crystal fiber measurements
°: N28W
$\Sigma\delta$l: 0.07
$\Sigma$L: 0.3
$e_i$: 0.233
$\sigma_1$: N26E

label: 2'
time: second of 1st set
style: right-shear
orientation: N55E
contents: fibrous calcite
system: stretched
crystal fiber measurements
°: N6E
$\Sigma\delta$l: 0.11
$\Sigma$L: 0.37

APPENDIX J (continued)

**Thin section label:** 9a (cont.)

label: 3'
time: third of 1st set
style: right-extension
orientation: N59E
contents: fibrous calcite
system: stretched
crystal fiber measurements
°: N32W
$\Sigma\delta$l: 0.02
$\Sigma$L: 0.72
$e_i$: 0.028
$\sigma_1$: N58E

label: 4'
time: fourth of 1st set
style: left-extension
orientation: N63E
contents: fibrous calcite
system stretched
crystal fiber measurements
°: N52W
$\Sigma\delta$l: 0.01
$\Sigma$L: 0.73
$e_i$: 0.014
$\sigma_1$: N38E

label: 5'
time: fifth of 1st set
style: right-extenison
orientation: N8E
contents: fibrous calcite
system: stretched
crystal fiber measruements
°: N70W
$\Sigma\delta$l: 0.015
$\Sigma$L: 0.735
$e_i$: 0.02
$\sigma_1$: N20E

label: 1"
time: first of2nd set
style: right-extension
orientation: N9E
contents: fibrous calcite
system: stretched
crystal fiber measurements
°: N73W
$\Sigma\delta$l: 0.01
$\Sigma$L: 0.475
$e_i$: 0.021
$\sigma_1$: N17E

label: 2"
time: second of 2nd set
style: right-shear
orientation: N5W
contents: equant calcite
system: -
crystal fiber measurements
°:
$\Sigma\delta$l:
$\Sigma$L:
$e_i$:
$\sigma_1$:

label: 3"
time: third of 2nd set
style: right-extension
orientation: N43E
contents: fibrous calcite
system: stretched
crystal fiber measurements
°: N31W
$\Sigma\delta$l: 0.01
$\Sigma$L: 0.485
$e_i$: 0.021
$\sigma_1$: N59E

APPENDIX J (continued)

**Thin section label:** 9a (cont.)

label: 4"
time: fourth of 2nd set
style: right-extension
orientation: N55E
contents: fibrous calcite
system: stretched
crystal fiber measurements
°: N28W
$\Sigma\delta l$: 0.005
$\Sigma L$: 0.495
$e_i$: 0.01
$\sigma_1$: N62E

label: 1C
time: first of set C
style: right-extension
orientation: N17W
contents: fibrous calcite
system stretched
crystal fiber measurements
°: N62E
$\Sigma\delta l$: 0.01
$\Sigma L$: 0.11
$e_i$: 0.091
$\sigma_1$: N28W

label: 2C
time: second of set C
style: right-extension
orientation: N47W
contents: fibrous calcite
system: stretched
crystal fiber measruements
°: N22E
$\Sigma\delta l$: 0.013
$\Sigma L$: 0.12
$e_i$: 0.108
$\sigma_1$: N68W

label: 3C
time: third of set C
style: left-extension
orientation: N47W
contents: fibrous calcite
system: stretched
crystal fiber measurements
°: N9E
$\Sigma\delta l$: 0.017
$\Sigma L$: 0.133
$e_i$: 0.128
$\sigma_1$: N81W

label:
time:
style:
orientation:
contents:
system:
crystal fiber measurements
°:

$\Sigma L$:

label:
time:
style:
orientation:
contents:
system:
crystal fiber measurements
°:

$\Sigma L$:

APPENDIX J (continued)

**Thin section label:** 10a

Orientation of thin section: dot represents 87,340. Thin section cut perpendicular to inclination.

Field Location: (x)2-4711

Photography: 6/9/86-13,14+15

**Drawing:**

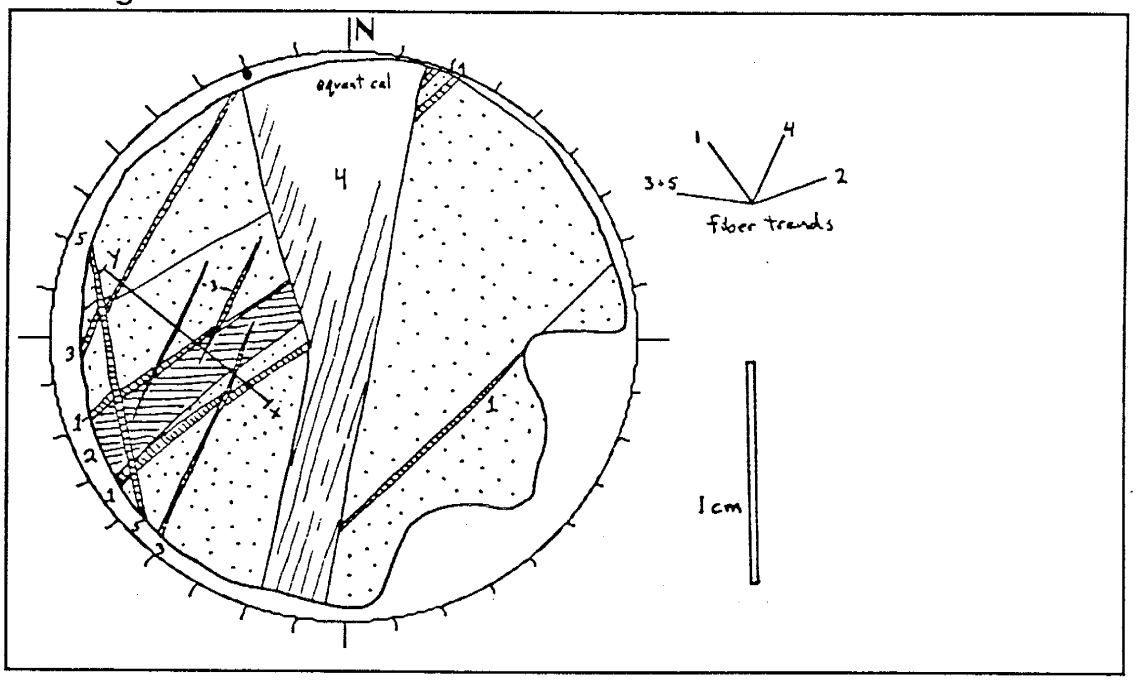


**Vein Descriptions**

Rock type: limestone-packstone, pelsparite

label: 1
time: first
style: normal-extension
orientation: N56E
contents: fibrous calcite
system: stretched
crystal fiber measurements
°: N34E
$\Sigma\delta$l: 0.04
$\Sigma$L: 0.79
$e_i$: 0.051
$\sigma_1$: N56E

label: 2
time: second
style: left-shear
orientation: N56E
contents: equant + fib' cal'
system: stretched
crystal fiber measurements
°: N70E
$\Sigma\delta$l: 0.13
$\Sigma$L: 0.87

APPENDIX J (continued)

**Thin section label:** 10a (cont.)

label: 3
time: third
style: left-extension
orientation: N24E
contents: fibrous calcite
system: stretched
crystal fiber measurements
°: N80W
$\Sigma\delta l$: 0.04
$\Sigma L$: 0.83
$e_i$: 0.048
$\sigma_1$: N10E

label: 4
time: fourth
style: left-shear
orientation: N14E
contents: equant + fib' cal'
system stretched
crystal fiber measurements
°: N25E
$\Sigma\delta l$:
$\Sigma L$:

label: 5
time: fifth
style: right-extension
orientation: N12W
contents: fibrous calcite
system: stretched
crystal fiber measruements
°: N80W
$\Sigma\delta l$: 0.005
$\Sigma L$: 1
$e_i$: 0.005
$\sigma_1$: N10E

label:
time:
style:
orientation:
contents:
system:
crystal fiber measurements
°:

$\Sigma L$:

label:
time:
style:
orientation:
contents:
system:
crystal fiber measurements
°:

$\Sigma L$:

label:
time:
style:
orientation:
contents:
system:
crystal fiber measurements
°:

$\Sigma L$:

label:
time:
style:
orientation:
contents:
system:
crystal fiber measurements
°:

$\Sigma L$:

APPENDIX J (continued)

**Thin section label:** 11a

Orientation of thin section: dot represents 84,50. Thin section cut perpendicular to inclination.

Field Location: (x)2-4711

Photography: 6/9/86-16

**Drawing:**

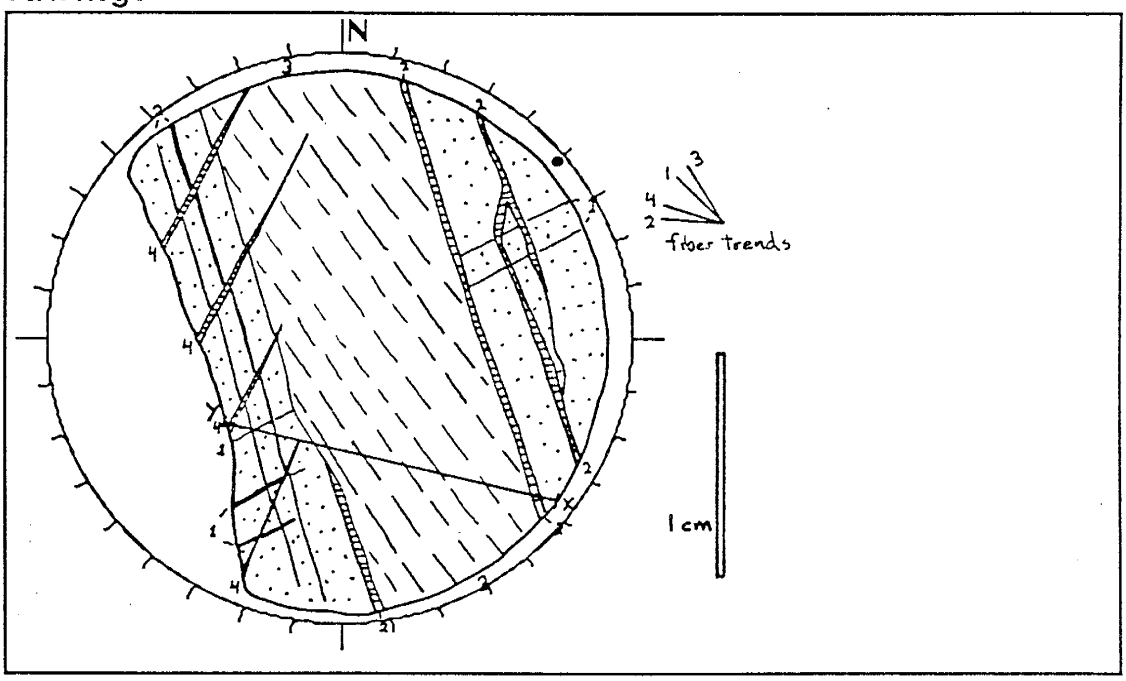


## Vein Descriptions

Rock type:

label: 1
time: first
style: left-extension
orientation: N62E
contents: fibrous calcite
system: stretched

crystal fiber measurements

°: N45W
$\Sigma\delta l$: 0.003
$\Sigma L$: 0.447
$e_j$: 0.007
$\sigma_1$: N45E

label: 2
time: second
style: right-extension
orientation: N12W
contents: equant + fib' cal'
system: stretched

crystal fiber measurements

°: N85W
$\Sigma\delta l$: 0.04
$\Sigma L$: 0.45
$e_j$: 0.089
$\sigma_1$: N5E

APPENDIX J (continued)

**Thin section label:** 11a (cont.)

label: 3
time: third
style: right-shear
orientation: N12W
contents: fibrous calcite
system: stretched
crystal fiber measurements
°: N32W
$\Sigma\delta l$: 1
$\Sigma L$: 0.49

label: 4
time: fourth
style: left-extension
orientation: N16E
contents: fib' + equant cal'
system stretched
crystal fiber measurements
°: N73W
$\Sigma\delta l$: 0.01
$\Sigma L$: 1.49
$e_i$: 0.007
$\sigma_1$: N17E

label:
time:
style:
orientation:
contents:
system:
crystal fiber measruements
°:

$\Sigma L$:

label:
time:
style:
orientation:
contents:
system:
crystal fiber measurements
°:

$\Sigma L$:

label:
time:
style:
orientation:
contents:
system:
crystal fiber measurements
°:

$\Sigma L$:

label:
time:
style:
orientation:
contents:
system:
crystal fiber measurements
°:

$\Sigma L$:

APPENDIX J (continued)

**Thin section label:** 12a

Orientation of thin section: dot represents 81,133. Thin section cut perpendicular to inclination.

Field Location: (x)2-4711

Photography: 6/9/86-17+18

**Drawing:**

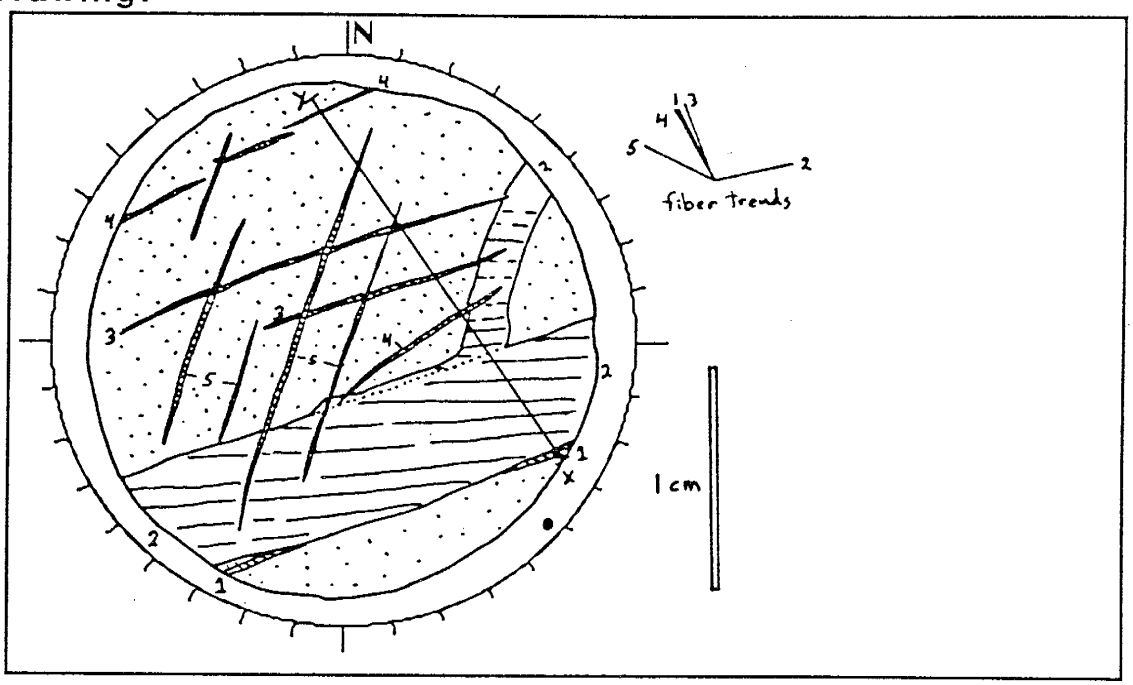


**Vein Descriptions**

Rock type: limestone-pack and wackestone, biomicrite

label: 1
time: first
style: left-extension
orientation: N70E
contents: fib' + equant cal'
system: stretched
crystal fiber measurements
°: N26W
$\Sigma\delta$l: 0.03
$\Sigma$L: 1.17
$e_j$: 0.026
$\sigma_1$: N64E

label: 2
time: second
style: left-shear
orientation: N70E
contents: fib' + equant cal'
system: stretched
crystal fiber measurements
°: N78E
$\Sigma\delta$l: 0.54
$\Sigma$L: 1.41

APPENDIX J (continued)

**Thin section label:** 12a (cont.)

label: 3
time: third
style: left-extension
orientation: N70E
contents: fibrous calcite
system: stretched
crystal fiber measurements
°: N21W
$\sigma_1$: 0.015
$\Sigma L$: 1.95
$e_i$: 0.008
$\sigma_1$: N69E

label: 4
time: fourth
style: right-extension
orientation: N52E
contents: fibrous calcite
system stretched
crystal fiber measurements
°: N28W
$\sigma_1$: 0.015
$\Sigma L$: 1.965
$e_i$: 0.008
$\sigma_1$: N62E

label: 5
time: fifth
style: right-extension
orientation: N20E
contents: fibrous calcite
system: stretched
crystal fiber measruements
°: N63W
$\sigma_1$: 0.02
$\Sigma L$: 1.98
$e_i$: 0.01
$\sigma_1$: N27E

label:
time:
style:
orientation:
contents:
system:
crystal fiber measurements
°:

$\Sigma L$:

label:
time:
style:
orientation:
contents:
system:
crystal fiber measurements
°:

$\Sigma L$:

label:
time:
style:
orientation:
contents:
system:
crystal fiber measurements
°:

$\Sigma L$:

label:
time:
style:
orientation:
contents:
system:
crystal fiber measurements
°:

$\Sigma L$:

APPENDIX J (continued)

**Thin section label:** 13e
Orientation of thin section: horizontal, dot represents north

Field Location: (x)26429
Photography:

**Drawing:**

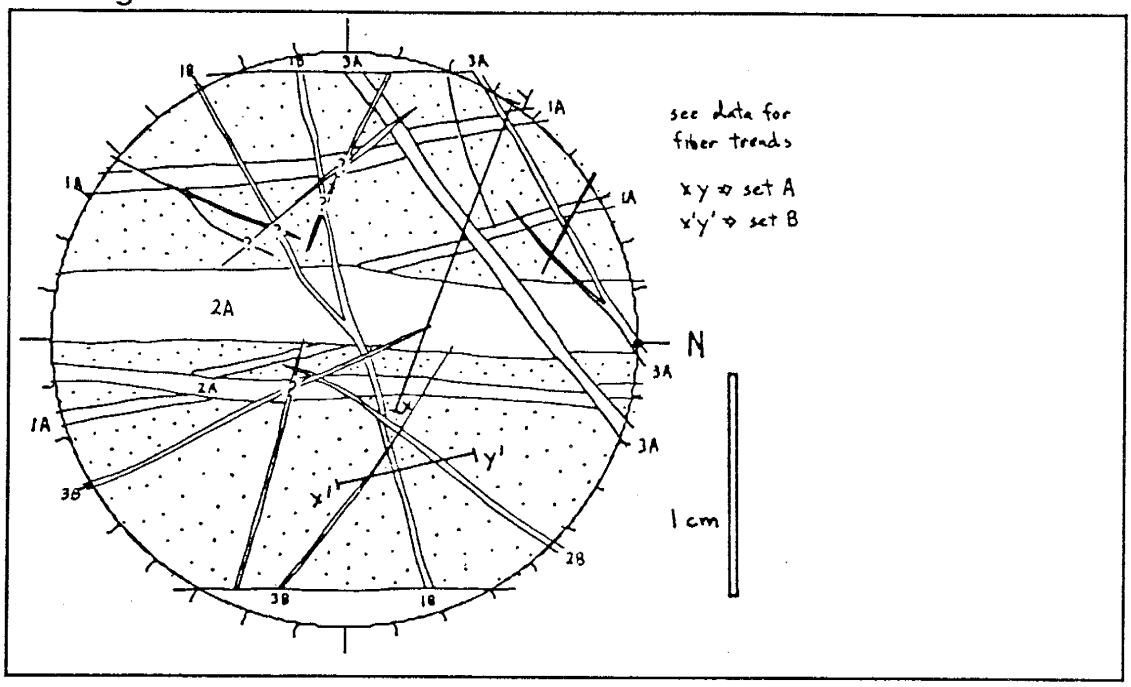


## Vein Descriptions

Rock type:

label: 1A
time: first of set A
style: right-extension
orientation: N8W
contents: fibrous calcite
system: stretched
crystal fiber measurements
°: N85E
$\Sigma\delta l$: 0.14
$\Sigma L$: 0.84
$e_j$: 0.167
$\sigma_1$: N5W

label: 2A
time: second of set A
style: left-extension
orientation: N7E
contents: fib' + equant cal'
system: stretched
crystal fiber measurements
°: N88E
$\Sigma\delta l$: 0.38
$\Sigma L$: 0.98
$e_j$: 0.388
$\sigma_1$: N2W

APPENDIX J (continued)

**Thin section label:** 13e (cont.)

label: 3A
time: third of set A
style: left-extension
orientation: N53E
contents: fib' + equant cal'
system: stretched
crystal fiber measurements
°: N46E
$\Sigma\delta l$: 0.09
$\Sigma L$: 1.36
$e_i$: 0.066
$\sigma_1$: N44E

label: 1B
time: first of set B
style: L+R-extension
orientation: N84E(L),N65E(R)
contents: fibrous calcite
system stretched
crystal fiber measurements
°: N21W
$\Sigma\delta l$: 0.025
$\Sigma L$: 0.65
$e_i$: 0.038
$\sigma_1$: N69E

label: 2B
time: second of set B
style: right-extension
orientation: N34E
contents: fibrous calcite
system: stretched
crystal fiber measruements
°: N42W
$\Sigma\delta l$: 0.02
$\Sigma L$: 0.675
$e_i$: 0.03
$\sigma_1$: N48E

label: 3B
time: third of set B
style: right-extension
orientation: N43W
contents: fibrous calcite
system: stretched
crystal fiber measurements
°: N45E
$\Sigma\delta l$: 0.005
$\Sigma L$: 0.695
$e_i$: 0.007
$\sigma_1$: N45W

label:
time:
style:
orientation:
contents:
system:
crystal fiber measurements
°:

$\Sigma L$:

label:
time:
style:
orientation:
contents:
system:
crystal fiber measurements
°:

$\Sigma L$:

# APPENDIX K

Vein styles and associated maximum principle stress trends for each thin section.

Vein styles: Vein timing indicated by numbers. (# in parentheses relates vein to maximum principal stress increment.) Veins in thin-section 9a are split into 1st and 2nd sets to prevent crowding the diagram, and thin sections 9a and 13a contain sets A and B, or C when timing between vein sets is indeterminable. Occasionally, one vein has two orientations, both developing at the same time.

——> right-extension, ·····> right-shear, ——> left-extension, ----> left-shear, ''''''''''> normal-extension.

Maximum principal stresses: Longitudinal normal to fibrous crystals in extension veins. Increment timing indicated by numbers.

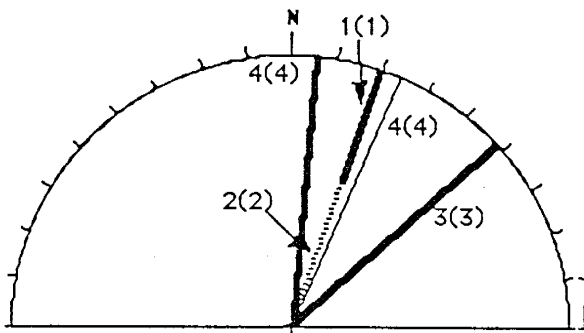


(a) Thin section 1a - vein styles

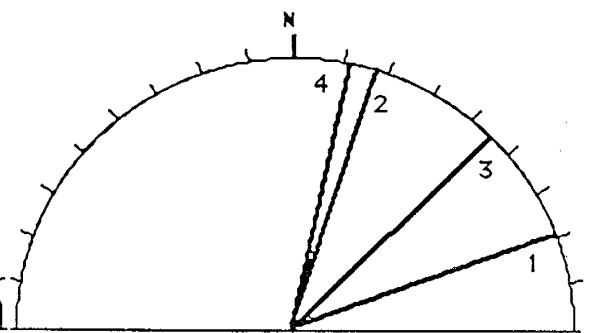


(aa) Thin section 1a - maximum principle stresses

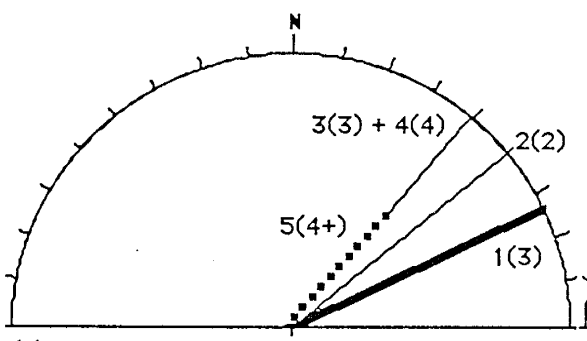


(b) Thin section 3a - vein styles

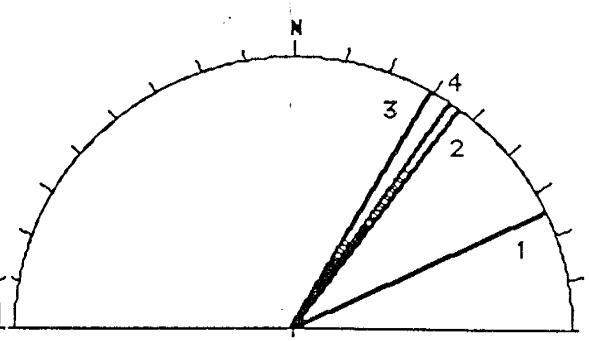


(bb) Thin section 3a - maximum principle stresses

# APPENDIX K (continued)

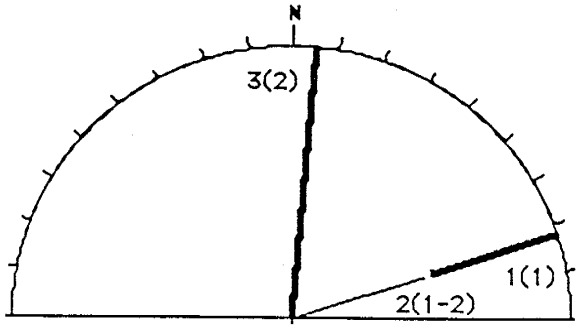


(c) Thin section 6a - vein styles

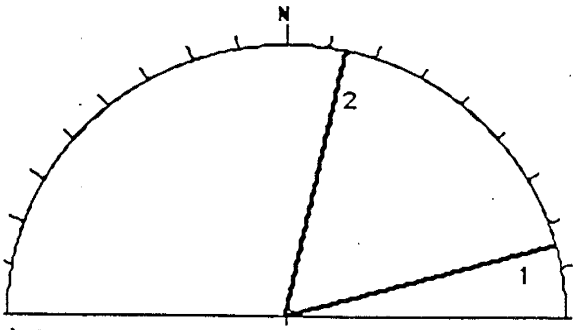


(cc) Thin section 6a - maximum principal stresses

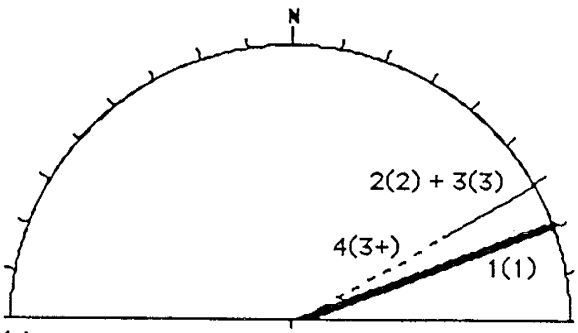


(d) Thin section 7a - vein styles

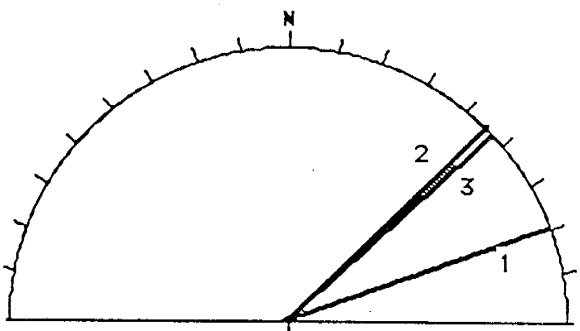


(dd) Thin section 7a - maximum principal stresses

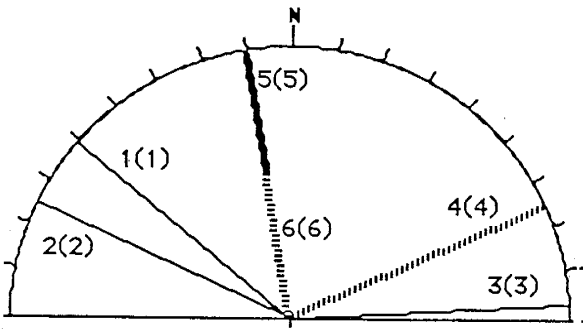


(e) Thin section 8a - vein styles

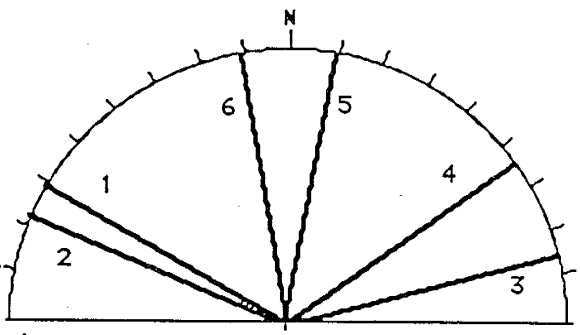


(ee) Thin section 8a - maximum principal stresses

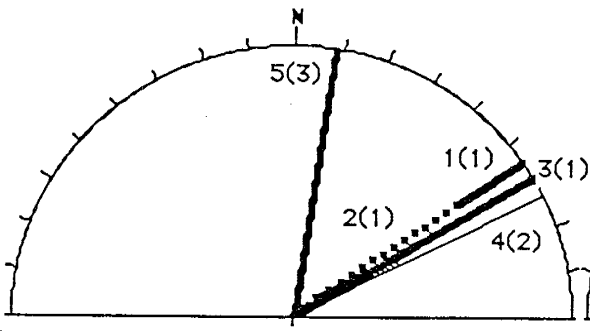


(f) Thin section 9a (1st set) - vein styles

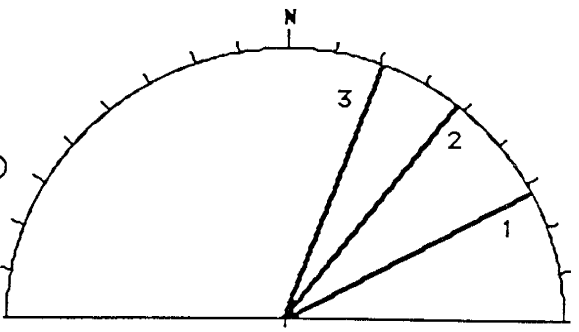


(ff) Thin section 9a (1st set) - max principal stresses

# APPENDIX K (continued)

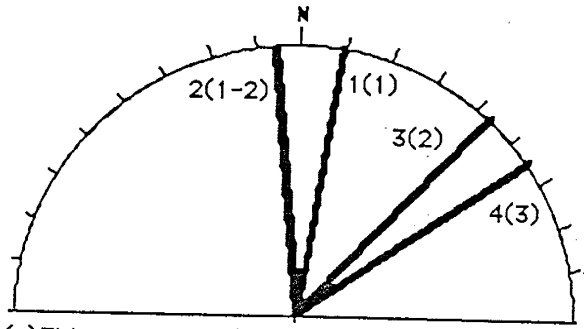


(g) Thin section 9a (2nd set) - vein styles

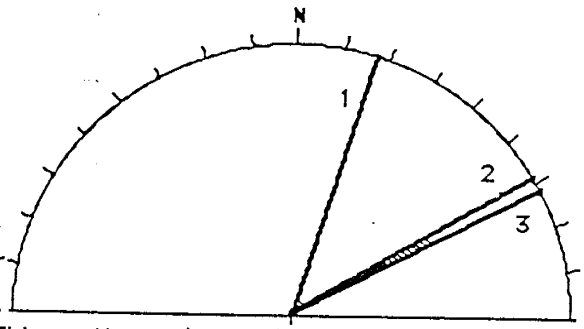


(gg) Thin section 9a (2nd set) - max principal stresses

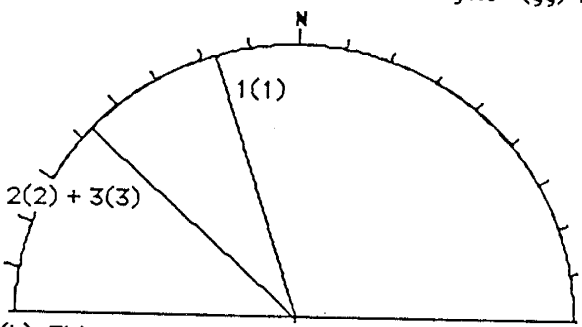


(h) Thin section 9a (set C) - vein styles

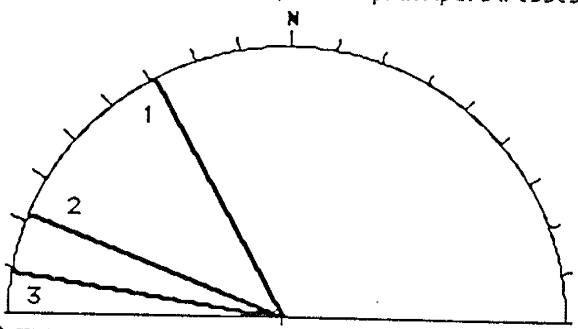


(hh) Thin section 9a (set C) - max principal stresses

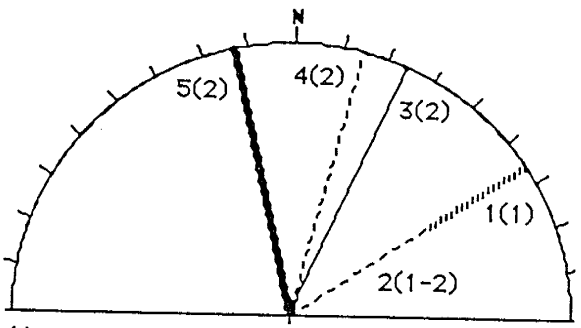


(i) Thin section 10a - vein styles

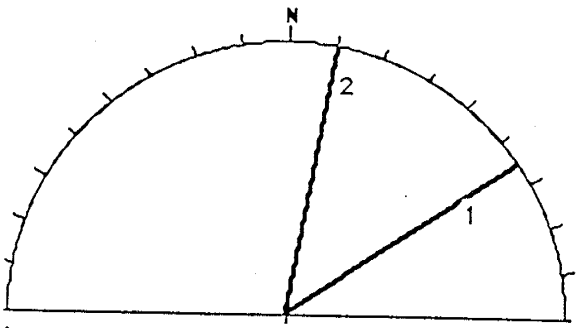


(ii) Thin section 10a - maximum principal stresses

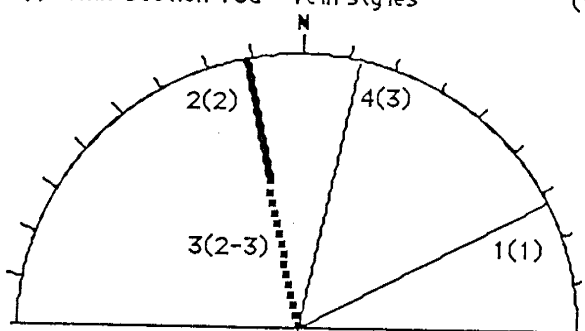


(j) Thin section 11a - vein styles

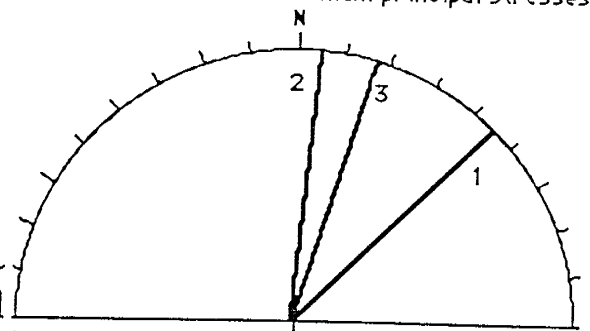


(jj) Thin section 11a - maximum principal stresses

# APPENDIX K (continued)

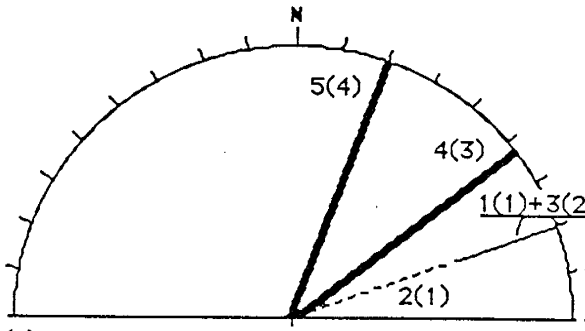


(k) Thin section 12a - vein styles

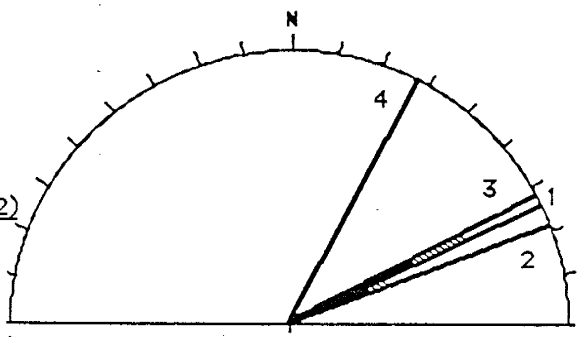


(kk) Thin section 12a - maximum principal stresses

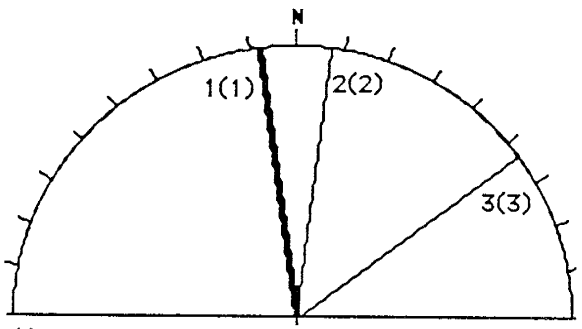


(l) Thin section 13e (set A) - vein styles

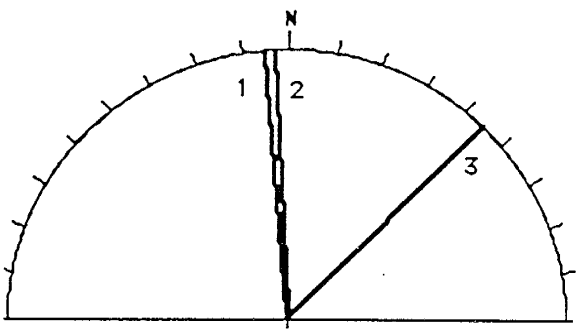


(ll) Thin section 13e (set A) - max principal stresses

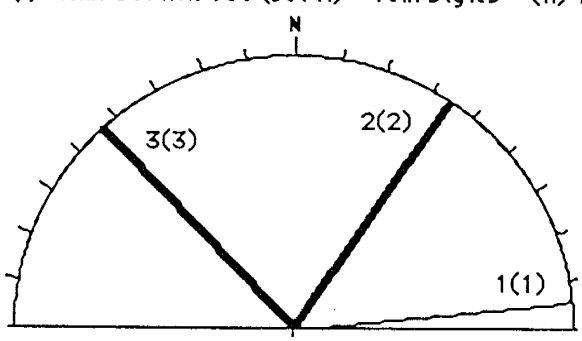


(m) Thin section 13e (set B) - vein styles.

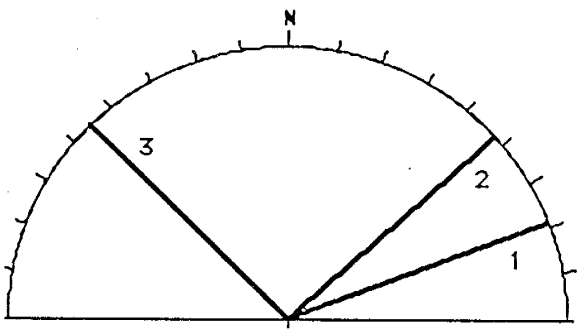


(mm) Thin section 13e (set B) - max principal stresses

# APPENDIX L

Summaries of veins and associated fibrous crystals from thin sections: (a) right-extension, (b) left-extension, (c) normal-extension, (d) right- shear, and (e) left-shear.

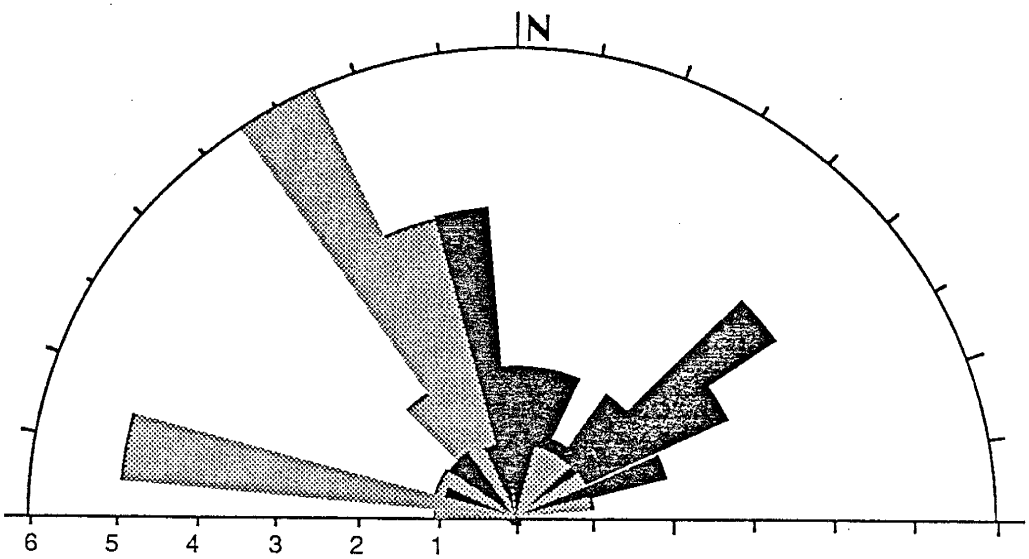


(a) Right-extension veins, N=26

Associated fibrous crystals, N=25

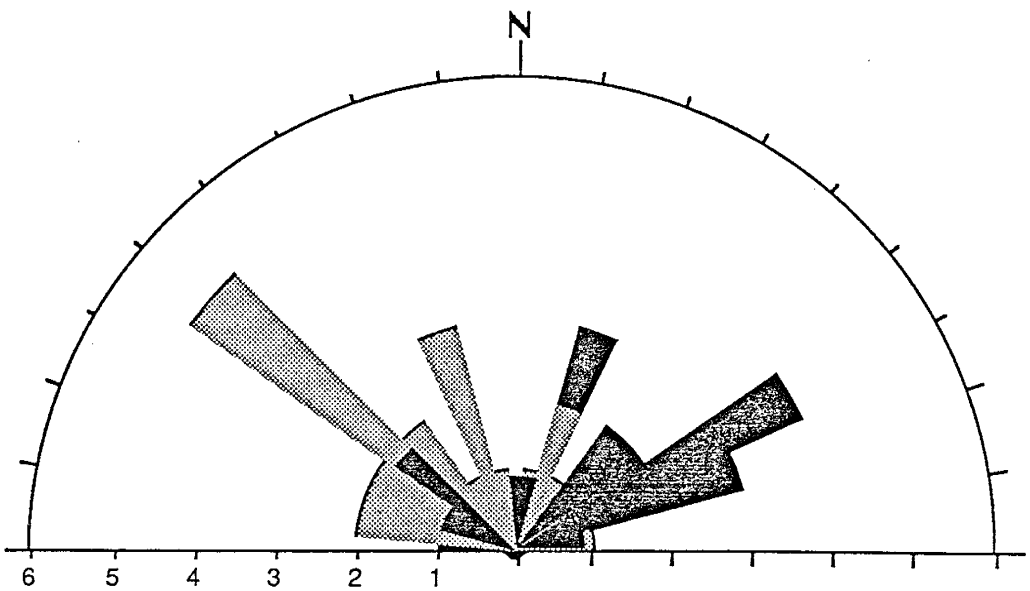


(b) Left-extension veins, N=23

Associated fibrous crystals, N=24

APPENDIX L (continued)

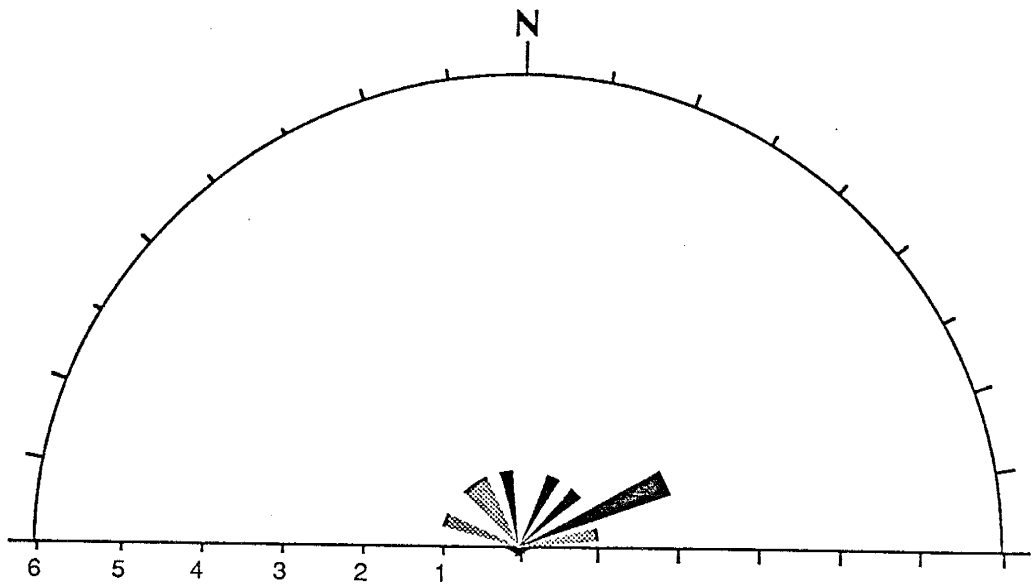


(c) Normal-extension veins, N=5

Associated fibrous crystals, N=4

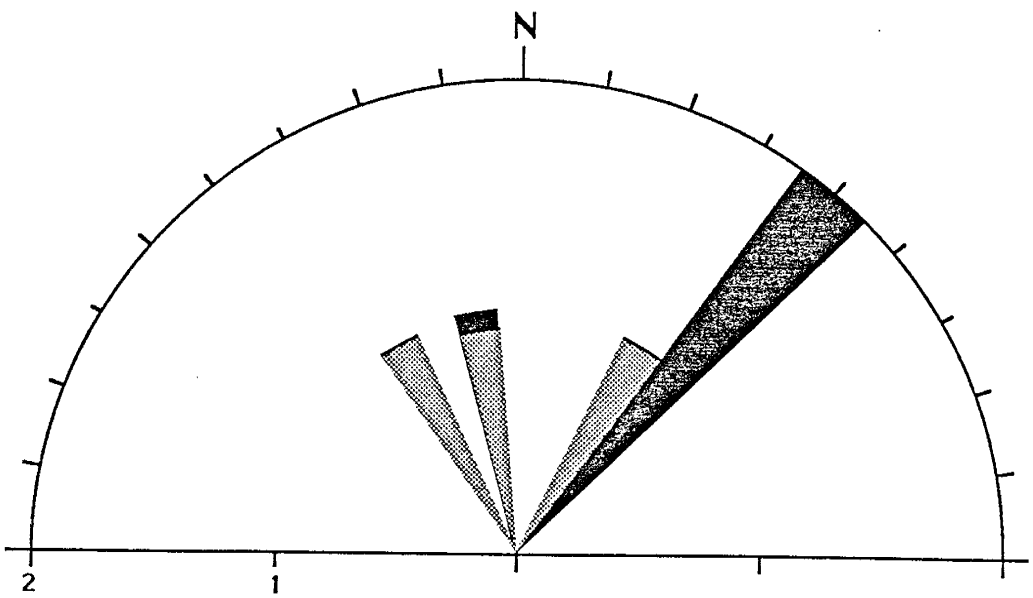


(d) Right-shear veins, N=3

Associated fibrous minerals, N=3

APPENDIX L (continued)

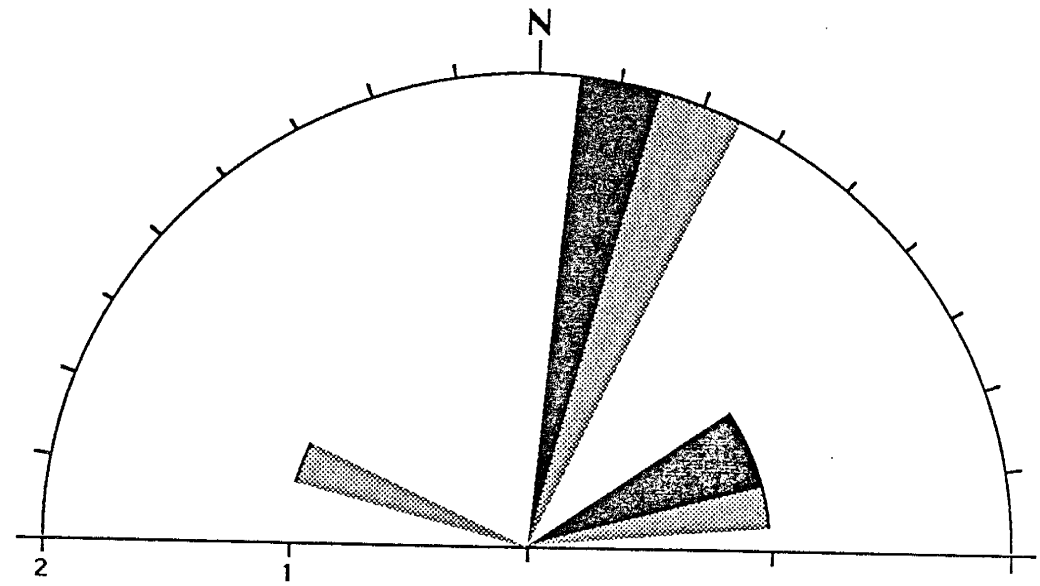


(e) Left-shear veins, N=4

Associated fibrous crystals, N=4

# APPENDIX M

Summaries of the trends in veins and associated fibrous crystals from field measurements: (a) right-extension linear, (b) left-extension linear, (c) left-echelon (right-slip), and (e) right-echelon (left-slip).

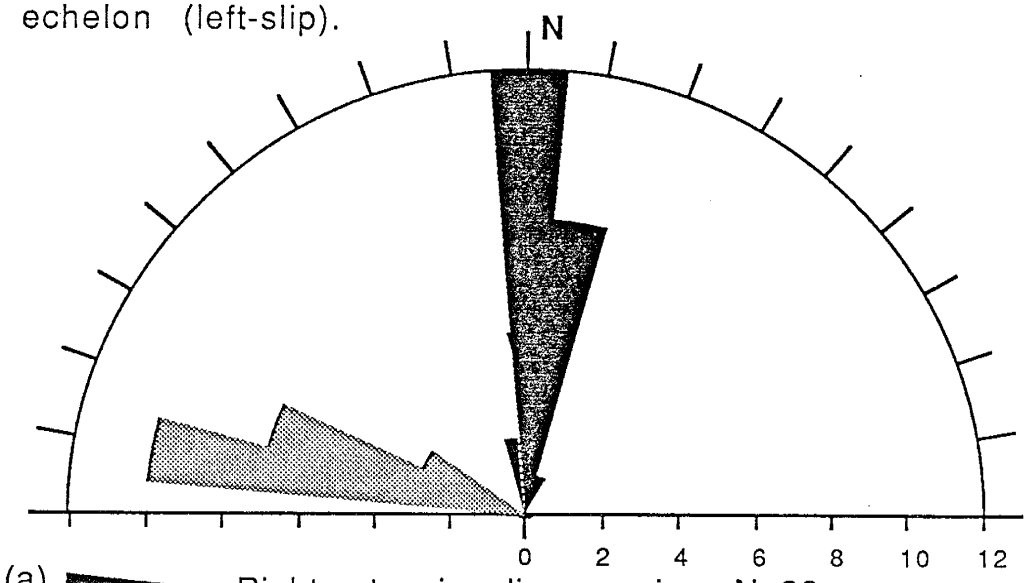


(a) Right-extension linear veins, N=22
associated fibrous crystals, N=22

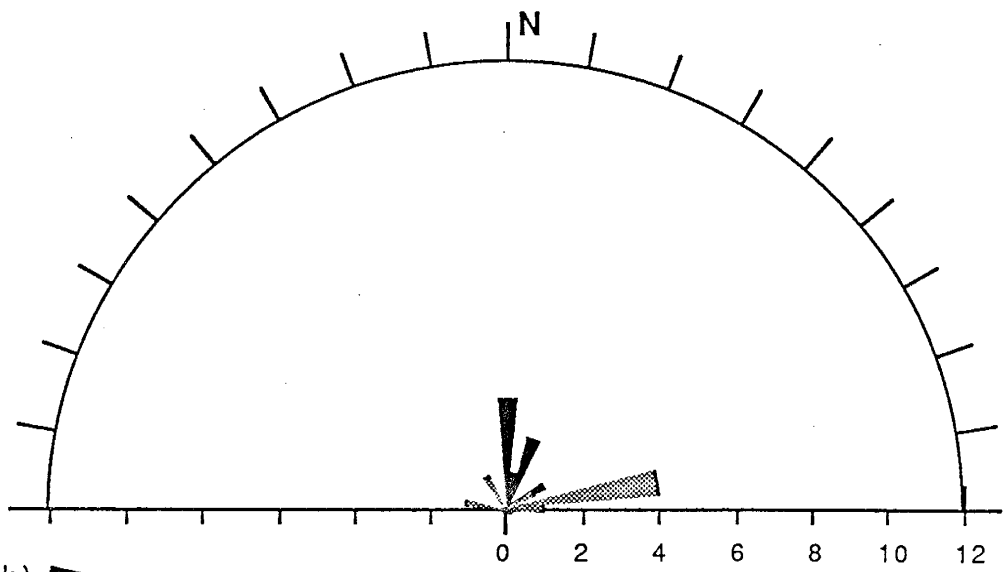


(b) Left-extension linear veins, N=7
associated fibrous crystals, N=9

APPENDIX M (continued)

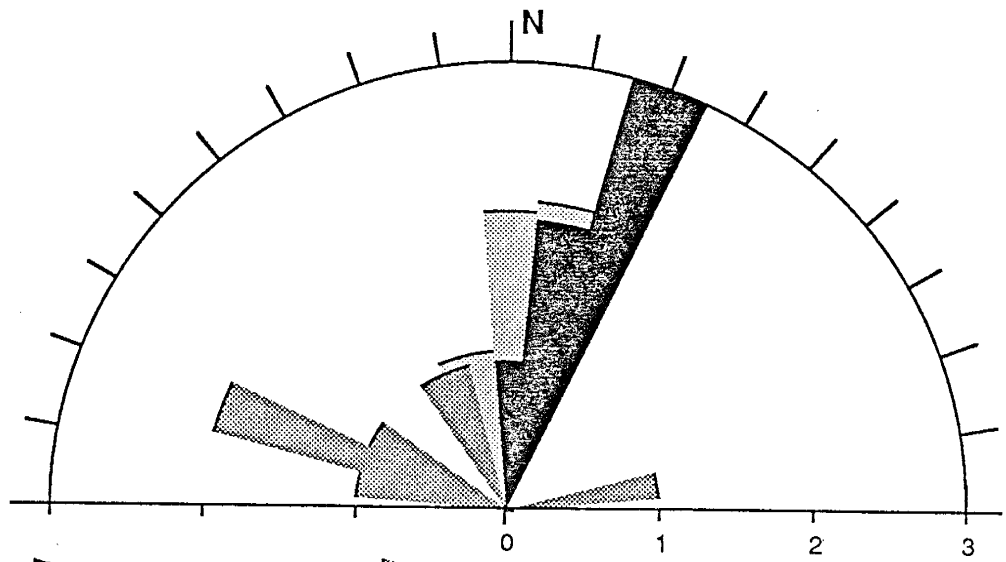


(c) Veins, N=6 Fibrous crystals, N=7

Left-en echelon arrays, or right-slip shear zones, N=6

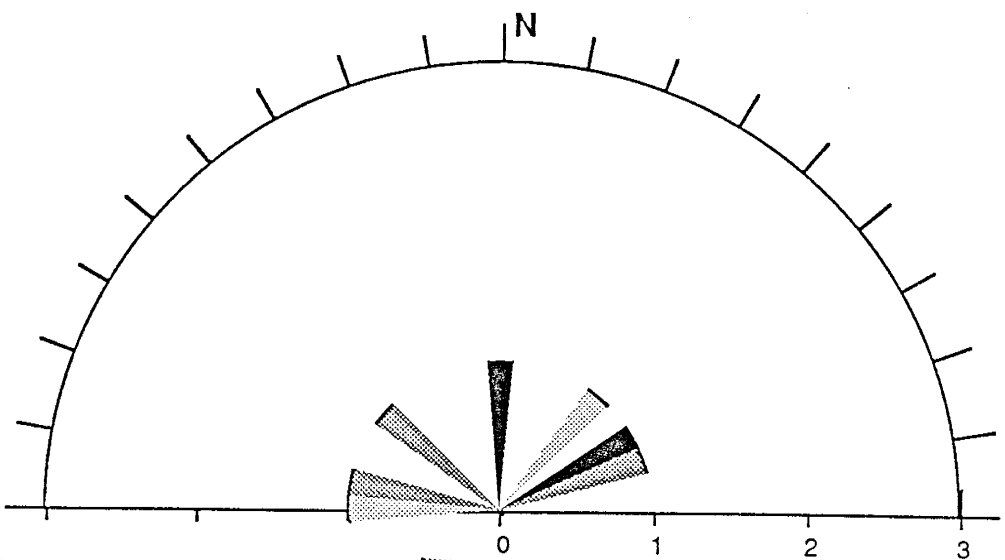


(d) Veins, N=2 Fibrous Crystals, N=3

Right-en echelon arrays, or left-slip shear zones, N=2

# APPENDIX N

Incremental strain ($e_i$) versus fibrous crystal orientation
See Figure 23 and text (pg. 102 ) for explanation and analysis.

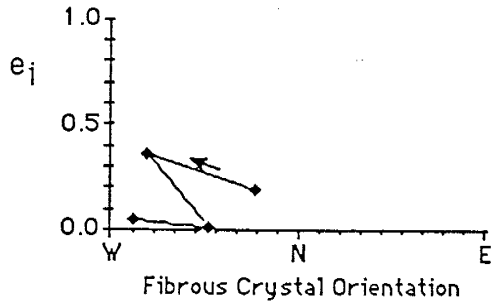


Thin section 1a

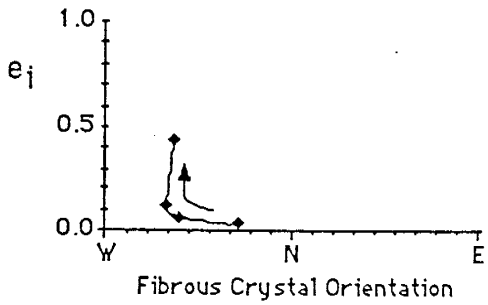


Thin section 3a

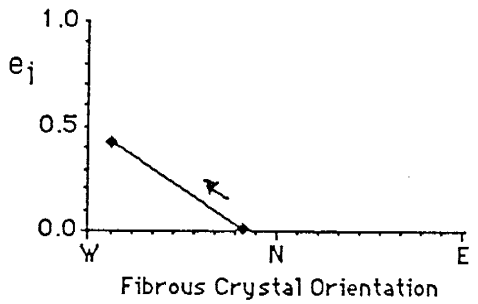


Thin section 6a

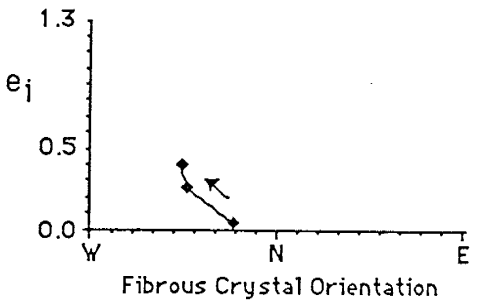


Thin section 7a

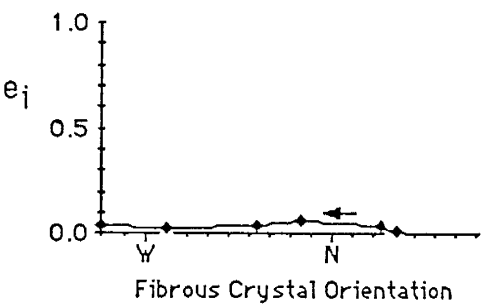


Thin section 8a

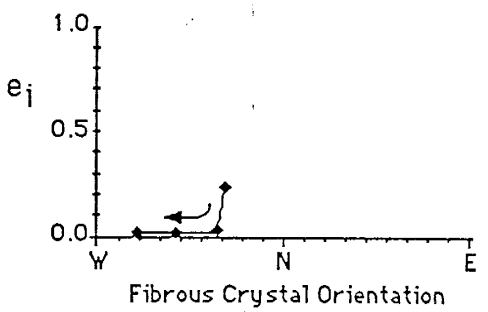


Thin section 9a, 1st set

APPENDIX N (continued)

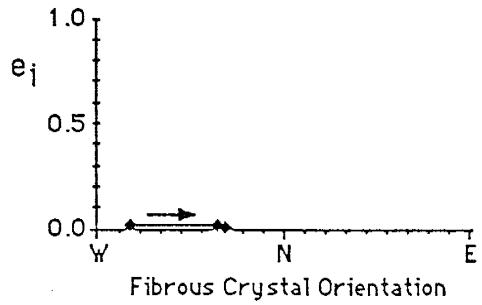


Thin section 9a, 2nd set

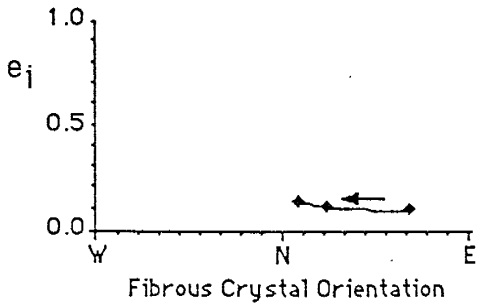


Thin section 9a, set C

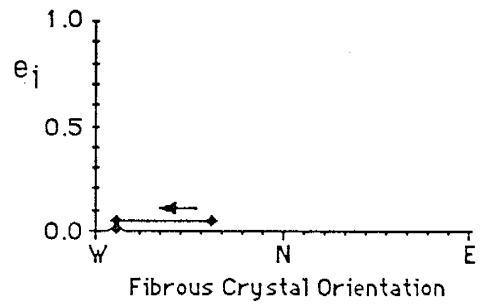


Thin section 10a

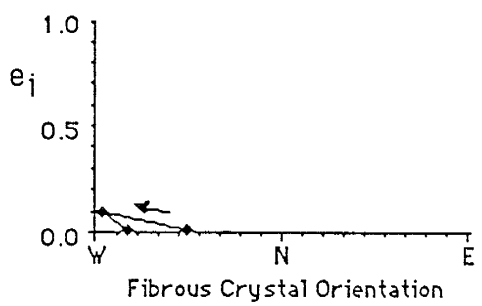


Thin section 11a

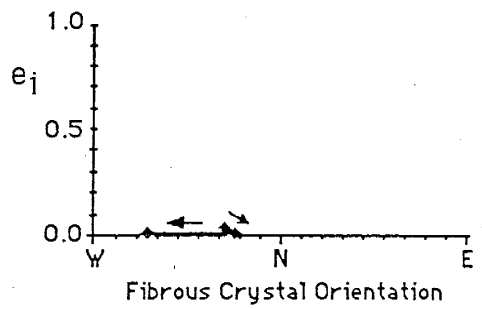


Thin section 12a

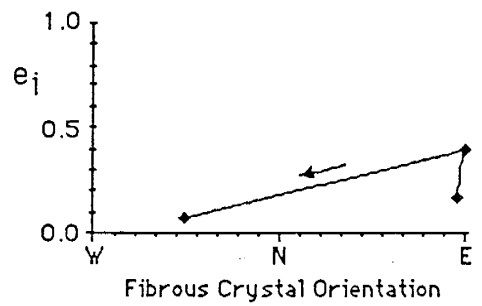


Thin section 13e, set A

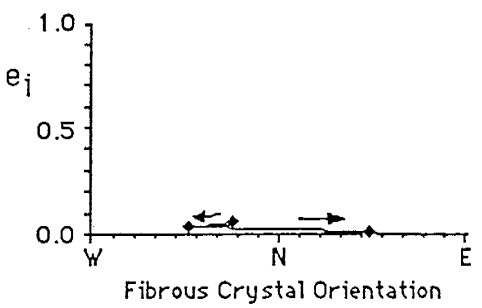


Thin section 13e, set B

This thesis is accepted on behalf of the faculty of the Institute by the following committee:

Advisor

8/25/87
Date